НАЦІОНАЛЬНА АКАДЕМІЯ НАУК УКРАЇНИ
НАВЧАЛЬНО-НАУКОВИЙ КОМПЛЕКС
«ІНСТИТУТ ПРИКЛАДНОГО СИСТЕМНОГО АНАЛІЗУ»
НАЦІОНАЛЬНОГО ТЕХНІЧНОГО УНІВЕРСИТЕТУ УКРАЇНИ
«КИЇВСЬКИЙ ПОЛІТЕХНІЧНИЙ ІНСТИТУТ ІМЕНІ ІГОРЯ СІКОРСЬКОГО»

СИСТЕМНІ ДОСЛІДЖЕННЯ ТА ІНФОРМАЦІЙНІ ТЕХНОЛОГІЇ

МІЖНАРОДНИЙ НАУКОВО–ТЕХНІЧНИЙ ЖУРНАЛ

У номері:

- **Теоретичні та прикладні проблеми і методи системного аналізу**

- **Проблеми прийняття рішень та управління в економічних, технічних, екологічних і соціальних системах**

- **Теоретичні та прикладні проблеми інтелектуальних систем підтримання прийняття рішень**

- **Проблемно- і функціонально-орієнтовані комп'ютерні системи та мережі**

- **Методи оптимізації, оптимальне управління і теорія ігор**

- **Математичні методи, моделі, проблеми і технології дослідження складних систем**

In the issue:

• **Theoretical and applied problems and methods of system analysis**

• **Decision making and control in economic, technical, ecological and social systems**

• **Theoretical and applied problems of intelligent systems for decision making support**

• **Problem- and function-oriented computer systems and networks**

• **Methods of optimization, optimum control and theory of games**

• **Mathematical methods, models, problems and technologies for complex systems research**

Шановні читачі!

Навчально-науковий комплекс «Інститут прикладного системного аналізу» Національного технічного університету України «Київський політехнічний інститут імені Ігоря Сікорського» видає міжнародний науково-технічний журнал

«СИСТЕМНІ ДОСЛІДЖЕННЯ ТА ІНФОРМАЦІЙНІ ТЕХНОЛОГІЇ».

Журнал публікує праці теоретичного та прикладного характеру в широкому спектрі проблем, що стосуються системних досліджень та інформаційних технологій.

Провідні тематичні розділи журналу:

Теоретичні та прикладні проблеми і методи системного аналізу; теоретичні та прикладні проблеми інформатики; автоматизовані системи управління; прогресивні інформаційні технології, високопродуктивні комп'ютерні системи; проблеми прийняття рішень і управління в економічних, технічних, екологічних і соціальних системах; теоретичні та прикладні проблеми інтелектуальних систем підтримання прийняття рішень; проблемно і функціонально орієнтовані комп'ютерні системи та мережі; методи оптимізації, оптимальне управління і теорія ігор; математичні методи, моделі, проблеми і технології дослідження складних систем; методи аналізу та управління системами в умовах ризику і невизначеності; евристичні методи та алгоритми в системному аналізі та управлінні; нові методи в системному аналізі, інформатиці та теорії прийняття рішень; науково-методичні проблеми в освіті.

Головний редактор журналу — ректор Національного технічного університету України «Київський політехнічний інститут імені Ігоря Сікорського», академік НАН України Михайло Захарович Згуровський.

Журнал «Системні дослідження та інформаційні технології» включено до переліку фахових видань ВАК України.

Журнал «Системні дослідження та інформаційні технології» входить до таких наукометричних баз даних: Scopus, EBSCO, Google Scholar, DOAJ, Index Copernicus, реферативна база даних «Україніка наукова», український реферативний журнал «Джерело», наукова періодика України.

Статті публікуються українською та англійською мовами.

Журнал рекомендовано передплатити. **Наш індекс 23918.** Якщо ви не встигли передплатити журнал, його можна придбати безпосередньо в редакції за адресою: 03056, м. Київ, просп. Перемоги, 37, корп. 35.

Dear Readers!

Educational and Scientific Complex «Institute for Applied System Analysis» of the National Technical University of Ukraine «Igor Sikorsky Kyiv Polytechnic Institute» is published of the international scientific and technical journal

«SYSTEM RESEARCH AND INFORMATION TECHNOLOGIES».

The Journal is printing works of a theoretical and applied character on a wide spectrum of problems, connected with system researches and information technologies.

The main thematic sections of the Journal are the following:

Theoretical and applied problems and methods of system analysis; theoretical and applied problems of computer science; automated control systems; progressive information technologies, high-efficiency computer systems; decision making and control in economic, technical, ecological and social systems; theoretical and applied problems of intellectual systems for decision making support; problem- and function-oriented computer systems and networks; methods of optimization, optimum control and theory of games; mathematical methods, models, problems and technologies for complex systems research; methods of system analysis and control in conditions of risk and uncertainty; heuristic methods and algorithms in system analysis and control; new methods in system analysis, computer science and theory of decision making; scientific and methodical problems in education.

The editor-in-chief of the Journal is rector of the National Technical University of Ukraine «Igor Sikorsky Kyiv Polytechnic Institute», academician of the NASU Michael Zaharovich Zgurovsky.

The articles to be published in the Journal in Ukrainian and English languages are accepted. Information printed in the Journal is included in the Catalogue of periodicals of Ukraine.

СИСТЕМНІ ДОСЛІДЖЕННЯ ТА ІНФОМАЦІЙНІ ТЕХНОЛОГІЇ

1 • 2023

ЗМІСТ

SYSTEM RESEARCH AND INFORMATION TECHNOLOGIES

1 • 2023

CONTENT

RESEARCH OF FOOD SECURITY PROBLEMS OF THE WAR-TORN REGIONS OF UKRAINE USING GEOMATICS METHODS

M. ZGUROVSKY, K. YEFREMOV, S. GAPON, I. PYSHNOGRAIEV

Abstract. Every year, the world faces new difficult challenges in maintaining global security. Compliance with food security principles is an important component of the global context of world development. Recent military conflicts have had a strong impact on the development of regions that provide food for millions of people around the world. Ukraine plays a key role in providing agricultural products to the population of countries from different continents. The article is devoted to the study of the state of agricultural crops in a regional section during the period of active hostilities by means of geomatics, which allow one to assess the degree of transformation of sustainable farming quickly, determine the trend of the development of the industry, and calculate the likely scale of changes in the obtained products in the coming years. As a result, with the help of deep learning models integrated into geoinformation systems, the boundaries of agricultural fields in the Kherson and Zaporizhia regions were determined, the state of moisture and bioproductivity of agricultural crops was determined for three years, an analysis of changes has been made in the state of agricultural fields under the influence of new factors of conducting active hostilities during the first half of 2022, the next harvest productivity forecast was made in two southern regions of Ukraine. The study was carried out by the team of the World Data Center for Geoinformatics and Sustainable Development of the Igor Sikorsky Kyiv Polytechnic Institute. It was part of research on the analysis of the behavior of complex socio-economic systems and processes of sustainable development in the context of the quality and safety of people's lives.

Keywords: food security, spatial data analysis, deep learning, agricultural fields, mathematical modeling.

INTRODUCTION

Intensification of extreme weather conditions, climate change processes, coronavirus pandemic, etc. led to an aggravation of the food situation for many countries of the world [1]. Before Russia`s full-scale invasion of Ukraine, the world was close to a global food crisis, but since February 24, 2022, the situation has significantly worsened [2]. Ukraine is a supplier of a large number of agricultural products to dozens of taps in the world. Ukraine has 15% of the global product market (UBTA) for individual grain crops [3]. Some countries of the world depend on certain types of agricultural products from Ukraine for more than 50%. The full-scale war led to a significant reduction in the area of cultivated agricul-

tural areas, a decrease in the number of people and equipment involved in the cultivation of agricultural crops. In addition, the structure of management in the field of irrigation was transformed.

Combat actions and specific management decisions in the temporarily occupied territories have significantly changed the irrigation system that has existed for many years. The canal systems, which were fed from the Dnieper and transported water hundreds of kilometers to the south and east of the country, are under temporary occupation and their state of functioning is difficult to investigate. At the same time, the region continues to be a supplier of a significant amount of agricultural products, so it is extremely important to understand the degree of transformation processes in order to assess possible losses and predict the degree of the food crisis. Due to constant military operations, direct access to the territory is extremely difficult, reliable statistical data on the volume and condition of the harvest, irrigation of the territory, etc. are not collected, the only possible methods of assessing the degree of transformation of agricultural fields are methods of remote sensing of the Earth, and geomatics in general. The most characteristic signs of the transformation of the water regime, especially for irrigated areas, are signs of a sharp change in indicators of bioproductivity and territory moisture. Such characteristics can be obtained with high accuracy based on the analysis of satellite images of medium resolution, which is not a limiting factor based on the realities of war.

This study is a continuation of the thematic research of the team of authors on the study of sustainable development of communities and territories of Ukraine and security processes in the regions of the state [4, 5] and research on the development of the applications of geomatics methods [6, 7].

DATA FRAMEWORK

Two southern regions of Ukraine: Kherson and Zaporizhzhya, were chosen to assess the impact of the processes associated with the occupation on the condition of agricultural plots (Fig. 1).

Fig. 1. The study area (black borders) with the indicated averaged zones of temporary occupation as of May 2022 (gray color)

For most of the first four months of the active phase of the war, these areas have been partially occupied, and this period completely coincides with the period of active agricultural work, in particular with the irrigation of the territory. Remote monitoring of the state of moisture in agricultural fields, analysis of the distribution of the Normalized Difference Moisture Index (NDMI) on the territory, its dynamics over different years will allow to assess the degree of changes in sustainable agricultural practices in the region and assess the state of the potential harvest, which in the pre-war period for years provided food for the population of Ukraine and residents of countries that import agricultural products. The selected areas have a high share of plowed territory, both irrigated and non-irrigated agricultural fields, and a dense and fairly even distribution of plots throughout the territory. This makes it possible to distinguish the anthropogenic influence of the occupation itself on the situation with the moisture of agricultural fields from the general background climatic influence. The condition of plots exclusively on traditionally irrigated lands can be analyzed separately. In addition to the analysis of the differentiation of the moisture index, it is necessary to investigate the change in the bioproductivity index: Normalized Difference Vegetation Index (NDVI), which on the one hand directly correlates with the moisture content of the territory, but allows to distinguish the vegetation state of the vegetation itself, which affects the indices of the moisture index itself (there may be weakly moistened territories, however, due to the high vegetation, give the moisture index high values). The condition of plots exclusively on traditionally irrigated lands can be analyzed separately. In addition to the analysis of the differentiation of the moisture index, it is necessary to investigate the change in the bio productivity index: NDVI, which on the one hand directly correlates with the moisture content of the territory, but allows to distinguish the vegetation state of the vegetation itself, which affects the indices of the moisture index itself (there may be weakly moistened territories, however, due to the high vegetation, it gives the moisture index of high values).

To assess the impact of the occupation, mainly data from remote sensing of the Earth (DSR) [8], data on the administrative and territorial structure of the country [9] and the borders of temporarily occupied territories from open online sources [10] were used. For the analysis of moisture and bio productivity, data were obtained from the Sentinel-2 mission satellite, platforms 2-A and 2-B and product type S2MSI1C with a cloud cover of no more than 10% in the study area [11]. The resolution of multispectral three-channel images is 10 m per pixel, single-channel 20 m per pixel. Channels B08 and B11, bio productivity index: B08 and B04 were used to calculate the moisture index.

$$NDMI = (B08 - B11)/(B08 + B11); \qquad (1)$$

$$NDVI = (B08 - B04)/(B08 + B04). \qquad (2)$$

Data on the boundaries of regions, districts and communities of the study area were obtained from the official website of the support for the decentralization reform [12].

The boundary of the line of contact of the troops is dynamic and has not yet been determined, therefore the boundaries of the temporarily occupied territories for the Kherson and Zaporizhzhia regions were drawn quite approximately based on an integrated analysis of data on the boundaries of the occupation zones as of the end of May 2022 according to publicly available web map data [13, 14].

RESEARCH FRAMEWORK

To analyze the impact of the occupation, mainly geomatics methods, systems analysis methods and machine learning methods were used. In particular, the overlay method and map algebra method were used in desktop GIS [15, 16] even before the beginning of 2022 to calculate bio productivity and moisture indices.

The papers consider aspects of integration of temporal statistical characteristics with spectral and textural characteristics extracted from high-quality Sentinel-2 images using Random Forest classification [17]. The performance and contribution of different combinations is evaluated based on classification accuracy. The results show that the statistical analysis of time series is an effective way of presenting information about the degree of soil moisture. The method uses clear pixels from dense, low-quality images to derive NDVI statistics, thus reducing the influence of random factors such as weather conditions.

Approaches to developing a linear mixed effects (LME) model for poorly calculated areas using time series of Sentinel 1A and 1B images and ground measurements of soil moisture are considered [18]. The model assumes a linear relationship that varies in both time and space between soil moisture and backscatter coefficient. The LSE model can be effectively applied to estimate soil moisture from multi-temporal Sentinel-1 images, which is useful for flood and drought monitoring and improving runoff forecasting.

Techniques for mapping soil moisture and irrigation at the scale of agricultural fields based on the synergistic interpretation of multitemporal optical and synthetic aperture radar (SAR) data (Sentinel-2 and Sentinel-1) were also presented [19]. The resulting irrigation maps were validated using reference fields in the study area. The best results were obtained with classifications based only on soil moisture indicators, with an accuracy of 77%.

An important aspect of the study was the separation of data on the NDVI and NDMI indices exclusively for the territory of the agricultural fields of the two regions, without considering the surrounding roads, settlements, water bodies, forested areas, etc. For this, the model was trained using the Image Analyst module, and the machine learning method integrated with desktop GIS was used: Detect Objects Using Deep Learning [20]. For training the model, the Non-Maximum Suppression parameter was used to detect and remove duplicate objects (Fig. 2).

Fig. 2. Reference set of polygons for training the model for identifying the boundaries of agricultural fields

The model tool processes the input geospatial images that are in the extent of the project map. The following approaches were used to train the model: MaskRCNN Object detection (Fig. 3) and Single Shot Detector (SSD) (Fig. 4) [21].
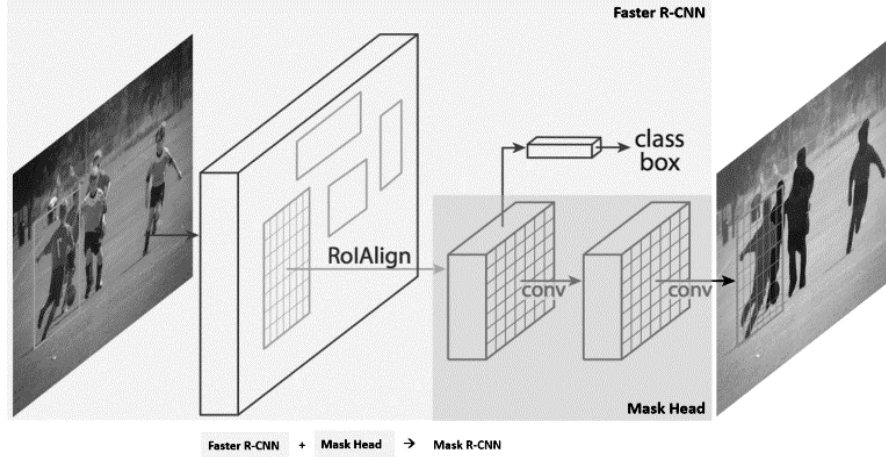
Fig. 3. The Mask R-CNN framework for instance segmentation [22]
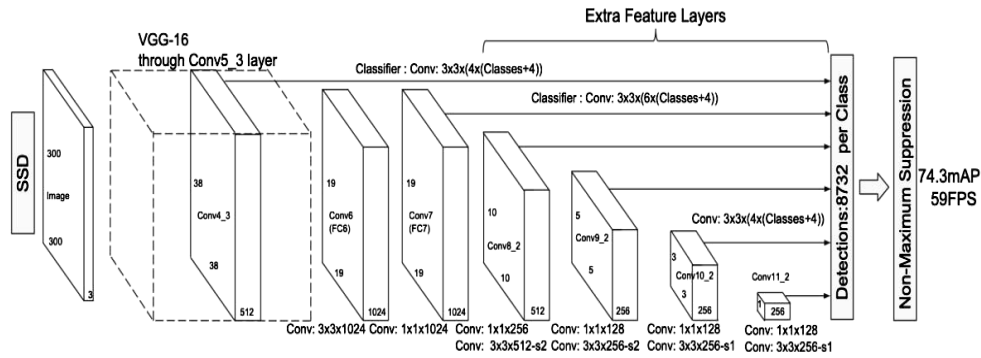
Fig. 4. SSD architecture [23]

The Mask R-CNN is obtainded rablacing the RoI pool by RoIAlign in Faster R-CNN. It helps to preserve spatial information which gets misaligned in case of RoI pool. RoIAlign uses binary interpolation to create a feature map that is of fixed size for e.g. 7 x 7. The output from RoIAlign layer is then fed into Mask head, which consists of two convolution layers. It generates mask for each RoI, thus segmenting an image in pixel-to-pixel manner.

During training our models we need to outline which default boxes correspond to a ground truth detection and train the network accordingly. To achieve this, we need to determine properly objective loss function for SSD model. The SSD training objective is gotten from [24]. Let $x_{ij}^{p} = \{1,0\}$ be an indicator for matching the *i*-th default box to the *j*-th ground truth box of category *p*. In the matching strategy were $\Sigma_i x_{ji}^{p} \geq 1$. The overall objective loss function is a weighted sum of the localization loss (loc) and the confidence loss (conf):

$$L(x,c,l,g) = \frac{1}{N}(L_{conf}(x,c) + \alpha L_{loc}(x,l,g)),$$

where *N* is the number of matched default boxes. If $N = 0$, the loss is set to 0. The localization loss is a Smooth L1 loss between the predicted box (l) and the ground truth box (g) parameters. It is regressed to offsets for the center (*cx, cy*) of the default bounding box (*d*) and for its width (*w*) and height *(h)*

$$L_{loc}(x,l,g) = \sum_{i \in Pos}^{N} \sum_{m \in \{cx,cy,w,h\}} x_{ij}^k smooth_{L1}(l_i^m - \hat{g}_j^m),$$

$$\hat{g}_j^{cx} = \frac{g_j^{cx} - d_i^{cx}}{d_i^w}, \quad \hat{g}_j^{cy} = \frac{(g_j^{cy} - d_i^{cy})}{d_i^h},$$

$$\hat{g}_j^w = \log\left(\frac{g_j^w}{d_i^w}\right), \quad \hat{g}_j^h = \log\left(\frac{g_j^h}{d_i^h}\right).$$

The confidence loss is the softmax loss over multiple classes confidences (*c*):

$$L_{conf}(x,c) = - \sum_{i \in Pos}^{N} x_{ij}^p \log(\hat{c}_i^p) - \sum_{i \in Neg} \log(\hat{c}_i^0),$$

where $\hat{c}_i^p = \dfrac{\exp(c_i^p)}{\sum_p \exp(c_i^p)}$ and the weight term α is set to 1 by cross validation.

MaskRCNN and SSD are used for segmentation and precise delineation of object boundaries on a space image.

All calculations of index values were carried out for territories that were within the boundaries of the identified plots. Based on the fact that in the resulting geospatial layers (GSP) there were several million individual values regarding the characteristics of moisture and bio productivity of agricultural fields, the processing results were processed in the R software environment.

Using the capabilities of the Copernicus Open Access Hub [25], images were uploaded to the territory of Kherson and Zaporizhzhia regions for the period May-June 2019–2022. Each image had to be covered by clouds no more than 10%. Due to the presence of many wet atmospheric fronts in the specified period of the year, such a wide permissible time period was chosen for uploading images, where priority was given to space images that were taken in the first half of June (70% of the received images). Due to the unsatisfactory state of cloud coverage of the images, the period of the end of May (12% of the images) and the second half of June (18% of the images) was chosen for the rest of the scenes. For each year, a minimum of 8 separate photo scenes were uploaded, which covered at least 97% of the territory of the selected regions (Fig. 5).

For each year, a new mosaic of both an integral image in the visible range (RGB) and a new mosaic of individual spectral channels (B04, B08, B11) was created from a series of separate images to calculate the moisture and bio productivity indices. Three-spectral rasters in the visible range and single-spectral rasters in the index range were obtained at the output. A raster in the visible range allows you to visually examine the area for artifacts of space images, and, if necessary, replace individual scenes with those that meet the requirements for the visibility of black and white fields. From the new mosaics of individual spectral channels, integral rasters of indices were calculated for each year (Fig. 6).
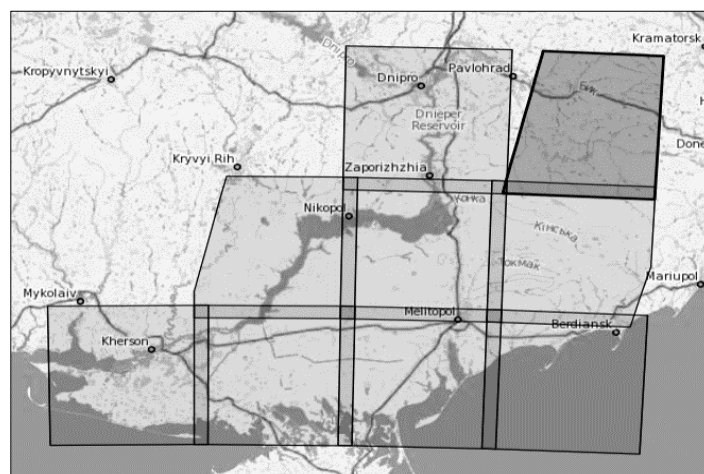
Fig. 5. Coverage of the research area with space images

Fig. 6. A fragment of the territory moisture index raster for 2022

The new image mosaics must be separated from the two areas to avoid analyzing areas that are outside the study ones. To do this, a process of raster extraction along the contours of the Kherson and Zaporizhzhia regions was carried out for all new raster mosaics obtained. The resulting GPS included both those necessary for the analysis of the territory of agricultural fields, as well as external water bodies, urbanized areas, infrastructure facilities, etc. For their illumination and selection of exclusively rural areas, training of a machine learning model integrated into the capabilities of the geographic information system (GIS) was carried out.

To carry out the model training process, it was necessary to manually highlight the boundaries of several thousand agricultural fields on space images for the selected period. The fields were vectorized evenly over the territory of the two regions with important identification of the borders of both irrigated and non-irrigated areas (Fig. 7). Often, irrigated areas have a rather specific contour of a regular circle, which, with insufficient training of the model on these fields, can lead to incorrect identification of boundaries.
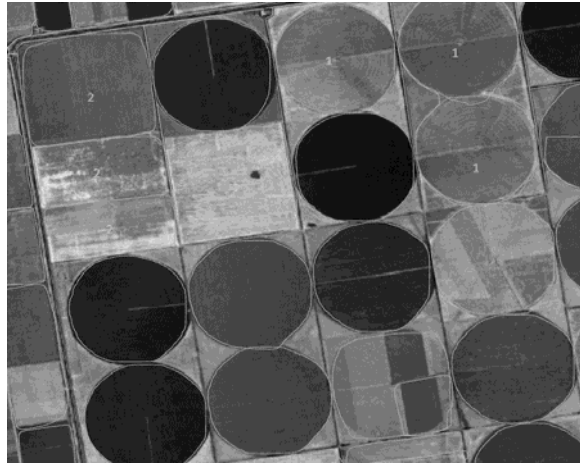
Fig. 7. Characteristic boundaries of irrigated (1) and non-irrigated (2) fields

The training process took place in a GIS environment where image tiles were first created as input layers to train the model. Image tile size was 448 pixels with metadata format: PASCAL Visual Object Classes and RCNN Masks. The image batch size type was 8, the model was run for 100 iterations (epochs). The additional pixel border around each field is 2 pixels. The maximum overlap of the resulting boundaries is 0.1, the minimum reliability of the selected boundaries is 60% (0.6). In total, the model consisted of 12 iterations of corrections and additional training.

As a result, the GIS was obtained with about 370,000 identified agricultural fields for the territory of two regions: 210.000 for the Kherson region and 160.000 for the Zaporizhia region (Fig. 8). The average reliability of the selected limits was 75%.
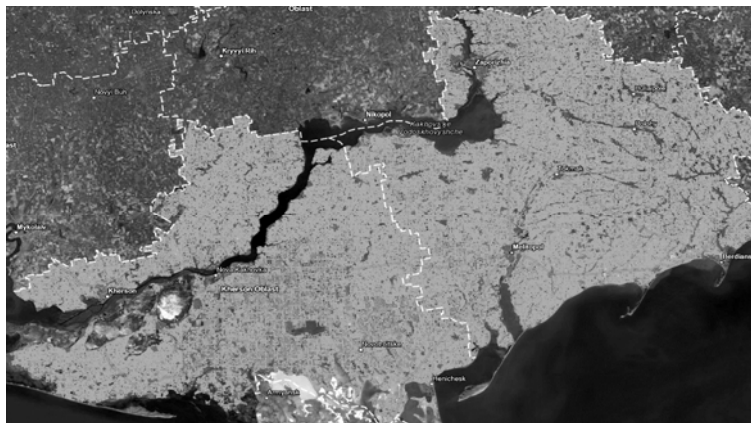
Fig. 8. Identified borders of agricultural fields for Kherson and Zaporizhzhia regions

Further improvement in model accuracy can be performed to achieve other applied goals in agriculture. For assessing the degree of transformation of the moisture regime and bio productivity of the fields, the obtained reliability is considered completely satisfying.

The extraction of new raster mosaics of the moisture index and bio productivity was carried out based on the obtained field mask. The final rasters began to calculate data exclusively for agricultural plots (Fig. 9).

Fig. 9. A fragment of the moisture index raster for agricultural fields in 2022

To assess the state of agricultural fields within individual regions, districts and communities, in the context of temporarily occupied and government-controlled territories, it is necessary to convert raster images into vector format and supplement the GIS with attributive data of the layers of the administrative-territorial system (ATU). After converting the data into a vector format, the area of each cell of the new GPS was calculated to obtain the ratio of the areas of areas with different humidity for each unit of ATU. The resulting layers consisted of more than 10 million records, the calculation of which was extremely difficult exclusively with GIS tools, so the corresponding statistical processing was carried out in the R software environment.

THE MOISTURE LEVEL ANALYSIS FOR THE IDENTIFIED FIELDS

Based on the rasters of the thematic indexes of agricultural fields, it is possible to make a preliminary integrated analysis for two regions, without dividing the regions into districts, communities, and the zone of occupation. Using the methods of zonal statistics, data were obtained on the average values of the moisture index rasters for 2019–2022 (Fig. 10). It can be seen from the graphs that over the past 4 years there has been a rather strong spread of index values: from 0.02 in 2020 to 0.07 in 2019. Moreover, the structure of the distribution of values is not uniform: normal or lognormal distribution in 2019 and 2020, and a distribution with two peaks in 2021 and 2022, indicating dry periods with a strong influence of irrigation systems in particular.

A normal or lognormal distribution indicates the classic case in which the average values of the wetness index cover a larger area. The values for 2019 correspond to this distribution, with a certain local peak on the graph for values that characterize low, poorly moistened vegetation. Most of the territory, according to the distribution, is covered with medium-low vegetation with low water stress. The log-normal distribution for 2020 is characterized by a large peak in the plot for coverage for low and dry vegetation, resulting in an overall lowest 4-year mean wetness index value. This situation strongly correlates with climate indicators, according to which 2020 was the driest year in terms of precipitation, which

caused a sharp drop in water levels in natural and anthropogenic reservoirs in the region. For 2021, two peaks on the graph are characteristic: for low and poorly moistened vegetation, and for medium-high, medium with low water stress. This distribution is caused by the contrasting weather conditions in May–June 2021, when the dry period ended with intense precipitation combined with a strong contrast in the wetness index for irrigated and non-irrigated areas. Where the high value of the index is characteristic mainly of irrigated fields, which occupy significant areas in the Kherson region. This statement is supported by further research. The year 2022 is also characterized by two peaks on the graph, among which the larger peak is responsible for poorly watered areas, and the smaller one is for vegetation with low water stress.
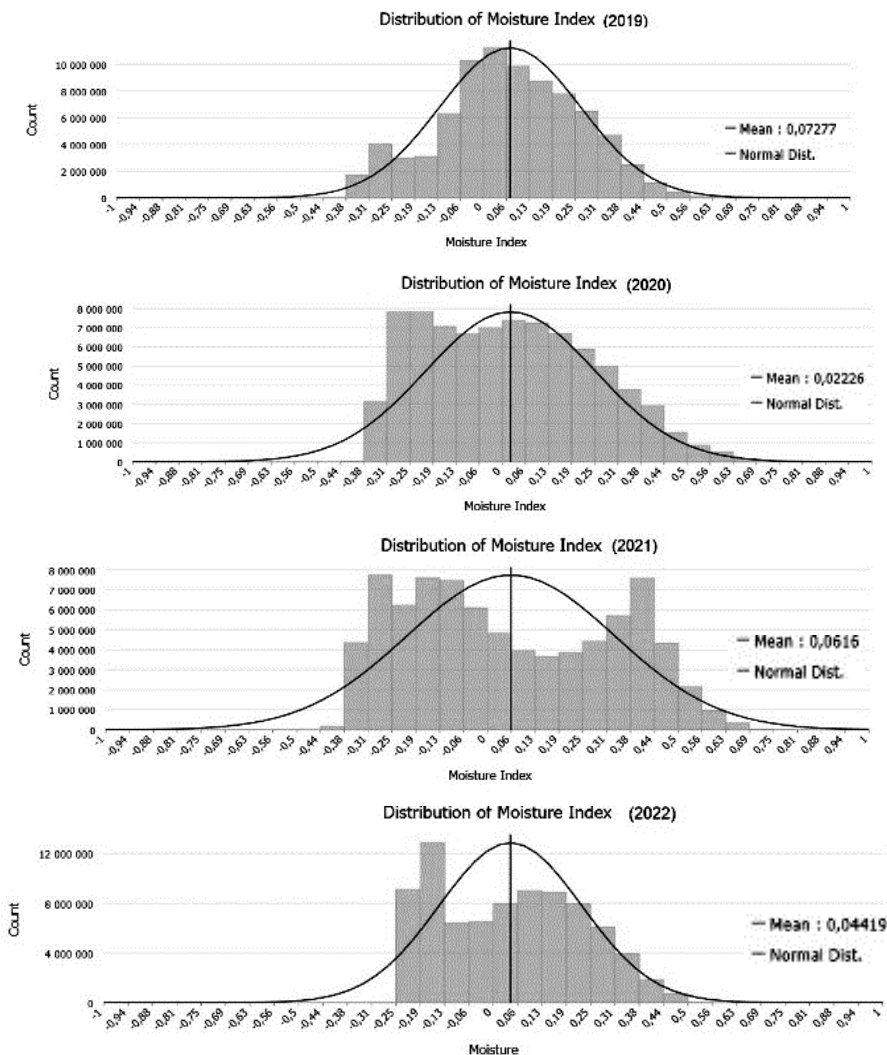
Fig. 10. Distribution of the humidity index for 2019–2022 in the Kherson and Zaporizhia regions

The territorial analysis of the moisture content of agricultural fields for 4 years showed a decrease in plots with medium-high vegetation cover and low water stress in two regions in 2022 (Fig. 11).
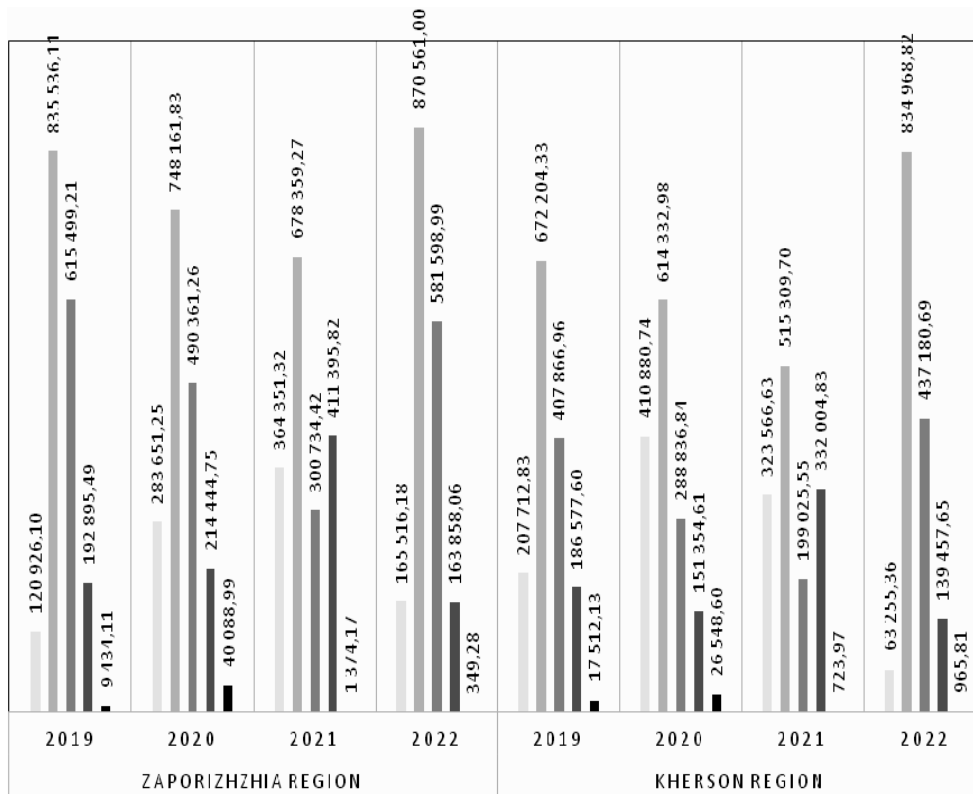
Fig. 11. Dynamics of the humidity index of the territory

■ Low coverage, dry or very low coverage

■ Medium-low vegetation cover, high water stress or low vegetation cover, low water stress

■ Medium vegetation cover, high water stress or medium-low vegetation cover, low water stress

■ Medium-high vegetation cover, high water stress or medium cover, low water stress

■ Other

Even compared to 2020, when a dry period was observed in both regions, the area of fields with low water stress in 2022 decreased by 8% in Kherson region and by 24% in Zaporizhzhya region. The Kherson region has a larger number of irrigated areas, which, most likely, continued to be actively irrigated in 2022, which quite strongly smoothed out the drop in the index value. Compared to the previous year 2021, for 2022 the drop was 60% for both Kherson and Zaporizhzhia regions. Such a rapid decrease in well-watered agricultural fields can be explained by the transformation in the conduct of irrigation and other processes in the agriculture of the region, which, in turn, is most likely directly related to the temporary occupation of the region. This statement requires further research in the context of expanding the experimental period of observations of the dynamics of the territory's moisture index. Most likely, there is a certain shift in the phases of irrigation, which leads to a shift in the vegetation phases of agricultural plants. From the graph of the dynamics of the index, it can be seen that in 2022 there is a significant increase in the area of fields with medium-low vegetation cover and low water stress compared to all other years: an increase of 119% in Kherson region and 93% in Zaporizhia region compared to 2021 However,

compared to 2019, there are almost no changes in areas, which most likely indicates a significant influence of climatic factors on the value of the indicator.

The influence of climatic factors, namely a rather cold and wet spring, also affected the distribution of areas with dry and very low vegetation cover (Fig. 12).

Low coverage, dry or very low coverage

Medium-low vegetation cover, high water stress or low vegetation cover, low water stress

Medium vegetation cover, high water stress or medium-low vegetation cover, low water stress

Medium-high vegetation cover, high water stress or medium cover, low water stress
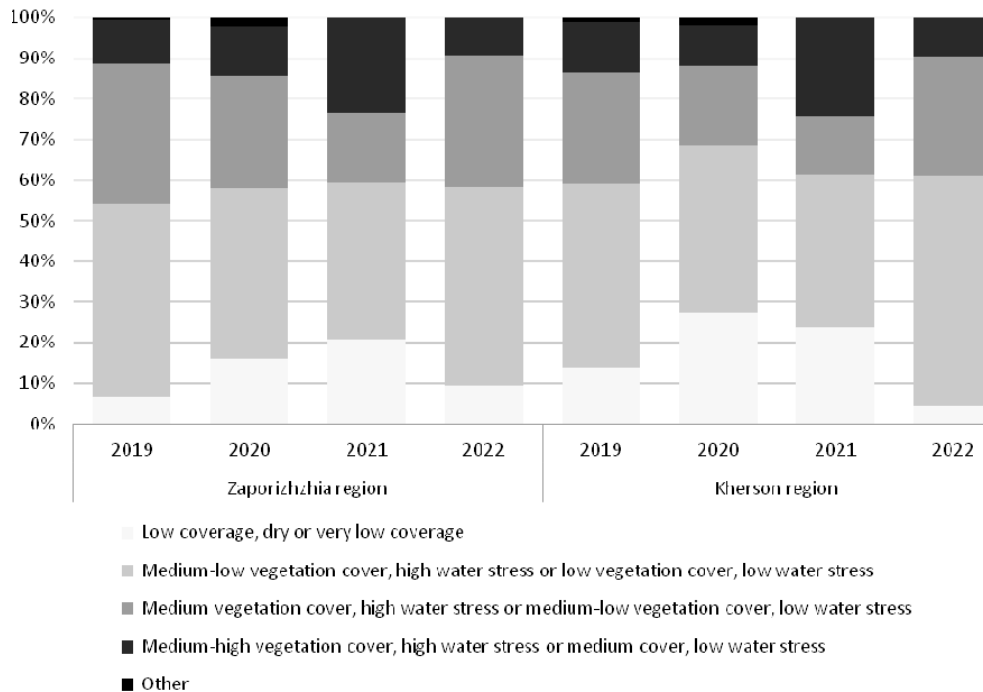
Other

Fig. 12. Percentage distribution of the territory's humidity index values

In 2022, there is a drop in this indicator compared to other years. This is especially characteristic of the Kherson region, where favorable synoptic conditions combined with artificial irrigation processes significantly reduced the index with low values.

An analysis was conducted exclusively for irrigated fields. For this purpose, those that are not reached by the system of irrigation canals were illuminated from the entire array of plots. The situation with the irrigated area is quite dynamic, so the average indicator of irrigated areas over 4 years was chosen. The Kherson region has a much higher density of canals and irrigated areas in general (Fig. 13). Therefore, fields with low water stress occupy much more area in the Kherson region, where there are almost no irrigated fields with dry vegetation (less than 4%).

Territorial analysis of the influence of occupation, in contrast to the temporal distribution, did not show any differences in the condition of agricultural fields in temporarily occupied and unoccupied areas of the region. Intense hostilities affect the entire territory of the regions, where the demarcation zone dynamically changes many times a month. Moreover, the most cultivated and irrigated parts of both the Kherson and Zaporizhzhia regions have been under temporary occupation since the first days of the war, the unoccupied territory consists of fields that are not reached by canal branches. This condition leads to a slight proportional increase in the area of poorly moistened areas precisely in the unoccupied territories (Fig. 14). However, all other index values remain proportionally almost the same.

Low coverage, dry or very low coverage

■ Medium vegetation cover, high water stress or medium-low vegetation cover, low water stress

■ Medium-high vegetation cover, high water stress or medium cover, low water stress

■ Medium-low vegetation cover, high water stress or low vegetation cover, low water stress

■ Other
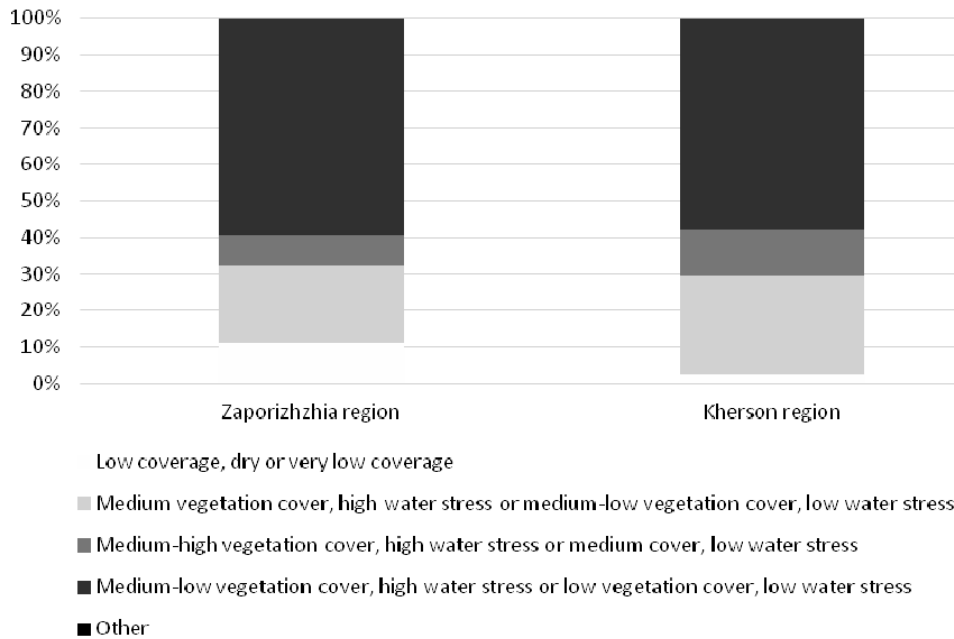
Fig. 13. Correlation of moisture index values for irrigated areas in 2022

Low coverage, dry or very low coverage

■ Medium-low vegetation cover, high water stress or low vegetation cover, low water stress

■ Medium vegetation cover, high water stress or medium-low vegetation cover, low water stress

■ Medium-high vegetation cover, high water stress or medium cover, low water stress

■ Other
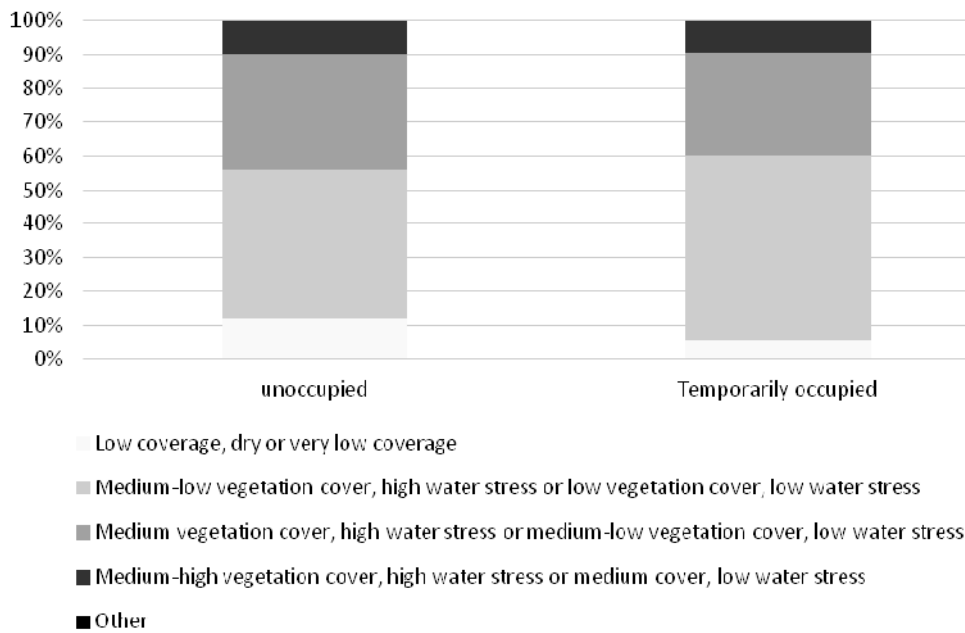
Fig. 14. Differentiation of the humidity index in temporarily occupied and unoccupied territories

CONCLUSIONS

1. The temporary occupation of the part of the Ukraine's southern regions leads to significant transformations in the structure of agriculture. Even though almost all the capacities of the irrigation systems of the Kherson and Zaporizhia regions was under the control of the occupiers, there is a significant decrease in

agricultural fields in a well-watered state (up to 60% compared to previous years). This may indicate the imperfect use of existing irrigation facilities and the reluctance of local farmers to cooperate with the occupation authorities.

2. However, at the same time, the catastrophic impact of temporary occupation on the state of agricultural land is not observed. Most of them are in a satisfactory condition, which makes it possible to predict a slight decrease in the amount of potentially harvested agricultural products. Active military actions do not allow agricultural works to be carried out fully in the unoccupied part of the regions, which affects the state of agricultural crops. However, even in such a difficult situation, the state of moistening of the fields of most of the unoccupied territory remains satisfactory. Which also indicates a favorable forecast for the collection of agricultural crops. However, the factor of conducting hostilities, which can significantly worsen the situation with the state of agricultural fields in both occupied and non-occupied territory, remains unpredictable.

3. The prepared machine learning model for identifying the boundaries of agricultural plots significantly improved the accuracy of the estimates made by illuminating all extraneous territories. In individual communities of the region, without considering the results of the model, the indicators of the state of hydration differed by 10–15% compared to the indicators of the indexes calculated exclusively within the boundaries of the plots.

4. The developed machine learning model can be applied to other regions of Ukraine, which will make it possible to assess the impact of military operations and/or temporary occupation for all affected regions. It is urgent to expand the research area in the following research to Mykolaiv region, which was also significantly affected by the temporary occupation of its territory.

5. Similar methods can be applied to those regions that have not undergone occupation, in the context of temporal and territorial analysis of the condition of agricultural fields under conditions of climate change, etc.

FUNDING INFORMATION

REFERENCES

1. P. Hebinck and H. Oostindie, "Performing food and nutritional security in Europe: claims, promises and limitations," *Food Sec.*, vol. 10, pp. 1311–1324, 2018. doi: 10.1007/s12571-018-0853-9.
2. M. Tanchum, *The Russia-Ukraine War has Turned Egypt's Food Crisis into an Existential Threat to the Economy*. Middle East Institute, MEI, 2022. CID: 20.500.12592/0h424d.
3. *Agricultural Production*. [Online]. Available: https://ourworldindata.org/ agricultural-production
4. Michael Zgurovsky, Andrii Boldak, Kostiantyn Yefremov, and Ivan Pyshnograiev, "Modeling and investigating the behavior of complex socio-economic systems,"

2017 IEEE First Ukraine Conference on Electrical and Computer Engineering (UKRCON), pp. 1113–1116, 2017. doi: 10.1109/UKRCON.2017.8100400.

5. M. Zgurovsky, K. Yefremov, I. Pyshnograiev, A. Boldak and I. Dzhygyrey, "Quality and Security of Life: A Cross-Country Analysis," *2022 IEEE 3rd International Conference on System Analysis & Intelligent Computing (SAIC), 2022*, pp. 1–5. doi: 10.1109/SAIC57818.2022.9923006.

6. M. Zgurovsky et al., "Parameterization of Sustainable Development Components Using Nightlight Indicators in Ukraine," *2018 IEEE First International Conference on System Analysis & Intelligent Computing (SAIC), 2018*, pp. 1–5. doi: 10.1109/SAIC.2018.8516726.

7. M. Zgurovsky, K. Yefremov, S. Gapon and I. Pyshnograiev, "Modeling of Potential Flooding Zones with Geomatics Tools," *2022 IEEE 3rd International Conference on System Analysis & Intelligent Computing (SAIC), 2022*, pp. 1–4. doi: 10.1109/SAIC57818.2022.99230.

8. Heike Schmidt and Arnon Karnieli, "Remote sensing of the seasonal variability of vegetation in a semi-arid environment," *Journal of Arid Environments*, vol. 45, iss. 1, pp. 43–59, 2000. doi: 10.1006/jare.1999.0607.

9. *Administrative boundaries of Ukraine*. [Online]. Available: https://data.humdata.org/dataset/ukraine-administrative-boundaries

10. *Interactive Map: Russia's Invasion of Ukraine*. [Online]. Available: https://www.understandingwar.org/

11. *European Union's Earth observation programme*. [Online]. Available: https://www.copernicus.eu/en

12. *Support site for Ukraine's decentralization reform*. [Online]. Available: https://atu.decentralization.gov.ua/

13. *DeepState Map: Russia's Invasion*. [Online]. Available: https://deepstatemap.live/

14. *Map tells story about war in Ukraine and Eastern Europe*. [Online]. Available: https://liveuamap.com/

15. M. Wu et al., "Monitoring cotton root rot by synthetic Sentinel-2 NDVI time series using improved spatial and temporal data fusion," *Sci. Rep.*, vol. 8, 2016 (2018). doi: 10.1038/s41598-018-20156-z.

16. M.S. Boori, K. Choudhary, R. Paringer, A.K. Sharma, A. Kupriyanov, and S. Corgne, "Monitoring Crop Phenology Using NDVI Time Series from Sentinel 2 Satellite Data," *2019 5th International Conference on Frontiers of Signal Processing (ICFSP), 2019*, pp. 62–66. doi: 10.1109/ICFSP48124.2019.8938078.

17. C. Huang et al., "Land Cover Mapping in Cloud-Prone Tropical Areas Using Sentinel-2 Data: Integrating Spectral Features with Ndvi Temporal Dynamics," *Remote Sens.*, 12(7): 1163, 2020. doi: 10.3390/rs12071163.

18. Y. Zhang, J. Gong, K. Sun, J. Yin, and X. Chen, "Estimation of Soil Moisture Index Using Multi-Temporal Sentinel-1 Images over Poyang Lake Ungauged Zone," *Remote Sens.*, 10(1), 12, 2018. doi: 10.3390/rs10010012.

19. S. Bousbih et al., "Soil Moisture and Irrigation Mapping in a Semi-Arid Region, Based on the Synergetic Use of Sentinel-1 and Sentinel-2 Data," *Remote Sens.*, 10(12), 1953, 2018. doi: 10.3390/rs10121953.

20. Z.-Q. Zhao, P. Zheng, S.-T. Xu and X. Wu, "Object Detection With Deep Learning: A Review," in *IEEE Transactions on Neural Networks and Learning Systems*, vol. 30, no. 11, pp. 3212–3232, Nov. 2019. doi: 10.1109/TNNLS.2018.2876865.

21. E.A. Alburshaid and M.A. Mangoud, "Palm Trees Detection Using the Integration between GIS and Deep Learning," *2021 International Symposium on Networks, Computers and Communications (ISNCC), 2021*, pp. 1–6. doi: 10.1109/ISNCC52172.2021.9615721.

22. Kaiming He, Georgia Gkioxari, Piotr Dollár, and Ross Girshick, *Mask R-CNN*. 2017. Available: http://arxiv.org/abs/1703.06870

23. J. Redmon, S. Divvala, R. Girshick, and A. Farhadi, "You only look once: Unified, real-time object detection," in *CVPR, 2016.*

24. W. Liu et al., "SSD: Single Shot MultiBox Detector," in *B. Leibe, J. Matas, N. Sebe, M. Welling (eds) Computer Vision – ECCV 2016. Lecture Notes in Computer Science*, vol. 9905. Springer, Cham, 2016. doi: 10.1007/978-3-319-46448-0_2.

25. *Copernicus Open Access Hub.* [Online]. Available: https://scihub.copernicus.eu/dhus/#/home

INFORMATION ON THE ARTICLE

Michael Z. Zgurovsky, ORCID: 0000-0001-5896-7466, National Technical University of Ukraine "Igor Sikorsky Kyiv Polytechnic Institute", Ukraine, e-mail: zgurovsm@hotmail.com

Kostiantyn V. Yefremov, ORCID: 0000-0003-3495-6417, National Technical University of Ukraine "Igor Sikorsky Kyiv Polytechnic Institute", Ukraine, e-mail: k.yefremov@wdc.org.ua

Sergii V. Gapon, ORCID: 0000-0002-8834-5825, National Technical University of Ukraine "Igor Sikorsky Kyiv Polytechnic Institute", Ukraine, e-mail: gapon@wdc.org.ua

Ivan O. Pyshnograiev, ORCID: 0000-0002-3346-8318, National Technical University of Ukraine "Igor Sikorsky Kyiv Polytechnic Institute", Ukraine, e-mail: pyshnograiev@gmail.com

ДОСЛІДЖЕННЯ ПРОБЛЕМ ПРОДОВОЛЬЧОЇ БЕЗПЕКИ, ОХОПЛЕНИХ ВІЙНОЮ РЕГІОНІВ УКРАЇНИ МЕТОДАМИ ГЕОМАТИКИ / М.З. Згуровський, К.В. Єфремов, С.В. Гапон, І.О. Пишнограєв

Анотація. Світ з кожним роком наражається на нові важкі виклики щодо підтримання глобальної безпеки. Важливою складовою глобального контексту світового розвитку є дотримання принципів продовольчої безпеки. Новітні військові конфлікти сильно впливають на стан розвитку регіонів, які забезпечують мільйони людей по всьому світу продовольством. Україна відіграє ключову роль у глобальних процесах забезпечення продукцією сільського господарства населення країн з різних континентів. Присвячено дослідженню станів сільськогосподарських культур у регіональному розрізі у період ведення активних бойових дій засобами геоматики, що дозволяє швидко оцінити ступінь трансформації сталого господарювання, визначити тренд розвитку галузі, обчислити ймовірні масштаби зміни отриманої про-дукції у найближчі роки. У результаті за допомогою інтегрованих у геоінформаційні системи моделей глибинного навчання визначено межі сільськогосподарських полів Херсонської та Запорізької областей, стан зволоженості та біопродуктивності сільськогосподарських культур за три роки, проаналізовано зміни станів сільськогосподарських полів під впливом нових факторів ведення активних бойових дій за першу половину 2022 р., зроблено прогноз продуктивності наступного врожаю у двох південних областях України. Наведене дослідження виконано командою Світового центру даних «Геоінформатика та сталий розвиток» КПІ ім. Ігоря Сікорського і є частиною досліджень з аналізу поведінки складних соціально-економічних систем та процесів сталого розвитку в контексті якості та безпеки життя людей.

Ключові слова: продовольча безпека, просторовий аналіз даних, глибинне навчання, сільськогосподарські поля, математичне моделювання.

DECISION-TREE AND ENSEMBLE-BASED MORTALITY RISK MODELS FOR HOSPITALIZED PATIENTS WITH COVID-19

Ya. VYKLYUK, S. LEVYTSKA, D. NEVINSKYI, K. HAZDIUK, M. ŠKODA, S. ANDRUSHKO, M. PALII

Abstract. The work is devoted to studying SARS-CoV-2-associated pneumonia and the investigating of the main indicators that lead to the patients' mortality. Using the good-known parameters that are routinely embraced in clinical practice, we obtained new functional dependencies based on an accessible and understandable decision tree and ML ensemble of classifiers models that would allow the physician to determine the prognosis in a few minutes and, accordingly, to understand the need for treatment adjustment, transfer of the patient to the emergency department. The accuracy of the resulting ensemble of models fitted on actual hospital patient data was in the range of 0.88–0.91 for different metrics. Creating a data collection system with further training of classifiers will dynamically increase the forecast's accuracy and automate the doctor's decision-making process.

Keywords: COVID-19, decision-making system, decision tree, ML-ensemble, ensemble of classification models.

BACKGROUND

The pandemic of SARS-CoV-2 infection, started in December 2019 has rapidly spread across the globe and affected all countries in two years. As of November 2021, the number of world-wide cases exceeded 262 million people, more than 5 million people died, including more than 85 thousand deaths in Ukraine [1]. The spread of coronavirus infection in Ukraine began from Chernivtsi and this city held the sad first place by the level of the SARS-CoV-2 morbidity during a year and a half. An emergency situation in medicine has obliged physicians of various specialties to help patients with SARS-CoV-2-associated pneumonia and to study the peculiarities of SARS-CoV-2 infection in their own practical experience.

Despite the huge accumulated clinical and laboratory material, the extraordinary attention of the medical community to the treatment of patients with SARS-CoV-2-associated pneumonia, it is still not clear why the disease became fatal for some patients [2].

Recent years decision-making and expert systems based on artificial intelligence have become widespread in medicine. Classification methods are one of the most urgent and necessary tasks in medicine. Classification shapes medicine and guides its practice. An understanding of classification should be part of the search for a better understanding of the social context and consequences of diagnosis. Classification is the part of human activity that provides the basis for recognizing and studying a disease. This means deciding how to extract significant parts from the vast expanse of nature, stabilizing and structuring disordered things [3], [4]. One of the most popular methods of classification is the diagnosic X-ray.

Different types of convolutional neural networks, or classical classifiers based on image features, are used as a classification model [5–7].

There are also investigations to determine mortality rate of patients depending on medical indicators. In particular, in the paper [8] Lactate dehydrogenase, neutrophils (%), lymphocyte (%), high-sensitivity C-reactive protein, and age (LNLCA), which were determined on hospital admission, were identified as key predictors of death from the multi-tree XGBoost model. The integrated score (LNLCA) was calculated with the corresponding probability of death. COVID-19 patients were divided into three subgroups: low-, middle-, and high-risk groups using LNLCA cutoff values of 10.4 and 12.65. The probability of death in each group is less than 5%, 5-50% and above 50%, respectively. The prognostic model, nomogram, and LNLCA assessment can help identify early high-risk mortality in patients with COVID-19, which will help physicians improve the management of patient stratification.

In the paper [9] the severity and outcome of COVID-19 cases has been associated with the percentage of circulating lymphocytes (LYM%), levels of C-reactive protein (CRP), interleukin-6 (IL-6), procalcitonin (PCT), lactic acid (LA), and viral load (ORF1ab Ct). However, the predictive power of each of these indicators in disease classification and prognosis remains largely unclear.

Similar results in work [10] indicate that the risk period for patients is 12–14 days, after which the probability of patient survival may increase. In addition, it is noted that the probability of death in COVID cases increases with age. It is established that the probability of death is higher in men than in women. SVM with Grid search methods showed the highest accuracy of about 95%, followed by the decision tree algorithm with an accuracy of about 94%.

Retrospective Cohort Study [11] included patients with COVID-19 who were admitted at three designated locations at Wuhan Union Hospital (Wuhan, China). Dynamic hematological and coagulation parameters were investigated with a linear mixed model, and coagulopathy screening with sepsis-induced coagulopathy and International Society of Thrombosis and Hemostasis overt disseminated intravascular coagulation scoring systems was applied.

The authors of paper [12] used the available information on pre-existing health conditions identified for deceased patients positive with severe acute respiratory syndrome coronavirus 2 (SARS-CoV-2)' in Italy. They estimated the total number of deaths for different pre-existing health conditions categories and calculated a conditional CFR based upon the number of comorbidities before SARS-CoV-2 infection morbidities before SARS-CoV-2 infection.

In the paper [13] was proved that High IL-6 level, C-reactive protein level, lactate dehydrogenase (LDH) level, ferritin level, d-dimer level, neutrophil count, and neutrophil-to-lymphocyte ratio all of them were predictors of mortality (area under the curve > 0.70), as well as low albumin level, lymphocyte count, monocyte count, and ratio of peripheral blood oxygen saturation to fraction of inspired oxygen (SpO_2/FiO_2). A multivariable mortality risk model including the SpO_2/FiO_2 ratio, neutrophil-to-lymphocyte ratio, LDH level, IL-6 level, and age was developed and showed high accuracy for the prediction of fatal outcome (area under the curve 0.94). The optimal cutoff reliably classified patients (including patients without initial respiratory distress) as survivors and nonsurvivors with a sensitivity of 0.88 and a specificity of 0.89.

As you can see there are not clearly defined factors that will affect mortality rate. There are no strict rules or decision trees for predicting patients' death.

Therefore, there is a great need to conduct research that will help the doctors predict the severity of the disease and its mortality.

The present studies and analysis unlock a way in the direction of attribute correlation, estimation of survival days, and the prediction of death probability. The findings of the present review clearly indicate that machine learning algorithms have strong capabilities of prediction and classification in relation to COVID-19 as well.

The aim of the study is the determination of the prognostic factors of fatal SARS-CoV-2-associated pneumonia and establishing a functional relationship between them and the mortality of the patient.

The main contribution of this article can be summarized as follows:

• based on the medical data of real patients of the hospital admitted with COVID-19, a heterogeneous data set was created, which became the basis for finding the relationship between the mortality rate of the patient;

• the method of validation, transformation and purification of the medical data set in preliminary preparation for the analysis was developed;

• an analysis to determine the impact of medical factors on mortality was conducted and a final set of data for the construction of classification models was formed;

• the train dataset for experimental modeling was created;

• the effectiveness of ten existing machine learning algorithms for solving the problem of determining the level of patient mortality was evaluated and a decision tree was constructed;

• a stacking model to predict mortality, which has prevented overfitting was developed and a significant increase in the accuracy of its operation and in comparison, with some existing machine learning algorithms was shown.

The resulting functional dependence can be implemented in expert systems that will allow the average physician to predict the degree of mortality of the patient, and therefore apply the necessary tools of intensive care to save human lives.

METHODS

Data Collection

A retrospective analysis of the results of treatment of 121 SARS-CoV-2-associated pneumonia patients who stayed in Chernivtsi City Hospital №1 (since March 2020 – the Chernivtsi Central COVID Hospital) was performed. The inclusion criterion was moderate or severe SARS-CoV-2-associated pneumonia as well as the exclusion criterion – the death before the fifth day staying in the hospital. According to the results, two groups were formed: the first group of the 60 SARS-CoV-2 associated pneumonia patients with the fatal outcome and the second group of the 61 patients with favorable course of the SARS-CoV-2 associated pneumonia.

Every patient could be described with a huge number of parameters. As potential prognostic factors we analyzed the 77 parameters divided into 9 parts according to the working hypothesis. This task can be attributed to the machine learning classification, where it is necessary to determine patients belonging to one of the classes (will die or live) based on many different factors. The stages of machine learning in this case should include preliminary data preparation, models selection, training and analysis of results.

Preliminary data preparation

There are several steps that are due to the peculiarities of obtaining and storing data at this stage. A Python script was written to implement each step.

Removing personalized data. Fields that contain personal information and those that do not clearly affect the diagnosis are removed from analysis. In particular: patient ID number, Name of patient, phone, diagnosis, complications, CT-scans etc.

Verification of human mistakes. The feature of the available data is that they are all entered by people, and this leads to technical mistakes. So, the first procedure is to verify the data and correct them automatically and manually. To do this, a script that identified and, if possible, corrected human errors was created.

Transformation and change of field values. A significant number of fields are not suitable for digital analysis, because they contain information in text format that is not suitable for analysis. The parse function was created that transformed all data for appropriate DataAnalysis form.

Handling features with missing data

The next step is removing the records that contain a lot of missing values. The large number of features leads to the removing records that contain at least one missing value. It can lead to a significant reduction in the DataSet and makes using classification methods impossible. To resolve this problem, empty values have been filled with the default values (if possible). Next, the features with the most missed data were identified.

It was decided to eliminate these features that consist more that 40% missed data from further calculation, as their presence will make further analysis impossible. This procedure of deletion of records with missing data reduced the DataSet by 19% (from 121 to 99 records). The total number of fields was 53 input and one output field that contain 49 – digital fields, 3 categorical and one logical.

Identification of factor importances

The Pearson's consistency criterion – χ^2 and mutual information (MI) as sorting method was used to determine the importance of factors for the classification of patients [14]–[16]. The magnitude of these criteria determines the significance of the field in the classification. The results are present in Table 1.

T a b l e 1. The top 10 of the most important features for classification

Features	χ^2	Features	MI
Leukocytes 2	434	Lymphocytes 2	0.3
Band-neutrofils 2	352	Leukocytes 2	0.28
Lymphocytes 2	352	Band-neutrofils 2	0.25
Hematocrit 2	250	Saturation without oxygen supply	0.23
Creatinine 2	226	The duration of the hospitalization	0.20
Saturation without oxygen supply	22	Hematocrit 2	0.19
The duration of the hospitalization	183	Creatinine 2	0.17
C-reactive protein 2	146	Hemoglobin 1	0.15
The pulmonary insufficiency	68	Age	0.13
Gender	50	The course of the disease	0.13

As can be seen from Table 1, the first seven factors in the two methods coincide. The only difference is their importance. Therefore, the DataSet was reduced to the first seven features.

The next step was to check the presence of correlation between features. The result of correlation analysis was presented in Fig. 1.
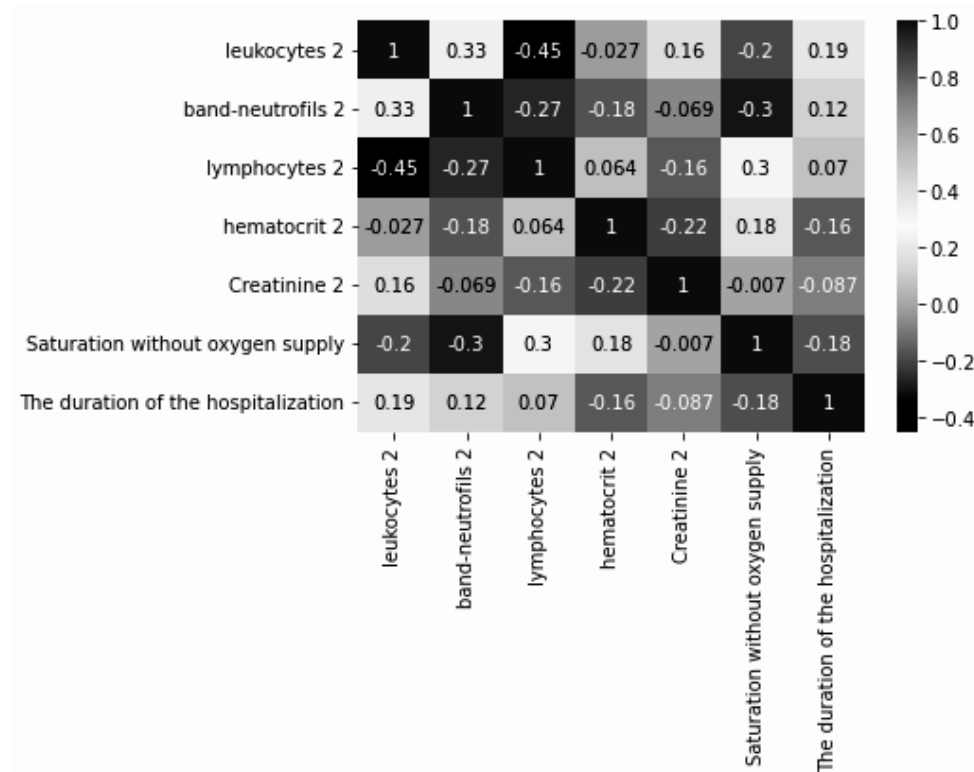
Fig. 1. Correlation matrix of input features

As can be seen from the Fig. 1, there is no correlation between the input factors. This means that you do not need to perform factor analysis and remove or convert factors.

Proposed models

This paper is aimed at building a forecast model, which will provide the highest accuracy in solving the problem on the one hand and will allow one to visualize the result in the form of a decision tree on the other hand. It is impossible to achieve this at the same time. After all, ensemble accuracy provides the highest accuracy. It is based on the use of a set of basic regressors, the results of which are summarized by the metaregressor. This will increase the accuracy compared to the use of single models that form such a model. However, it is not possible to visualize such a decision result in the form of a decision tree.

Therefore, we considered two approaches to prognosis. One is based on the decision tree; the other is ensemble.

Decision tree model. The decision tree method was used to determine the classification rules and visualize the results [17]. The main advantage of choosing this method is the ability to visualize the result of classification analysis in the form of a decision tree. However, the accuracy of this method is not the best.

The Gini coefficient was chosen as the criterion for measuring the cleavage threshold [18] – an indicator of the inequality of the distribution of some value of numbers, which takes values between 0 and 1, where 0 means absolute equality

(the value takes only one value), and 1 denotes complete inequality. The strategy used to select the split in each node is to find the best distribution.

Ensemble of classification models. The literature considers three main approaches to constructing ensemble models: boosting, bagging, and stacking.

In this work, we build a prediction model based on the stacking approach. The model assumes the presence of basic N-algorithms that will form a stacking ensemble. The meta-algorithm will weigh the results of their work. The work of the meta-algorithm will determine the impact of solving the stated task.

The data set collected by us to solve the problem of predicting the level of mortality contains many independent attributes. In addition, there are complex and nonlinear, unobvious and unexplored relationships between different features. It is evident that, in particular, many linear machine learning methods will not provide sufficient accuracy. If such algorithms are included in the general ensemble model, they will reduce the accuracy of their work. That is why we propose to perform a preliminary selection of basic algorithms that will form a stacking ensemble. It is based on initial modeling of machine learning algorithms and evaluation of their efficiency using the next four performance metrics: Accuracy, Precision, Recall and F1 Scope.

Accuracy means that the set of labels predicted for a sample must exactly match the corresponding set of labels in target.

Precision is the ratio:

$$precision = tp / (tp + fp),$$

where tp is the number of true positives and fp — the number of false positives. The precision is intuitively the ability of the classifier not to label as positive a sample that is negative.

Recall is the ratio:

$$recall = tp / (tp + fn).$$

The recall is intuitively the ability of the classifier to find all the positive samples.

F1 Scope is the harmonic mean of precision and recall, where an F1 score reaches its best value at 1 and worst score at 0. The relative contribution of precision and recall to the F1 score are equal. The formula for the F1 score is:

$$F1 = 2 * (precision * recall) / (precision + recall).$$

The Precision of classifier is the fraction of samples in the DataSet it labeled, for example, as death is really death. Its Recall is the percentage of all death samples in the dataset that it correctly labeled as death. The F1 score is the harmonic mean of precision and recall.

RESULTS AND DISCUSSIONS

Performance evaluation of the investigated decision tree model

The DataSet was splitted into train and test in the proportion of 70/30 to fit and determine the accuracy of the algorithm. The resulting decision tree is presented in Fig. 2.

Fig. 2. The decision tree determines whether the patient will die (False) or remain alive (True). Gini - distribution inequality, samples - the number of cases, value - the value of the classifier function, class - belonging to the class

Performance metrics on train DataSets consisted: accuracy = 0.90, precision = 0.89, recall = 0.88 and f1 = 0.89. We get accuracy = 0.88, precision = 0.86, recall = 0.86 and f1 = 0.86 for test DataSet. The small variance between test and training datasets indicates good fitting of this method. That is mean this model predicts unknown (new) data in the same level accuracy like know data. The high values of all metrics indicate the accuracy and adequacy of the model. It allows the doctor to personally guide the patient through this tree and quickly determine the class to which he belongs. Creating an automated decision-making program

based on trees is not a problem. The construction of the decision tree made it possible to establish the importance of features for this classifier (Table 2).

T a b l e 2. The importance of the decision tree features

Feature	Importance
Lymphocytes 2	0.62
Band-neutrofils 2	0.13
Saturation without oxygen supply	0.12
Creatinine 2	0.04
The duration of the hospitalization	0.04
Leukocytes 2	0.03
Hematocrit 2	0.02

As can be seen from the Table 2, the most important factor in the decision tree is the number of lymphocytes a week after hospitalization (lymphocytes 2). The decreased level of the lymphocytes as the marker of the severe SARS-CoV-2-infection was described in [19], [20]. Instead, our study proves the importance of this parameter as the risk marker of the fatal outcome. The further depression of the lymphocytes a week after the beginning of the intensive treatment of the SARS-CoV-2-patient points to the exhaustion of the immune defense and increases the probability of the fatal outcome.

The next important factor is the good-known indicator of the activity of the inflammatory process – the amount of the band-neutrophils [21] measured on the 7th day of the beginning of the intensive care of the SARS-CoV-2-patient. The prognostic non-favorable marker was the combination of the increasing amount of the band-neutrofils and the decreasing amount of the lymphocytes. The SARS-CoV-2-pneumonia patient's chances to survive are reduced in case of the severe activation of the inflammatory process with depression of the specific immune response.

The third important factor in the decision tree is the blood saturation without oxygen supply at the moment of the hospitalization. The low level of the blood saturation indirectly reflects the severity of the patient's condition and lungs affection, points to the exhaustion of the defensive and compensatory possibilities of the organism, the cardio-circulatory decompensation, severe tissue hypoxia [22]. The value of this indicator as a predictor of an unfavorable prognosis of the disease turned out to be quite logical.

Here are some examples of using the decision tree. The patient 1 was admitted to the hospital with blood saturation 85%, the amount of the leukocytes — 34,9 G/l, band-neutrofils — 24, lymphocytes — 3, hematocrit — 43,1, kreatinin-142 were revealed in his blood analysis in a week. Let's take the patient through the decision tree: lymphocytes ≤ 9.5 (yes) $\geq$ saturation without oxygen supply ≤ 92.5 (yes) $\to$ leukocytes ≤ 7.05 (no) $\to$ lymphocytes ≤ 7.75 (yes) $\to$ band-neutrofils ≤ 7.5 (no) $\to$ Class False, it means the prognosis is non-favorable. Indeed, on the 12th day after admission, the patient's death was fixed.

The patient 12 was admitted to the hospital with blood saturation 91%, the amount of the leukocytes — 6,1 G/l, band-neutrofils — 2, lymphocytes — 9, hematocrit — 46, kreatinin- 117 were revealed in his blood analysis in a week. Let's take the patient through the decision tree: lymphocytes ≤ 9.5 (yes) $\to$ satu-

ration without oxygen supply ≤ 92.5 (yes) $\rightarrow$ leukocytes ≤ 7.05 (yes) $\rightarrow$ saturation without oxygen supply ≤ 79.5 (no) $\rightarrow$ Class True, that shows on the favorable prognosis. And this patient was discharged from the hospital on the 13th day of the treatment.

Performance evaluation of the investigated ML-ensemble

It was decided to increase the train DataSet and use an ensemble of classification models to improve the quality of fitting and eliminate overfitting. For this purpose, all available records were used as a training set. An additional 83 patients were studied to obtain a test DataSet. New data were obtained in the same hospital department that is why the distribution of the test DataSet was the same.

The choice of classifiers for the ensemble was based on the analysis of the accuracy of each of them. The availability of overfitting on the train DataSet was also assessed. An experimental comparison of the efficiency of ten existing machine learning methods using the four performance metrics on train and test DataSets was carried out (Table 3 and 4).

T a b l e   3. The results of prediction based on performance criteria using all the studied machine learning algorithms (Train Data Set)

Machine learning method	Performance metric			
	Accuracy	Precision	Recall	F1 Scope
Logistic regression (CR)	0.89	0.90	0.84	0.87
Decision tree (DT)	0.89	0.87	0.87	0.87
Quadratic discriminant analysis (QDA)	0.84	0.94	0.68	0.79
Naive Bayesian classifier (NB)	0.84	0.91	0.70	0.79
Random forest classifier (RF)	0.95	0.93	0.95	0.94
Adaptive Boosting classifier (AB)	1.00	1.00	1.00	1.00
Support Vector Classification (SVC)	0.89	0.95	0.80	0.86
Stochastic Gradient Descent (SGD)	0.75	0.64	0.98	0.77
Neural Network (NN)	0.98	0.97	0.97	0.97
Gradient Boosting (GB)	1.00	1.00	1.00	1.00

T a b l e   4. The results of prediction based on performance criteria using all the studied machine learning algorithms (Test Data Set)

Machine learning method	Performance metric			
	Accuracy	Precision	Recall	F1 Scope
Logistic regression (LR) [23]	0.78	0.74	0.74	0.74
Decision tree (DT)	0.86	0.85	0.84	0.85
Quadratic discriminant analysis (QDA)[24]	0.75	0.77	0.57	0.66
Naive Bayesian classifier (NB) [25]	0.72	0.73	0.54	0.62
Random forest classifier (RF) [26]	0.62	0.56	0.57	0.56
Adaptive Boosting classifier (ABC) [27]	0.66	0.59	0.69	0.63
Support Vector Classification (SVC) [28]	0.77	0.79	0.63	0.70
Stochastic Gradient Descent (SGD) [29]	0.48	0.44	0.91	0.60
Neural Network (NN) [30–32]	0.77	0.70	0.80	0.75
Gradient Boosting (GB) [33, 34]	0.63	0.55	0.68	0.61

As you can see in Table 3, Decision Tree, AdaBoost and Gradient Boost had problems with overfitting. They have 100% accuracy on train DataSet and very low on test DataSet. Therefore, we exclude them from future analysis. All other seven classifiers had similar accuracy. Therefore, for improving accuracy we combined them into ensemble. A joint solution to these methods was found by the Voting Classifier [35]. The basic idea of a voting classifier is to combine conceptually different machine learning classifiers and use the majority of votes (hard voting) or average predicted probabilities (soft voting) to predict class labels. In our case, "hard" voting was used i.e., the choice of class was determined by the majority of "votes" of the classifiers. Results of accuracy of this ensemble are present in Table 5.

T a b l e 5. The results of prediction based on performance criteria using ensemble of machine learning algorithms

Voting Classifier	Performance metric			
	Accuracy	Precision	Recall	F1 Scope
Train Data Set	0.94	0.95	0.91	0.93
Test Data Set	0.91	0.88	0.88	0.88

For comparison we presented results on one plot (Fig. 3).
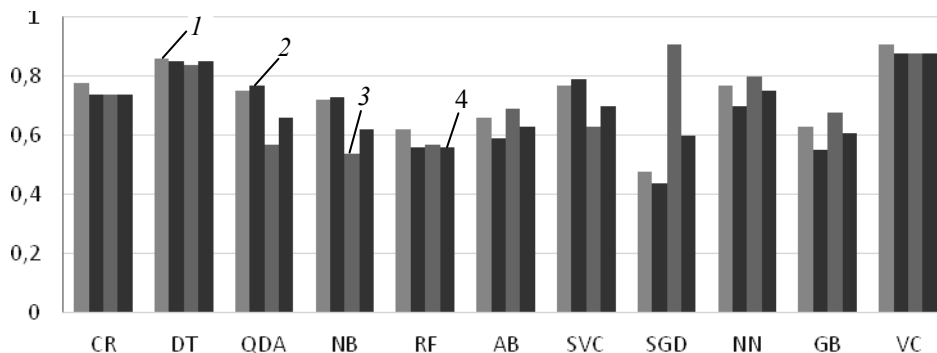
Fig. 3. Comparison of performance metrics of investigated classifiers and their ensemble: *1* — Accuracy, *2* —Precision, *3* — Recall, *4* — F1Scope

As you can see from the plot, ensemble has the biggest performance. You can also see that Recall for SGD is bigger than for ensemble. But other their performance metrics are smaller. Ensemble is stable in joint decision because Precision and Recall have the same big value. Thus, using an ensemble of ML models made it possible to avoid overfitting and increase the accuracy and stability of the forecast. The forecast error (bias) on the train DataSet is 6% and the variance of the test DataSet from the training set is 3%. So, we can conclude that to reduce the variance (reduce the error of the test DataSet) it is enough to simply increase the train DataSet. This will lead to a slight decrease in the accuracy of bias of the train DataSet and a increase in the accuracy of the test DataSet.

Further increase in the accuracy of the two indicators is possible provided the simultaneous growth of the train DataSet and the inclusion in the calculation of new factors, or the complexity of classification models, such as joining the ensemble of classifiers based on neural networks.

CONCLUSIONS

The only one marker of the non-favorable outcome of the SARS-CoV-2-associated pneumonia presented on the day of admission of the patient was the blood saturation less than 92.5%. This is the first and the basic indicator checked in every patient and doctors determine the necessity of the oxygen supply based on this parameter. In contrast to the severity of the general condition, diabetes mellitus, the duration of the disease does not increase the probability of the lethal outcome. The severity of the lung's affection based on the results of CT- or ultrasound examination don't influence the chances to die because of SARS-CoV-2-pneumonia.

But after a week of intensive treatment, we could reveal the informative markers of the lethal outcome. They are the amount of the lymphocytes and band-neutrophils in peripheral blood. The increasing of the activity of the inflammatory process reflected in the increase amount of the band-neutrophils and leukocytes as well as the decreasing of the lymphocyte points to the exhaustion of the specific immune response, the loss of the immunological control of the inflammation and to the high probability of the lethal outcome.

Using the good-known parameters that are routinely used daily in clinical practice, an accessible and understandable decision tree will allow the physician to determine the prognosis in a few minutes and, accordingly, to understand the need for treatment adjustment, transfer of the patient to the emergency department.

Creating a data collection system with further training of classifiers will dynamically increase the accuracy of the forecast and automate the decision-making process by the doctor.

DECLARATIONS

Ethics approval and consent to participate
Not applicable.
Consent for publication
Not applicable.
Availability of data and materials
Data were obtained from the medical histories of patients who were hospitalized at the Central Hospital in Chernivtsi, Ukraine. The data is available on the link: https://github.com/vyklyuk/COVID_Chernivtsi
Competing interests
The authors declare that they have no competing interests.
Funding
This research received no external funding.
Authors' contributions
Conceptualization, software, investigation, writing — original draft preparation Yaroslav Vyklyuk and Denys Nevinskyi; methodology Svitlana Levytska; software, validation, writing–review and editing Kateryna Hazdiuk; formal analysis, funding acquisition Miroslav Škoda; resources, data curation Stanislav Andrushko and Maryna Palii. All authors have read and agreed to the published version of the manuscript.

REFERENCES

1. *Worldometer COVID-19 Coronavirus Pandemic. 2020.* Accessed on: November 28, 2021. [Online]. Available: https://www.worldometers.info/coronavirus/

2. S. Priya, M. Selva Meena, J. Sangumani, P. Rathinam, C. Brinda Priyadharshini, and V. Vijay Anand, "Factors influencing the outcome of COVID-19 patients admitted in a tertiary care hospital, Madurai. -a cross-sectional study," *Clin Epidemiol Glob Health,* 2021. doi: 10.1016/j.cegh.2021.100705.

3. Annemarie Jutel, "Classification, Disease, and Diagnosis," *Perspectives in Biology and Medicine, Project MUSE*, vol. 54 no. 2, pp. 189–205, 2011. doi: 10.1353/pbm.2011.0015.

4. Aiping Lu, Miao Jiang, Chi Zhang, and Kelvin Chan, "An integrative approach of linking tradi-tional Chinese medicine pattern classification and biomedicine diagno-sis," *Journal of Ethnopharmacology*, vol. 141, issue 2, pp. 549–556, 2012. Available: https://doi.org/10.1016/j.jep.2011.08.045

5. O.S. Albahri et al., "Systematic review of artificial intelligence techniques in the de-tection and classification of COVID-19 medical images in terms of evaluation and benchmarking: Taxonomy analysis, challenges, future solutions and methodological aspects," *Journal of Infection and Public Health*, vol. 13, issue 10, pp. 1381–1396, 2020. Available: https://doi.org/10.1016/j.jiph.2020.06.028

6. Gonçalo Marques, Deevyankar Agarwal, and Isabel de la Torre Díez, "Automated medical diagnosis of COVID-19 through EfficientNet convolutional neural network," *Applied Soft Computing*, 2020, vol. 96. Available: https://doi.org/10.1016/j.asoc.2020.106691

7. X. Wang et al., "A Weakly-Supervised Framework for COVID-19 Classification and Lesion Localization from Chest CT," *IEEE Transactions on Medical Imaging*, vol. 39, no. 8, pp. 2615–2625, 2020. doi: 10.1109/TMI.2020.2995965.

8. M.E.H. Chowdhury et al., "An Early Warning Tool for Predicting Mortality Risk of COVID-19 Patients Using Machine Learning," *Cogn. Comput.*, 2021. Available: https://doi.org/10.1007/s12559-020-09812-7

9. Li Tan et al., "Validation of Predictors of Disease Severity and Outcomes in COVID-19 Patients: A Descriptive and Retrospective Study," *Med*, vol. 1, issue 1, pp. 128–138, 2020. Available: https://doi.org/10.1016/j.medj.2020.05.002

10. Ashutosh Kumar Dubey, Sushil Narang, Abhishek Kumar, Sasubilli Satya Murthy, and Vicente García-Díaz, "Performance Estimation of Machine Learning Algorithms in the Factor Analysis of COVID-19 Dataset," *Computers, Materials, & Continua*, 66(2), pp. 1921–1936, 2021.

11. Danying Liao et al., "Haematological characteristics and risk factors in the classifi-cation and prognosis evaluation of COVID-19: a retrospective cohort study," *The Lancet Haematology*, vol. 7, issue 9, pp. e671–e678, 2020. Available: https://doi.org/10.1016/S2352-3026(20)30217-9

12. M. Aguiar and N. Stollenwerk, "Condition-specific mortality risk can explain differ-ences in COVID-19 case fatality ratios around the globe," *Public Health*, vol. 188, pp. 18–20, 2020.

13. Rocio Laguna-Goya et al., "IL-6–based mortality risk model for hospitalized patients with COVID-19," *Journal of Allergy and Clinical Immunology*, vol. 146, issue 4, pp. 799–807, 2020. Available: https://doi.org/10.1016/j.jaci.2020.07.009

14. R. Rana and R. Singhal, "Chi-square test and its application in hypothesis testing," *J. Pract. Cardiovasc. Sci.*, 1, pp. 69–71, 2015. doi: 10.4103/2395-5414.157577.

15. B.C. Ross, "Mutual Information between Discrete and Continuous Data Sets," *PLoS ONE*, 9(2), 2014. Available: https://doi.org/10.1371/journal.pone.0087357

16. E. Archer, I.M. Park, and J. Pillow, "Bayesian and Quasi-Bayesian Estimators for Mutual Information from Discrete Data," *Entropy*, 15 (12), pp. 1738–1755, 2013. doi: 10.3390/e15051738.

17. S.R. Safavian and D. Landgrebe, "A survey of decision tree classifier methodology", *Systems Man and Cybernetics IEEE Transactions*, vol. 21, no. 3, pp. 660–674, 1991.

18. Laura Elena Raileanu and Kilian Stoffel, "Theoretical Comparison between the Gini Index and Information Gain Criteria," *Annals of Mathematics and Artificial Intelligence*, vol. 41, pp. 77–93, 2004. doi: 10.1023/B:AMAI.0000018580.96245.c6.

19. J. Wagner, A. DuPont, S. Larson, B. Cash, and A. Farooq, "Absolute lymphocyte count is a prognostic marker in Covid-19: A retrospective cohort review," *Int. J. Lab. Hematol.*, vol. 42(6), pp. 761–765, 2020. doi: 10.1111/ijlh.13288.

20. A. Mazzoni, L. Salvati, L. Maggi, F. Annunziato, and L. Cosmi, "Hallmarks of immune response in COVID-19: Exploring dysregulation and exhaustion," *Semin. Immunol.*, 2021. doi: 10.1016/j.smim.2021.101508.

21. J. Wang, M. Jiang, X. Chen, and L.J. Montaner, "Cytokine storm and leukocyte changes in mild versus severe SARS-CoV-2 infection: Review of 3939 COVID-19 patients in China and emerging pathogenesis and therapy concepts," *J. Leukoc. Biol.*, 108(1), pp. 17–41, 2020. doi: 10.1002/JLB.3COVR0520-272R.

22. D. Böning, W.M. Kuebler, and W. Bloch, "The oxygen dissociation curve of blood in COVID-19," *Am. J. Physiol. Lung. Cell. Mol. Physiol.*, vol. 321(2), L349–L357, 2021. doi: 10.1152/ajplung.00079.2021.

23. J. Tolles and W.J. Meurer, "Logistic Regression: Relating Patient Characteristics to Outcomes," *JAMA*, vol. 316(5), pp. 533–534, 2016. doi: 10.1001/jama.2016.7653.

24. Alaa Tharwat, "Linear vs. quadratic discriminant analysis classifier: a tutorial," *International Journal of Applied Pattern Recognition*, vol. 3.2, pp. 145–180, 2016.

25. P. Domingos and M. Pazzani, "On the optimality of the simple Bayes-ian classifier under zero-one loss," *Machine Learning*, vol. 29, pp. 103–137, 1997.

26. Leo Breiman, "Random Forests," *Machine Learning*, 45 (1), pp. 5–32, 2001. doi: 10.1023/A:1010933404324.

27. Zhao Yan, Xing Chen, and Jun Yin, "Adaptive boosting-based computational model for predicting potential miRNA-disease associations," *Bioinformatics*, vol. 35.22, pp. 4730–4738, 2019.

28. Chih-Wei Hsu, Chih-Chung Chang, and Chih-Jen Lin, *A Practical Guide to Support Vector Classification*. Department of Computer Science, National Taiwan University (Hrsg.), 2003.

29. L. Bottou, "Large-scale machine learning with stochastic gradient descent," *Proceedings of COMPSTAT*, Physica-Verlag HD, 2010, pp. 177–186.

30. Shaohua Wan et al., "Deep multi-layer perceptron classifier for behavior analysis to estimate parkinson's disease severity using smartphones," *IEEE Access*, 6, pp. 36825–36833, 2018.

31. D.C. Liu and J. Nocedal, "On the limited memory BFGS method for large scale optimization," *Mathematical Programming*, vol. 45, pp. 503–528, 1989. Available: https://doi.org/10.1007/BF01589116

32. Ph. Moritz, N. Robert, and M. Jordan, "A linearly-convergent stochastic L-BFGS algorithm," *Proceedings of the 19th International Conference on Artificial Intelligence and Statistics, PMLR,* 51, pp. 249–258, 2016.

33. S. Madeh Piryonesi and Tamer El-Diraby, "Data Analytics in Asset Management: Cost-Effective Prediction of the Pavement Condition Index," *Journal of Infrastructure Systems*, 26 (1): 04019036, 2020. doi: 10.1061/(ASCE)IS.1943-555X.0000512.

34. T. Hastie, R. Tibshirani, and J.H. Friedman, "Boosting and Additive Trees," *The Elements of Statistical Learning* (2nd ed.). New York: Springer, 2009, pp. 337–384.

35. Onan Aytuğ, Serdar Korukoğlu, and Hasan Bulut, "A multiobjective weighted voting ensemble classifier based on differential evolution algorithm for text sentiment classification," *Expert Systems with Applications*, vol. 62, pp. 1–16, 2016.

INFORMATIONON THE ARTICLE

Yaroslav I. Vyklyuk, ORCID: 0000-0003-4766-4659, Lviv Polytechnic National University, Ukraine, e-mail: vyklyuk@ukr.net

Svitlana A. Levytska, ORCID: 0000-0001-6616-3572, Bukovinian State Medical University, Ukraine, e-mail: levitska.svitlana@bsmu.edu.ua

Denys V. Nevinskyi, ORCID: 0000-0002-0962-072X, Lviv Polytechnic National University, Ukraine, e-mail: nevinskiy90@gmail.com

Kateryna P. Hazdiuk, ORCID: 0000-0002-7568-4422, Yuriy Fedkovych Chernivtsi National University, Ukraine, e-mail: kateryna.gazdyik@gmail.com

Miroslav Škoda, ORCID: 0000-0001-6658-2742, DTI University, Slovakia, e-mail: skoda@dti.sk

Stanislav D. Andrushko, Chernivtsi central hospital, Ukraine, e-mail: stanislav.andrushko14@gmail.com

Maryna A. Palii, Chernivtsi central hospital, Ukraine, e-mail: marinapaljj90@gmail.com

МОДЕЛІ РИЗИКУ СМЕРТНОСТІ НА ОСНОВІ ДЕРЕВА РІШЕНЬ І АНСАБЛЮ ДЛЯ ГОСПІТАЛІЗОВАНИХ ПАЦІЄНТІВ ІЗ COVID-19 / Я.І. Виклюк, С.А. Левицька, Д.В. Невінський, К.П. Газдюк, М. Шкода, С.Д. Андрушко, М.А. Палій

Анотація. Присвячено вивченню пневмонії, асоційованої із SARS-CoV-2 та дослідженню основних показників, що призводять до смертності хворих. Використовуючи добре відомі параметри, які регулярно застосовуються в клінічній практиці, отримано абсолютно нові функціональні залежності на основі доступного та зрозумілого дерева рішень і моделей класифікаторів ML, що дозволить лікарю визначити прогноз за кілька хвилин і, відповідно, зрозуміти необхідність коригування лікування, переведення хворого до відділення невідкладної допомоги. Точність отриманого ансамблю моделей, підібраних за реальними даними пацієнтів лікарні, становила 0,88–0,91 для різних показників. Створення системи збирання даних з подальшим навчанням класифікаторів дасть змогу динамічно підвищити точність прогнозу та автоматизувати процес прийняття рішення лікарем.

Ключові слова: COVID-19, система прийняття рішень, дерево рішень, ML-ансамбль, ансамбль класифікаційних моделей.

STUDY OF THE UNDERGROUND TUNNEL PLANNING.
COGNITIVE MODELLING

N.D. PANKRATOVA, D.I. MUSIIENKO

Abstract. A study of the underground tunnel planning reliability for megacities is proposed based on the use of foresight and cognitive modeling methodologies. Using the foresight methodology allows, with the help of expert estimation procedures, to identify critical technologies and build alternatives of scenarios with quantitative characteristics. For the justified implementation of a particular scenario, cognitive modeling is used, which allows to build causal relationships based on knowledge and experience, understand and analyze the behavior of a complex system for a strategic perspective with a large number of interconnections and interdependencies. The suggested study allows the reliability planning of underground tunnels on the basis of reasonable scenarios selection and justification of their creation priority.

Keywords: cognitive, impulse modelling, planning, scenarios, underground tunnel.

INTRODUCTION

The global trend of increasing urbanization poses challenges for both expanding and newly developing cities. Population growth leads to an increased demand for reliable infrastructure, which in the current war times is combined with the need for increased safety and environmental awareness of the population. The use of underground space can help cities meet these increased needs while remaining compact, or find the space needed to incorporate new features into the existing urban landscape. When underground solutions are considered and evaluated from the planning or initial stages of a project, better solutions become possible. Efficient and rational placement of numerous structures of transport, energy, economic, municipal, social and creation of large-scale engineering infrastructure sets the task of strategic planning of underground space of megacities [1]. Underground urban development is a complex system in many aspects. Firstly, this system consists of many interconnected subsystems and objects. Secondly, the processes flowing in this system both during construction and operation are also complicated and in some cases poorly predictable, because they are largely related to different geological processes. The problems accompanying the underground urban planning can be referred to the weakly structured problems. Underground urbanism, which is an integral part of the modern megacity, has already gone beyond the individual local objects and is becoming a system factor in the

development of cities. Let us consider urbanism as a global super-system in the form of an ordered set of structurally interconnected and functionally interdependent global systems.

The implementation of underground transport tunnel projects requires a detailed study of the surrounding facilities, taking into account the reduced capacity, increased travel time delay, fuel consumption, the number of traffic accidents, which lead to unaccounted economic losses. Thus, it becomes necessary to study and quantify the impact of construction work zones of high-speed public transport system on the transport environment, which will further help to assess economic losses due to the construction work zone of underground transport facilities [2].

According to the "optimistic scenario" over 20 km of transport tunnels can be built in Kiev in the next ten years. At the same time it is necessary to justify the expediency and reliability of the tunnel construction taking into account the development characteristic to the territory in question, the road network, and the characteristics of traffic in the area of the potential tunnel.

All of the above allows us to propose a methodology for anticipation and cognitive modeling of complex systems [3–5] for modeling and analysis of planning the development of the metropolitan underground tunnels under conditions of environmental, man-made and terrorist threats.

RELATED PAPERS

Practical guidance on assessing the impact of soft ground tunneling in urban areas on existing structures and services is provided in paper [6]. Various empirical approaches to the definition of the surface settlement zone are summarized and the assessment of the magnitude and distribution of surface movements is compared with case history data. A tentative risk classification related to settlement and maximum slope criteria is proposed, which will allow rapid optimization of route adjustments and thereby identification of those buildings particularly at risk and requiring a more detailed assessment. Predicting anomalous geological structures before tunneling (ahead of exploration) has become an important routine in tunneling, providing particularly important a priori information for safe, economical and efficient tunneling. Article [7] analyzes the characteristics, advantages and applicability of various methods. Preliminary exploration should be aimed at determining the properties of the rock before the tunnel is closed, and not at assessing the structure. Life safety issues associated with fires and explosions are critical issues in the design of large underground structures. In [8] these issues are considered and discussed from the viewpoint of existing life safety codes.

Much attention when planning underground facilities is paid to environmental issues, reducing ground noise sources, minimizing vibrations in the environment, both caused by the railway and created by the explosion of rocks [9–11]. Actual problems of underground urbanization of the central part of Lviv are considered in [12]. The questions of interaction of natural and technogenic components during the development of the underground space of the city are covered. The main risk-forming factors in the construction of multi-level underground parking have been identified. The relief, geological structure and hydrogeological conditions of the central part of the city are analyzed. A spatial analysis of the

risk-forming components of the geological environment has been carried out. Zones with varying degrees of geological risk have been identified. Reference [13] presents a numerical model for predicting vibrations and re-radiated noise in buildings caused by rail traffic. A three-dimensional numerical model capable of simulating the propagation and transmission of ground vibrations near high-speed railways is presented in [14]. It is used to study the effect of the material that makes up the embankment on the level of ground vibration at different distances from the track. The paper [15] discusses the design, installation, and also experimental and numerical evaluation of the effectiveness of a rigid wave barrier in the ground as a measure to mitigate the effects of railway-induced vibration.

Ground vibration from underground tunnels is a major environmental problem in urban areas. To study this problem, various studies have been carried out, mainly based on numerical methods [16]. This article presents a study of the influence of changes in soil properties with depth (soil heterogeneity) on soil vibration from an underground tunnel. Comparison of experimental and numerical results shows that a homogeneous model can give acceptable estimates of tunnel behavior. However, a clear improvement in the estimates of soil behavior is observed when the change in soil properties with depth is taken into account in the numerical model. In [17], the range disturbed by earthworks and a model for numerical analysis of underground engineering and surface structures are determined, and the relationship between stress and deformation of surface buildings caused by deformation is obtained. The feedback of the results of the analysis with the data management of the GIS platform has been received. By comparing with the relevant standard damage assessment rules, it can provide technical support to decision makers. By analyzing and verifying the case study of the impact on buildings caused by the excavation of the underwater tunnel terminal, it is possible to ensure the safety of the above-ground buildings affected by the excavation.

It follows from the above review that one of the complex problems is underground tunnels, which ensure the vital activity of both surface and underground urban planning. This paper examines the issue of the construction of underground tunnels and the rationale for the priority of their creation.

MODELS AND METHODS

The development of the strategy of innovative planning of underground construction development belongs to the class of weakly structured tasks, in which the goals, structure and conditions are known only partially and are characterized by a large volume of non-factors: imprecision, incompleteness, uncertainty, and fuzzy data describing the object. Such problems are characterized by many contradictions and uncertainties. The most important of them are:

- ambiguity and inconsistency of requirements for the product;
- inconsistency of goals and ambiguity of the conditions of application of the product;
- uncertainty and unpredictability of possible actions of competitors;
- infinity and unpredictability of risk situations at different stages of the product life cycle.

In these conditions, using heterogeneous, usually incomplete, empirical, experimental, casual and other background information, the developer must formalize and solve the problem of product design, in particular to formulate and justify the goals of its creation. The results of the solution of this problem should prove the practical necessity, technological possibility and economic feasibility of production of the designed product [3].

Solving approximated to reality tasks of anticipation, at its different stages use different methods of qualitative analysis in a single man-machine procedure. In this study, the method of morthological analysis is used to select the characteristic parameters of the cognitive model [4].

The cognitive approach to the solution of this problem required the definition and description of the main elements (parameters, factors, concepts), causes and consequences characterizing the natural-technical geosystem ("underground construction – environment"). As a result of cognitive modeling, scenarios of possible development of a complex system arising under the influence of changes in the internal and external environment of an underground structure must be obtained. It is especially important for knowledge and prevention of negative consequences, minimization of damage in conditions of influence of the most unfavorable combination of negative factors: external and internal static and dynamic loads, all kinds of technogenic influences inside an underground construction, harmful natural manifestations from the rock mass, etc.

A systematic approach to the modeling and scenario analysis of infrastructure planning of the megacity under environmental, man-made and terrorist threats, based on the joint application of the methodologies of foresight and cognitive modeling [18]. It is proposed to use these methodologies together: at the first stage to apply the methodology of foresight using the method of morphological analysis. The results obtained are used as background information to find ways to build an alternative of this or that scenario in the form of a cognitive map. To justify the implementation of this or that scenario alternative, cognitive modeling methodology is involved, which allows to build cause-effect relationships on the basis of knowledge and experience, understand and analyze the behavior of a complex system (SS) for a strategic perspective with a large number of relationships and interdependencies, applying a scientifically sound strategy for implementing the priority scenario [19].

Cognitive modeling begins with the development of a cognitive map of the object. A cognitive map – a structural scheme of cause-and-effect relationships in a system that interprets the judgments and views of the LPR – is constructed in order to understand and analyze the behavior of a complex system. Let the underground infrastructure in question consist of many individual elements. Two elements of the system and patterns can be depicted as separate point-to-points, and if an element is connected to an element by a causal relationship, they are connected by an oriented arc. It is quite possible that consequences can be the cause of changes in other factors. Causal chains can be quite long and complex. The analysis of cause-and-effect chains is necessary, for example, for forecasting of development of a situation, realization of various controls of processes in a system. After the cause-and-effect diagrams are constructed, the decision-making strategies in a given subject area are determined. As a result of cognitive structu-

ration, an informal description of knowledge about the subject area is developed, which can be visualized as a scheme, graph, matrix, table or text [5].

In the study of the problem of justification of land suitability for underground tunnel construction at the first stage were used cognitive models such as a cognitive map – sign oriented graph and a functional graph in the form of a weighted sign orograph

$$G = V, E,$$

where V — set of nodes $V_i \in V$, $i = 1, 2, \ldots, k$, which are elements of the system under study; E — set of arcs $e_{ij} \in E$; $i, j = 1, 2, \ldots, N$, reflecting the relationship between the nodes V_i and V_j; the impact can be positive (sign "+" above the arc), when the increase (decrease) of one factor leads to an increase (decrease) of another, negative (sign "-" above the arc), when the increase (decrease) of one factor leads to a decrease (increase) of another, or absent (0).

Vector graph

$$\Phi = G, X, F(X, E), \Theta,$$

where G is a cognitive map; X is a set of node parameters; Θ — vertex parameter space; $F(X, E)$ — arc transformation functional.

At the third stage of cognitive modeling, a pulse process model (cognitive modeling of perturbation propagation) was used to determine the possible development of processes in a complex system and develop development scenarios [28]:

$$x_{v_i}(n+1) = x_{v_i}(n) + \sum_{j=1}^{N} f(x_i, x_j, e_{ij}) P_j(n) + Q_{v_i}(n),$$

where $x(n)$, $x(n+1)$ are the values of the index in the vertex V_i at the simulation steps at the moment $t = n$ and following it $t = n+1$; $P_j(n)$ is the momentum in the vertex V_j at the moment $t = n$; $Q_{v_i}(n) = \{q_1, q_2, \ldots, q_k\}$ is the vector of external momentum (disturbing or controlling actions) introduced in the vertices V_i at time n.

Simulation cognitive modeling, especially at the design stage of underground space development, is extremely necessary. A serious reason for this may be the fact that it is necessary to anticipate and exclude or reduce the risks, which are inevitably inherent in the underground urban development. One of the complex problems is the underground tunnels providing life for both surface and underground urban development. This paper explores the construction of underground tunnels and the justification of the priority and reliability of their construction.

CASE STUDY

Let us carry out a study of the reliability planning of two types of underground tunnels: Tunnel 1 through the built-up part of the city and Tunnel 5 through the Dnipro River. Table 1 present the data of the vertices (concepts) of the cognitive models G_1 of Tunnel 1.

T a b l e   1. The vertices of the hierarchical cognitive map Tunnel 1

Code	Name of the vertex	Assignment of the vertex
V1	V1. State of the Tunnel 1	Indicative
V2	V2. Anthropogenic activities	Perturbing
V2.1	V2.1. The Evil Mind: Fighting, Terrorism	Perturbing
V2.2	V2.2. Without malice	Perturbing
V3	V3. Technogenic events	Perturbing
V3.1	V3.1. Technical	Perturbing
V3.2	V3.2. Technological	Perturbing
V4	V4. Natural disasters, weather catastrophes	Perturbing
V4.1	V4.1 Shifts	Perturbing
V5	V5. Protection of the object	Basic
V6	V6. The scale of the impact of an undesirable event	Disturbing
V7	V7. Ability to function	Disturbing
V8	V8. Time to restore functioning	Disturbing
V9	V9. Environmental consequences	Disturbing
V10	V10. Economic consequences	Disturbing
V11	V11. Consequences for life	Disturbing
V12	V12. The number of injured	Disturbing
V13	V13. Organizational, technical, etc. capabilities	Basic
V14	V14. Investor	Basic
V15	V15. Level of damage	Disturbing
V15.1	V15.1. Integrity of the ruin system	Basic
V16	V16. Material damage	Disturbing
V17	V17. Geotechnology of construction	Basic
V18	V18. Capacity of land routes	Basic
V19	V19. Population	Basic
V20	V20. Intensity of movement	Disturbing
V21	V21. Average speed	Disturbing
V22	V22. Undeground vibrations	Disturbing
V23	V23. Atmospheric pollution	Disturbing

Before using the cognitive model to determine its possible behavior of modeling analyzes the various properties of the model is fulfilled. In this case, the stability properties of the model must be analyzed. The initial cognitive map was unstable. Taking into account the weight characteristics obtained from the results of the morphological analysis, a stable cognitive map was obtained for Tunnel 1, and then and for Tunnel 5. The cognitive model was reduced to a stable form with respect to perturbations. According to the adopted criterion [5]: the maximal modulo root of the graph relation matrix characteristic equation is $M = 0.96931$. The cognitive map also is stable according to the initial value. An analysis of the ratio of the number of stabilizing cycles (5 negative feedbacks) and process accelerator cycles (3 positive feedbacks) indicates the structural stability of such a system. For structural stability, the number of negative cycles must be odd [5].

Fig. 1 shows the sustainable cognitive map G_1 of Tunnel 1.

The solid lines of arcs in Fig. 1 mean that with an increase (or decrease) in the signal at the vertex V_i, the same changes occur at the vertex V_j — an increase (or decrease). The dashed lines of arcs in Fig. 1 mean: an increase (or decrease) in the pulse at the vertex V_i leads to a decrease (or increase) in the pulse at the vertex V_j.
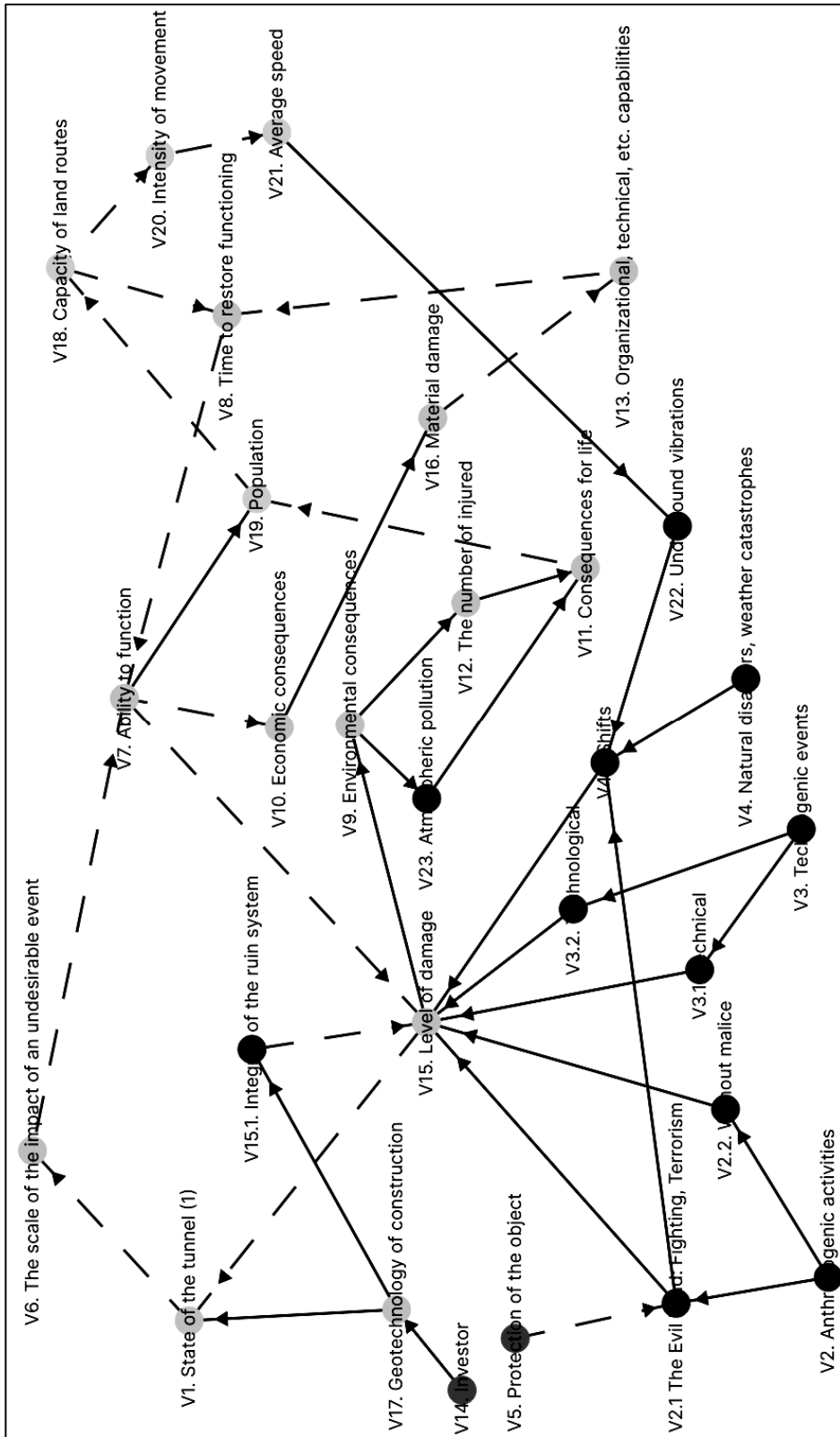
Fig. 1. Sustainable cognitive map G_1 of Tunnel 1

Now analyze the model 2 connected with cognitive map G_2 Tunnel 5 presented in Fig. 2. Vertices V2–V23 of the cognitive map G_2 correspond to the vertices of the cognitive map G_1 shown in Table 1. Vertices V1, V24 for the cognitive map G_2 Tunnel 5 are added to the model 2 (Table 2).

Fig. 2. Sustainable cognitive map "Tunnel 5"

According to the adopted criterion [5]: the maximal modulo root of the graph relation matrix characteristic equation is $M = 0.99902$. The cognitive map also is stable according to the initial value.

T a b l e 2. The vertices of the hierarchical cognitive map G_2 Tunnel 5

Code	Name of the vertex	Assignment of the vertex
V1	State of the Tunnel 5	Indicative
V24	Flooding	Perturbing

An analysis of the ratio of the number of stabilizing cycles (15 negative feedbacks) and process accelerator cycles (3 positive feedbacks) indicates the structural stability of such a system [5].

NUMERICAL INVESTIGATIONS. IMPULSE MODELING

Involving impulse modeling, is investigated the planning reliability of the tunnels in question under different types of impacts on them. Figs. 4–9 show the distribution of pulse processes for the three scenarios.
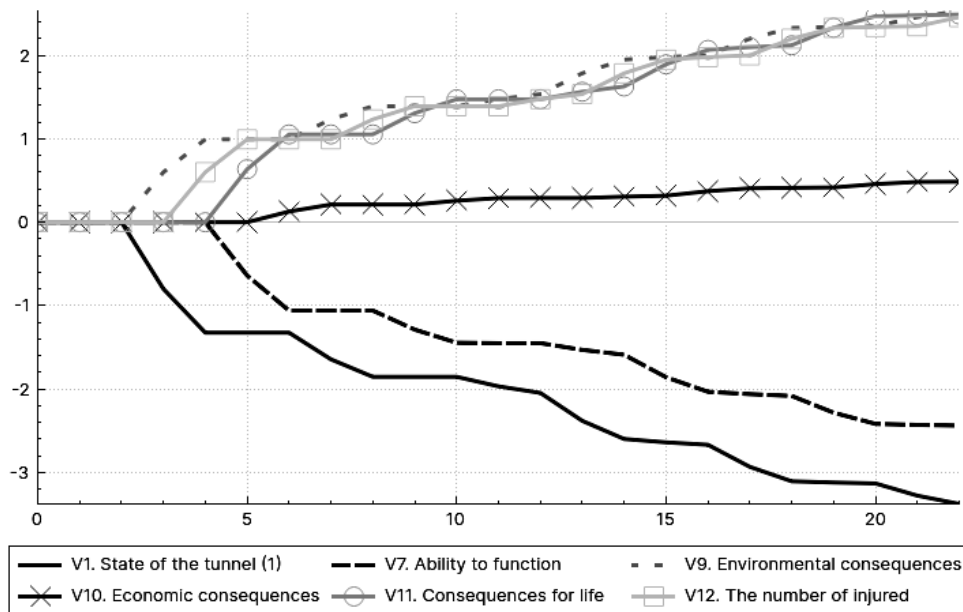
Fig. 3. The distribution of pulse processes for the Tunnel 1 (Scenario 1)

Scenario 1. Let's conduct a study for Tunnel 1 and Tunnel 5. Assume to the vertex V2.1 — The Evil Mind: Fighting, Terrorism the control action is introduced $Q = (q_{V_1} = 0, \ldots, q_{V_{2.1}} = +1, \ldots)$. Figs. 3 and 4 show the distribution of pulse processes for the Tunnel 1 and Tunnel 5.

The first scenario is needed to analyze the consequences of strong explosions directed at the tunnel. Based on the simulation results, it can be concluded that Tunnel 1 is more resistant to threats associated with a clear intention, namely terrorist acts and hostilities. This is primarily due to the underwater dislocation of

Tunnel 5. A large explosion could cause the tunnel to flood, resulting in a larger impact than the same scenario in the case of Tunnel 1.
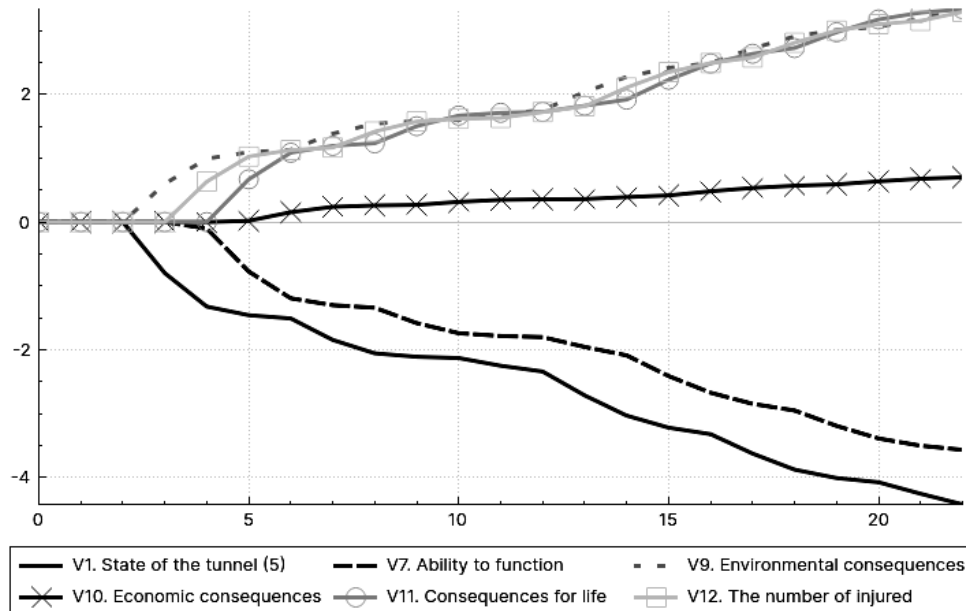
Fig. 4. The distribution of pulse processes for the Tunnel 5 (Scenario 1)

Scenario 2. Assume to the vertex V4.1 – Shifts the control action is introduced $Q = (q_{V_1} = 0, \ldots, q_{V_{4.1}} = +1, \ldots)$. Figs. 5 and 6 show the distribution of pulse processes for the Tunnel 1 and Tunnel 5.
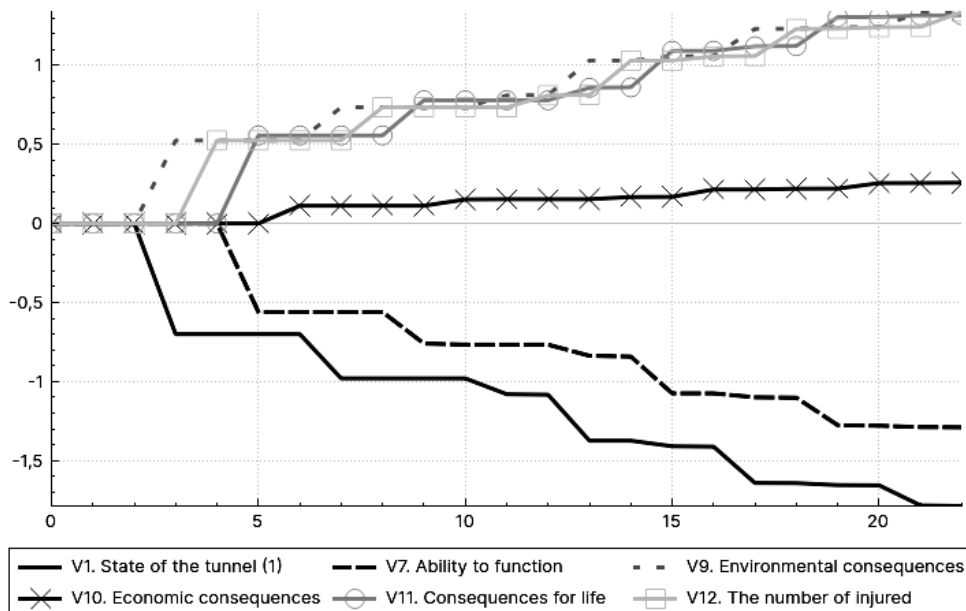
Fig. 5. The distribution of pulse processes for the Tunnel 1 (Scenario 2)

This scenario is needed to analyze the impact of natural factors on each tunnel. As in the previous scenario, Tunnel 1 turned out to be more stable. The rea-

son still remains the possibility of tunnel flooding due to hard rock shear, which significantly affects the performance of the tunnel.
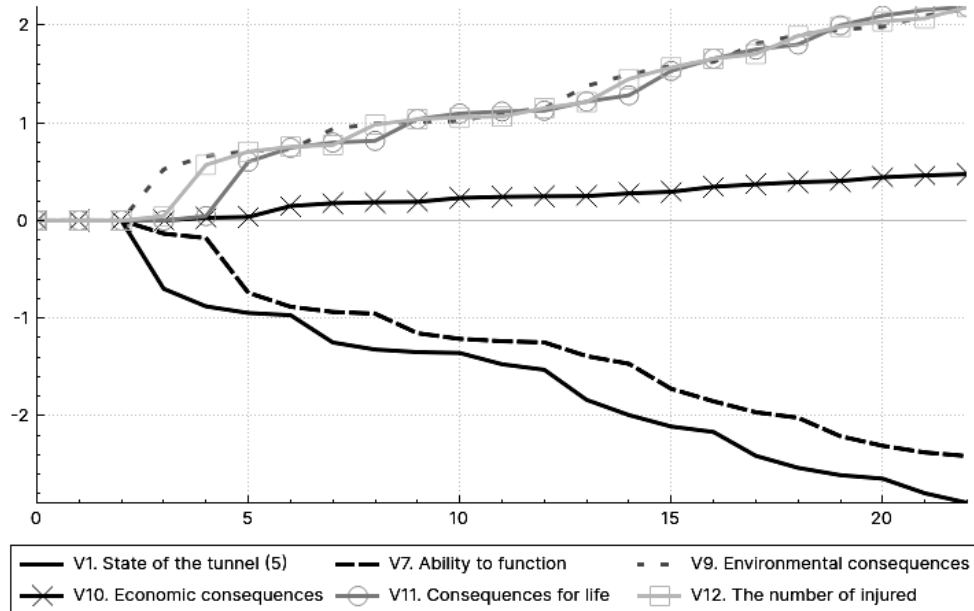
Fig. 6. The distribution of pulse processes for the Tunnel 5 (Scenario 2)
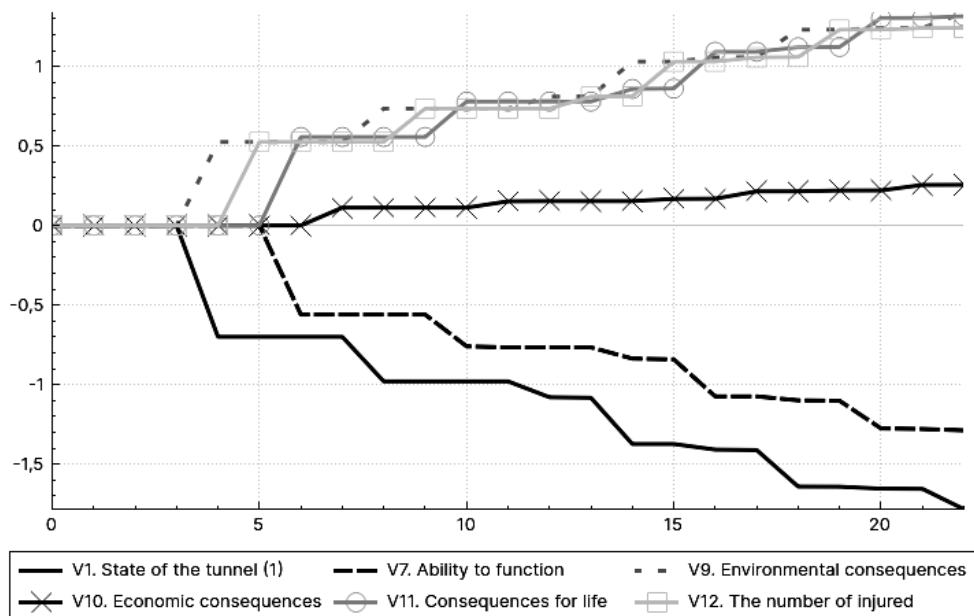
Fig. 7. The distribution of pulse processes for the Tunnel 1 (Scenario 3)

Scenario 3. Assume to the vertex V3 – Technogenic events, the control action is introduced $Q = (q_{V_1} = 0, \dots, q_{V_3} = +1, \dots)$. Figs. 7 and 8 show the distribution of pulse processes for the Tunnel 1 and Tunnel 5.

The distribution of pulse processes for the Tunnel 5 (Scenario 3) is shown in Fig. 8. This scenario demonstrates the resilience of tunnels to industrial threats. In

contrast to the previous scenarios, the numerical differences between the results obtained are not so significant. This may indicate the similarity of tunnels to industrial threats. However, Tunnel 1 still showed greater resilience to such scenarios.
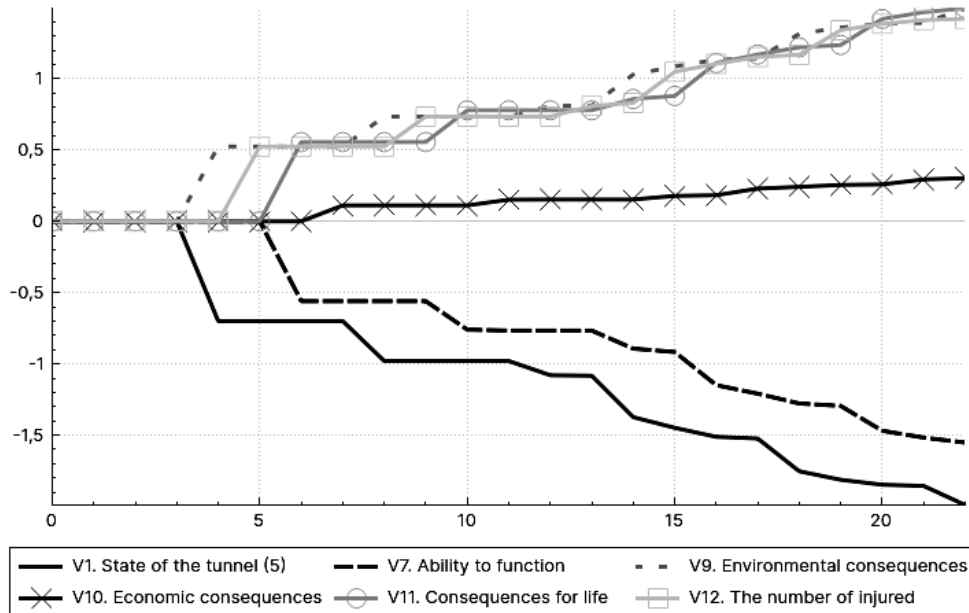
Fig. 8. The distribution of pulse processes for the Tunnel 5 (Scenario 3)

CONCLUSION

Modeling of scenarios of possible processes of events development in the analyzed types of underground tunnels is carried out under the influence of various external disturbances and control impulse influences. The results of the conducted cognitive modeling make it possible to judge that cognitive models that systematize and structure different information about the tunnel underground construction system correspond to the real system and can be used to anticipate possible processes of development of situations in the system under the influence of various disturbing and controlling factors. The developed author's software complex allows in the process of pulse modeling and analysis of the obtained results to introduce controlling or excitatory influences at any stage of modeling. This allows changing (correcting) scenarios in the dynamics of model creation, determining effects that bring processes closer to the desired ones. The developed system approach is applied to the study of planning reliability of underground tunnels of different types in order to choose reasonable scenarios for their future development.

REFERENCE

1. S. Durmisevic, "The future of the underground space," *Cities*, vol. 16, no. 4, pp. 233–245, 1999.
2. R. Bhutani, S. Ram, and K. Ravinder, "Impact of Metro Rail Construction Work Zone on Traffic Environment," *Transportation Research Procedia*, 17, pp. 586–595, 2016. doi: 10.1016/j.trpro.2016.11.11.

3. N. Pankratova, G. Gorelova, and V. Pankratov, "The Strategy of Underground Construction Objects Planning Based on Foresight and Cognitive Modelling Methodologies. Book Chapter 5," in *Springer book M. Zgurovsky and N. Pankratova (eds.), System Analysis & Intelligent Computing, Studies in Computational Intelligence*, vol. 1022, pp. 69–91, 2022. Available: doi.org/10.1007/978-3-030-94910-5_5

4. N.D. Pankratova, I.A. Savchenko, and G.I. Gayko, *Development of underground urbanism as a system of alternative design configurations*, (in Ukrainian). Kyiv: Scientific thought, 2019.

5. *Innovative development of socio-economic systems based on methodologies of foresight and cognitive modelling*, (in Russian). Collective monograph edited by G.V. Gorelova, N.D. Pankratova. Kyiv: Naukova Dumka, 2015, 464 p.

6. W.J. Rankin, "Ground movements resulting from urban tunnelling: predictions and effects," *Geological Society, London, Engineering Geology Special Publications*, 5(1), pp. 79–92, 1988. doi: 10.1144/gsl.eng.1988.005.0.

7. S. Li et al., "An overview of ahead geological prospecting in tunnelling," *Tunnelling and Underground Space Technology*, 63, pp. 69–94, 2017. doi: 10.1016/j.tust.2016.12.011.

8. R. Sterling, J. Carmody, and W.H. Rockenstein, "Case study of life safety standards for a large mined underground space facility in minneapolis, minnesota," *Tunnelling and Underground Space Technology*, 7(2), pp. 119–125, 1992. doi:10.1016/0886-7798(92)90041-f.

9. L. Andersen and S.R.K. Nielsen, "Reduction of ground vibration by means of barriers or soil improvement along a railway track," *Soil Dynamics and Earthquake Engineering*, 25(7–10), pp. 701–716, 2005. doi: 10.1016/j.soildyn.2005.04.

10. L. Auersch, "Mitigation of railway induced vibration at the track, in the transmission path through the soil and at the building," *Procedia Engineering*, 199, pp. 2312–2317, 2017. doi: 10.1016/j.proeng.2017.09.1.

11. G. Berta, "Blasting-induced vibration in tunnelling," *Tunnelling and Underground Space Technology*, 9(2), pp. 175–187, 1994. doi: 10.1016/0886-7798(94)90029-9.

12. Nadiya Kremin and Yuriy Andreychuk, "Geoecological risks of underground space development in the central part of L'viv (Ukraine)," *Proceedings Conference: Constructive geography and cartography: state, problems, perspectives: International scientific and practical online conference materials, dedicated to 20th anniversary of Department of Constructive Geography and Cartography of Ivan Franko National University of L'viv, 2020*, pp. 15–20.

13. A. Colaço, P.A. Costa, P. Amado-Mendes, L. Godinho, and R. Calçada, "Mitigation of vibrations and re-radiated noise in buildings generated by railway traffic: a parametric study," *Procedia Engineering*, 199, pp. 2627–2632, 2017. doi:10.1016/j.proeng.2017.09.4.

14. D. Connolly, A. Giannopoulos, and M.C. Forde, "Numerical modelling of ground borne vibrations from high speed rail lines on embankments," *Soil Dynamics and Earthquake Engineering*, 46, pp. 13–19, 2013. doi: 10.1016/j.soildyn.2012.12.

15. P. Coulier, V. Cuéllar, G. Degrande, and G. Lombaert, "Experimental and numerical evaluation of the effectiveness of a stiff wave barrier in the soil," *Soil Dynamics and Earthquake Engineering*, 77, pp. 238–253, 2015. doi: 10.1016/j.soildyn.2015.04.

16. . Yang, M.F.M. Hussein, and A.M. Marshall, "Centrifuge and numerical modelling of ground-borne vibration from an underground tunnel," *Soil Dynamics and Earthquake Engineering*, 51, pp. 23–34, 2013. doi: 10.1016/j.soildyn.2013.04.

17. C. Yuan, X. Wang, N. Wang, and Q. Zhao, "Study on the Effect of Tunnel Excavation on Surface Subsidence Based on GIS Data Management," *Procedia Environmental Sciences*, 12, pp. 1387–1392, 2012. doi: 10.1016/j.proenv.2012.01.4.

18. N. Pankratova, I. Savchenko, H. Haiko, and V. Kravets, "System approach to planning urban underground development," *Int. Journal "Information Content and Processing"*, 6(1), pp. 3–17, 2019.

19. N.D. Pankratova, G.V. Gorelova, and V.A. Pankratov, "Study of the Plot Suitability for Underground Construction: Cognitive Modelling," *ISDMCI 2020: Lecture Notes in Computational Intelligence and Decision Making*, pp. 246–264. Available: https://doi.org/10.1007/978-3-030-54215-3_16

20. F. Roberts, *Graph Theory and its Applications to Problems of Society*. Philadelphia: Society for Industrial and Applied Mathematics, 1978.

INFORMATION ON THE ARTICLE

Nataliya D. Pankratova, ORCID: 0000-0002-6372-5813, Educational and Scientific Institute for Applied System Analysis of the National Technical University of Ukraine "Igor Sikorsky Kyiv Polytechnic Institute", Ukraine, e-mail: natalidmp@gmail.com

Danylo I. Musiienko, Educational and Scientific Institute for Applied System Analysis of the National Technical University of Ukraine "Igor Sikorsky Kyiv Polytechnic Institute", Ukraine

ДОСЛІДЖЕННЯ ПЛАНУВАННЯ ПІДЗЕМНИХ ТУНЕЛІВ. КОГНІТИВНЕ МОДЕЛЮВАННЯ / Н.Д. Панкратова, Д.І. Мусієнко

Анотація. Запропоновано дослідження надійності планування підземних тунелів для мегаполісів на основі використання методологій форсайту та когнітивного моделювання. Методологія форсайту дозволяє за допомогою процедур експертного оцінювання виявити критичні технології та побудувати альтернативи сценаріїв з кількісними характеристиками. Для обґрунтованої реалізації того чи іншого сценарію використовується когнітивне моделювання, яке дає змогу побудувати причинно-наслідкові зв'язки на основі знань та досвіду, зрозуміти та проаналізувати поведінку складної системи на стратегічну перспективу з великою кількістю взаємозв'язків та взаємозалежностей. Запропоноване дослідження дозволяє планувати надійність підземних тунелів на основі вибору обґрунтованих сценаріїв та обґрунтування пріоритетності їх створення.

Ключові слова: когнітивне, імпульсне моделювання, планування, сценарії, підземні тунелі.

MODIFIED SEIRD MODEL FOR DESCRIBING THE COVID-19 EPIDEMIC

A.I. KLYMENKO, G.B. PODKOLZIN

Abstract. This article is devoted to mathematical models in epidemiology, in particular SIR, SEIR, and SEIRD models. It explores the importance of these models in predicting the spread of infectious diseases and evaluating the effectiveness of control measures. These models allow for assessing important epidemic parameters such as the speed of infection transmission, the number of people infected, and the number of deaths. This data can help in making decisions regarding the imposition and lifting of quarantine restrictions, opening and closing of schools and other institutions, as well as in developing vaccination strategies and other control measures. In summary, mathematical models such as SIR, SEIR, and SEIRD are important tools in the fight against epidemics. They enable epidemiologists and medical professionals to predict and control the spread of diseases, thus preserving the health and lives of people.

Keywords: epidemiology, epidemiological models, modified mathematical models, COVID-19 modeling SEIR, SEIRD model, unvaccinated people, virus, division of the population, new strains.

INTRODUCTION

Modeling is a widely used tool to support the evaluation of various disease interventions. The value of epidemiological models lies in their ability to explore "what if" scenarios and provide decision makers with a priori knowledge of the consequences of disease emergence and the impact of control strategies.

To be useful, models must be fit for purpose and properly validated and verified. The complexity and variability inherent in biological systems should limit the use of models as predictive tools during actual outbreaks. Models will be most useful when used prior to an outbreak, particularly in the areas of retrospective analysis of past outbreaks, contingency planning, resource planning, risk assessment, and training. Models are only one tool for providing scientific advice, and results should be evaluated in conjunction with experimental data, field experience, and scientific knowledge.

SIR, SEIR, SEIRD MODELS

The severity and global reach of the COVID-19 pandemic has spurred research in many areas, including disease dynamics modeling, with the goal of using such models to better understand the impact of intervention strategies on disease control [1]. Several factors are known to influence disease dynamics, including incidence rates, recovery rates, quarantine strategies, and the impact of awareness [2]. In the literature, classical epidemic models of susceptible infectious diseases

(SIR, SEIR, SEIRD models) have been widely used to model infectious diseases [3].

The SIR model is based on the number of susceptible (S), infectious (I), and recovered (R) individuals. The classical epidemic model is shown below:

$$\begin{cases} \dfrac{dS(t)}{dt} = -\beta \dfrac{S(t)I(t)}{N}; \\ \dfrac{dI(t)}{dt} = \beta \dfrac{S(t)I(t)}{N} - \gamma I(t); \\ \dfrac{dR(t)}{dt} = \gamma I(t), \end{cases}$$

where $S(t)$ — the number of people who can be infected; $I(t)$ — the number of infected people; $R(t)$ — the number of people who have been isolated from transmission (died or recovered); β — the transmission rate; γ — the recovery rate.

Each group contains a certain number of people each day. However, this number changes from day to day as people move from one group to another. For example, people in Group S will move to Group I when they become infected. Similarly, infected individuals will move to group R after they recover. It is assumed that the total population in the three groups $(S + I + R)$ always remains the same.

The SIR model assumes that recovered individuals cannot be reinfected [2]. The SEIR model has an additional group for individuals who become infected and contagious after the incubation period (E — Exposed). In other words, the SEIR model includes a latency period.

The SEIR model is described by the following system of equations:

$$\begin{cases} \dfrac{dS(t)}{dt} = -\beta \dfrac{S(t)I(t)}{N}; \\ \dfrac{dE(t)}{dt} = \beta \dfrac{S(t)I(t)}{N} - \alpha E(t); \\ \dfrac{dI(t)}{dt} = \alpha E(t) - \gamma I(t); \\ \dfrac{dR(t)}{dt} = \gamma I(t), \end{cases}$$

where α — the rate of transition of the disease from the latent period to the overt stage; β — the rate of infection transmission; γ is the rate of recovery; $S(t)$ — the number of people susceptible to the virus; $E(t)$ — the number of people with the virus in the incubation period; $I(t)$ — the number of people who get sick; $R(t)$ — the number of recovered people who have come into contact with the pathogen and have gained stable immunity.

To describe the COVID-19 epidemic, the most appropriate of the above models is the SEIRD model, in which group D — Death appears, i.e. this model takes into account the dead.

The classical SEIRD model is shown below:

$$
\begin{cases}
\dfrac{dS(t)}{dt} = -\beta \dfrac{S(t)I(t)}{N}; \\[2mm]
\dfrac{dE(t)}{dt} = \beta \dfrac{S(t)I(t)}{N} - \alpha E(t); \\[2mm]
\dfrac{dI(t)}{dt} = \alpha E(t) - (\gamma + \mu)I(t); \\[2mm]
\dfrac{dR(t)}{dt} = \gamma I(t); \\[2mm]
\dfrac{dD(t)}{dt} = \mu I(t),
\end{cases}
\tag{1}
$$

where β — the coefficient that can be interpreted as the probability of contracting the disease in case of contact between a susceptible individual and an infected person; μ — the mortality rate; γ — the recovery rate; α — the rate of transition from the latent period to the overt stage; $S(t)$ — the number of people susceptible to the virus; $E(t)$ — the number of people with the virus in the incubation period; $I(t)$ — the number of people who fall ill; $R(t)$ — the number of recovered people who have come into contact with the pathogen and have gained stable immunity.

MODIFIED SEIRD-MODEL

Modified models can take into account more realistic factors such as population mobility, different variants of the disease, carrier effects, vaccination, and other factors. For example, the SIR model typically assumes that people in each group interact with each other, but in some cases there may be groups that interact less frequently or not at all. In this case, modified models can be used to describe more complex scenarios.

In epidemiology, it is very important to have a model that covers all stages of the disease, including incubation, clinical course, recovery, and death. The SIR model does not include a parameter responsible for the incubation period of the disease, and SIR and SEIR cannot be used when the epidemic includes mortality and fertility. For this reason, the SEIRD model has become the most relevant in epidemiology, since it includes all the parameters necessary to study the different stages of the disease and allows more accurate predictions of the spread of the disease and the effectiveness of control measures.

The advantages of the proposed model are related to the fact that the population can be divided into vaccinated and unvaccinated. In addition, the modified SEIRD model takes into account fertility and natural mortality unrelated to disease mortality, which allows for the most accurate reproduction of the situation, bringing it as close as possible to real conditions.

The basic SEIRD model is shown in (1). In the modified model, each component is divided into two parts: vaccinated and unvaccinated members of the population (susceptible, exposed, infectious, recovered). The fertility parameter applies only to unvaccinated susceptibles, because by default, people are born unvaccinated.

So, the model is:

$$
\left\{
\begin{aligned}
\frac{dS_{unvac}}{dt} &= l - \mu S_{unvac} - \frac{S_{unvac}(\beta_{uu}I_u + \beta_{uv}I_v)}{N}; \\
\frac{dS_{vac}}{dt} &= -\mu S_{vac} - \frac{S_{vac}(\beta_{vu}I_u + \beta_{vv}I_v)}{N}; \\
\frac{dE_{unvac}}{dt} &= \frac{S_{unvac}(\beta_{uu}I_u + \beta_{uv}I_v)}{N} - (\mu + \alpha_{unvac})E_{unvac}; \\
\frac{dE_{vac}}{dt} &= \frac{S_{vac}(\beta_{vu}I_u + \beta_{vv}I_v)}{N} - (\mu + \alpha_{vac})E_{vac}; \\
\frac{dI_{unvac}}{dt} &= \alpha_{unvac}E_{unvac} - (\gamma_{unvac} + \mu + \theta_{unvac})I_{unvac}; \\
\frac{dI_{vac}}{dt} &= \alpha_{vac}E_{vac} - (\gamma_{vac} + \mu + \theta_{vac})I_{vac}; \\
\frac{dR_{unvac}}{dt} &= \gamma_{unvac}I_{unvac} - \mu R_{unvac}; \\
\frac{dR_{vac}}{dt} &= \gamma_{vac}I_{vac} - \mu R_{vac}; \\
\frac{dD}{dt} &= \theta_{vac}I_{vac} + \theta_{unvac}I_{unvac} + \mu\left(\begin{array}{c}S_{vac} + S_{unvac} + E_{vac} + E_{unvac} + \\ + I_{vac} + I_{unvac} + R_{vac} + R_{unvac}\end{array}\right),
\end{aligned}
\right. \tag{2}
$$

where S_{unvac} — susceptible unvaccinated persons who are not infected but can become infected through contact with an infected person (unvaccinated or vaccinated); S_{vac} — susceptible to the virus are vaccinated persons in the population who are not infected but can become infected through contact with an infected person (unvaccinated or vaccinated); E_{unvac} — the number of unvaccinated people with the disease in latent mode (they contacted with an infected person); E_{vac} — the number of vaccinated people with the disease in latent mode (they contacted with an infected person); I_{unvac} — the number of unvaccinated sick people who transmit the virus to unvaccinated and vaccinated susceptible persons; I_{vac} — the number of vaccinated patients who transmit the virus to unvaccinated and vaccinated susceptible persons; R_{unvac} — the number of unvaccinated survivors who are susceptible to reinfection, although the probability is lower; R_{vac} — the number of vaccinated survivors who are susceptible to re-infection, although the probability is lower; D — people who died from the virus and other causes; θ_{unvac} — deaths from the virus in infected unvaccinated people; θ_{vac} — deaths from the virus in infected vaccinees; β_{uu} — the probability of transmission of the virus from infected unvaccinated persons to unvaccinated persons; β_{uv} — the probability of transmission of the virus from infected unvaccinated persons to vaccinated persons; β_{vu} — the probability of transmission of the virus from infected vaccinated to unvaccinated persons; β_{vu} — the probability of virus transmission from infected vaccinated to vaccinated persons; α_{unvac} — the probability of the disease transition from the latent phase to the overt phase in unvaccinated persons; α_{vac} — the probability of the disease transition from the latent phase to the overt phase in vaccinated persons; γ_{unvac} — recovery of infected unvaccinated

people from the virus; γ_{vac} — recovery of infected vaccinated persons from the virus; μ — mortality not due to infection; l — birth rate.

The main difference between this model and the classical SEIRD model is the division of the population into vaccinated and unvaccinated individuals. Probability of infection of vaccinated persons (S_{vac}) is much lower than that of unvaccinated persons (S_{unvac}). Sick vaccinated persons (I_{vac}) are less contagious and less likely to die than unvaccinated infectious people (I_{unvac}).

IMPLEMENTING THE MODIFIED SEIRD MODEL FOR COVID-19 IN UKRAINE IN 2021

Let's model the situation with COVID-19 in Ukraine. To do this, we need to calculate the appropriate coefficients to substitute them. To do this, we will use information for 2021.

The number of Ukrainians in 2021 (excluding the occupied territories) is 41 million 167 thousand people [4]. The mortality rate for 2021 is 714 263 people, of which COVID-19 accounts for 86 015 cases [5]. The birth rate for 2021 will be 271 984 children [6].

The number of all deaths per day averages 714 263/365 = 1 956.88 people. That is, 1 956.88/41 167 300 = 0.0000475349 of the total population dies per day. This number includes deaths from COVID-19. The death rate from COVID-19 is (86 015/365)/41 167 300 = 0.0000057244.

Unfortunately, no mortality statistics for vaccinated and unvaccinated people could be found for Ukraine. However, you can calculate this coefficient yourself if the data mentioned in an interview with Professor Leanne Wen of the School of Public Health [14] are true: that vaccinated people are six times less likely to be infected than unvaccinated people and 11 times less likely to die from coronavirus. In this case, the mortality rate of vaccinated people per day is 0.0000004770, and that of unvaccinated people is 0.0000052474. Accordingly, we have $\Theta_{unvac} = 0.0000052474$ $\Theta_{vac} = 0.0000004770$.

Accordingly, the mortality rate per day not due to COVID-19 is 0.0000475349 - 0.0000057244 = 0.0000418105, i.e. $\mu = 0.0000418105$.

The birth rate per day is (271 984 /365)/41 167 300 = 0.0000181008, so $l = 0.0000181008$.

Since the modeling requires both vaccinated and unvaccinated populations, we need to provide data on these. In 2021, 15 201,112 people have been vaccinated with two vaccines in Ukraine [7]. That is, 15 201 112/41 167,300 = 0.3692521006. Accordingly, if you want to model a population of only 100 people, and one of each of the vaccinated and unvaccinated gets sick, 36.1867058563 will be the vaccinated who have not yet gotten sick, and 61.8132941437 will be the unvaccinated who have not yet gotten sick.

The incubation period is the number of days between the moment of infection and the moment of symptoms. To calculate the coefficient responsible for the rate of transition of the virus from the latent period to the fully infected state, we use formula:

$$\alpha = \frac{1}{T_{inc}},$$

where α — the rate of transition of the disease from the latent to the overt phase; T_{inc} — the average incubation time of the virus.

Viruses are constantly changing, sometimes resulting in the emergence of new strains. Different strains of COVID-19 may have different incubation periods. On average, symptoms appear in a newly infected person about 5.6 days after exposure [8]. So, $T_{inc} = 5.6$, accordingly, $\alpha = 1/5.6 = 0.17858$. According to studies, the incubation period for vaccinated and unvaccinated individuals is the same number of days [9], i.e. $\alpha_{unvac} = \alpha_{unvac} = 0.17858$.

Some studies have shown that it may take the body 2 weeks to recover from a mild illness, or up to 6 weeks in severe or critical cases [10]. Other sources say [11] that recovery usually takes one to two weeks. So let's use the average recovery time of two weeks.

Let's calculate γ according to the formula for calculating the recovery rate coefficient:

$$\gamma = \frac{1}{T_{rec}},$$

where γ — the recovery rate of infected people from the virus; T_{rec} — average recovery time.

So, $T_{rec} = 14$ days. Accordingly, $\gamma = \gamma_{unvac} = 1/14 = 0.0714$.

When the population is divided into vaccinated and unvaccinated, the recovery time will be different. Different sources report different recovery times: some studies show that the overall recovery time was six to seven days shorter than for unvaccinated people [12]. Another study from the Centers for Disease Control and Prevention found that vaccinated participants spent an average of two to six days less in bed than unvaccinated participants [13]. Let's assume that, on average, the vaccinated are sick six days less, that is $\gamma_{vac} = 1/8 = 0.125$.

Now let's calculate the probability of disease transmission. To calculate the data for vaccinated people, we need statistics on the effectiveness of the vaccine (let's take the Pfizer vaccine). According to [15], Pfizer has 95% protection against mild COVID-19. This means that you are less likely to get sick if you are vaccinated:

$$p_{get\ infected\ if\ you\ are\ vaccinated} = 0.05.$$

It should also be noted that vaccinated people are less likely to transmit the disease, even if they become infected. At a press conference in November, WHO Director-General Tedros Ghebreyesus said that vaccines protect against the spread of the virus by 60 percent before the delta variant emerges [16, 19]. This means:

$$p_{transmit\ the\ disease\ if\ you\ are\ vaccinated} = 0.4.$$

According to the same study [16, 17], vaccinated people are ten times less likely to be infected [18], and the likelihood of me being infected is half, judging by the above figures.

So, $p_{get\ infected\ if\ you\ are\ not\ vaccinated} = p_{get\ sick\ if\ you\ are\ vaccinated} \times 10 = 0.5$.

A $p_{transmit\ the\ disease\ if\ you\ are\ not\ vaccinated} = 0.4 \times 2 = 0.8$.

Now we can calculate the disease transmission rates.

$\beta_{uu} = p_{transmit\ the\ disease\ if\ you\ are\ not\ vaccinated} \times p_{get\ infected\ if\ you\ are\ not\ vaccinated} =$

$$= 0.8 \times 0.5 = 0.4 .$$

$\beta_{uv} = p_{transmit\ the\ disease\ if\ you\ are\ not\ vaccinated} \times p_{get\ sick\ if\ you\ are\ vaccinated} =$

$$= 0.8 \times 0.05 = 0.04 .$$

$\beta_{vu} = p_{get\ infected\ if\ you\ are\ vaccinated} \times p_{get\ infected\ if\ you\ are\ not\ vaccinated} =$

$$= 0.4 \times 0.5 = 0.2 .$$

$\beta_{vv} = p_{get\ infected\ if\ you\ are\ vaccinated} \times p_{get\ sick\ if\ you\ are\ vaccinated} =$

$$= 0.4 \times 0.05 = 0.02 .$$

Let's simulate the model with these parameters. In Fig. 1 you can see the results for one hundred days:

Fig. 1. Modified SEIRD model for 100 days

Fig. 1 shows how the number of people who have not had the disease is decreasing, while the number of people who have had the disease is increasing.

The number of unvaccinated patients is growing faster, which seems logical given the vaccination rate [13]. The number of deaths is growing relatively slowly. The number of uninfected, unvaccinated people is decreasing faster because they are more likely to contract the disease, while vaccinated people are slower to get sick.

If we look at a much longer time period (e.g., 8,000 days), we can see in Fig. 2 how the number of deaths increases and the number of deaths in the rest of the population decreases. The number of people who became ill also decreases because model (2) also takes into account natural mortality, which in this case does not include deaths from COVID-19.
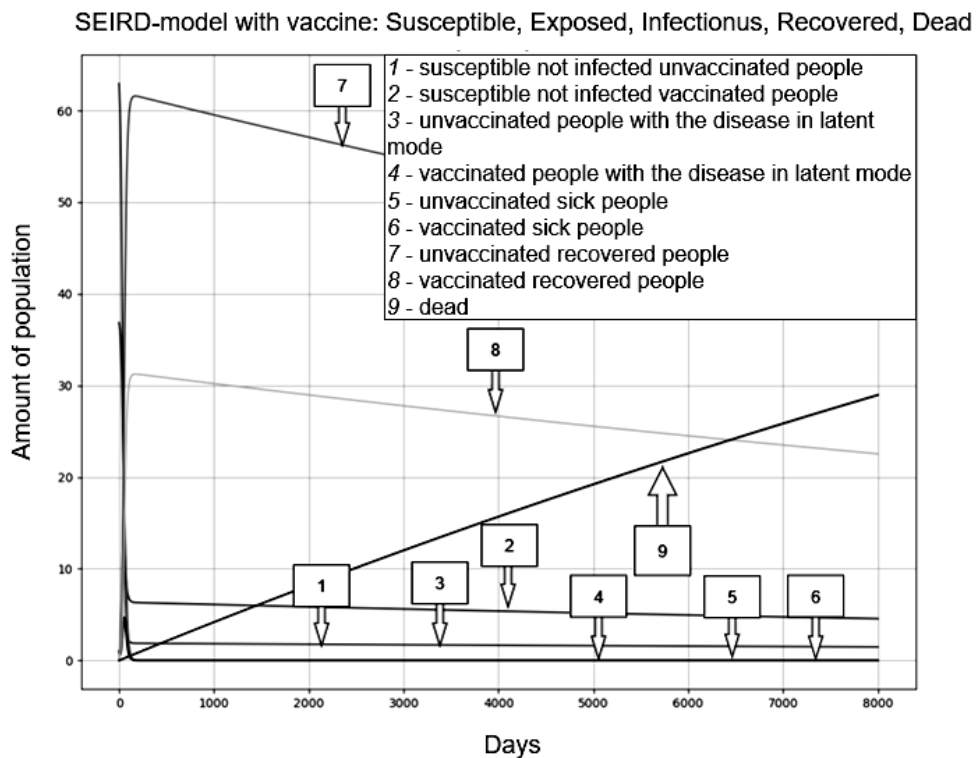
Fig. 2. Modified SEIRD model for 8000 days

This situation with fertility and mortality is due to the fact that in Ukraine the birth rate is lower than the death rate [20]. If we increase the fertility rate so that it exceeds the mortality rate, the situation looks different (fertility $l = 0.0500181008$) (Fig. 3):

Only the number of unvaccinated people who have not yet become ill increases, because this model does not include vaccination and the corresponding transition from unvaccinated to vaccinated people. The entire birth population is unvaccinated by default. From Fig. 3, you can also see how the disease process progresses over time: on the thousandth and two thousandth day, you can see waves of sick unvaccinated people, and accordingly, the number of unvaccinated people who have not yet become sick decreases over time.

SEIRD-model with vaccine: Susceptible, Exposed, Infectionus, Recovered, Dead

1 - susceptible not infected unvaccinated people
2 - susceptible not infected vaccinated people
3 - unvaccinated people with the disease in latent mode
4 - vaccinated people with the disease in latent mode
5 - unvaccinated sick people
6 - vaccinated sick people
7 - unvaccinated recovered people
8 - vaccinated recovered people
9 - dead
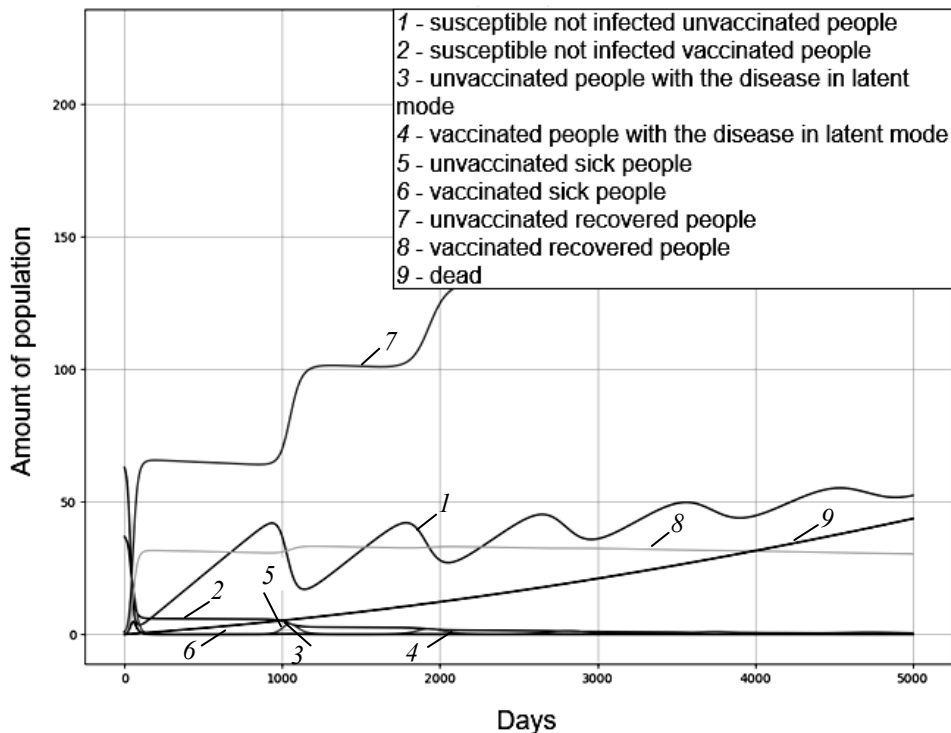
Fig. 3. Modified SEIRD model for 5000 days with a birth rate of l = 0.0500181008

CONCLUSIONS

The modified mathematical epidemiological SEIRD model is an important tool for assessing epidemic outbreaks and implementing disease control strategies. It is especially important that this model takes into account vaccination and non-vaccination, as this reflects the real situation with COVID-19 and other diseases for which vaccines exist. This model also allows for the impact of different vaccine variants on the effectiveness of its use.

To effectively combat epidemic outbreaks, it is necessary to know what factors influence the spread of the disease and which control strategies are most effective in specific conditions. The developed modified SEIRD model not only takes into account vaccination and non-vaccination, but also has coefficients responsible for birth and death, and that is why it can reflect a realistic picture. This model can help solve these problems by providing scientists and policymakers with a tool for forecasting, planning, and decision-making to control the epidemic.

Also, for the modified SEIRD model, all parameters were calculated from real statistical data from Ukraine to be able to simulate the situation as close to reality as possible. These data are important for making decisions on the development of medical infrastructure, the provision of medical equipment and medicines, as well as for determining the need for large-scale vaccinations and other epidemic control measures.

REFERENCES

1. H. Hethcote, "Qualitative analyses of communicable disease models," *Math. Biosci.*, 28 (3-4), pp. 335–356, 1976.

2. V. Capasso, *The Mathematical Structure of Epidemic Systems*. Springer Verlag, 1993.

3. Gergely Röst and Jianhong Wu, "SEIR epidemiological model with varying infectivity and infinite delay," *Math Biosci Eng.*, pp. 389–402, 2008.

4. *Population of Ukraine*. Accessed on: November 18, 2022. [Online]. Available: https://index.minfin.com.ua/ua/reference/people/

5. *Mortality rate of Ukraine for 2021*. Accessed on: November 18, 2022. [Online]. Available: https://index.minfin.com.ua/ua/reference/people/deaths/2021/

6. *Birth rate in Ukraine*. Accessed on: November 15, 2022. [Online]. Available: https://uk.wikipedia.org/wiki/Birth_in_Ukraine

7. *Vaccination in Ukraine*. Accessed on: November 13, 2022. [Online]. Available: https://index.minfin.com.ua/ua/reference/coronavirus/vaccination/ukraine/

8. *Coronavirus Incubation Period*. Accessed on: November 18, 2022. [Online]. Available: https://www.webmd.com/lung/coronavirus-incubation-period#1

9. *SARS-Cov-2 incubation period according to vaccination status during the fifth COVID-19 wave in a tertiary-care center in Spain: a cohort study*. Accessed on: November 18, 2022. [Online]. Available: https://bmcinfectdis.biomedcentral.com/articles/10.1186/s12879-022-07822-4

10. *Coronavirus Recovery*. Accessed on: November 15, 2022. [Online]. Available: https://www.webmd.com/lung/covid-recovery-overview#2

11. *Diagnosed with covid-19 what to expect*. Accessed on: November 14, 2022. [Online]. Available: https://www.hopkinsmedicine.org/health/conditions-and-diseases/coronavirus/diagnosed-with-covid-19-what-to-expect

12. *COVID-19 Vaccine Reduces Severity, Length, Viral Load for Those Who Still Get Infected*. Accessed on: November 14, 2022. [Online]. Available: https://news.arizona.edu/story/covid-19-vaccine-reduces-severity-length-viral-load-those-who-still-get-infected

13. *It's not just severity—the types of Covid symptoms you get depend on the vaccines you've received, new data says*. Accessed on: November 14, 2022. [Online]. Available: https://www.cnbc.com/2022/10/26/covid-symptoms-differ-based-on-vaccination-status-zoe-health-study.html

14. *Why vaccinated people dying from Covid-19 doesn't mean the vaccines are ineffective*. Accessed on: November 12, 2022. [Online]. Available: https://edition.cnn.com/2021/10/18/health/covid-19-vaccination-colin-powell-death-wen-wellness/index.html

15. *COVID-19 vaccine efficacy explained*. Accessed on: November 12, 2022. [Online]. Available: https://www.nebraskamed.com/COVID/covid-19-vaccine-efficacy-explained

16. *Modelling of COVID-19*. Accessed on: November 10, 2022. [Online]. Available: https://www.doherty.edu.au/our-work/institute-themes/viral-infectious-diseases/covid-19/covid-19-modelling/modelling

17. *Your unvaccinated friend is roughly 20 times more likely to give you COVID*. Accessed on: November 12, 2022. [Online]. Available: https://theconversation.com/your-unvaccinated-friend-is-roughly-20-times-more-likely-to-give-you-covid-170448

18. *Vaccinated NSW residents to be allowed into Victoria as the state records 2,179 COVID-19 cases and six deaths*. Accessed on: November 10, 2022. [Online]. Available: https://www.skynews.com.au/australia-news/coronavirus/watch-live-vic-health-officials-to-provide-covid19-update/news-story/863cdc24d57dd787251a8ccff26b5ec5

19. *The Risk of Vaccinated COVID Transmission Is Not Low*. Accessed on: November 10, 2022. [Online]. Available: https://www.scientificamerican.com/article/the-risk-of-vaccinated-covid-transmission-is-not-low/

20. *The birth rate in Ukraine continues to fall and is preparing to set a new anti-record of the last 30 years*. Accessed on: November 10, 2022. [Online]. Available: https://opendatabot.ua/analytics/depopulation-2021

INFORMATION ON THE ARTICLE

Anastasiia I. Klymenko, ORCID: 0000-0001-9595-8155, National Commission for State Regulation of Energy and Public Utilities, Ukraine, e-mail: asja653@gmail.com

Gleb B. Podkolzin, ORCID: 0000-0002-7120-2772, Educational and Scientific Institute for Applied System Analysis of the National Technical University of Ukraine "Igor Sikorsky Kyiv Polytechnic Institute", Ukraine, e-mail: podkolzin.gleb@lll.kpi.ua

МОДИФІКОВАНА SEIRD-МОДЕЛЬ ОПИСУ ЕПІДЕМІЇ COVID-19 / А.І. Клименко, Г.Б. Подколзін

Анотація. Присвячено математичним моделям в епідеміології, зокрема SIR, SEIR і SEIRD. Досліджено важливість цих моделей у прогнозуванні поширення інфекційних захворювань та оцінювання ефективності контрольних заходів. Ці моделі дають змогу оцінити важливі параметри епідемії, такі як швидкість поширення інфекції, кількість людей, які зазнають захворювання, та померлих від цього захворювання. Ці дані можуть допомогти у прийнятті рішень про введення та зняття карантинних обмежень, відкриття і закриття шкіл та інших установ, а також у розробленні стратегій вакцинації та інших контрольних заходів. Загалом математичні моделі SIR, SEIR і SEIRD є важливим інструментом з боротьби з епідеміями. Вони дозволяють епідеміологам і медичним працівникам прогнозувати та контролювати поширення захворювань, що зберігає здоров'я та життя людей.

Ключові слова: епідеміологія, епідеміологічні моделі, модифіковані математичні моделі, SEIR-моделювання COVID-19, SEIRD-модель, невакциновані люди, вірус, поділ популяції, нові штами.

GENERALIZATION OF THE THERMODYNAMIC APPROACH TO MULTI-DIMENSIONAL QUASISTATIC PROCESSES

A.S. KUTSENKO, S.V. KOVALENKO, S.M. KOVALENKO

Abstract. A method of mathematical modeling of multidimensional quasi-static processes, a generalization of quasi-static processes of equilibrium thermodynamics, is proposed and substantiated. The authors obtain a generalization of the first and the second law of thermodynamics in the form of Carathéodory to multidimensional quasi-static processes. The idea of generalization is to construct an orthogonal system of functionals similar to the work and heat functionals of classical thermodynamics along families of phase trajectories corresponding to different types of influences on a multidimensional quasi-static system. The representation of quasi-static processes by systems of ordinary differential equations containing control variables is substantiated. The obtained results make it possible to use a wide arsenal of methods of the theory of control of dynamical systems to solve problems of control of quasi-static processes.

Keywords: quasi-static processes, equilibrium thermodynamics, mathematical modeling, work, energy, controllability, entropy.

INTRODUCTION

The concepts of "quasi-static system" and "quasi-static process" owe their appearance to the fundamental branch of physics – thermodynamics. Thermodynamics originated and was further developed on the basis of the phenomenological approach, i.e. considering only the observed properties of thermodynamic systems (TS) without a detailed analysis of the mechanisms of their manifestation. As a result of this approach to the formation of thermodynamics, its main provisions: terminology, axiomatics and logical constructions in the form of physical laws have not changed significantly over the past few centuries. In the same time real practical results confirming theoretical backgrounds with a sufficiently high degree of accuracy have made thermodynamics, along with mechanics, a model of applied science. The quasi-static nature of processes in TS is one of the main postulates of thermodynamics, along with such concepts as reversibility and equilibrium. From the standpoint of thermodynamics, a quasi-static process is an infinitely slow process consisting of a sequence of equilibrium states infinitely close to each other. An essential limitation of the thermodynamics of equilibrium processes is the exclusion from consideration of the time coordinate and the representation of processes in the form of segments of trajectories in the phase space.

The mathematical support of thermodynamics is based on two postulates: the first and second laws, on the basis of which mathematical models of the main thermodynamic processes are introduced.

Despite the apparent limitation of the object of study in the form of quasi-static TS, a number of concepts and approaches of thermodynamics can be adapted to a relatively wide class of technological systems similar in external properties to TS. In this regard, the problem of constructing a mathematical theory of quasi-static processes arises, covering both the TS and other systems with the quasi-static property. In this article, an attempt to propose the mathematical foundations of the theory of quasi-static processes with a focus on the control problem is made.

REVIEW AND ANALYSIS OF INFORMATION SOURCES

The classical substantiation of thermodynamics as a system of knowledge is almost completely described in the works of Carnot, Clausius, Boltzmann, Planck [1–3] and other "classics" of thermodynamics [4, 5]. This branch of thermodynamics has survived without fundamental changes to the present day.

One of the principal ways to involve mathematical methods in thermodynamics and generalize the latter to other physical and technical processes can be considered the approach outlined in [6]. A feature of Gukhman's ideas is the substantiation of the uniformity of the components of the differential equation of the first law of thermodynamics in the form of products of certain potentials and a change in the corresponding coordinate of the state of the TS. At the same time, the thermal effect was included as a particular type of the set of effects on the TS, and the concepts of energy and amount of effect received a generalized interpretation suitable for any similar processes. The versatility of the ideas presented in [6] is clearly demonstrated in studies in the field of ecosystems [7].

Summarizing the results of thermodynamics related to the first law or the law of conservation of energy, we can conclude that the mathematical methods that allow adapting classical equilibrium thermodynamics to a wide range of similar processes in nature, technology and society are limited. The fundamental disadvantage of the considered approach is the absence of any time dependences linking changes in the state of the TS with the intensity (power) of actions.

In this regard, the authors of this work previously obtained some results of the "dynamization" of quasi-static processes. This made it possible to obtain mathematical models in the form of ordinary differential equations relating the change in time of the state vector of a quasi-static system to changes in the power of control actions. The results obtained in [8–10] require further generalization.

The greatest difficulty in the formation of thermodynamics was caused by its second law, and in particular the concept of entropy. For instance, in [4] there are 18 formulations of the 2nd law, each of which ultimately has the same meaning of the impossibility of obtaining mechanical work using only one source of heat. Unfortunately, the abundance of formulations and interpretations of the 2nd law of thermodynamics has led to some conservatism in the mathematization and formalization of thermodynamic methods and their adaptation to quasi-static processes of a different nature. The works of Schiller, Carathéodory, Afanasieva-Ehrenfest, Belokon were a qualitative shift in the direction of axiomatization in

thermodynamics, where a generalized theory of quasi-static processes was formulated in the language of mathematical formulations. Among the studies in this direction, the article by Carathéodory [11] should be especially singled out, where he elegantly formulated the 2nd law of thermodynamics in the language of Pfaffian forms. This article gave impetus to the wide application of the axiomatic approach in the thermodynamics of multidimensional processes [12–15].

MATHEMATICAL MODEL OF A CONTROLLED QUASI-STATIC PROCESS

We will consider multidimensional quasi-static processes in terms similar to the terms of classical thermodynamics: state, action, phase trajectory, work, energy, etc. The fundamental difference from thermodynamics will be the inclusion of the concept of heat in the category of works, as proposed in [6]. Thus, in our further constructions, heat or other effects will not take any priority position among the many possible effects on the system under consideration.

Let the state of the system under consideration Σ is given by the state vector $x \in R^n$. State change over time $x(t)$ represents a trajectory Σ in $(n+1)$-dimensional space. Any change of the vector x in time is associated with the presence of one or more actions from a given set W. In the absence of actions on a quasi-static system, the latter remains in the state in which all actions were interrupted. That is any condition $x \in R^n$ of a quasi-static system is an equilibrium position, in contrast to dynamical systems, for which the set of equilibrium positions is a subset of the space R^n.

Associate with each $m \le n$ of the types of actions W_k a vector field $\varphi_k(x)$, $k = \overline{1,m}$. We will assume that the system of vector fields $\varphi_1(x), \varphi_2(x), ..., \varphi_m(x)$ at every point $x \in R^n$ is linearly independent. For k-th action the trajectory Σ in phase space can be represented as a solution to the system of differential equations

$$\frac{dx}{dt} = \varphi_k(x)u_k(t), \tag{1}$$

where $u_k(t)$ is a scalar function of the parameter t, which has the meaning of the action intensity W_k. Absolute value $u_k(t)$ determines the speed of movement of the representative point along the phase trajectory, and its sign determines the direction of movement.

Let now several actions be simultaneously applied to the system. They correspond to the vector field $\varphi(x)$. Let's decompose the vector $\varphi(x)$ at some point x along linearly independent vectors $\varphi_1(x), \varphi_2(x), ..., \varphi_m(x)$. We get

$$\varphi(x) = \sum_{k=1}^{m} \varphi_k(x)u_k,$$

where u_k are decomposition coefficients.

Then the movement of the system along an arbitrary phase trajectory corresponding to the complex action will correspond to the system of differential equations

$$\frac{dx}{dt} = \sum_{k=1}^{m} \varphi_k(x)u_k(t), \tag{2}$$

and the coefficients u_k can be interpreted as the intensity of the corresponding actions.

If time t is chosen as a parameter, and values $u_k(t)$ are considered as controls, then the mathematical model of the quasi-static process in the form (2) is a controlled system linear in controls. Since the vectors are linearly independent, then the equilibrium of system (2) is $\varphi_1(x), \varphi_2(x),..., \varphi_m(x)$ achieved only in the case $u_1 = u_2 = ... = u_m = 0$. That is, the effects cannot compensate each other.

The proposed mathematical models of quasi-static processes with single (1) and complex action (2) give a qualitative model of behavior Σ. The point is that the vector fields $\varphi_k(x)$ $(k = \overline{1,m})$ specify only the directions of the corresponding fields and can be normalized arbitrarily. In this case, the form of phase trajectories will remain unchanged. At the same time, the trajectory Σ in time will depend both on the normalization of the vector $\varphi_k(x)$, as well as on the size $u_k(t)$, forming the speed of movement Σ along the phase trajectory defined by the vectors $\varphi_k(x)$ and some starting point x_0 of the specific process.

ENERGY MEASURE OF THE ACTION

The previously introduced concept of the action intensity, which has the meaning of controlling a quasi-static process, requires a quantitative measurement. To do this, as an analogy, we use the classical thermodynamic approach for thermal deformation systems, i.e., TS subject only to mechanical and thermal effects, the phase trajectories of which have the form $pV^{\gamma} = \text{const}$ and $p = \text{const}$ respectively, where p, V are the pressure and volume of the gas in relative units and γ is adiabatic exponent $(\gamma \approx 1.3 \div 1.5)$, depending on the chemical composition of the substance.

It is known from thermodynamics [5] that the first law of thermodynamics is valid for a thermal deformation system, which is formulated as follows:

$$dU = \Delta L + \Delta Q, \tag{3}$$

where dU is an increment of internal energy, ΔL is a deformation work, ΔQ is a supplied heart. In (3) internal energy $U(x)$ is a function of state and quantities ΔL and ΔQ are functions of trajectories in a state space.

For ideal gases [5] the internal energy U has the form

$$U = \frac{1}{\gamma - 1} pV, \tag{4}$$

and the mechanical work and heart are calculated as curvilinear integrals along the phase trajectory l:

$$\Delta L = -\int\limits_{(l)} p \, dV; \tag{5}$$

$$\Delta Q = \int\limits_{(l)} \left(\frac{1}{\gamma - 1} V dp + \frac{\gamma}{\gamma - 1} p \, dV \right). \tag{6}$$

Thus, ratio (5) and (6) can be interpreted as a quantitative measure of the action on the TS in the form of the mechanical work (5) and heat (6). For fixed initial x_0 and final x_f process points $U(x_f) - U(x_0) = \text{const}$ for any trajectories connecting x_0 and x_f, the sum ΔL and ΔQ in accordance with (3) will be constant for various ratios ΔL and ΔQ.

Let us generalize the thermodynamic approach (4) as applied to finding similar quantitative measures of actions for an arbitrary n-dimensional quasi-static process with $m = n$ actions. Let us introduce R^n the scalar continuous function in static space – the energy:

$$U(x) = U(x_1, x_2, \ldots, x_n). \tag{7}$$

The energy increment (7) in some point $x \in R^n$ will look like:

$$dU = \frac{\partial U}{\partial x_1} dx_1 + \frac{\partial U}{\partial x_2} dx_2 + \ldots + \frac{\partial U}{\partial x_n} dx_n. \tag{8}$$

Denoting $\frac{\partial U}{\partial x} \overset{\Delta}{=} g(x)$ — the gradient $U(x)$, write down (8) as

$$dU = (g, dx), \tag{9}$$

and along the trajectory of the solution (1), or along the phase trajectory of the k-th action, the (8) takes the form

$$dU = (g, \varphi_k) dt. \tag{10}$$

Ratio (10) will also be valid for any phase trajectory generated by an arbitrary vector field $\varphi(x)$

$$dU = (g, \varphi) dt. \tag{11}$$

Let us denote the set of possible phase trajectory l_k corresponding to k-th type of action as L_k, and the set $\bigcup L_k \overset{\Delta}{=} L$. The set of all feasible trajectories corresponding to an arbitrary composition of actions is denoted by L^*. Then there is the system of inclusions

$$L_k \subset L \subset L^*, \quad \forall k = \overline{1, m}.$$

We will call the energy measure $J(l)$ of any phase trajectory l the value

$$J(l) = \int_{(l)} (g, dx). \tag{12}$$

Due to (9) the energy measure (12) depends only on the initial x_0 and final x_f points of the curve l:

$$J(l) = U(x_f) - U(x_0) = J(x_0, x_f). \tag{13}$$

The energy measure (13) satisfies the following axioms:

1) $J(x, x) = 0$;

2) $J(x, y) = -J(y, x)$; $\tag{14}$

$$3)\ J(x,y) = J(x,z) + J(z,y).$$

Axioms 2 and 3 in (14) differ from the symmetry and triangle axioms known from the theory of metric spaces:

$$J(x,y) = J(y,x);$$

$$J(x,y) \le J(x,z) + J(z,y).$$

By analogy with first law of thermodynamics, we will look for the quantities of each type of actions in the form of functionals $A_k(l)$, calculated along phase trajectories similar to the mechanical work and heat for the simplest thermodynamic system (5), (6):

$$A_k(l) = \int\limits_{(l)} (q_k(x), dx), \quad k = \overline{1,n}. \tag{15}$$

Functionals $A_k(l)$ we will call the works of action W_k. Vectors $q_k(x)$ we will be chosen so that following conditions are satisfied:

$$A_k(l) = \begin{cases} J(l), & \text{if } l \in L_k, \\ 0, & \text{if } l \in L_i, \end{cases} \quad i,k = \overline{1,n},\ i \ne k. \tag{16}$$

Requirements (16) will by met under the following conditions to choose from $q_k(x)$:

$$(q_k, \varphi_i) = \delta_{ik}(g, \varphi_i), \quad i,k = \overline{1,n}, \tag{17}$$

where δ_{ik} is the Kronecker symbol.

The conditions (17) are essentially conditions for the quasi-biorthogonality of vector systems $(\varphi_1, \varphi_2 \ldots \varphi_n)$ and $(q_1, q_2 \ldots q_n)$.

Rewrite the last equation in matrix form:

$$Q\Phi = \text{diag}\left(\Phi^T g\right), \tag{18}$$

where the rows of matrix Q are desired vectors $(q_1, q_2 \ldots q_n)$ and the columns of the matrix Φ are vector fields $(\varphi_1, \varphi_2 \ldots \varphi_n)$ of actions on the system.

Since vectors $\varphi_k(x)$ are assumed to be linearly independent for $\forall x \in R^n$, matrix Φ is non-degenerate, therefore the solution (18) can be written as

$$Q = \text{diag}(\Phi^T g)\Phi^{-1}. \tag{19}$$

Let us now show that for the system of works $A_1, A_2 \ldots A_n$ with vector fields, defined in accordance with (19), $\forall l \in L^*$ the following relation in true:

$$J(l) = \sum_{k=1}^{n} A_k(l). \tag{20}$$

To prove (20), we sum relations (17) over k. As a result, we get:

$$\sum_{k=1}^{n} (q_k, \varphi_i) = \sum_{k=1}^{n} \delta_{ik}(g, \varphi_i), \quad i = \overline{1,n};$$

$$\left(\sum_{k=1}^{n} q_k, \varphi_i \right) = (g, \varphi_i), \quad i = \overline{1, n} \,.$$

It follows directly from the latter:

$$\sum_{k=1}^{n} q_k = g = \frac{\partial U}{\partial x} \,. \tag{21}$$

Let us sum over k the values $A_k(l)$, determined in accordance with (15). As a result, we get

$$\sum_{k=1}^{n} A_k(l) = \int_l (\sum_{k=1}^{n} q_k, dx) \,. \tag{22}$$

Taking into account relations (12) and (21), and from (22) we get (20), i.e. the sum of the work calculated along an arbitrary trajectory is equal to the increment in the energy of the system at the ends of this trajectory.

As an example consider thermodynamic system with actions in the form of mass transfer, deformation, and heat transfer The vector fields of such actions are well known [5] and are represented by the matrix $\Phi(p, V, m)$, looking like

$$\Phi = \begin{pmatrix} \gamma \dfrac{p}{m} & -\gamma \dfrac{p}{V} & 1 \\ 0 & 1 & 0 \\ 1 & 0 & 0 \end{pmatrix}, \tag{23}$$

where p, V, m are pressure, volume and mass of the system. The columns of the matrix (22) are vector fields of mass transfer, deformation and thermal effects, respectively.

Let us introduce the energy of system in the form of a known relation for ideal gases (3), then

$$\frac{\partial U}{\partial x} = \left(\frac{1}{\gamma - 1} V, \frac{1}{\gamma - 1} p, 0 \right) = (g_1, g_2, g_3) \,. \tag{24}$$

Substituting the (23) and (24) in the formula (19), we get a matrix

$$Q = \begin{pmatrix} 0 & 0 & \dfrac{\gamma}{\gamma - 1} \dfrac{pV}{m} \\ 0 & -p & 0 \\ \dfrac{V}{\gamma - 1} & \dfrac{\gamma p}{\gamma - 1} & -\dfrac{\gamma}{\gamma - 1} \dfrac{pV}{m} \end{pmatrix},$$

the rows of which are the components of the vectors of the quantities of the corresponding actions

$$A_1 = \int_{(l)} \frac{\gamma}{\gamma - 1} \frac{pV}{m} dm \,; \quad A_2 = \int_{(l)} -p dV \,;$$

$$A_3 = \int_{(l)} \left(\frac{V}{\gamma - 1} dp + \frac{\gamma}{\gamma - 1} p dV - \frac{\gamma}{\gamma - 1} \frac{pV}{m} dm \right),$$

where A_1 is a work of mass transfer, A_2 is a mechanical work, A_3 is a heat.

It is easy to verify that sum of the rows of the matrix Q coincides with the internal energy gradient, and

$$A_1(l) + A_2(l) + A_3(l) = J(l).$$

The considered approach to constructing a system of functionals satisfying the additivity condition (20) can also be extended to the case when the number of actions m is less than the dimension of the system n. In this case, the matrix Φ in the system of equations (18) is rectangular, and, consequently, constructions (19)–(24) lose their meaning. A way out of this situation can be obtained as a result of redefining the system of actions with the missing $n - m$ dummy actions. These dummy actions are chosen so that the square matrix $\Phi = (\Phi_1 \vdots \Phi_2)$, where $\Phi_1 - (n \times m)$ – the matrix given actions, and $\Phi_2 - (n \times (n - m))$ – the matrix of dummy actions will be nondegenerate. Substituting the matrix Φ obtained this way in relation (19) we get the matrix of works, which will depend on an arbitrary matrix Φ_2.

INVERSE PROBLEM

The performed analysis showed that if the laws of change of the phase coordinates of the thermodynamic system depending on the type of influences are known, then for an arbitrarily given state function $U(x)$, a system of functionals can be chosen that satisfies the structure of the energy conservation law. The question arises, is it possible to solve the inverse problem: for a given functional corresponding to the work of some action, construct the corresponding function $U(x)$, which has the meaning of the energy of the thermodynamic system. This approach is quite pragmatic, since it allows to "join" various physical processes that have the same types of external influences. For example, in mechanics and thermodynamics, such an action is deformation, and the corresponding work in both cases is calculated by similar functionals:

$$A = -\int_{(l)} f ds \quad \text{is mechanics};$$

$$L = -\int_{(l)} p dV \quad \text{is thermodynamics}.$$

So, let's formulate the problem as follows. Let some reference action be given, which corresponds to the phase trajectories of the system of differential equations

$$\dot{x} = \varphi(x), \quad x \in R^n,$$

where $\varphi(x)$ is a known vector function.

Let the known functional correspond to the standard action, with the help of which the work of the standard action is calculated:

$$L = \int_{(l)} q_1(x)dx_1 + q_2(x)dx_2 + \ldots + q_n(x)dx_n = \int_{(l)} (q, dx).$$

Then, due to relation (17), the vector functions $\varphi(x)$, $q(x)$ and $g(x)$ must satisfy the condition

$$(q,\varphi)=(\varphi,g) \,.$$

The last equation can be interpreted as a linear differential equation in partial derivatives with respect to the function of the energy of the thermodynamic system $U(x)$:

$$\left(\frac{\partial U}{\partial x},\varphi\right)=(q,\varphi) \,.$$

To solve it, we use the method of characteristics. The system of differential equations of characteristics in symmetrical form can be written as

$$\frac{dx_1}{\varphi_1(x)}=\frac{dx_2}{\varphi_2(x)}=\ldots=\frac{dx_n}{\varphi_n(x)}=\frac{dU}{(q(x),\varphi(x))} \,. \tag{25}$$

Since all $\varphi_k(x)$ included in (25) do not depend on the desired function $U(x)$, then the set of first integrals of the subsystem of differential equations (25)

$$\frac{dx_1}{\varphi_1(x)}=\frac{dx_2}{\varphi_2(x)}=\ldots=\frac{dx_n}{\varphi_n(x)} \tag{26}$$

will also be a subset of the set of integrals of the complete system (25).

Let

$$\Psi_k(x)=C_k \,, \ k=\overline{1,n-1} \tag{27}$$

be the first integrals of the system (26). Based on (27), we express the first $x_1,x_2,\ldots,x_{n-1}$ through x_n and $C_1,C_2,\ldots,C_{n-1}$:

$$\begin{aligned}
x_1 &= \lambda_1(x_n,C_1,C_2,\ldots,C_{n-1}); \\
x_2 &= \lambda_2(x_n,C_1,C_2,\ldots,C_{n-1}); \\
&\ldots\ldots\ldots\ldots\ldots\ldots\ldots\ldots\ldots\ldots\ldots \\
x_{n-1} &= \lambda_{n-1}(x_n,C_1,C_2,\ldots,C_{n-1}),
\end{aligned} \tag{28}$$

and substitute the obtained relations into the last of equations (25)

$$\frac{dx_n}{\varphi_n(x)}=\frac{dU}{(q(x),\varphi(x))} \,.$$

As a result of such a substitution, we obtain a differential equation with separable variables x_n and U

$$\frac{dx_n}{\overline{\varphi_n}(x_n,C)}=\frac{dU}{(\overline{\beta}(x_n,C),\overline{\varphi}(x_n,C))} \,,$$

where $\overline{\varphi_n}$, $\overline{\varphi}$, $\overline{q}$ are the functions of the vector x_n and the vector of constants $C=\left(C_1,C_2,\ldots,C_{n-1}\right)$ obtained after substituting (28) into the expressions for φ_n, φ, q respectively.

Integrating the last differential equation, we obtain the n-th first integral of the original system of differential equations of characteristics (25) in the form

$$U + \lambda_n(x_n, C) = C_n. \tag{29}$$

Substituting into (29) the expressions for the components of the vector of constants C in the form (27), we finally obtain

$$U + \Psi_n(x) = C_n.$$

As is known from the theory of partial differential equations, the general solution $U(x)$ satisfies the equation

$$\Phi\big(U + \Psi_n(x), \Psi_1(x), \Psi_2(x), \ldots, \Psi_{n-1}(x)\big) = 0,$$

where Φ is an arbitrary function of its arguments.

Solving the last equation with respect to the first argument, we finally obtain

$$U = U_0(x) + \Phi[\Psi_1(x), \Psi_2(x), \ldots, \Psi_{n-1}(x)], \tag{30}$$

where $U_0(x) = -\Psi_n(x)$, and Φ is an arbitrary function of its arguments.

Let's analyze the result. As can be seen from (30), the function $U(x)$ that satisfies the differential equation for the operation of a given action consists of two terms. The first term $U_0(x)$ is determined both by the type of the phase trajectory of the system subject to the reference action and by the type of the standard functional (vector $q(x)$). The second term depends only on the phase trajectories and is an arbitrary function of the first integrals of the system of differential equations that model the behavior of the thermodynamic system under the reference action.

Thus, all $\Psi_i(x)$ $i = \overline{1, n-1}$ that are arguments of an arbitrary function Φ are constants, and therefore $\Phi[\Psi_1, \Psi_2, \ldots, \Psi_{n-1}]$ also an arbitrary constant. Thus,

$$U(x) = U_0(x) + C,$$

i.e. the energy of a quasi-static system is determined up to some constant C.

Consider an example of finding the internal energy $U(p, V)$ for the simplest thermodynamic system subjected to a standard deformation effect, the work of which is defined as

$$L = -\int_{V_1}^{V_2} p\, dV.$$

The system of differential equations modeling the deformation effect, as follows from [5], has the form

$$\frac{dp}{dt} = -\gamma \frac{p}{V}, \quad \frac{dV}{dt} = 1,$$

and differential equation (24) for $U(p, V)$ can be written in the form

$$-\gamma \frac{p}{V} \frac{\partial U}{\partial p} + \frac{\partial U}{\partial V} = -p.$$

The corresponding system of ordinary differential equations of characteristics can be written as

$$\frac{dp}{-\gamma\frac{p}{V}} = \frac{dV}{1} = \frac{dU}{-p}. \tag{31}$$

The first integral $\Psi_1(p,V)$, which is the equation of the adiabatic phase curve, is obtained by integrating the differential equation

$$\frac{dp}{-\gamma\frac{p}{V}} = \frac{dV}{1}$$

and has a well-known form

$$pV^\gamma = C_1. \tag{32}$$

Expressing p through C_1 and V, and substituting the result into (31), we obtain a differential equation for determining the energy $U(p,V)$. Thus

$$p = C_1 V^{-\gamma}, \ dU = -C_1 V^{-\gamma} dV, \ U = -C_1 \int V^{-\lambda} dV, \ \text{and} \ U = -C_1 \frac{V^{-\gamma+1}}{1-\gamma} + C.$$

Substituting expression (32) for C_1 into the last relation, we finally obtain the expression, well known from thermodynamics for the internal energy of an ideal gas,

$$U = \frac{1}{\gamma-1} pV + C.$$

It should be noted that this result was obtained only on the basis of the known experimental adiabatic curves without involving the results of the well-known experiment of Gay–Lussac and Joule, which showed the invariance of the gas temperature during its expansion into a vacuum.

Let us now return to the original mathematical model of the thermodynamic system (2) and find the physical meaning of the quantities u_k – an action intensities of W_k. To do this, we proceed as follows: let the work A_j be given by an integral of the form:

$$A_j = \int\limits_{(l)} (q_j, dx), \tag{33}$$

where q_j is previously defined vector of j-th work. Multiply the left and right parts of (2) scalarly by the vector q_j, as a result we get

$$(q_j, \dot{x}) = \sum_{k=1}^{n} (q_j, \varphi_k) u_k. \tag{34}$$

Taking into account the conditions of orthogonality of works (12), from relations (33)–(34) we get

$$\frac{dA_j}{dt} = (q_j, \varphi_j) u_j.$$

From the last expression, and also from (17) it follows

$$u_j = \frac{1}{(q_j, \varphi_j)} \dot{A}_j = \frac{1}{(g, \varphi_j)} \dot{A}_j, \quad j = \overline{1, n}. \tag{35}$$

Let us substitute (35) into original differential equation (2). As result we get

$$\frac{dx}{dt} = \sum_{k=1}^{n} \frac{\varphi_k(x)}{(g, \varphi_k)} \dot{A}_k. \tag{36}$$

From (36) it follows that if the column vectors $\varphi_k(x)$ of matrix $\Phi(x)$ divide accordingly into dot products (g, φ_k), then each of the controls u_k will match the intensity of the corresponding work $\dot{A}_k$, i. e., using electromechanical terminology, u_k with this normalization corresponds to the action power W_k. In addition, the original system of equations (2) can be immediately normalized in accordance with (36), which will in no way affect the form of phase trajectories corresponding to certain types of action and the corresponding work vector $q_k(x)$.

Thus, without loss of generality, we can assume that the right side of the system of equations (2) is normalized in accordance with (34), and the control vector u_j corresponds to the power vector $\dot{A}_j$. Therefore, any of the works can be calculated both in the form of a curvilinear integral (33) and in the form of an integral over the time

$$A_j = \int_{t_0}^{t_1} u_j(t) dt.$$

QUASI-STATIC CONTROL SYSTEM OF GENERAL VIEW

Let us consider an empirical approach to the construction of mathematical models of quasi-static systems, given by families of phase trajectories $L_1, L_2, ..., L_n$, corresponding to the impacts $W_1, W_2, ..., W_n$. Let L_k it look like

$$\begin{aligned}
f_1(x_1, x_2, ..., x_n) &= C_1; \\
f_2(x_1, x_2, ..., x_n) &= C_2; \\
&\cdots\cdots\cdots\cdots\cdots\cdots \\
f_{n-1}(x_1, x_2, ..., x_n) &= C_{n-1},
\end{aligned} \tag{37}$$

of $(n-1)$-parametric family of lines in n-dimensional phase space. The set of constants $C_1, C_2, ..., C_{n-1}$ set a specific phase trajectory $l_k \in L_k$, and a change in one of the variables (for example, x_n) determines all the coordinates of the points of the selected phase trajectory as a result of solving system (37). Let's associate the change x_n with some parameter $t \in R^1$, which can be taken as time. Then all x_k will also be functions of time due to equations (37). To find the vector field corresponding to trajectories from L_k, we differentiate (37) with respect to t. As a result, we get

$$\frac{\partial f_1}{\partial x_1}\dot{x}_1 + \frac{\partial f_1}{\partial x_2}\dot{x}_2 + ... + \frac{\partial f_1}{\partial x_n}\dot{x}_n = 0;$$

$$...$$ (38)

$$\frac{\partial f_{n-1}}{\partial x_1}\dot{x}_1 + \frac{\partial f_{n-1}}{\partial x_2}\dot{x}_2 + ... + \frac{\partial f_{n-1}}{\partial x_n}\dot{x}_n = 0.$$

Complementing (38) with the equation

$$\dot{x}_n = 1,$$

we obtain $n \times n$ a linear system of algebraic equations with respect to $\dot{x}_1, \dot{x}_2, ..., \dot{x}_n$, the solution of which gives the vector field of the k-th action or the corresponding system of differential equations

$$\frac{dx_k}{dt} = \varphi_k(x_1, x_2, ..., x_n), \quad k = \overline{1,n}.$$ (39)

Thus, from a family of phase trajectories of some process (37) we can get a quasi-static model of the same process, which has the structure of a system of differential equations (39).

The transition to the environment of differential equations allows us to use a wide arsenal of modern methods of control theory for solving all kinds of control problems for technical systems.

REACHABILITY, CONTROLLABILITY, AND ENTROPY OF QUASI-STATIC SYSTEMS

In the previous sections, the concepts of energy and work of various action were formalized and substantiated, which made it possible to interpret quasi-static systems as controlled dynamic ones. One of the central concepts of control theory is the concepts of reachability and controllability [16], which qualitatively characterize the fundamental possibility of solving a control problem, i.e., the existence of a certain control law that implements the transition between two reassigned points of the phase space. Let us extend these concepts to controlled multidimensional quasi-static processes.

If the system of actions on the TS is complete, i.e. $m = n$, then it is obvious that it is always possible to choose such a sequence of actions that the phase trajectory will pass through any predetermined point of the state space. So the whole space R^n is achievable, and the TS is fully controllable. In another limiting case, when all controls except u_k are identically equal to zero, i.e. $m = 1$, the reachable set is some isolated phase trajectory $l_k \in L_k$, on which the represented point is currently located, and the system becomes uncontrollable. Bellow the obtain a criterion for the controllability of quasi-static systems for the general case $1 < m < n$, relying, as before, on the methods of equilibrium thermodynamics.

It is easy to see that the concept of controllability of quasi-static systems is closely related to the concept of adiabatic inaccessibility introduced by Carathéodory [11] when formulating the second law of thermodynamics. Accord-

ing to Carathéodory, in the vicinity of an arbitrary state of the TS, there are adia-batically inaccessible states. In other words, in the absence of thermal action, the phase trajectories of the TS belong to some hypersurfaces, which are a one-parameter family

$$f(x) = c .$$

To curry out to the transition of the representative point from a hypersurface $f(x) = c_1$ on a hypersurface $f(x) = c_2$ it is necessary to involve thermal action. Carathéodory proved that in this case the differential form included in the integral (15) for the elementary amount of heat dQ is holonomic, i.e must have an integrating factor $\psi(x)$:

$$dQ = (q(x), dx) = \psi(x)(\overline{q}(x), dx) = \psi(x) dS(x) .$$

Function $S(x)$, which remains constant in the absence of thermal interaction, corresponds to the entropy of the TS. In [17], general criteria for the holonomy of differential Pfaffian forms are formulated.

Thus, the second law of thermodynamics in the formulation of Carathéodory from the point of view of control theory is a criterion for the controllability of a n–dimensional dynamical system of the form (1) under a $n-1$ control action. Since this paper presents an abstract approach to equilibrium thermodynamics, the authors consider it fundamental to extend the Carathéodory method to an arbitrary number of control actions. In other words, below we will analyze the controllability of dynamic systems of the form (1) with the $m \leq (n-1)$ numbers of actions.

To solve the formulated problem, we study the structure of the set of phase trajectories of solution of differential equations corresponding to m action

$$\frac{dx}{dt} = \varphi_1(x), \dots, \frac{dx}{dt} = \varphi_m(x) . \tag{40}$$

Regarding the set of phase trajectories of m systems (40), we assume that it belongs to some invariant one-parameter manifold

$$S(x) = c , \tag{41}$$

i.e. all points $x(t)$ of phase trajectories of the set of systems (32), satisfy the condition

$$S(x(t)) = c , \quad \forall t \in [0, \infty) ,$$

where the constant c is determined from the initial condition

$$c = S(x(t_0)) .$$

In this case, the set of states, that do not satisfy condition (41) will be inaccessible for a given set of actions, and from the point of view of control theory, such a system will be uncontrollable.

To find the surface $S(x)$ we compose the system of differential equations in partial derivatives, which it must satisfy

$$\left(\frac{\partial S}{\partial x}, \varphi_1(x) \right) = 0, \dots, \left(\frac{\partial S}{\partial x}, \varphi_m(x) \right) = 0 . \tag{42}$$

The system (42) the conditions of orthogonality for the gradient vector of the function $S(x)$ and for all vector fields that determined the TS trajectories for a given structures of actions. Thus the problem of inaccessibility of a TS of an arbitrary set of actions is reduced to the analysis of the solvability of the system of equations (42), which is the system of linear differential equations in partial derivatives with respect to the function $S(x)$.

The theory of linear partial differential equations is quite well developed and contains a solution algorithm, including an analysis of the conditions for the existence of a solution [18]. This condition can be represented as

$$\text{rank}\{\varphi_1, \varphi_2, ..., \varphi_m, [\varphi_1, \varphi_2], [v]...[\varphi_{m-1}, \varphi_m], [\varphi_1, [\varphi_2, \varphi_3]]...\} < n, \quad (43)$$

where $[\varphi, \psi]$ is the commutator of the vector fields φ and ψ.

$$[\varphi, \psi] = \frac{\partial \psi}{\partial x}\varphi - \frac{\partial \varphi}{\partial x}\psi.$$

Thus, this fulfilment of the condition (43) indicates that there is an invariant surface $S(x) = c$, to which all possible trajectories of the TS motion belong, i.e. (43) is a criterion for the uncontrollability of the generalized thermodynamic system.

THE DISCUSSION OF THE RESULTS

The thermodynamic approach to mathematical modeling of multidimensional quasi-static processes is generalized. The concepts of energy and work corresponding to each of the feasible actions on the controlled system are introduced. The conditions for the orthogonality of the vectors of the coefficients of the differentials of work made it possible to formulate the law of conservation of energy, similar to the first law of thermodynamics, in the most general form without involving any physical laws.

The axiomatic approach to the formation of the 2nd law of thermodynamics has been further developed as applied to multidimensional quasi-static systems. The concept of controllability of a quasi-static system is introduced.

Conditions for the existence of an invariant set of states of a quasi-static system are obtained for the number of actions less than the dimension of the system. It is shown that the existence of an invariant set is equivalent to the criterion of uncontrollability of a quasi-static system.

REFERENCES

1. M. Plank, *Thermodynamics*. Leningrad-Moscow : GIZ, 1925, 311 p .
2. S. Carnot, *Reflections on the driving force of fire and machines capable of developing this force: Series "Classics of natural science"*. Moscow: Kniga po Trebovaniju, 2013, 80 p.
3. R. Clauzilus, "Mechanical theory of heat. Mathematical introduction," *The second law of thermodynamics*. Moscow-Leningrad: Goztekhizgrad, 1934, pp. 73–157.
4. K.A. Putilov, *Thermodynamics*. Moscow: Kniga po Trebovaniju, 2013, 375 p.
5. R. Kubo, *Thermodynamics*. Moscow: Mir, 1970, 304 p.
6. A.A. Gukhman, *On the foundations of thermodynamics*. Moscow: LKI, 2010, 384p.
7. G.V. Averyn, *System Dynamics*. Donetsk: Donbass, 2014, 403 p.

8. A.S. Kutsenko, "Optimal control of thermodynamic processes," *Mechanics and machine building*, no.1, pp. 93–97, 1999.

9. A.S. Kutsenko, "Equilibrium thermodynamics from the point of view of control theory," *Integration technologies and energy saving*, no.4, pp. 35–41, 2001.

10. A.S. Kutsenko, S.V. Kovalenko, and V.I. Tovazhnyanskii, "Structural and Parametric Synthesis of a Stabilization System for a Quasistatic Technological Process," *Bulletin of the National Technical University "KhPI". Series: System analysis, management and information technology*, no. 58 (1167), pp. 24–28, 2015.

11. K. Carathéodory, "On the foundations of thermodynamics,"*Development of modern physics*. Moscow, 1964, pp. 188–222.

12. P.T. Landsberg, "On Suggest Simplification of Carateodory's Thermodynamics," *Phys. Status Solidi*, vol. 1, no. 2, pp. 120–126, 1961.

13. G.V. Averin, A.V. Zvyagintseva, and M.V. Shevtsova, "On the Question of Substantiation of Thermodynamic Statements by the Method of Differential Geometry of Multidimensional Spaces," *Scientific statements of NRU BelSU, Ser. Mathematics, Physics*, issue 45, no. 27(248), pp. 36–44, 2016.

14. G. Falk and H. Jung, *Axiomatik der Thermodynamik. Handbuch der Physik*, III/2, pp. 119–175, 1959.

15. E.H. Lieb and J. Yngvason, "The phisics and mathematics of the second law of thermodynamics," *Physics Reports*, vol. 310, no. 1, pp. 1–96, 1999.

16. Yu.N. Andreev, *Control of finite-dimensional linear objects*. Moscow: Nauka, 1976, 424 p.

17. N.I. Belokon, *Thermodynamics*. Moscow–Leningrad: Gosenergoizdat, 1954, 416 p.

18. I. Gorn, *Introduction to the theory of differential equations with partial derivatives*. Moscow: GONTI NKTP USSR, 1938, 274 p.

INFORMATION ON THE ARTICLE

Alexander S. Kutsenko, ORCID: 0000-0001-6059-3694, National Technical University "Kharkiv Polytechnic Institute", Ukraine, e-mail: kuzenko@i.ua

Sergii V. Kovalenko, ORCID: 0000-0001-8763-0862, National Technical University "Kharkiv Polytechnic Institute", Ukraine, e-mail: adbc@ukr.net

Svitlana M. Kovalenko, ORCID: 0000-0001-6770-6778, National Technical University "Kharkiv Polytechnic Institute", Ukraine, e-mail: svetkovalenko@gmail.com

УЗАГАЛЬНЕННЯ ТЕРМОДИНАМІЧНОГО ПІДХОДУ ДО БАГАТОВИМІРНИХ КВАЗІСТАТИЧНИХ ПРОЦЕСІВ / О.С. Куценко, С.В. Коваленко, С.М. Коваленко

Анотація. Запропоновано і обґрунтовано метод математичного моделювання багатовимірних квазістатичних процесів, які є узагальненням квазістатичних процесів рівноважної термодинаміки. Отримано узагальнення першого, а також другого закону термодинаміки у формі Каратеодорі на багатовимірні квазістатичні процеси. Ідея узагальнення — побудова ортогональної системи функціоналів, аналогічних функціоналам роботи і теплоти класичної термодинаміки уздовж сімей фазових траєкторій, що відповідають різним видам впливів на багатовимірну квазістатичну систему. Обґрунтовано подання квазістатичних процесів системами звичайних диференціальних рівнянь, що містять керувальні змінні. Отримані результати дозволяють залучити широкий арсенал методів теорії керування динамічними системами до розв'язання задач керування квазістатичними процесами.

Ключові слова: квазістатичні процеси, рівноважна термодинаміка, математичне моделювання, робота, енергія, керованість, ентропія.

ALGORITHMS OF STATISTICAL ANOMALIES CLEARING FOR DATA SCIENCE APPLICATIONS

O. PYSARCHUK, D. BARAN, Yu. MIRONOV, I. PYSARCHUK

Abstract. The paper considers the nature of input data used by Data Science algorithms of modern-day application domains. It then proposes three algorithms designed to remove statistical anomalies from datasets as a part of the Data Science pipeline. The main advantages of given algorithms are their relative simplicity and a small number of configurable parameters. Parameters are determined by machine learning with respect to the properties of input data. These algorithms are flexible and have no strict dependency on the nature and origin of data. The efficiency of the proposed approaches is verified with a modeling experiment conducted using algorithms implemented in Python. The results are illustrated with plots built using raw and processed datasets. The algorithms application is analyzed, and results are compared.

Keywords: anomaly removal, anomaly detection, noise removal, statistical techniques, data analysis, big data, data cleaning.

INTRODUCTION

The Data Science techniques and approaches are widely used to solve modern day technical problems. One of frequent use-cases is implementing Back-End software components for distributed CRM and ERP with intellectual features. A possible format of input data for such systems is Big Data arrays that could be interpreted as numeric statistical samples. This kind of data is used in a variety of application domains, such as Commodity Trade and Risk Management systems, automotive applications like automated driver assistants, Unmanned Aerial Vehicle software, Computer Vision software responsible for raster-to-vector conversion et cetera [1–6].

In solutions from the aforementioned application domains, the underlying mathematical models are a priory known. Therefore, dataset processing is reduced to mapping data features to model properties. This allows to determine the trend line of a considered process both within observation range and beyond it (by means of interpolation and extrapolations – retrospective and perspective prognoses) [2–4]. This paper suggests treating the process of analytical model configuring as an unsupervised learning activity, since any solution of Artificial Intelligence problem, in its first iteration, is implemented as a process of parameters configuration with respect to input dataset [2–4]. Moreover, such models could be associated with artificial intelligence technologies because of the aforementioned and because of their prognosis features.

Statistical dataset processing is based on the hypothesis of accidental factors model that result in input dataset bias. Statistical data are usually obtained through experiments and sampling.

The first stage of step-by-step statistical analysis includes a preparatory stage — data research [2–4, 7]. Tasks of this stage include checking input Big Data array for anomalies. Any value that has a significant difference from the other dataset values could be treated as anomaly. Abnormal data is a result of various miscalculations and malfunctions during the data sampling. Two major types of anomalies are value skips and crude measurements. Both of these anomaly types, if not handled during next stages, will result in distorted results of statistical analysis. The distortions are represented with increased dispersion of scoring and/or with bias of scoring result [2–4, 7]. Possible ways to address the problem of distorted data are smoothing or evaluation.

In order to reduce influence of anomalies on further data processing, it is necessary to detect abnormalities and to restore or remove abnormal values. These actions could be translated to a tuple of stages that will represent the entire process of clearing dataset from abnormal values [3, 4, 7–10].

Anomaly detection is based on their analyzing properties with respect to absolute values, trend dynamics and statistical properties change [3, 4, 7, 9–10].

Related works. A significant amount of known approaches to anomaly clearing has been considered [7, 8]. They possess a common flaw – it is necessary to manually tune parameters with respect to input dataset and anomaly properties. Moreover, the majority of them will result in NP problems when applied to Big Data array. This makes their application impossible.

Therefore, the task of designing simple and efficient data clearing algorithms for Data Science purposes remains relevant.

Goal. The goal of the paper is proposing precise, performant, efficient and relatively simple algorithms for clearing datasets from anomalies.

Proposal. Experience of multiple IT proejcts related to Data Science allows to formulate practical requirements to algorithms responsible for anomaly detection and clearing. They include:

1. High efficiency of detection, integrity and adequacy of output, precise values of dispersion and standard deviation.

2. Relatively low computing complexity, therefore high performance with large datasets.

3. Automatic adjustment of parameters with respect to the input data properties, or minimal amount of manual settings;

Three algorithms of anomaly detection and removal have been developed to address these requirements.

Data preprocessing algorithm – the "sliding_wind" algorithm

The main idea of the algorithm is application of smoothing within a trivial sliding window. Within the window, an arithmetic mean value is calculated. The size of the sliding window is calculated in accordance to the demand of quasi-linear trend that describes the change considered process withing the window.

Sliding_wind algorithm stages:

1. Considering statistical sample $X = \{x_i\}$, $i = 1...n$ as an input.

2. Formulating *Nwin*-dimensional sliding window.

3. Calculating an arithmetic mean:

$$j = 1,...,N_{win}.$$

4. Formulating a clean dataset $\hat{X} = \{\hat{x}_i\}$, $i = 1...n$ by replacing elements of X sample with arithmetic mean $\hat{x}_j$: $x_{i=Nwin} = \hat{x}_j$, starting from the last entry within sliding window.

5. Shifting the sliding window to the next dataset dimension to the right – to $i = i + 1$.

6. Repeating steps 2–5 within input statistical sample $i = 1...n$.

7. After processing the entire dataset, in order to adjust data within the first sliding window, a subset *N=2Nwin* is created. After that, steps 2–5 are applied to this subset, traversing it in reverse.

The advantages of sliding_wind algorithm are its simplicity, minimum number of manual settings (only window size), potential for effective usage on datasets with fuzzy trend properties and anomalies and equal sizes of input and output.

It could be possible to include nonlinear estimation model for $\hat{x}_j$ inside sliding_wind algorithm, but it is inadvisable due to major increase in complexity. This would especially affect Big Data inputs.

Results of modeling and efficiency estimation of sliding_wind algorithm. For the modeling, a $n = 10000$ dataset has been considered. Quadratic trend and normal distribution are present in the dataset. Normal distribution has expected value of 0 and standard deviation $\sigma_X = 5.0$. Abnormal entries are evenly distributed within selection and constitute 10% of values. The model of trend and stochastic components is additive. Computations are conducted using Python implementation of algorithm [5, 6] using features of numpy and matplotlib libraries.

Results of sliding_wind execution are provided in Fig. 1.
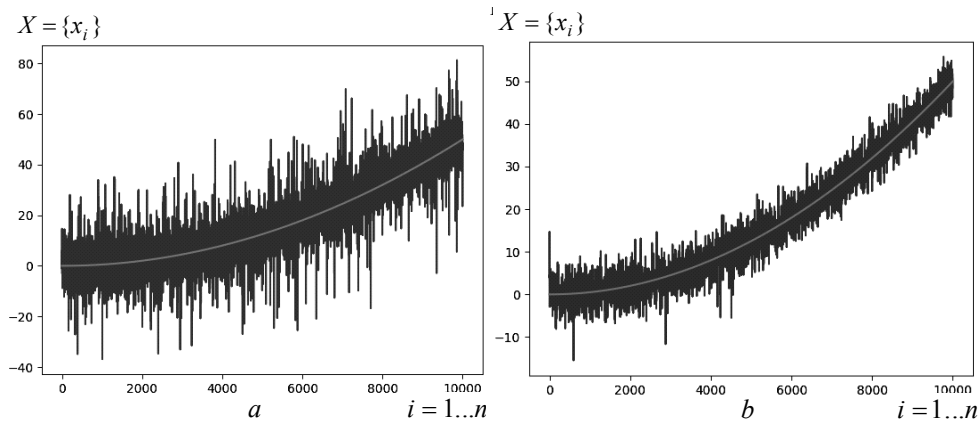
Fig. 1. Results of sliding_wind execution: *a* — input dataset, $\sigma_X = 6.64$; *b* — processed dataset, $\sigma_X = 2.95$

Fig. 1, *a* represents a plot built from input dataset $X = \{x_i\}$, $i = 1,...,n$ with normal noise and anomalies, as well as the trend line obtained via least squares method [3, 4]. Standard deviation of input dataset with anomalies is $\sigma_X = 6.64$. Fig. 1, *b* represents a plot built from dataset cleared from anomalies by means of sliding_wind algorithm. Standard deviation of such a dataset is $\sigma_X = 2.95$. Comparing plots 1, *a* and 1, *b*, as well as reduced value of standard deviation indicates efficiency of the sliding_wind algorithm.

Algorithm of dataset statistic properties control – the "medium" algorithm

The main idea of the algorithm is detecting abnormal elements by determining etalon parameters of dataset (expected value, standard deviation) without anomalies and comparing them with initial statistical features. Detected anomalies are replaced with arithmetic mean. Etalon and initial statistical features are derived from datasets that formulate initial initial and current sliding windows respectively.

Stages of medium algorithm:

1. Considering statistical sample $X = \{x_i\}$, $i = 1,...n$.

2. Within the first sliding window with size of *Nwin* dimensions, estimation of etalon expected value, standard deviation and dispersion is conducted:

$$\hat{x}_j^{\text{etalon}} = \frac{1}{Nwin} \sum_{j=1}^{Nwin} x_j \, , \quad \hat{D}_j^{\text{etalon}} = \frac{1}{Nwin-1} \sum_{j=1}^{Nwin} (\hat{x}_j - x_j)^2 \, ,$$

$$\hat{\sigma}_j^{\text{etalon}} = \sqrt{\hat{D}_j} \, , \quad j = 1...Nwin.$$

3. Formulating the next sliding window with size of *Nwin* dimensions is conducted.

4. Determining expected value, dispersion and standard deviation for sliding windows:

$$\hat{x}_j = \frac{1}{Nwin} \sum_{j=1}^{Nwin} x_j \, , \quad \hat{D}_j = \frac{1}{Nwin-1} \sum_{j=1}^{Nwin} (\hat{x}_j - x_j)^2 \, , \quad \hat{\sigma}_j = \sqrt{\hat{D}_j} \, , \quad j = 1...Nwin.$$

5. If the following condition is true

$$\hat{\sigma}_j > Q\hat{\sigma}_j^{\text{etalon}} \, ,$$

(Q — weighting factor), then current j-th dimension, added to sliding window is considered to be abnormal.

Abnormal j-th dimension is replaced with estimated expected value of current sliding window $x_i = \hat{x}_j$ inside $X = \{x_i\}$ dataset.

If condition $\hat{\sigma}_j > Q\hat{\sigma}_j^{\text{etalon}}$ is false, then the $X = \{x_i\}$ dataset is not modified.

6. Repeating steps 3–5 within statistical sample of $i = 1...n$.

7. The result of algorithm is dataset $\hat{X} = \{\hat{x}_i\}$, $i = 1...n$ clear of anomalies.

The main advantages of suggested algorithm are simplicity of implementation, statistical approach to determining abnormality of values, immutability of dataset when no anomalies detected, keeping the same size of dataset after processing.

One peculiarity of the algorithm is that etalon dataset should contain no anomalies. Also, Q weighting factor is determined proportionally to the size of abnormality bias.

Results of modeling and efficiency estimation of medium algorithm. Modeling conditions are the same as for sliding_wind algorithm. Research results are provided on Fig. 2, in equivalence to Fig. 1.
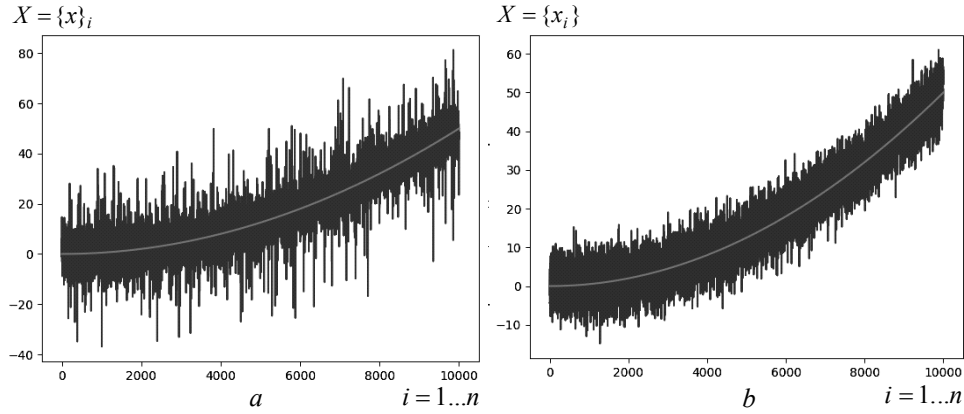
Fig. 2. Results of medium algorithm execution: *a* — input dataset $\sigma_X = 6.64$; *b* — rocessed dataset $\sigma_X = 4.45$

Comparing plots depicted at Fig. 2, *a* and 2, *b*, as well as standard deviation reduction ($\sigma_X = 4.45$) tells of medium algorithm efficiency.

Algorithm of control over dataset dynamic properties change — the LSM algorithm

The idea of the algorithm is in detecting abnormal values by determining etalon parameters of trend dynamic change speed, and comparing them to current properties using Least Squares Method. Etalon values of speed are calculated according to input dataset, and current values – according to sliding window selections. During comparison, the statistical estimation errors are respected.

LSM algorithm steps:

1. Considering input dataset $X = \{x_i\}$, $i = 1...n$.

2. Using polynomial model LSM, the etalon speed is calculated within dataset:

$Speed^{\text{etalon}} = c_2$, with LSM polynomial $T(x) = c_0 + c_1 x + c_2 x^2 + ...$

3. Formulating sliding window with $Nwin$ dimensions.

4. Determining current estimation of expected value, dispersion and standard error for the sliding windows:

$$\hat{x}_j = \frac{1}{Nwin} \sum_{j=1}^{Nwin} x_j \ , \ \hat{D}_j = \frac{1}{Nwin-1} \sum_{j=1}^{Nwin} (\hat{x}_j - x_j)^2 \ , \ \hat{\sigma}_j = \sqrt{\hat{D}_j} \ , \ j = 1...Nwin.$$

5. Determining controlled parameters for abnormality that are scaled up to size of the datasets with scores and respecting dimension errors:

$$\text{Ind\_1} = \left| Speed^{\text{etalon}} \cdot \sqrt{n} \right|, \ \text{Ind\_2} = \left| Q \cdot \hat{\sigma}_j \cdot Speed^{\text{etalon}} \cdot \sqrt{Nwin} \right|,$$

(Q — setting weighting factor).

6. If condition is true

$$\text{Ind\_2} > \text{Ind\_1} \ ,$$

then current j-th dimension added to sliding window is treated as anomaly.

Abnormal j-th dimension is replaced with LSM score $x_i = T(x = \hat{x}_j)$ inside dataset $X = \{x_i\}$.

If condition $\text{Ind\_2} > \text{Ind\_1}$ is false, $X = \{x_i\}$ dataset remains immutable.

6. Repeating steps 3–5 within input dataset $i = 1...n$.

7. The result of algorithm is dataset $\hat{X} = \{\hat{x}_i\}$, $i = 1...n$ clear of anomalies.

The main advantages of suggested algorithm are simplicity of implementation, dynamic criteria of abnormality, modification of abnormal elements only, same size of input and result datasets.

One peculiarity of algorithm is that it does not require parameter control when determining etalon values; the weighting factor Q is determined proportionally to the size of abnormality bias.

Results of modeling and efficiency estimation of LSM algorithm. Modeling conditions are the same as for sliding_wind algorithm. Results are depicted at Fig. 3. Equivalent to Fig. 1.

$X = \{x_i\}$
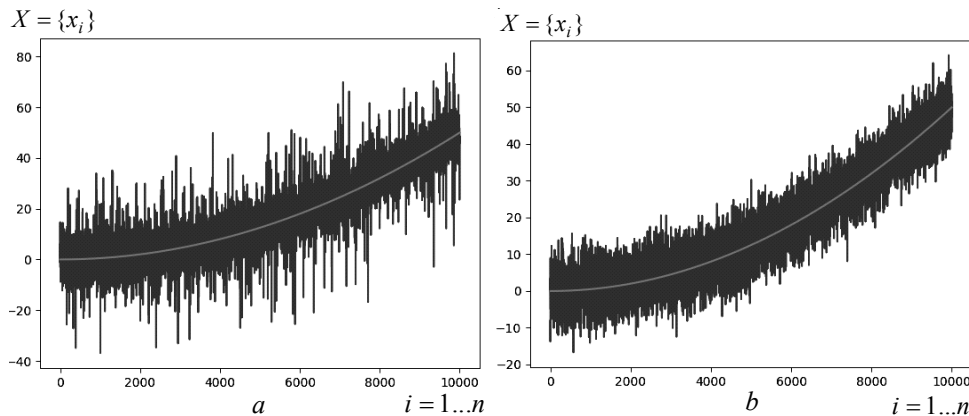
Fig. 3. Results on MNK algorithm execution: *a* — raw dataset $\sigma_X = 6.64$; *b* — processed dataset $\sigma_X = 4.71$

Comparison of plots depicted at Fig. 3, *a* and 3, *b*, as well decreasing standard deviation ($\sigma_X = 4.7$) illustrates algorithm efficienccy.

Generalized statistical properties and reduction of bias with three proposed algorithms are depicted at table.

Generalized statistical properties of three proposed algorithms

Raw data with abnormalities	sliding_wind	medium	MNK
$\sigma_X = 6.64$	$\sigma_X = 2.95$	$\sigma_X = 4.45$	$\sigma_X = 4.71$

Data from table demonstrate that sliding_wind algorithm is the most successful precision-wise — it has the least standard deviation. This algorithm is also the most productive and has no need for configuration. However, it may be unapplicable to dynamic strongly nonlinear processes — its usage may result in biases. Medium and MNK algorithms are the opposites to sliding_wind. In order to choose specific algorithm, dataset properties and anomaly features (such as margin of error or the nature of the trend model) have to be considered. Comparing proposed methods with more sophisticated alternatives gave no results, since using data of equivalent complexity (*N*=10000) yielded no results from these alternatives in sensible time.

Conclusions. The proposed algorithms are not expensive to implement, they do not require major manual tuning and show acceptable precision and performance for Big Data arrays processing.

REFERENCES

1. F. Provost and T. Fawcett, *Data Science for Business.* USA: O'Reilly Media, Inc, 2013, 409 p.
2. D. Dietrich, *Data Science & Big Data Analytics: Discovering, Analyzing, Visualizing and Presenting Data.* Indianapolis, Indiana, USA: John Wiley & Sons, Inc, 2015, 420 p. doi: 10.1002/9781119183686.ch1.
3. O. Pysarchuk and V. Kharchenko, *Nonlinear multi-criteria process modeling in traffic management systems*, (in Ukrainian). Kyiv: Institute of Gifted Child, 2015, 248 p.
4. S. Kovbasiuk, O. Pysarchuk, and M. Rakushev, *Least Squares Method and its practical applications*, (in Ukrainian). Zhytomyr: Zhytomyr Military Institute, 2008, 228 p.
5. S. Raschka, Y. Liu, and V. Mirjalili, *Machine Learning with PyTorch and Scikit-Learn: Develop machine learning and deep learning models with Python.* Birmingham: Packt, 2022.
6. P. Joshi, *Artificial Intelligence with Python.* Birmingham: Packt, 2017.
7. G. Kishan, K. Chilukuri, and H. HuaMing, *Anomaly Detection Principles and Algorithms.* Switzerland, Springer, 2017, 229 p. doi: 10.1007/978-3-319-67526-8.
8. O. Pysarchuk and Y. Mironov, *Chromosome Feature Extraction and Ideogram-Powered Chromosome Categorization.* Switzerland, Springer, 2022. doi: 10.1007/978-3-031-04812-8_36.
9. H. Blomquist and J. Möller, *Anomaly detection with Machine learning. Quality assurance of statistical data in the Aid community.* Uppsala: Uppsala University, 2015, 60 p.
10. S. Thudumu, P. Branch, J. Jin, and J. Singh, *A comprehensive survey of anomaly detection techniques for high dimensional big data.* Switzerland, Springer, 2017, 30 p. doi: 10.1186/s40537-020-00320-x.

INFORMATION THE ARTICLE

Oleksii O. Pysarchuk, ORCID: 0000-0001-5271-0248, National Technical University of Ukraine "Igor Sikorsky Kyiv Polytechnic Institute", Ukraine, e-mail: PlatinumPA2212@gmail.com

Danylo R. Baran, ORCID: 0000-0002-3251-8897, "Codeimpact B.V", Ukraine, e-mail: danil.baran15@gmail.com

Yurii G. Mironov, ORCID: 0000-0002-2291-5864, National Aviation University, Ukraine, e-mail: yuriymironov96@gmail.com

Illya O. Pysarchuk, ORCID: 0000-0003-4343-0142, National Technical University of Ukraine "Igor Sikorsky Kyiv Polytechnic Institute", Ukraine, e-mail: flimka134@gmail.com

АЛГОРИТМИ ОЧИЩЕННЯ СТАТИСТИЧНОЇ ВИБІРКИ ВІД АНОМАЛІЙ ДЛЯ ЗАДАЧ DATA SCIENCE / О.О. Писарчук, Д.Р. Баран, Ю.Г. Міронов, І.О. Писарчук

Анотація. Розглянуто природу даних, що використовуються в задачах сучасних прикладних областей. Запропоновано декілька алгоритмів очищення статистичної вибірки від аномалій в конвеєрі задач Data Science. Відзнакою та перевагою запропонованих алгоритмів є їх відносна простота та обмежена кількість параметрів налаштувань, що визначаються за технологіями навчання відповідно до властивостей вхідних статистичних даних. Запропоновані алгоритми є достатньо гнучкими у використанні і не залежать від природи та походження даних. Результати модельного експерименту запропонованих підходів у вигляді скриптів мовою Python та базових бібліотек довели їх ефективність. Результати проілюстровано графіками, побудованими з використанням початкових даних та даних, що змінені за допомогою запропонованих алгоритмів. Застосування алгоритмів проаналізовано та порівняно результати виконання алгоритмів.

Ключові слова: очищення від аномалій, виявлення аномалій, видалення шуму, статистичні методи, аналіз даних, великі дані, очищення даних.

OPTIMIZATION OF ROUTE DISTANCE USING K-NN ALGORITHM FOR ON-DEMAND FOOD DELIVERY

PRADIP M. PAITHANE, SARITA JIBHAU WAGH, SANGEETA N. KAKARWAL

Abstract. Customers are now more able to purchase goods over the phone or the Internet, and the ability for those purchases to be delivered safely to the customer's location is proliferating. On-request meal delivery, where customers submit their food orders online, and riders deliver them, is growing in popularity. The cutting-edge urban food application necessitates incredibly efficient and adaptable continuous delivery administrations toward quick delivery with the shortest route. However, signing up enough food parcels and training them to use such food-seeking frameworks is challenging. This article describes a publicly supported web-based food delivery system. IoT (Internet of Things) and 3G, 4G, or 5G developments can attract public riders to act as publicly sponsored riders delivering meals using shared bikes or electric vehicles. The publicly funded riders are gradually distributed among several food suppliers for food delivery. This investigation promotes an online food ordering system and uses K-Nearest Neighbor calculations to address the Traveling Salesman Problem (TSP) in directing progress. The framework also uses the Global Positioning System (GPS) on Android-compatible mobile devices and the TOM-TOM Routing API to obtain coordinates for planning purposes. To evaluate the presentation of the proposed approach, recreated limited scope and certifiable enormous scope on-request food delivery occurrences are used. Compared to the conventional methodology, the proposed strategy reduces the delay time. Each rider will receive the most direct route to the order delivery address. The delivery delay time is reduced by approximately 10–15 minutes for every order. The food supplier can determine whether an item is available to the rider; thus, the food supplier can add an order to the rider having the shortest way.

Keywords: crowd-sourcing, hybrid optimization on-demand food-delivery, *k*-nearest neighbor algorithm (KNN), route optimization, traditional search (ts), urban logistic.

INTRODUCTION

The development of mobile Internet over the past few decades has made it possible to use smartphones for online ordering and delivery (like Domino's deliveries). By enhancing client happiness, a service provider can grow their customer base [1]. To make it better, you'll have a food ordering system that enables consumers to purchase products without physically going to the store, but also possibly using a phone or the internet, and after delivering them safely and in good condition to the specific customer's home. Users of the OCD service should place online orders for delivery of takeout food from crowd-sourced riders.

OCD framework enables food supply shops to accept food orders booked by customers through their computers or smartphones and then prepare personalized food and drinks[2]. With the help of on-demand couriers, customers of small catering businesses and food businesses can receive omnipresent scalable and affordable food service.

Deliveries make sure that the appropriate consumers receive the requested meal as quickly as feasible. The online-food in a sector where numerous small food suppliers often enter and exit. For these little food merchants, hiring a fleet of shipment boys would be quite expensive [3]. Additionally, because catering orders vary, it is challenging to modify the delivery team accordingly. However, some customers may be impatient and unable to wait many days for their food [4].

This suggested framework has encouraged a creative publically supported strategy framework to deliver parcels using already-existing taxicabs, hence reducing the task's time cost. This pioneering study demonstrated the viability of public funding in the last-mile transportation sector [5]. Food delivery is contingent on public support when requested. An online business known as "crowd-sourced delivery" for food is made up of riders, restaurants, customers, and publicly backed cargo[6]. Customers can order meals from catering shops via Food-Net. Cooking establishments accept customer orders to produce personalized food packages that are subsequently delivered by volunteers in place of the cafés' delivery personnel. The publicly supported riders register with the Online Crowd Sourced Delivery system, accept their assigned delivery commitments, visit the cafés, purchase the food packages, and deliver them to the relevant customers [7].

The food cloud attracts members of society at large to travel as delivery riders. Such crowded drivers can complete delivery tasks using shared bikes or electric motor bicycles using IoT and 3G, 4G, and 5G advancements[8]. In this way, the recently created online crowd-sourced delivery system can adapt to meet changing client requests [9]. The online crowd-sourced delivery method can reduce the cost of hiring delivery staff, in the opinion of the food suppliers[10]. The OCD method will aid vulnerable people, alleviate traffic congestion, and reduce emissions from fossil fuels. To reduce the absolute trip expense and delivery delay, a numerical model of the widely accepted delivery issue is developed [11]. The planning system makes use of Google Maps, an innovation of the Global Positioning System (GPS) [12]. By using one of the TSP solutions, heuristics calculation, the framework may speed up the delivery direction cycle. The matching of riders and suppliers is done via an expense-based coordination formula. Every rider's and supplier's respective moving costs are calculated. The problem is solved using a crossover meta-heuristic calculation that combines the Tabu Search and Adaptive Large Neighborhood Search methodologies for flexible large-area searches. Systems in Shenzhen that are both copied and truly demonstrate the validity, effectiveness, and distinctive advancement structure of the system that is being presented.

MOTIVATION

Today's unemployment is a growing issue, and this approach is suggested as a solution. The delivery wait time is longer than with more modern route optimization techniques. According to reports, it will lessen traffic problems during the delivery. To satisfy customer demands for prompt and accessible meal delivery [13]. A quick and comparatively simple way to get lunch delivered on demand

and on the same day. Since not every restaurant can afford to pay someone to deliver food, this approach will also solve that issue. A crowdsourced online delivery method that organizes between restaurants, clients, and crowdsourced riders can travel to the food supplier using this system while minimizing their overall travel costs and optimizing their route [10]. To distribute food delivery jobs and create high-quality delivery training in real-time. Overcome both the carbon emissions that result from transportation congestion. The on-demand food vendor is provided with a crowdsourced shipping method. Food delivery services that are quick to deliver food are essential, as demonstrated by the meals on call for the transport industry. Through an online dynamic optimization framework [14], the time options of the customers and crowd-sourced riders are addressed. The neighbor customer order details and the quickest route are managed using the *K*-Nearest Neighbor algorithm in this study. Following each food delivery, the rider and supplier can calculate the shortest route and closest location for the food order because they are exchanging information with one another.

METHODOLOGY

We conducted the research, and the authors followed a set of processes to determine the optimal path for the rider to deliver the food on time.

In each step, the activities are:

1. Observe the business process of different meal delivery services in the local area near the city. The proposed On-Demand Food Delivery via Online Crowdsourced in this study is based on these observed business processes.

2. Study of GPS technology to gain information, data, and expertise for the system's development. The developed application in this study makes use of Android handsets' GPS capability.

3. Examine the Tom-Tom API. This procedure seeks to investigate the characteristics and capabilities of Tom-Tom API for Maps. The research makes use of the internet and university library resources.

4. The author conducts analysis using the results of phases (1), (2), and (3) to create comprehensive knowledge for designing the system.

5. The author designs the system in the design phase utilizing the information gathered during the analysis phase. The blueprint for the created system is provided in this phase.

6. The application is developed utilizing the specified technology and tools during the implementation phase.

7. A testing phase is initiated to confirm the application's functionalities, during which the program is tested using many test cases

Food Ordering System via Online Crowdsourcing

Figure 1 depicts the architecture of the created online food ordering system. The main applications of the food ordering system are:

On-Demand Online Crowdsourcing application on the web. A rider has access to this application and can deliver orders after logging in. For the admin, this app is used to log in a rider who has placed an online purchase, input the order into the program, and create information about the outlet that will handle the re-

quest and the route that Delivery Staff should follow. The application is also used by the administrator to receive orders and prepare food. Customers can also use this web-based tool to check the status of their orders.
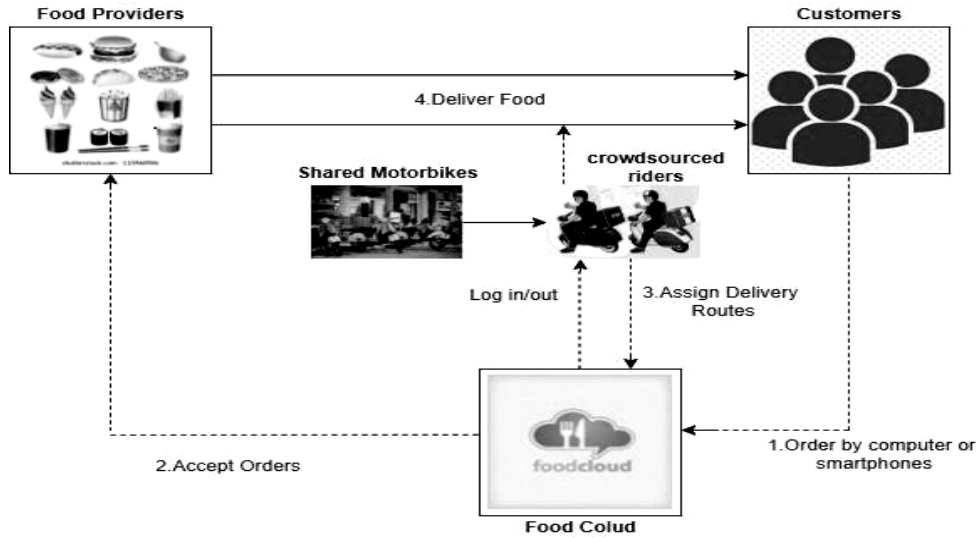

Fig. 1. The Crowdsourced on-demand Food Delivery System

K-Nearest Neighbor Algorithm for Routing Optimization

Steps:

Algorithm 1: K-Nearest Neighbor Algorithm

Input: *I*: The order set, *J*: The provider set, *K*: The rider set, $C_{a,b}$: Travel Cost, $T_{a,b}$: Travel Time, *i*: order, $a =$ placed by provider

Output: The initial routes *K*
1. sort_orders(I)
2. inserted node set $D =$ empty
3. for all $i \in I$ do
4. $f_{\min} \leftarrow \infty, i_{best} = -1$
5. for all $a \in D$ Do
6. initialize route for $a : k \leftarrow (a)$
7. if $f_{\min} > insert\_\cos t(a,i)$ and $Q_k < q_k$ Then
8. $f_{\min} = insert\_\cos t(a,i)$
9. $i_{best} = a$
10. end if
11. insert_node (i_{best}, i)
12. $D \leftarrow D \cup i$
13. end for
14. end for

The below algorithm is used for demand match between rider and provider for a new shortest path for the next location address.

Algorithm 2: Rider Provider Matching

Input: J: The provider set, K: the rider set

Output: The initial routes $k(p)$

$C_{kj} \leftarrow calculate\_travel\_\cos t(K,J)$, for all K and all J

2. Store step 1 cost in a queue L,

3. Initialize rider status for route: $s_k = $ false

4. Initialize current total load of route: $q_j = 0$

5. for all $c_{kj} \in L$ do

6. if $s_k = $ false and $q_j + q_k < Q_j$, then apply K-Nearest Neighbor algorithm

7. $s_k = $ True, $q_j^+ = q_k$

Above equation is used for update shortest path with rider data.

8. update the rider's provider: $k_j = j$

9. end if

10. end for

The Q_j is total number of provider orders. The above algorithm is used for the determination of the shortest path for new orders as per the current status of the order and the location of a rider.

The Rider Provider Matching algorithm is working on the total calculated travel cost and a queue of riders available for the same route. In the first step, the initial route will be calculated as per the travelsellsman algorithm. In the second step, collect the status of all riders and the status of available food items in the basket. The new cost of distance will be calculated from the current status of riders. The proposed algorithm is used to get an updated route with the help of step number 7 and 10.
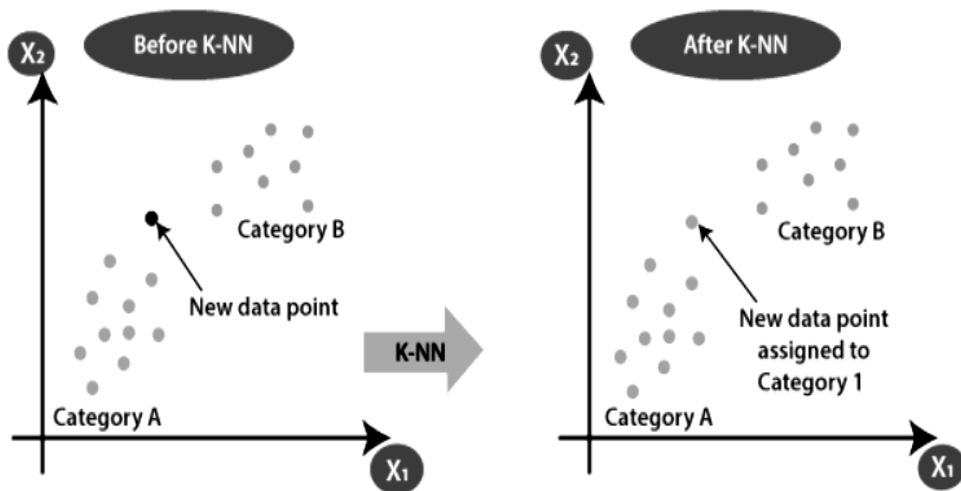

Fig. 2. K-Nearest Neighbor Graph

The output of this algorithm is the sequence of steps as the TSP solution. A simple web-based application was developed to test the heuristic algorithm for routing optimization. This testing application also utilizes TOM-TOM API for

Map [15]. In this application, the user can input several locations/addresses, and then Maps API will return the coordinate of those locations [16]. This function can be seen in Fig. 3, which shows an example of the optimized route for four addresses. In this application, point 1 is the initial and end point. The table with blue cells contains the data about the distance between two points that are generated using Google Maps API. Meanwhile, the table with red and yellow cells contains the solution for optimized routes [17].
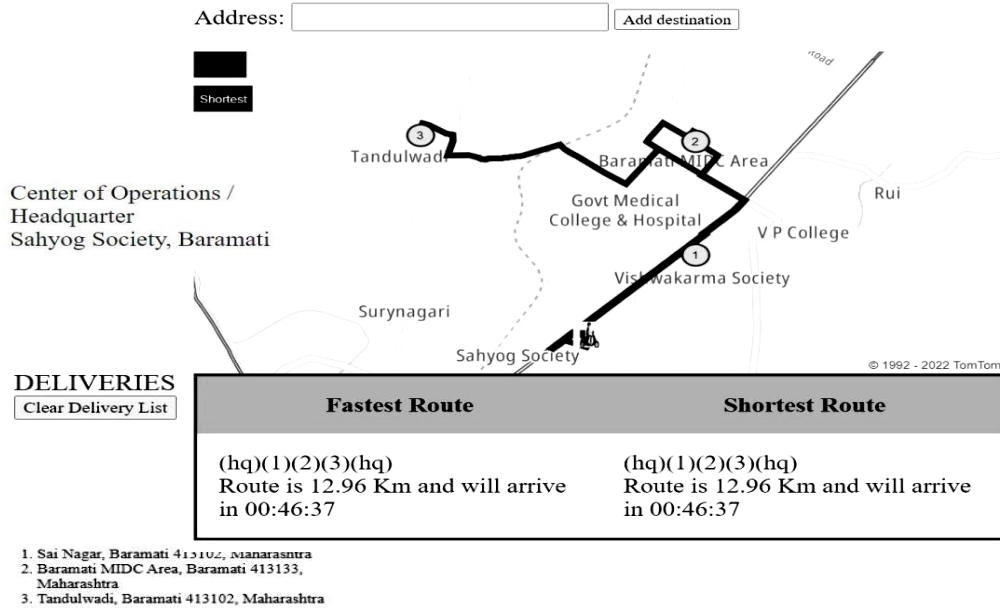

Fig. 3. Shortest Route for Food Delivery

As the Customer and Admin want to know the real-time location of the Rider for tracking purposes as shown in Fig. 4.

Fig. 4. Location of Rider

Mathematical Model

$$F = \beta_1 \sum_{k \in K} \sum_{a \in A} \sum_{b \in A} x_{ab}^k * c_{ab} + \beta_2 \sum_{a \in I} \max(0, T_a^k - t_a^e). \qquad (1)$$

The objective of OCD is the weighted travel cost and delivery delay, as shown in Eq. 1, where $\beta1, \beta2 \in [0,1]$ are weight parameters, a,b — source delivery and destination delivery location respectively, k — rider's index, T_a^k — arrival time of rider for delivery at node a, t_a^e — arrival time of rider from node a to provider location e, e- provider location, $C_{a,b}$ — weighted traffic cost from a to b delivery station

$$\sum_{a \in I \cup J} \sum_{k \in K} x_{ab}^k = 1 \quad \forall b \in I, \qquad (2)$$

where I-the set of users, b-next destination location, x-travelling distance cost, J: The provider set, K: the rider set

$$\sum_{b \in I \cup J} \sum_{k \in K} x_{ab}^k = 1 \quad \forall a \in I, \qquad (3)$$

The certain restrictions defined in Eq. 2 and Eq. 3 require that all accepted user orders must be provided and delivered.

$$\sum_{a \in I \cup J} x_{ab}^k = \sum_{a \in I \cup J} x_{ba}^k \quad \forall b \in I, \ \forall k \in K. \qquad (4)$$

Eq. 4 requires a crowd-sourced rider to leave a user's location after delivering that user's delivery order.

$$T_a^k + t_{ab} = T_b^k \leftarrow x_{abk} = 1 \qquad \forall a \in I. \qquad (5)$$

Eq. 5 states that the arrival time at user "b" is equal to the arrival time at the previous user "a" plus the travel time from node "a" to node "b", $t_{a,b}$. Note that the travel time $t_{a,b}$ can be updated using dynamic transportation analysis techniques, "x_{abk}" is travelling distance cost by k rider from "a" to "b".

$$Q_a^k \leq q_k \leftarrow \sum_{b \in I} x_{ab}^k = 1 \quad \forall k \in K. \qquad (6)$$

Eq. 6 ensures that the total amount delivered by crowd-sourced rider R does not exceed its capacity q_K.

$$x_{ab}^k \in \{0,1\} \quad \forall a, b \in I \cup J, \ \forall k \in K. \qquad (7)$$

Eq. 7 defines the decision-variables.

In the above diagram, the *K*-Nearest Neighbor algorithm is used for the identification of the shortest path for the initial stage as well as the new order launch in the system. After improving the shortest path, the system is going to check the availability of riders for the next delivery order location and transfers or updated route share with an available rider. The *K*-Nearest Neighbor algorithm is focusing on neighbor values with the help of distance values. The closer neighbor distance value is performing a vital role in the identification of the shortest path route only [18].
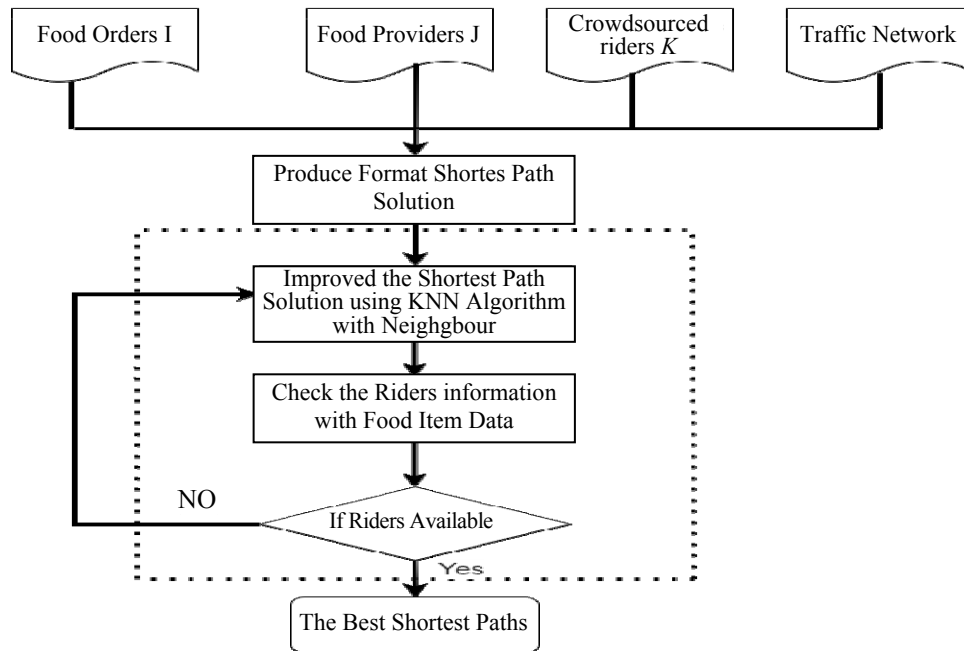
Fig. 5. Shortest Path Identification

EXPERIMENTAL RESULT

Result Analysis for Online Crowd-sourced Delivery vs. Traditional Approach

The proposed method is compared with a traditional method. The traditional method is used for food delivery with additional time for searching for the correct destination. In the OCD method, riders are getting updated information on their destination with location and delay time[19]. Based on the above information, Rider can transfer the same order to the nearest rider for delivery of the order so the waiting period is reduced.

The real-world OCD dataset consists of 10 instances from Baramati, Pune. The dataset covers the central business area as well citywide area of Baramati. Each instance consists of 435–1250 orders along with a set of providers and crowdsourced riders. The customers' preferred delivery times span the lunch period, from 11:00 AM to 2:00 PM, and another slot from 6.00 PM to 9.00 PM.

The travel speed is set to the average of the speeds of a bicycle and a motorcycle. The population of Baramati city is near about 200.000 and many people from Baramati MIDC are using food delivery applications for fast delivery. Heavy traffic and a limited number of a rider are major constraints to delivering food items at a scheduled time. The proposed system overcomes this drawback with updated delivery address information and updated rider details[20].

The presented dynamic crowdsourced food delivery framework was implemented in Python. The experiment was conducted on a personal computer equipped with an Intel(R) Core(TM) i7-4790 CPU @3.60 GHz and 16 GB of RAM. Two baseline algorithms were employed to solve the OCD instances for comparison with the presented hybrid solution method. The computing time for CPLEX was limited to 7200 seconds. The second algorithm used for comparison was the normal TS metaheuristic implemented in Python [21].

T a b l e 1. Detail Comparison of Proposed Method with Traditional Method

Sr.No	Provider Location	User Location	Rider Number	Time (Min)	Distance by Proposed KNN Method(Km)	Distance by Proposed Tra- ditional Search(Km)	Waiting Time using Proposed Method(Min)	Waiting Time using Traditional Method (Min)
1	Saily Nagar	Rui Hospital	R1	8	4	4	2	6
2		Tandulwadi	R2	10	12	18	4	8
3		Muktai Lawns	R3	6	3	13	3	9
4		Reliance Mart	R1	12	20	25	5	12
5	Vivekanad Nagar	Vidyanagari	R1	11	18	22	7	20
6		Suryanagari	R2	5	3	8	2	4
7		Shriram Nagar	R2	12	5	5	4	22
8	Kasaba	Baramati Bus Stand	R1	13	3	3	5	8
9		Malegoan	R3	8	10	10	3	16
10		Desai Estate	R1	18	5	5	2	19

T a b l e 2. Performance analysis of OCD with the tradition method according to distance and time parameter

Sr.No	Distance OCD	Distance Travel by Traditional Way	Extra Distance	Time OCD	Time Travel(Min) Traditional Way	Delay(min)
1	3.7	3.7	0	0+8	8	0
2	4	5+4	5	0+10	13+10	13
3	2.9	4.8+2.9	4.8	R1=8+6	9+6	9
4	6.2	1.2+6.2	1.2	R3=0+11	4+11	4
5	1.1	5.1+1.1	5.1	R2=10+5	12+5	12
Total	17.9	34	16.1	58	78	38

Comparision between OCD and Traditional Method using Distance
*1* — OCD Distance; *2* — Traditional Distance
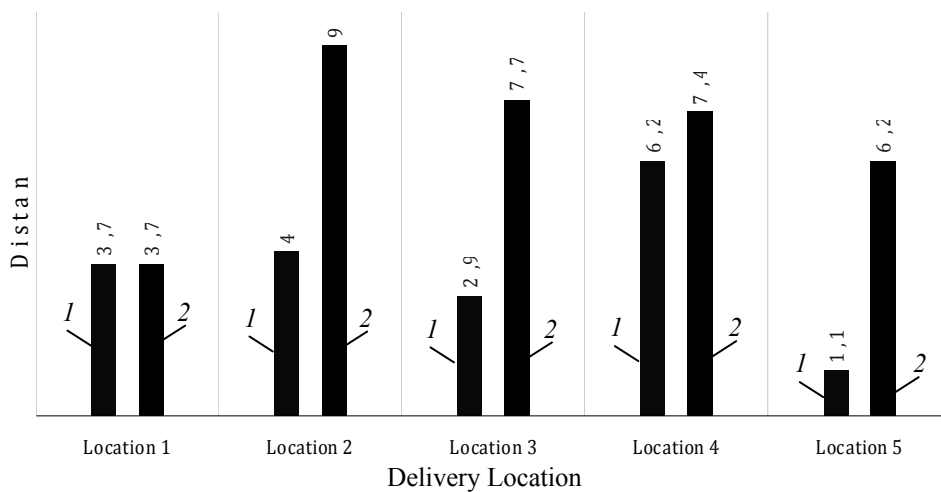
Fig. 6. Comparison between OCD and Traditional Method for Food delivery

Comparison between OCD and Traditional Method using Distance

*1* OCD Method Time   *2* Traditional Method Time
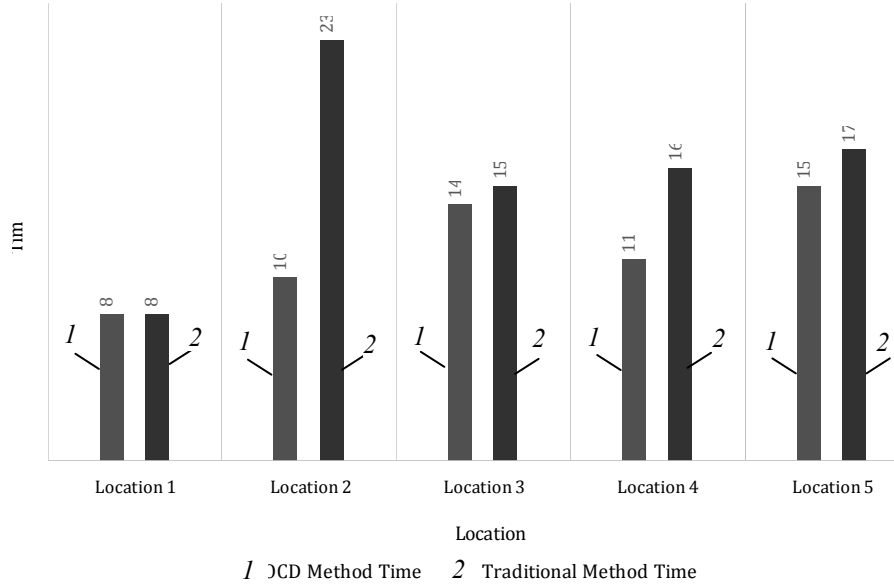
Fig. 7. Comparison between OCD and Traditional Method for Food delivery using Time Parameter

- A key feature of the proposed OCD method is that crowd-sourced riders are not tied to a single supplier, unlike the traditional approach, and can move between food suppliers. By limiting each passenger to a single vendor, the system simulated traditional food delivery logistics and compared the results.

- Crowd-Sourced food delivery goes beyond traditional logistics. As riders are spread across food vendors, which results in a reduction in median-total-travel-distance, and at the same time, the median total delivery delay is improved.

Above Table 3 depicted the detail comparison of traditional and K-Nearest Neighbor approach performance using time, distance and delay parameter.

T a b l e 3. Performance Analysis of the Traditional Approach and KNN approach

| Loca-tion	Rider No	Traditional Approach				KNN Approach			
		Obj	Time (Min)	Dist (Km)	Delay (Min)	Obj	Time (Min)	Dist (Km)	Delay (Min)
L1	R1	32.52	8	4	6	30.21	2	4	2
L2	R2	56.24	10	12	8	54.34	4	3	4
L3	R3	51.33	6	3	9	48.53	3	1	3
L4	R1	68.22	12	20	12	65.20	5	12	5
L5	R1	28.4	11	18	20	25.64	7	12	7
L6	R2	49.25	5	3	4	46.35	2	1	2
L7	R2	65.33	12	5	22	62.53	4	2	4
L8	R1	74.44	13	3	8	72.47	5	1	5
L9	R3	67.22	8	10	16	64.24	3	2	3
L10	R1	33.4	18	5	19	32.4	2	1	2
Average		52.64	10.3	8.3	12.4	50.20	3.7	3.9	3.7
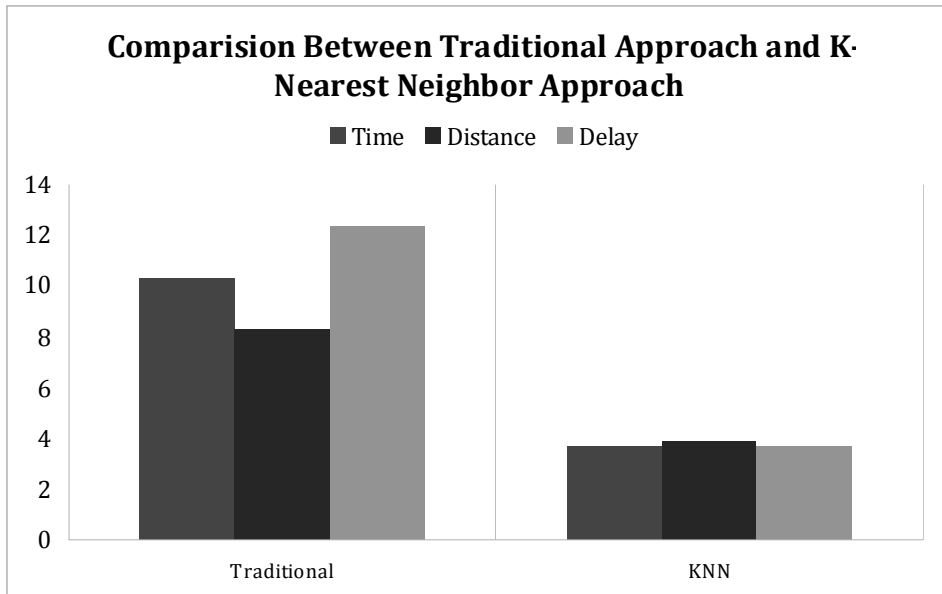
Fig. 8. Comparison between Traditional Approach and K-Nearest Neighbor Approachs

The K-Nearest Neighbor approach is reduced the time, delay and distance value for online food delivery process.

In above Fig. 9, the food delivery process is performed by the traditional method among all food suppliers. In this 3 food suppliers, 3 riders, and 6 customer locations are mentioned. The red line indicates the route path of rider 1 for provider A, the green line indicates the route of rider 2 for provider B and the blue line indicates the route path of rider 3 for provider C. Traditionally, the total 78 distance is covered by providers with 38 min minimum delay delivery time. The shortest path is not identified by Google Maps for the same process so an additional delay has been added to this method. Google map fails to detect the next order location with the shortest path because of the unavailability of food and other rider location data.

The proposed OCD system consists of information available for food item information, nearest neighbor rider information, and updated order with shortest path information. The proposed OCD method reduced the delivery delay time and identified the shortest path for the next order location.

From Fig. 9 and Fig. 10, we can claim that the KNN method is reduced the distance for food delivery location.

In Fig. 9, the traditional search algorithm has been used and the total distance covered by Rider is near about 56 km in figure 10, the K-Nearest Neighbor approach has been used and the total distance covered by the rider is 33 km only.
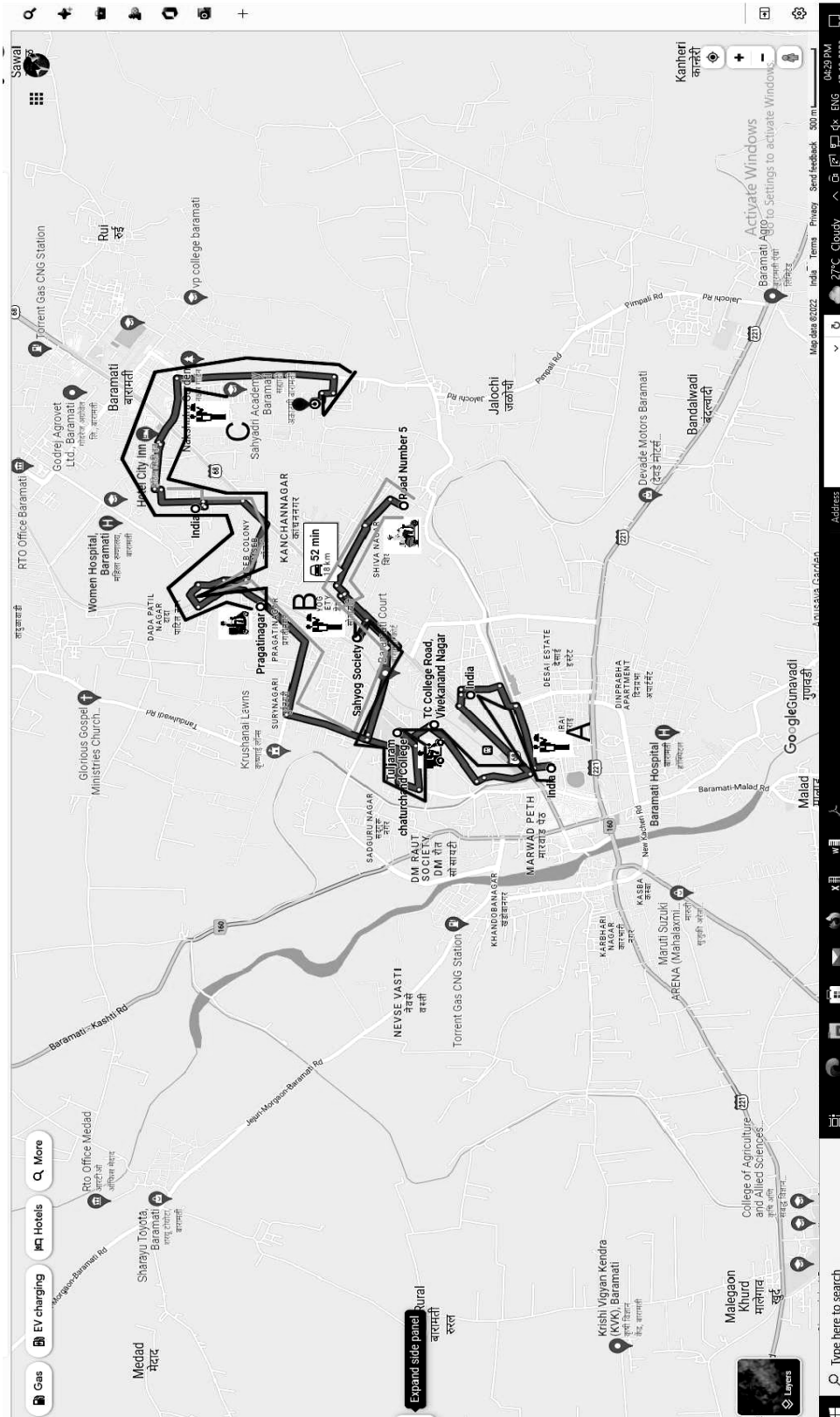
Fig. 9. Traditional Method for Food Delivery
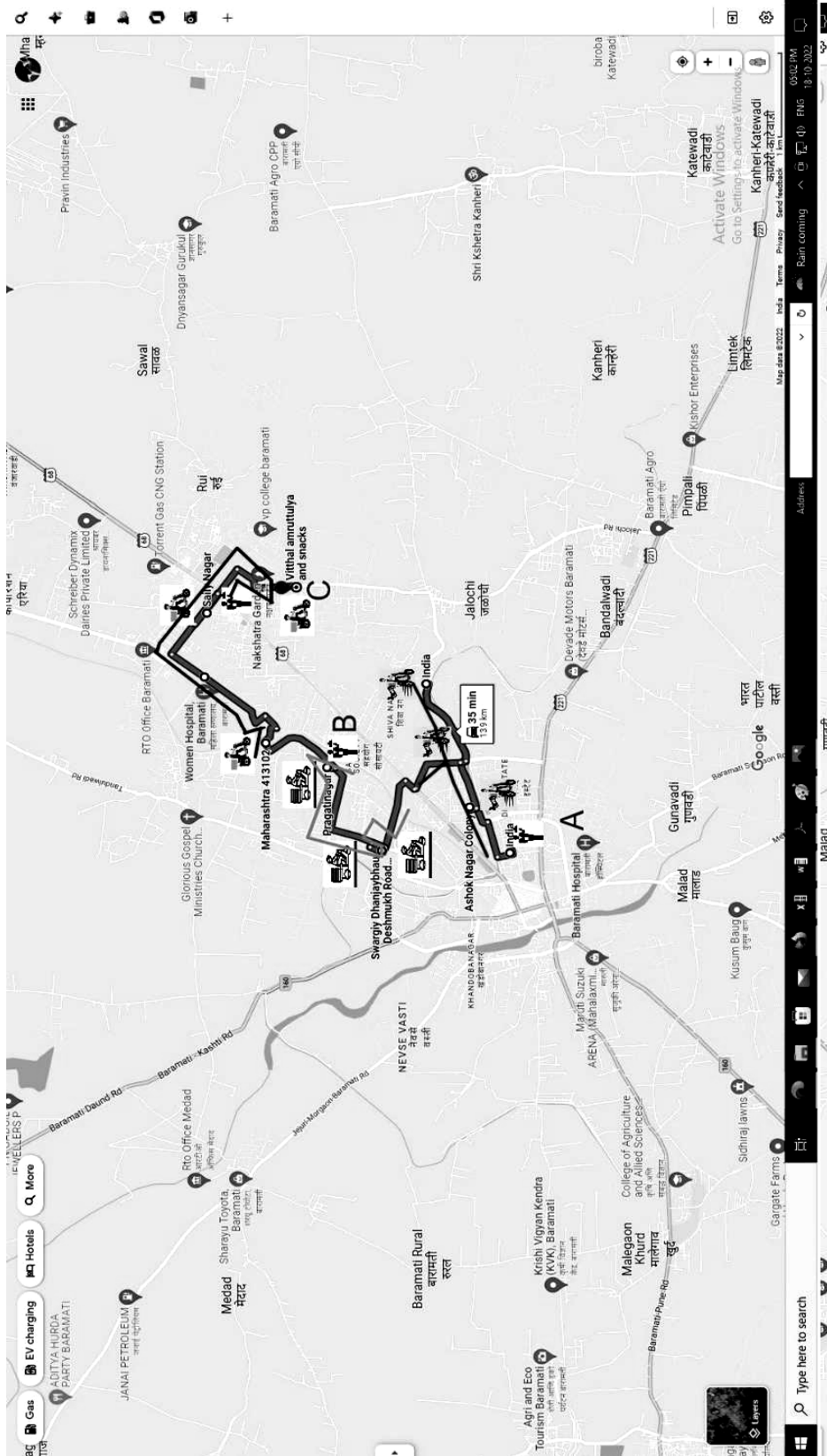
Fig. 10. K-Nearest Neighbor Shortest Path for Food Delivery Application

User Characteristics and Main Functions

The following are the major functions of the delivery system:

1. The registration of customers. This allows customers to save personal information for future orders. Customers must also register before they can place an order in the system.

2. The ability to delegate outlets. This function selects the most appropriate outlet to handle the order. The distance between the outlet and the customer's address is taken into account.

3. Create a delivery address routing that is optimum. The system generates optimized routing to provide detailed information about the sequence of delivery routes.

4. Management of orders. Order management allows the restaurant's workers to get order information and track the progress of each step.

5. Verification of order status. This feature allows customers to keep track of the status of their orders.

6. Order closure is a feature that allows you to close an order. This function is used to close an order by changing the order's status to "handled" and reporting the payment.

Aside from that, the application should be able to configure the following:

1. The outlet's address and exact coordinates.

2. An outlet's opening and closing times. This setting ensures that the order is handled by the only accessible outlet.

3. A delivery fee is a sum of money that the customer must pay to receive delivery service. This fee will be applied to the order bill automatically.

4. A food menu from which the customer can order.

5. The number of vehicles and delivery personnel available.

Web Service

A web service mediates data transmission between web-based applications. Users can obtain order information generated by the web-based application through the web service. The web services additionally provide a function that allows the Rider to update his current location.

The development tools for developing Online Crowd-Sourced Food Delivery can be seen in Table 4.

T a b l e 4 Development Tools

USER	ACTIVITIES
Platform	Microsoft Windows
Application Server	XAMP Server ,MySQL Server
IDE	Sublime Text
Technology	Web Service, CSS, Apache HTTP Server
Database	MySQL
Programming Languages	PHP, Java, Javascript, HTML
API	TOM TOM

After coding the application, the screenshot of the web-based food ordering system homepage can be seen in Fig. 11
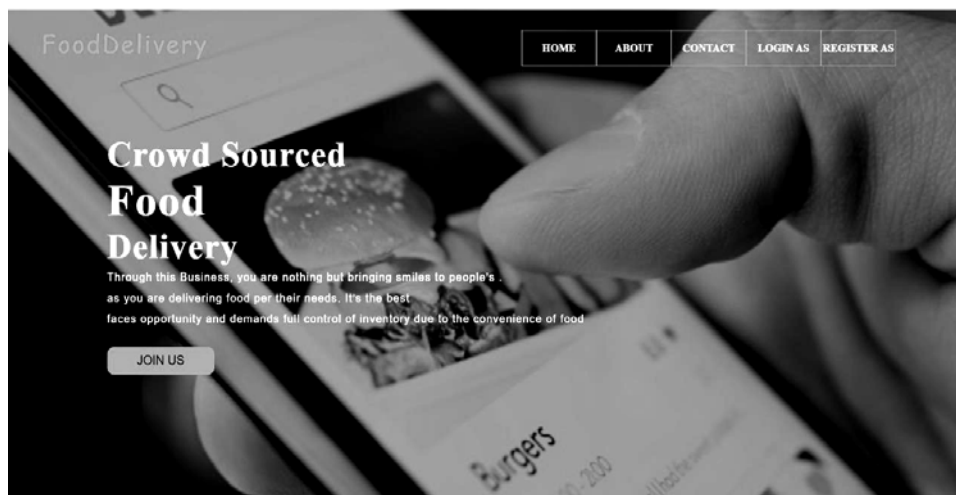

Fig. 11. Screenshot of the web-based food ordering system

CONCLUSION

This study suggested and created a web-based application for On-Demand Food Ordering using Online Crowdsourcing. In this research work, the utilization of riders with proper order delivery is performed. The traditional shortest method takes more time to deliver an order as compared to the OCD method. The OCD method minimizes the delay time and identifies the shortest path with the help of available Rider information. In future research, the author advises including more variables in the route optimization process, such as vehicle type, food package size, holiday season, Delivery Service's driver license type, and the maximum capacity of a vehicle type. These additional factors will increase the routing optimization's complexity.

Conflict of Interest

No conflict of Interest

REFERENCES

1. R.D.H. Tobing, "A food ordering system with delivery routing optimization using global positioning system (GPS) technology and google maps," *Internetworking Indonesia Journal*, 8(1), pp.17–21, 2016.
2. O.F. Aydin, I. Gokasar, and O. Kalan, "Matching algorithm for improving ride-sharing by incorporating route splits and social factors," *PloS one*, 15(3), p. e0229674, 2020.
3. D. Chen, Y. Yuan, W. Du, Y. Cheng, and G. Wang, "Online route planning over time-dependent road networks," in *2021 IEEE 37th International Conference on Data Engineering (ICDE)*, pp. 325–335.
4. Y. Liu et al., "FooDNet: Toward an optimized food delivery network based on spatial crowdsourcing," *IEEE Transactions on Mobile Computing*, 18(6), pp. 1288–1301, 2018.

5. W. Tu, T. Zhao, B. Zhou, J. Jiang, J. Xia and Q. Li, "OCD: Online crowdsourced delivery for on-demand food," *IEEE Internet of Things Journal*, 7(8), pp. 6842–6854, 2019.

6. Pradip M. Paithane, S.N. Kakarwal, and D.V. Kurmude, "Top-down method used for pancreas segmentation," *Int. J. Innov. Exploring Eng.(IJITEE)*, vol. 9, iss. 3, pp. 1790–1793, 2020.

7. J. Wang et al., "Multi-task allocation in mobile crowd sensing with individual task quality assurance," *IEEE Transactions on Mobile Computing*, 17(9), pp. 2101–2113, 2018.

8. P. Li, J. Lai, and Y. Wu, "Accountable attribute-based authentication with fine-grained access control and its application to crowdsourcing," *Front. Comput. Sci.*, **17**, 171802, 2023. Available: https://doi.org/10.1007/s11704-021-0593-4

9. C. Chen et al., "Crowddeliver: Planning city-wide package delivery paths leveraging the crowd of taxis," *IEEE Transactions on Intelligent Transportation Systems*, 18(6), pp. 1478–1496, 2016.

10. A.M. Arslan, N. Agatz, L. Kroon, and R. Zuidwijk, "Crowdsourced delivery—a dynamic pickup and delivery problem with ad hoc drivers," *Transportation Science*, 53(1), pp. 222–235, 2019.

11. Y. Ding et al., "A City-Wide Crowdsourcing Delivery System with Reinforcement Learning," *Proceedings of the ACM on Interactive, Mobile, Wearable and Ubiquitous Technologies*, 5(3), pp. 1–22, 2021.

12. P.M. Paithane and S.N. Kakarwal, "Automatic determination number of cluster for multi kernel NMKFCM algorithm on image segmentation," in *International Conference on Intelligent Systems Design and Applications. Springer, Cham, 2018*, pp. 870–879.

13. P.M. Paithane, S.N. Kakarwal, and D.V. Kurmude, "Automatic Seeded Region Growing with Level Set Technique Used for Segmentation of Pancreas," in *International Conference on Soft Computing and Pattern Recognition. Springer, Cham, 2020*, pp. 374–382.

14. P.M. Paithane and S.N. Kakarwal, "Automatic Pancreas Segmentation using A Novel Modified Semantic Deep Learning Bottom-Up Approach," *International Journal of Intelligent Systems and Applications in Engineering*, 10(1), pp. 98–104, 2022.

15. Pradip Mukundrao Paithane, "Yoga Posture Detection Using Machine Learning," *Artificial Intelligence in Information and Communication Technologies, Healthcare and Education: A Roadmap Ahead*, 2022: 27.

16. S.N. Kakarwal and P.M. Paithane, "Automatic pancreas segmentation using ResNet-18 deep learning approach," *System Research and Information Technologies*, no. 2, pp.104–116, 2022.

17. N. Wang et al., "Collecting and analyzing key-value data under shuffled differential privacy," *Front. Comput. Sci.*, **17**, 172606, 2023. Available: https://doi.org/10.1007/s11704-022-1572-0

18. A. Maatoug, G. Belalem, and S. Mahmoudi, "A location-based fog computing optimization of energy management in smart buildings: DEVS modeling and design of connected objects," *Front. Comput. Sci.*, **17**, 172501, 2023. Available: https://doi.org/10.1007/s11704-021-0375-z

19. A. Biswas et al., "OCSO-CA: opposition based competitive swarm optimizer in energy efficient IoT clustering," *Front. Comput. Sci.*, **16**, 161501, 2022. Available: https://doi.org/10.1007/s11704-021-0163-9

20. C. Zhu, B. Han, and Y. Zhao, "A bi-metric autoscaling approach for *n*-tier web applications on kubernetes," *Front. Comput. Sci.*, **16**, 163101, 2022. Available: https://doi.org/10.1007/s11704-021-0118-1

INFORMATION ON THE ARTICLE

Dr. Pradip M. Paithane, ORCID: 0000-0002-4473-7544, Vidya Pratishthan's Kamalnayan Bajaj Institute of Engineering and Technology, India, e-mail: paithanepradip@gmail.com

Sarita Jibhau Wagh, ORCID: 0000-0003-4798-2147, T.C. College Baramati, Maharashtra, India

Dr. Sangeeta N. Kakarwal, ORCID: 0000-0003-4828-5247, ICEEM College, India

ОПТИМІЗАЦІЯ МАРШРУТНОЇ ДИСТАНЦІЇ З ВИКОРИСТАННЯМ АЛГОРИТМУ *K*-NN ДЛЯ ДОСТАВКИ ЇЖІ НА ВИМОГУ / Прадіп М. Пайтане, Саріта Джібхау Ваг, Сангіта Н. Какарвал

Анотація. Сьогодні можливість клієнтів купувати товари в Інтернеті чи по телефону і безпечно транспортувати до місця розташування клієнта швидко зростає. Стає поширеною послуга доставки їжі за запитом, коли клієнти розміщують запити на їжу в Інтернеті, а пасажири передають ці замовлення. Нове застосування столичних харчових продуктів вимагає продуктивних і універсальних безперервних адміністрацій транспортування для швидкої доставки найкоротшим шляхом. Складно зареєструвати достатню кількість пакетів їжі та навчити їх працювати з такими структурами запиту їжі. У цій роботі подано загальнодоступний веб-підхід до транспортування їжі за запитом. У співпраці з IOT (Інтернет речей) і досягненнями 3G, 4G або 5G громадські гонщики можуть бути залучені до подорожей як громадські гонщики, які перевозять їжу за допомогою спільних велосипедів або електромобілів. Підтримувані громадськістю райдери поступово розподіляються між різними постачальниками їжі для її транспортування. У дослідженні створено систему запитів на їжу в Інтернеті та застосовано обчислення KNN для вирішення проблеми комівояжера (TSP). Платформа додатково використовує технологію глобальної системи позиціонування (GPS) у мобільних пристроях, що підтримують Android, і використовує API маршрутизації TOM-TOM для координат для планування розташування. Для оцінювання запропонованого підходу використовуються відтворені події обмеженого обсягу та сертифікованого великого обсягу за запитом. Такий підхід зменшує час затримки доставки (до 10–15 хв). Кожен пасажир отримає оновлене місце призначення доставки замовлення найкоротшим маршрутом. Постачальник продуктів харчування може отримати статус харчового продукту, доступного на райдері.

Ключові слова: краудсорсинг, гібридна оптимізація, доставка їжі на вимогу, алгоритм *k*-найближчих сусідів, оптимізація маршруту, традиційний пошук, міська логістика.

МОДИФІКАЦІЯ МЕРЕЖ ПЕТРІ З АНТИСИПАЦІЄЮ ПО ПОЗИЦІЇ

В.М. СТАТКЕВИЧ

Анотація. Запропоновано модифікацію мережі Петрі з урахуванням сильної антисипації по позиції. Розширення реалізовано за допомогою введення в правило запуску переходу нового доданка, який містить цілочислову функцію від нової кількості фішок у позиції. Знайдено важливі відмінності від класичних мереж Петрі, наприклад, множина маркувань, досяжних з поточного маркування запуском дозволеного переходу, може бути як порожньою, так і містити більше одного маркування. Розглянуто питання побудови графу досяжності та дерева покриття. Указано умови, за яких дерево покриття існує, а для його побудови запропоновано алгоритм, який узагальнює відомий класичний алгоритм. Основні ідеї та конструкції проілюстровано на прикладах.

Ключові слова: мережа Петрі, антисипація, умова запуску переходу, граф досяжності, дерево покриття.

Пам’яті Юрія Вікторовича Богданського (10.06.1949–21.11.2021)

ВСТУП

Мережі Петрі, запропоновані К.А. Петрі в 1962 р., є зручним засобом для проектування, аналізу та моделювання різних процесів та мереж [1–3]. Багатьма авторами були розглянуті та досліджені різні модифікації мереж Петрі: інгібіторні, часові, стохастичні, кольорові, неперервні та інші [1–6]. У деяких з цих мереж правила запуску переходу можуть відрізнятись від класичного правила запуску переходу, запропонованого К.А. Петрі. Наприклад, в інгібіторних мережах вводиться інгібіторна дуга, яка проведена від позиції до переходу та яка забороняє запуск цього переходу, якщо в позиції наявна фішка. Також в неперервних мережах правило запуску відрізняється від класичного і пристосоване до ситуації, коли кількість фішок у позиції може бути будь-яким дійсним невід’ємним числом і перехід може бути запущений нецілу кількість разів, а саме вводиться поняття ступеня запуску переходу.

У 1992 р. Д. Дюбуа [7–9] запропонував поняття інкурсії, антисипації або передбачення, коли новий стан об’єкта залежить не тільки від певних попередніх станів, а і від певних майбутніх станів (сильна антисипація) або їх оцінок (слабка антисипація). Об’єкти можуть бути різної природи: диференціальні рівняння з неперервним часом та їх скінченно-різницеві аналоги з дискретним часом, диференціальні рівняння звичайні та з частинними похідними, клітинні автомати досліджувались, наприклад, у працях [7–12], диференціальні рівняння з випереджальним аргументом – у працях [13–15].

У цій роботі пропонується модифікувати правило запуску переходу класичної мережі Петрі з урахуванням сильної антисипації, а саме: ввести новий доданок, який містить функцію від нової кількості фішок у позиції. Якщо функція $f : \mathbf{N} \cup \{0\} \to \mathbf{N} \cup \{0\}$, то кількість фішок у позиції також буде цілим невід’ємним числом, як і у випадку класичних мереж Петрі. Наскіль-

ки відомо автору, такі модифікації мереж Петрі з антисипацією в літературі не розглядались.

ПОПЕРЕДНІ ВІДОМОСТІ

Мережею Петрі називають набір $\langle P,T,W,\mu_0 \rangle$, де $P = \{p_1,\ldots,p_m\}$ – скінченна множина позицій, $T = \{t_1,\ldots,t_n\}$ – скінченна множина переходів, $W = (T \times P) \cup (P \times T) \to \mathbf{N} \cup \{0\}$ – вагова функція, $\mu_0 : P \to \mathbf{N} \cup \{0\}$ – початкове маркування. Для зображення мереж Петрі використовують дводольний орієнтований мультиграф [1–3]. Перехід t називають дозволеним, якщо для кожної вхідної позиції p виконується нерівність $\mu(p) \geq W(p,t)$. Якщо перехід t дозволений, то він може бути запущений (але не обов'язково має бути запущеним), після його запуску нова кількість фішок у позиції p дорівнює

$$\mu_{k+1}(p) = \mu_k(p) - W(p,t) + W(t,p). \tag{1}$$

Модифікуємо правило запуску переходу (1). А саме розглянемо розширення класичної мережі Петрі $\langle P,T,W,\mu_0,\{f_{p_1},\ldots,f_{p_m}\} \rangle$, де функція $f_{p_i} : \mathbf{N} \cup \{0\} \to \mathbf{N} \cup \{0\}$ відповідає позиції p_i, $1 \leq i \leq m$ (також будемо використовувати позначення $f_i = f_{p_i}$). Перехід t, як і раніше, називаємо дозволеним, якщо для кожної вхідної позиції p виконується нерівність $\mu(p) \geq W(p,t)$. Нехай після запуску дозволеного переходу t нова кількість фішок $\mu_{new}(p)$ у позиції p задовольняє рівняння запуску переходу:

$$\mu_{new}(p) = \mu_k(p) - W(p,t) + W(t,p) + f_p(\mu_{new}(p)). \tag{2}$$

Рівняння (2) запуску переходу узагальнює правило запуску переходу (1) в класичній мережі Петрі. Запропоноване розширення назвемо мережею Петрі з антисипацією по позиції.

ВИКОНАННЯ МЕРЕЖ ПЕТРІ З АНТИСИПАЦІЄЮ ПО ПОЗИЦІЇ

Розглянемо виконання мереж Петрі з антисипацією по позиції по декількох прикладах.

Приклад 1. Розглянемо класичну мережу Петрі, зображену на рис. 1. Її граф досяжності зображено на рис. 1. Для функції наступного стану $\delta : (\mathbf{N} \cup \{0\})^2 \times T \to (\mathbf{N} \cup \{0\})^2$, яка природним чином узагальнюється для довільної скінченної послідовності запусків переходів [1], виконується, наприклад, рівність

$$\delta(\mu_0, t_1 t_2) = \delta(\mu_0, t_2 t_1) = (1,0). \tag{3}$$
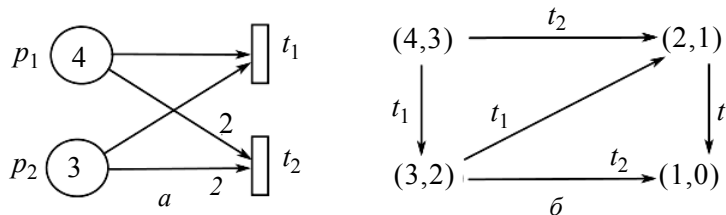

Рис. 1

Розширимо дану класичну мережу, а саме введемо антисипацію по позиції. Нехай позиціям p_i відповідають функції $f_i : \mathbf{N} \cup \{0\} \to \mathbf{N} \cup \{0\}$, $i = 1,2$,

$$f_1(k) = 0, \ 0 \le k \le 3; \ f_1(k) = k - 2, \ 4 \le k \le 5; \ f_1(k) = 2k, \ k \ge 6; \qquad (4)$$

$$f_2(k) = 0, \ k \notin \{3,4,5\}; \ f_2(k) = k - 2, \ k \in \{3,4\}; \ f_2(5) = 5.$$

Обидва переходи t_1 і t_2 дозволені в початковому маркуванні.

Рівняння запуску переходу t_1 з маркування μ_0 згідно з рівнянням (2) мають вигляд

$$\mu_{new}(p_1) = \mu_0(p_1) - 1 + f_1(\mu_{new}(p_1)) = 3 + f_1(\mu_{new}(p_1)); \qquad (5)$$

$$\mu_{new}(p_2) = \mu_0(p_2) - 1 + f_2(\mu_{new}(p_2)) = 2 + f_2(\mu_{new}(p_2)).$$

Тоді $\mu_{new}(p_1) = 3$, $\mu_{new}(p_2) \in \{2,3,4\}$. Аналогічні рівняння запуску t_2 такі:

$$\mu_{new}(p_1) = \mu_0(p_1) - 2 + f_1(\mu_{new}(p_1)) = 2 + f_1(\mu_{new}(p_1)); \qquad (6)$$

$$\mu_{new}(p_2) = \mu_0(p_2) - 2 + f_2(\mu_{new}(p_2)) = 1 + f_2(\mu_{new}(p_2)).$$

Тоді $\mu_{new}(p_1) \in \{2,4,5\}$, $\mu_{new}(p_2) = 1$. Таким чином, на відміну від класичної однозначної функції стану $\delta : (\mathbf{N} \cup \{0\})^2 \times T \to (\mathbf{N} \cup \{0\})^2$, для мережі рис. 1 отримуємо з введенням антисипації по позиції багатозначну функцію:

$$\delta : (\mathbf{N} \cup \{0\})^2 \times T \to 2^{((\mathbf{N} \cup \{0\})^2)};$$

$$\delta(\mu_0, t_1) = \{\mu_1 = (3,2), \mu_2 = (3,3), \mu_3 = (3,4)\}; \qquad (7)$$

$$\delta(\mu_0, t_2) = \{\mu_4 = (2,1), \mu_5 = (4,1), \mu_6 = (5,1)\}. \qquad (8)$$

З'ясуємо, чи виконується рівність (3), тобто як саме співвідносяться множини $\delta(\mu_0, t_1 t_2)$ і $\delta(\mu_0, t_2 t_1)$?

Розглянемо рівняння запуску переходу t_2 з маркувань $\mu_k \in \delta(\mu_0, t_1)$, $k = 1, 2, 3$:

$$\mu_{new}(p_1) = 1 + f_1(\mu_{new}(p_1)), \ \mu_{new}(p_2) = \mu_k(p_2) - 2 + f_2(\mu_{new}(p_2)). \qquad (9)$$

Із першого рівняння отримуємо $\mu_{new}(p_1) = 1$. Для другого рівняння розглянемо випадки:

1) для $k = 1$ маємо $\mu_{new}(p_2) = f_2(\mu_{new}(p_2))$, $\mu_{new}(p_2) \in \{0,5\}$;

2) для $k = 2$ маємо $\mu_{new}(p_2) = 1 + f_2(\mu_{new}(p_2))$, $\mu_{new}(p_2) = 1$;

3) для $k = 3$ маємо $\mu_{new}(p_2) = 2 + f_2(\mu_{new}(p_2))$, $\mu_{new}(p_2) \in \{2,3,4\}$.

Таким чином, $\delta(\mu_0, t_1 t_2) = \{(1,0), (1,1), (1,2), (1,3), (1,4), (1,5)\}$.

Тепер розглянемо рівняння запуску переходу t_1 з маркувань $\mu_k \in \delta(\mu_0, t_2)$, $k = 4, 5, 6$:

$$\mu_{new}(p_1) = \mu_k(p_1) - 1 + f_1(\mu_{new}(p_1)), \ \mu_{new}(p_2) = f_2(\mu_{new}(p_2)).$$

Для першого рівняння розглянемо випадки:

1) для $k = 4$ маємо $\mu_{new}(p_1) = 1 + f_1(\mu_{new}(p_1))$, $\mu_{new}(p_1) = 1$;

2) для $k = 5$ маємо $\mu_{new}(p_1) = 3 + f_1(\mu_{new}(p_1))$, $\mu_{new}(p_1) = 3$;

3) для $k = 6$ маємо $\mu_{new}(p_1) = 4 + f_1(\mu_{new}(p_1))$, розв'язків немає.

Із другого рівняння отримуємо $\mu_{new}(p_2) \in \{0,5\}$. Отже, остаточно отримуємо $\delta(\mu_0, t_2 t_1) = \{(1,0),(1,5),(3,0),(3,5)\}$.

Підсумовуючи маємо, що рівність (3) у загальному випадку не виконується. Множини $\delta(\mu, t_1 t_2)$ та $\delta(\mu, t_2 t_1)$ у загальному випадку різні, більш того жодна з цих множин не обов'язково у загальному випадку має бути підмножиною іншої: $\delta(\mu, t_1 t_2) \not\subset \delta(\mu, t_2 t_1)$, $\delta(\mu, t_2 t_1) \not\subset \delta(\mu, t_1 t_2)$.

Зауваження 1. Для мережі Петрі з антисипацією по позиції, яка містить m позицій, функція $\delta : (\mathbf{N} \cup \{0\})^m \times T \to 2^{((\mathbf{N} \cup \{0\})^m)}$.

Приклад 2. Модифікуємо умову прикладу 1, а саме: в рівності (4) покладемо

$$\widetilde{f_1}(k) = 0, \ 0 \le k \le 3; \ \widetilde{f_1}(k) = k - 4, \ 4 \le k \le 5; \ \widetilde{f_1}(k) = 2k, \ k \ge 6.$$

Тоді замість рівняння (5) отримуємо $\mu_{new}(p_1) = 3 + \widetilde{f_1}(\mu_{new}(p_1))$, $\mu_{new}(p_1) = 3$, замість рівняння (6) маємо $\mu_{new}(p_1) = 2 + \widetilde{f_1}(\mu_{new}(p_1))$, $\mu_{new}(p_1) = 2$. Таким чином, множина (7) не змінюється, а множина (8) стає одноелементною: $\delta(\mu_0, t_2) = \{\mu_4 = (2,1)\}$. Інакше кажучи, із запуском переходу t_2 з маркування μ_0 настає маркування, визначене однозначно, як і у випадку класичних мереж Петрі. Зазначимо, що перехід t_2 у маркуванні μ_4 не дозволений.

Рівняння (9) із заміною функції f_1 на $\widetilde{f_1}$ мають такі самі розв'язки, тому $\delta(\mu_0, t_1 t_2) = \{(1,0),(1,1),(1,2),(1,3),(1,4),(1,5)\}$. Рівняння запуску переходу t_1 з маркування $\mu_4 \in \delta(\mu_0, t_2)$ набувають вигляду $\mu_{new}(p_1) = 1 + \widetilde{f_1}(\mu_{new}(p_1))$, $\mu_{new}(p_2) = f_2(\mu_{new}(p_2))$. Тоді $\mu_{new}(p_1) = 1$, $\mu_{new}(p_2) \in \{0,5\}$. Таким чином, $\delta(\mu_0, t_2 t_1) = \{(1,0),(1,5)\} \subset \delta(\mu_0, t_1 t_2)$.

Наведений приклад показує, що в окремому випадку може виконуватись вкладення $\delta(\mu, t_2 t_1) \subset \delta(\mu, t_1 t_2)$.

Зауваження 2. У прикладі 2 маркування $(1,0)$ слід назвати тупиковим за аналогією із класичними мережами Петрі, оскільки жоден перехід у ньому не дозволений. У маркуванні $(1,5)$ перехід t_2 не дозволений, а перехід t_1 хоча формально і дозволений, але друге з рівнянь запуску переходу t_1 $\mu_{new}(p_1) = \widetilde{f_1}(\mu_{new}(p_1))$, $\mu_{new}(p_2) = 4 + f_2(\mu_{new}(p_2))$ не має розв'язків. У цьому і є відмінність ситуації від класичної. А саме, у мережі Петрі з антисипацією по позиції перехід може бути дозволений в тому сенсі, що кількості фішок у вхідних позиціях не менші, ніж ваги відповідних дуг, але рівнян-

ня запуску такого переходу не має розв'язків і $\delta(\mu,t) = \varnothing$. Таке маркування $(1,5)$ назвемо некласичним тупиковим маркуванням.

Зауваження 3. Якщо у прикладі 1 у рівності (4) вибрати

$$\widetilde{\widetilde{f_1}}(k) = 0, \ 0 \le k \le 3; \ \widetilde{\widetilde{f_1}}(k) = k - 2, \ 4 \le k \le 5; \ \widetilde{\widetilde{f_1}}(k) = k - 3, \ k \ge 6,$$

то рівніння (5) набуде вигляду $\mu_{new}(p_1) = 3 + \widetilde{\widetilde{f_1}}(\mu_{new}(p_1))$ і має нескінченну множину розв'язків $\mu_{new}(p_1) \in \{3,6,7,8,\ldots\}$. Отже, множина $\delta(\mu,t)$ у загальному випадку зліченна.

**Приклад 3.** Розглянемо мережу Петрі з антисипацією по позиції, зображену на рис. 2, і нехай позиції p_1 відповідає функція $f_1: \mathbf{N} \cup \{0\} \to \mathbf{N} \cup \{0\}$, де $f_1(k) = 0$ для $k \notin \{3,4\}$, $f_1(k) = k - 2$ для $k \in \{3,4\}$, а позиції p_2 відповідає тотожно нульова функція $f_2(k) \equiv 0$. Рівняння запуску переходу t з поточного маркування μ мають вигляд
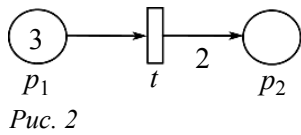
Рис. 2

$$\mu_{new}(p_1) = \mu(p_1) - 1 + f_1(\mu_{new}(p_1)), \quad \mu_{new}(p_2) = \mu(p_2) + 2. \qquad (10)$$

Кожний запуск переходу t додає по дві фішки в позицію p_2, як і в класичних мережах Петрі. Очевидна рівність $\delta(\mu_0,t) = \{\mu_1 = (2,2), \ \mu_2 = (3,2), \ \mu_3 = (4,2)\}$.

Рівняння запуску переходу t з маркування μ_1 згідно з рівняннями (10), мають вигляд $\mu_{new}(p_1) = 1 + f_1(\mu_{new}(p_1))$, $\mu_{new}(p_2) = \mu(p_2) + 2$, звідки випливає $\delta(\mu_1,t) = \{(1,4)\}$. Аналогічним чином $\delta((1,4),t) = \{(0,6)\}$, а маркування $(0,6)$ тупикове, оскільки в ньому перехід t не дозволений.

Маркування μ_2 є покривним для маркування μ_0, з рівнянь (10) випливає

$$\delta(\mu_2,t) = \{(2,4),(3,4),(4,4)\};$$

$$\delta((3,2k),t) = \{(2,2k+2),(3,2k+2),(4,2k+2)\}, \ k \in \mathbf{N} \cup \{0\}.$$

Нарешті, маркування μ_3 теж є покривним для маркування μ_0, але в ньому перше з рівнянь (10) набуває вигляду $\mu_{new}(p_1) = 3 + f_1(\mu_{new}(p_1))$ і не має розв'язків $\delta(\mu_3,t) = \varnothing$. Тому згідно із зауваженням 2 маркування μ_3 некласичне тупикове. Отримана ситуація, яка суперечить класичним мережам Петрі: у загальному випадку з маркування μ', яке є покривним для маркування μ'', неможливо запустити ті самі переходи, що з маркування μ'', яке покривається. Тому введення елемента $\omega = +\infty$ потребує додаткових умов.

Отже, можемо побудувати граф досяжності, зображений на рис. 3. Для даної мережі граф нескінченний, є деревом і має єдину нескінченну гілку $\{(3,2k): k \in \ \in \mathbf{N} \cup \{0\}\}$. Інші гілки скінченні і завершуються або тупиковими маркуваннями $\{(0,2k): k = 3,4,\ldots\}$, або некласичними тупиковими маркуваннями $\{(4,2k): k \in \mathbf{N}\}$. Зазначимо, що у працях [4, гл. 4; 6] для ілю-

страції досяжних маркувань неперервних мереж Петрі з двома (трьома) позиціями використовуються двовимірні (тривимірні) графіки відносно координат $\mu(p_1)$, $\mu(p_2)$ ($\mu(p_1)$, $\mu(p_2)$, ($\mu(p_3)$ відповідно).

Також зазначимо, що в побудові дерева покриття для класичної мережі Петрі кількість нових маркувань дорівнює кількості дозволених переходів у відповідному маркуванні [1, 2]. Проте для мережі з антисипацією по позиції кількість нових маркувань визначається рівняннями запуску переходів і у загальному випадку може бути зліченною (див. зауваження 3).

Перехід від нескінченного графу досяжності до скінченного дерева покриття пов'язаний із введенням елемента $\omega = +\infty$. Тоді виникає питання, чи можна з маркування μ', яке є покривним для маркування μ'', запустити ті самі послідовності переходів, що з

Рис. 3

маркування μ'', яке покривається. Наприклад, обидва маркування μ_2 і μ_3 є покривними для маркування μ_0, але множина $\delta(\mu_2, t)$ непорожня, а $\delta(\mu_3, t) = \varnothing$ Зазначимо, що умова обмеженості носіїв усіх функцій не дає відповіді на це питання: $\operatorname{supp} f_1 = \{3,4\} < \infty$, $\operatorname{supp} f_2 = \varnothing < \infty$. Причому недостатньо лише знати всі некласичні тупикові маркування — множина послідовностей запусків переходів може бути вужчою, але вона може бути непорожньою.

Зазначимо, що граф досяжності може бути також і скінченним: для мережі прикладу 2 граф досяжності скінченний (рис. 4). Таким же способом можна переконатись, що і граф досяжності для мережі прикладу 1 скінченний, всі маркування з множини μ з множини $\{0,1,2,3,4,5\}^{\times 2}$ досяжні. У цьому неважко переконатись, якщо записати відповідні рівняння запусків переходів t_1 і t_2 з кожного досяжного маркування.
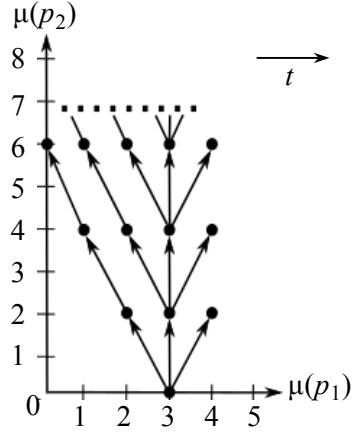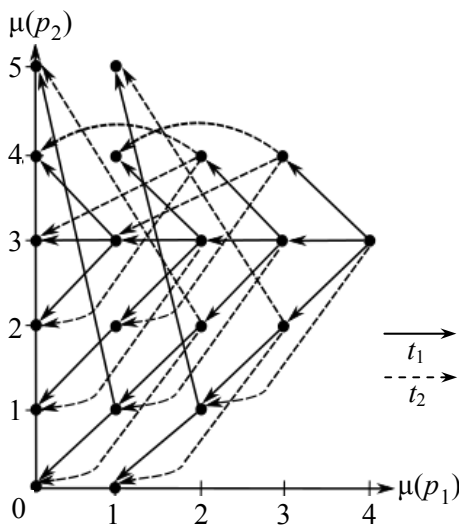

Рис. 4

Приклад 4. Розглянемо мережу Петрі з антисипацією по позиції, зображену на рис. 5, і нехай позиціям p_i відповідають функції $f_i : \mathbf{N} \cup \{0\} \to \mathbf{N} \cup \{0\}$, $i = 1, 2$;

$$f_1(k) = \operatorname{sgn} k = \begin{cases} 1, & k \in \mathbf{N}, \\ 0, & k = 0, \end{cases} \quad f_2(k) = \overline{\operatorname{sgn}} k = \begin{cases} 0, & k \in \mathbf{N}, \\ 1, & k = 0. \end{cases}$$

Поточне маркування позначимо через $\mu = (\mu(p_1), \mu(p_2))$.

Розглянемо рівняння запуску переходу t_1 з поточного маркування:

$$\mu_{new}(p_1) = \mu(p_1) - 1 + \operatorname{sgn} \mu_{new}(p_1), \ \mu_{new}(p_2) = \mu(p_2) + 1 + \overline{\operatorname{sgn}} \mu_{new}(p_2).$$

Якщо $\mu(p_1) = 0$, то перехід t_1 не дозволений. Якщо $\mu(p_1) = 1$, то $\mu_{new}(p_1) \in \{0,1\}$. Якщо ж $\mu(p_1) \geq 2$, то оскільки $\mu_{new}(p_1) \geq 1$, $\operatorname{sgn} \mu_{new}(p_1) = 1$, отримуємо $\mu_{new}(p_1) = \mu(p_1)$. Друге рівняння з урахуванням того, що $\mu_{new}(p_2) \geq 1$, $\overline{\operatorname{sgn}} \mu_{new}(p_2) = 0$, має єдиний розв'язок $\mu_{new}(p_2) = \mu(p_2) + 1$. Таким чином, у поточному маркуванні $(0, \mu(p_2))$ перехід t_1 не дозволений, $\delta((1, \mu(p_2)), t_1) = \{(0, \mu(p_2) + 1), (1, \mu(p_2) + 1)\}$, а для $\mu(p_1) \geq 2$ $\delta((\mu(p_1), \mu(p_2)), t_1) = \{(\mu(p_1), \mu(p_2) + 1)\}$.
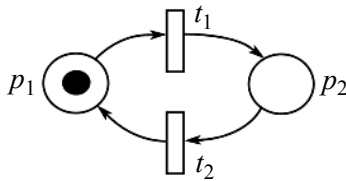
Тепер розглянемо рівняння запуску переходу t_2 з поточного маркування:

$$\mu_{new}(p_1) = \mu(p_1) + 1 + \operatorname{sgn} \mu_{new}(p_1), \ \mu_{new}(p_2) = \mu(p_2) - 1 + \overline{\operatorname{sgn}} \mu_{new}(p_2).$$

Перше рівняння, $\mu_{new}(p_1) \geq 1$, $\operatorname{sgn} \mu_{new}(p_1) = 1$, має єдиний розв'язок $\mu_{new}(p_1) = \mu(p_1) + 2$. Якщо $\mu(p_2) = 0$, то перехід t_2 не дозволений. Якщо $\mu(p_2) = 1$, то друге рівняння набуде вигляду $\mu_{new}(p_2) = \overline{\operatorname{sgn}} \mu_{new}(p_2)$ і не має розв'язків. Якщо ж $\mu(p_2) \geq 2$, то з урахуванням того, що $\mu_{new}(p_2) \geq 1$, $\overline{\operatorname{sgn}} \mu_{new}(p_2) = 0$, отримуємо $\mu_{new}(p_2) = \mu(p_2) - 1$. Таким чином, у поточному маркуванні $(\mu(p_1), 0)$ перехід t_2 не дозволений, $\delta((\mu(p_1), 1), t_2) = \varnothing$, $\delta((\mu(p_1), \mu(p_2)), t_2) = \{(\mu(p_1) + 2, \mu(p_2) - 1)\}$ для $\mu(p_2) \geq 2$.


Рис. 5
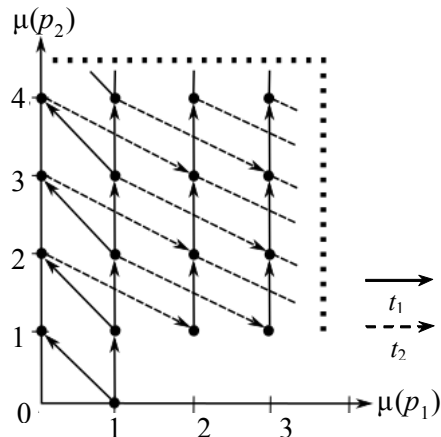
Отже, можемо побудувати граф досяжності, зображений на рис. 6. Для даної мережі граф нескінченний, має єдине некласичне тупикове маркування $(0,1)$ (оскільки в ньому перехід t_1 не дозволений, а перехід t_2 хоча і дозволений, але $\delta((0,1), t_2) = \varnothing$) і не є деревом ($\delta((2,2), t_1 t_2) = \delta((2,2), t_2 t_1) = \{(4,2)\}$). Зазначимо, що для класичної мережі Петрі без антисипації, зображеної на рис. 5, граф досяжності був би скінченним і містив би всього два марку-

Рис. 6

вання $(1,0)$ і $(0,1)$. Також зазначимо, що умова обмеженості носіїв усіх функцій не виконується: $\operatorname{supp} f_1 = \mathbf{N}$, $\operatorname{supp} f_2 = \{0\}$.

Нарешті, зазначимо, що запуском переходу t_1 з маркування $(1,1) \in$ $\in \delta((1,0), t_1)$, яке є покривним для маркування $(1,0)$, можна отримати маркування $(0,2)$, яке вже не є покривним для маркування $(1,0)$. Крім того, з маркування $(1,1)$ можна запускати перехід t_1 нескінченну кількість разів і отримувати маркування $(1,k)$, $k \in \mathbf{N} \setminus \{1\}$, а в маркуванні $(0,2) \in \delta((1,1), t_1)$ перехід t_1 хоча і дозволений, але $\delta((0,2), t_1) = \varnothing$. Таким чином, проблема введення елемента ω (див. приклад 3) для даної мережі зберігається.

ДЕРЕВО ПОКРИТТЯ ДЛЯ МЕРЕЖ ПЕТРІ З АНТИСИПАЦІЄЮ ПО ПОЗИЦІЇ

Розглянемо мережу Петрі з антисипацією по позиції з початковим маркуванням μ_0. Нагадаємо, що множину маркувань, досяжних з маркування μ, позначають через $R(\mu)$ [1–3]. Нехай мережа задовольняє дві додаткові умови 1 і 2.

Умова 1. Існує константа $C \in \mathbf{N}$, яка залежить від мережі та від функцій f_i ($1 \le i \le m$), що для кожного маркування $\mu \in R(\mu_0)$ і для кожного переходу t, дозволеного в маркуванні μ, рівняння запуску переходу t мають не більше ніж C розв'язків.

Умова 2. Якщо маркування μ' досяжне з маркування $\mu'' \in R(\mu_0)$ послідовністю запусків переходів σ і є покривним для маркування μ'', і до того ж для певної позиції p $\mu'(p) > \mu''(p)$, то:

а) або заздалегідь відоме скінченне число $N \in \mathbf{N}$, що послідовність σ можна запустити з маркування μ' не більше ніж N разів;

б) або заздалегідь відомо, що послідовність σ можна запустити з маркування μ' нескінченну кількість разів, і причому жодне з отриманих цими запусками маркувань не є некласичним тупиковим, а для всіх $k \in \mathbf{N} \cup \{0\}$ довільне маркування $\mu_k \in \delta(\mu', \sigma^k)$ покривається кожним маркуванням $\mu_{k+1} \in \delta(\mu_k, \sigma)$ і для вказаної позиції p $\mu_{k+1}(p) > \mu_k(p)$.

Зазначимо, що для класичної мережі Петрі без антисипації по позиції умови 1, 2 і 2б виконуються завжди ($C = 1$), умова 2а ніколи не виконується. Проте з введенням антисипації по позиції з'являються мережі, для яких може не виконуватись

– або умова 1 – див., наприклад, зауваження 3;

– або умова 2 – у прикладі 3 маркування $(3,2) \in \delta(\mu_0, t)$ є покривним для маркування μ_0, послідовність $\delta = t$ можна запускати з маркування $(3,2)$ нескінченну кількість разів та отримувати маркування $(3,2k)$, $k \in \mathbf{N} \setminus \{1\}$, але маркування $(2,4) \in \delta((3,2), t)$ вже не є покривним для маркування $(3,2)$, більш того маркування $(4,4) \in \delta((3,2), t)$ некласичне тупикове.

Також зазначимо, що умова 2б є формалізацією нескінченного зростання по кожній гілці.

Якщо додаткові умови 1 і 2 виконуються, стає можливим ввести елемент $\omega = +\infty$. Пропонується такий алгоритм побудови скінченного дерева покриття, який узагальнює добре відомий класичний алгоритм [2, с. 51; 1, с. 94; 3, с. 23; 4, с. 39–40].

Крок 1. Позначити початкове маркування μ_0 як корінь та присвоїти йому мітку "нове".

Крок 2. Поки існують нові маркування, виконувати такі операції:

Крок 2.1. Вибрати нове маркування μ.

Крок 2.2. Якщо μ збігається з одним з маркувань на шляху від кореня до μ, присвоїти μ мітку "старе" та перейти до іншого нового маркування.

Крок 2.3. Якщо для маркування μ немає дозволених переходів, присвоїти μ мітку "тупикове"; якщо ж для кожного дозволеного переходу t рівняння запуску t не мають розв'язків, присвоїти μ мітку "некласичне тупикове".

Крок 2.4. Поки для маркування μ існують дозволені переходи t, рівняння запуску яких мають розв'язки, для кожного з них виконати такі операції:

Знайти множину маркувань $\delta(\mu,t)$ і для кожного маркування $\mu' \in \delta(\mu,t)$ виконати такі операції:

– якщо на шляху від кореня до маркування μ існує маркування μ'', яке покривається маркуванням μ', і для них виконується умова 2б, то замінити $\mu'(p)$ на ω для кожної позиції p, указаної в умові 2;

– ввести μ' як вузол, з'єднати μ з μ' дугою, помітити дугу символом t і присвоїти μ' мітку "нове".

Очевидно, що певні операції наведеного алгоритму точно збігаються з операціями класичного алгоритму [2, с. 51]. Відмінності обумовлені способом введення ω, а також множиною $\delta(\mu,t)$, яка для дозволеного переходу t може бути в загального випадку як порожньою, так і містити більше одного маркування.

Теорема 1. Нехай для певної мережі Петрі з антисипацією по позиції виконуються умови 1 і 2. Тоді дерево покриття для такої мережі скінченне.

Доведення точно повторює доведення теореми 4.1 [1, с. 97–98]. Використані в ньому леми 4.1–4.3 [1, с. 95–97] запозичуються без змін, а в доведення самої теореми 4.1 вносяться такі два коригування:

1) наявність нескінченного шляху $x_0, x_1, x_2, \ldots$, який виходить з кореня x_0, свідчить про те, що в умові 2 виконується саме пункт 2б, а не пункт 2а – таким чином введення елемента ω коректне;

2) кількість вершин, які слідують за кожною вершиною в дереві, обмежена не кількістю переходів, а константою C з умови 1.

Для мережі прикладу 4 побудова дерева покриття викликає складності: вказані у прикладі 4 міркування свідчать про те, що умова 2 не виконується.

Приклад 5. Змінимо початкове маркування мережі в прикладі 4, нехай $\mu_0 = (2,1)$. Тоді умови 1 і 2 виконуються і в результаті застосування наведеного алгоритму отримуємо дерево покриття, зображене на рис. 7.

Зазначимо, що можливість побудови дерева покриття за допомогою наведеного алгоритму, тобто виконання умов 1 і 2, залежить у тому числі і від початкового маркування μ_0 та множини $R(\mu_0)$. Тут ситуація відрізняється від класичної: для мережі Петрі без антисипації по позиції від початкового маркування залежить конкретний вигляд самого дерева покриття, але аж ніяк не можливість його побудови. Як і у прикладі 4 умова обмеженості носіїв усіх функцій не виконується, але на відміну від прикладу 4 дерево покриття побудоване.
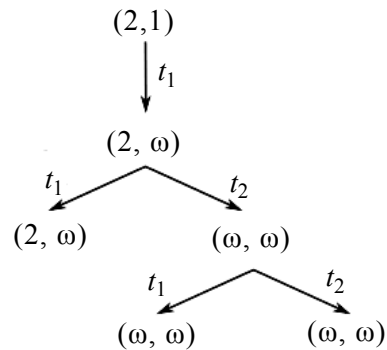
Рис. 7

Як і у випадку класичних мереж Петрі, у дереві покриття не відображається певна інформація. Наприклад, послідовність $t_1 t_2^2$ запустити неможливо, але на рис. 7 це не відображається.

Граф покриття будується за таким же принципом, як і у випадку класичних мереж Петрі [2]. Граф покриття для мережі прикладу 5 зображено на рис. 8.

Зауваження 4. Якщо послабити умову 2б і дозволити отримувати некласичні тупикові маркування, то дерево покриття залишиться скінченним. Але виникне інша проблема — можуть з'явитись зайві недосяжні маркування. А саме, якщо в дереві покриття буде наявне певне маркування μ, яке міститиме ω, то не можна буде зрозуміти чи повинне це маркування μ бути насправді наявним, чи наявність некласичних тупикових маркувань виключатиме появу маркування μ. Один зі способів розв'язання цієї проблеми
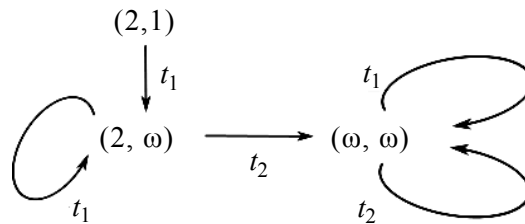
Рис. 8

може полягати у введенні нового додаткового елемента [ω/н.т.], але це може призвести до суттєвого збільшення кількості маркувань у дереві покриття, хоча дерево і залишиться скінченним.

ВИСНОВКИ

Запропоновано мережі Петрі з урахуванням сильної антисипації по позиції, які розширюють класичні мережі Петрі за допомогою модифікації правила запуску переходів. Наведено приклади виконання таких мереж; розглянуто питання побудови графу досяжності та дерева покриття. Виявлені відмінності від класичних мереж Петрі, які вказують на необхідність подальшого дослідження мереж такого типу.

ЛІТЕРАТУРА

1. J. Peterson, *Theory of Petri nets and system modeling*. M.: Mir, 1984, 264 p.
2. T. Murata, "Petri nets: Properties, analysis, applications," *TIIER*, vol. 77, no. 4, pp. 41–85, 1989.
3. V.E. Kotov, *Petri nets*. M.: Nauka, 1984, 160 p.

4. R. David and H. Alla, *Discrete, Continuous, and Hybrid Petri Nets*. Springer, Berlin, Heidelberg, 2005.

5. T. Gu and R. Dong, "A novel continuous model to approximate time Petri nets: modeling and analysis,"*International Journal of Applied Mathematics and Computer Science*, vol. 15, no. 1, pp. 141–150, 2005.

6. C.R. Vazquez, C. Mahulea, J. Julvez, and M. Silva, "Introduction to Fluid Petri nets", Chapter in Book: "Control of Discrete-Event Systems," *Lecture Notes in Control and Information Sciences*, vol. 433, Eds. C. Seatzu, M. Silva, J.H. van Schuppen, Springer-Verlag London, pp. 365–386, 2013. doi: 10.1007/978-1-4471-4276-8_18.

7. D. Dubois, "Incursive and hyperincursive systems, fractal machine and anticipatory logic," *Computing Anticipatory Systems: CASYS 2000 – Fourth International Conference. AIP Conference Proceedings 573*, pp. 437–451, 2001. doi: 10.1063/1.1388710.

8. D. Dubois, "Theory of Incursive Synchronization and Application to the Anticipation of the Chaotic Epidemic,"*International Journal of Computing Anticipatory Systems*, vol. 10, pp. 3–18, 2001.

9. D. Dubois, "Generation of fractals from incursive automata, digital diffusion and wave equation systems," *Biosystems*, vol. 43, pp. 97–114, 1997. doi: 10.1016/S0303-2647(97)01692-4.

10. A. Makarenko, "Multivaluedness Aspects in Self-Organization, Complexity and Computations Investigations by Strong Anticipation,"*Chapter in Book: Recent Advances in Nonlinear Dynamics and Synchronization*; Eds. K. Kyamakya, W. Mathis, R. Stoop, J. Chedjou, Z. Li, Springer, Cham, pp. 33–54, 2018. doi: 10.1007/978-3-319-58996-1_3.

11. A. Makarenko, "Neural Networks with Strong Anticipation and Some Related Problems of Complexity Theory," *Chapter 12 in Series*: *Studies in Systems, Decisions and Control*, vol. 55. Ed. George H. Dimirovski, Springer, 2016, pp. 267–281. doi: 10.1007/978-3-319-28860-4_12.

12. A. Makarenko, "Toward Multivaluedness Aspects in Self-Organization, Complexity and Computations Investigations," *Forth International Workshop on Nonlinear Dynamics and Synchronization INDS'15*, Klagenfurt, Austria, Alpen-Adria University, July 31, 2015, pp. 84–93.

13. L.E. Elsgolts and S.B. Norkin, *Introduction to the theory of differential equations with deviating argument*. M.: Nauka, 1971, 296 p.

14. G.A. Kamensky and A.L. Skubachevskii*, Linear boundary value problems for differential-difference equations*. M.: Ed. MAI, 1992, 190 p.

15. V.G. Pimenov and D.A. Korotkiy, "On solving systems of differential equations with lead and lag," *Izvestiya UrGU*, 2006, no. 44, pp. 113–139.

INFORMATION ON THE ARTICLE

Vitalii M. Statkevych, ORCID: 0000-0001-5210-9890, Educational and Scientific Institute for Applied System Analysis of the National Technical University of Ukraine "Igor Sikorsky Kyiv Polytechnic Institute", Ukraine, e-mail: mstatckevich@yahoo.com

A MODIFICATION OF PETRI NETS WITH ANTICIPATION ON A POSITION / V.M. Statkevych

Abstract. We propose a modification of Petri nets with strong anticipation on a position. The extension modifies a transition rule by adding a new term that contains an integer function of the new marking in the position. The differences from classic Petri nets are found; for example, the set of markings that are reachable from a current marking by firing the enabled transition can either be empty or contain more than one marking. We consider the construction of a reachability graph and a coverability tree. We give the conditions for the existence of the coverability tree and propose the algorithm for constructing the coverability tree that generalizes the well-known classic algorithm. The main ideas and constructions are illustrated in the examples.

Keywords: Petri net, anticipation, transition rule, reachability graph, coverability tree.

RESEARCHES AND APPLICATIONS OF THE COMBINATORIAL CONFIGURATIONS FOR INNOVATIVE DEVICES AND PROCESS ENGINEERING[1]

V.V. RIZNYK

Abstract. This paper is devoted to the memory of Solomon Wolf Golomb (1932–2016) — a famous American mathematician, engineer, and professor of electrical engineering. He was interested in developing techniques for improving the quality indices of engineering devices and systems with respect to performance reliability, transmission speed, positioning precision, and resolving ability based on novel combinatorial configurations. In 1996 S. Golomb have supported the project "Researches and Applications of the Combinatorial Configurations for Innovative Devices and Process Engineering" as a scientific collaboration with the Former Soviet Union (FSU) research team from Lviv Polytechnic State University (Ukraine) under the Cooperative Grant Program by CRDF (U.S.). The underlying project to be edited by S. Golomb is presented, and short information on the development of the researches and applications of optimized systems with ring structure given.
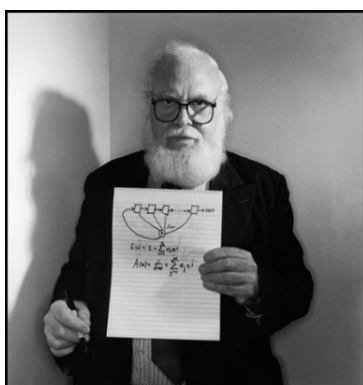
Keywords: project, combinatorial configuration, Ideal Ring Bundle, optimization, model, scientific school.

INTRODUCTION

Solomon Wolf Golomb was a world-famous American scientist, specialist in the field of telecommunications, digital electronics, cellular automata and information theory. He was a world leader in the application of combinatorial mathematics in coding theory and radiophysics. Golomb was the inventor of Golomb coding, a form of entropy coding, the Golomb rulers used in astronomy and data encryption, also named after him, as was one of the main methods for generating Costas arrays, the Lempel–Golomb generation method.

S. Golomb developed the idea of using the advantages of multi-bit shift registers with a balanced number of 0 and 1, or 00, 01, 10, 11, revealing in them the absence of autocorrelation, which made it possible to improve encoding systems –

decoding signals with correction of errors using sequences generated by shift registers. S. Golomb used versions of these sequences (Reed-Solomon codes) to encode video images of Mars, in CDMA cell phones (Codé Division Multiple Access) with multiple access and code separation of communication channels. In 1956, he joined Glenn L. Martin Company, which later became a defense contractor [1]. This explains all his further scientific activities under conditions of strict secrecy, developing military and space communications. Continuing to study sequences on shift registers to improve radio control systems for missiles, S. Golomb with the help of the 85-foot Golstone radio antenna located in the Mojave Desert, specified data on the distances Earth – Venus and the Earth – the Sun. The sequences generated by the sequence shift registers made it possible to clarify the distance to Venus using a radar system. In 1985, Golomb received the Shannon Prize of the IEEE Society of Information Theory, and later the Medal of the U.S. National Security Agency. He was also the winner of the Lomonosov Medal of the Russian Academy of Sciences and the Kapitsa Medal of the Russian Academy of Natural Sciences. In 2000, Golomb was awarded the Richard W. Hemming IEEE Medal for his exceptional contributions to information science and systems engineering. In 2016, he was awarded the Benjamin Franklin Medal in Electrical Engineering for his pioneering work in space communications and digital signal processing, secure data forwarding, improving methods for deciphering cryptographic texts, rocket guidance systems, cellular communications, radars, sonar, GPS [1].

In 1996, S. Golomb have supported the proposal of the Lviv State Polytechnic University (Ukraine) to cooperate with the University of Southern California on the project "Researches and Applications of the Combinatorial Configurations for Innovative Devices and Process Engineering", which was sent to the U.S. Civilian Research & Development Foundation (CRDF). This non-profit organization was founded in 1995 by the National Science Foundation of the United States in accordance with the decision of the U.S. Congress in order to promote international scientific and technical cooperation with the provision of grants, technical resources, training for scientists and researchers. S. Golomb has edited the text of the project, motivating the advantages of the proposed combinatorial configurations with a ring topological structure over chain sequences.

NARRATIVE PROJECT

Research and Applications of Combinatorial Configurations for Innovative Devices and Process Engineering

- The objectives of the proposed project are as follows:

1. Research into the underlying mathematical principles relating to the optimal placement of structural elements in spatially or temporally distributed systems, including the appropriate algebraic constructions based on cyclic groups in extensions of Galois field; development of the scientific basis for technologically optimum distributed systems theory; and the generalization of these methods and results to the improvement and optimization of a larger class of technological systems.

2. Experimental verification of the effectiveness of this new methodology, as it affects the whole range of new high-performance devices, systems, or technolo-

gies to which it can be applied, including applications to coded design of signals for communications and radar, positioning of elements in an antenna array, and other areas to which the mathematical apparatus of contemporary combinatorial theory can be applied.

- Expected results of the completed project:

1. Mathematical results – development of new algebraic results and techniques, based on the idea of "perfect" combinatorial constructions, and expanding the applicability of cyclic group relationships in Galois fields, and a variety of results in number theory.

2. Physical results – a better understanding of the role of geometric structure in the behavior of natural and man-made objects.

3. Technological results – the development of new directions in fundamental and applied research in systems engineering, for improving such quality indices as reliability, precision, speed, resolving ability, and functionality, using innovative methodologies based on combinatorial techniques, with direct applications to radio- and electronic engineering, radio astronomy, applied physics, and other engineering areas.

"Ideal Ordered Chain" Combinatorial Constructions. The "ordered chain" approach to the study of elements and events is known to be of widespread applicability, and has been extremely effective when applied to the problem of finding the optimum ordered arrangement of structural elements in a distributed technological system.

Sums on ordered-chain numbers. Let us calculate all S_n sums of the terms in the numerical *n*-stage chain sequence of distinct positive integers $C_n = \{K_1, K_2, \ldots, K_n\}$, where we require all terms in each sum to be consecutive elements of the sequence. Clearly the maximum such sum is the sum $K_1 + K_2 + \ldots + K_n = T$ of all *n* elements; and the maximum number of distinct sums is

$$S_n = 1 + 2 + \ldots + n = n(n+1)/2. \tag{1}$$

If we regard the chain sequence C_n as being *cyclic*, so that K_n is followed by K_1, we call this a ring sequence. A sum of consecutive terms in the ring sequence can have any of the *n* terms as its starting point, and can be of any length (number of terms) from 1 to $n-1$. In addition, there is the sum T of all *n* terms, which is the same independent of the starting point. Hence the maximum number of distinct sums $S(n)$ of consecutive terms of the ring sequence is given by

$$S(n) = n(n-1) + 1. \tag{2}$$

Comparing the equations (1) and (2), we see that the number of sums $S(n)$ for consecutive terms in the ring topology is nearly double the number of sums S_n in the daisy-chain topology, for the same sequence C_n of *n* terms.

Ideal Numerical Rings. An *n*-stage ring sequence $C_n = \{K_1, K_2, \ldots, K_n\}$ of natural numbers for which the set of all $S(n)$ circular sums consists of the numbers from 1 to $S(n) = n(n-1) + 1$ (each number occurring exactly once) is called

an "Ideal Numerical Ring" (INR). Here is an example of an IRN with *n*=5 and $S(n) = 21$, namely $\{1,3,10,2,5\}$. To see this, we observe:

$$
\begin{aligned}
&1 = 1 && 6 = 5+1 && 11 = 2+5+1+3 && 16 = 1+3+10+2 \\
&2 = 2 && 7 = 2+5 && 12 = 10+2 && 17 = 10+2+5 \\
&3 = 3 && 8 = 2+5+1 && 13 = 3+10 && 18 = 10+2+5+1 \\
&4 = 1+3 && 9 = 5+1+3 && 14 = 1+3+10 && 19 = 5+1+3+10 \\
&5 = 5 && 10 = 10 && 15 = 3 = 10 = 2 && 20 = 3+10+2+5 \\
& && && && 21 = 1+3+10+2+5
\end{aligned}
$$

Note that if we allow summing over more than one complete revolution around the ring, we can obtain all positive integers as such sums. Thus:

$$22 = 1+3+10+2+5+1, \quad 23 = 2+5+1+3+10+2 \text{, etc.}$$

Next, we consider a more general type of INR, where the $S(n)$ ring-sums of consecutive terms give us each integer value from 1 to M, for some integer M, exactly R times, as well as the value of $M+1$ (the sum of all n numbers) exactly once. Here we see that:

$$M = n(n-1)/R.$$

An example with $n = 4$ and $R = 2$, so that $M = 6$, is the ring sequence (1, 1, 2, 3), for which the sums of consecutive terms are:

$$
\begin{aligned}
&1, 1, 2, 3; \\
&1+1 = 2, && 1+2 = 3, && 2+3 = 5, && 3+1 = 4, \\
&1+1+2 = 4, && 1+2+3 = 6, && 2+3+1 = 6, && 3+1+1 = 5, \\
&1+1+2+3 = 7.
\end{aligned}
$$

We see that each "circular sum" from 1 to 6 occurs exactly twice $(R = 2)$. We say that this INR has the parameters $n = 4$, $R = 2$.

- The individual competence of the FSU research team:

1. Theoretical research on the ideal configurations named Ideal Numerical Bundles (INB), in particular, Ideal Numerical Rings (INR), as modifications of certain combinatorial block-designs (existence, enumeration, classification).

2. Cyclic difference sets and some properties of Galois Field cyclic groups.

3. Construction of BIB designs, using INRs and Golomb rulers, and the reverse.

4. Software for construction of BIB designs using INRs.

5. Compiling a general catalogue of INRs and Golomb rulers.

6. Circuit design for the high performance technology of information coding and modulation.

7. Applied research and engineering design of concrete innovative devices and technologies based on combinatorial theory.

8. INBs and some problems of harmony and optimization of systems.

- The individual competence of the US research team:

1. Theoretical research on Golomb rulers and their relationships with difference (existence, enumeration, classification).

2. Construction of difference sets and Golomb rulers.

3. Compiling a general catalogue Golomb rulers.

4. Circuit design of high performance technology for coding of information and the design of communication signals.

5. Applied research and engineering design of innovative devices and technologies based on combinatorial theory.

6. Using combinatorial designs to obtain sequences with favorable correlation properties.

For carrying out the project, it is necessary to combine the achievements of Golomb ruler theory (US) and possibilities of Ideal Bundles theory (FSU) for extending the sphere of practical applications, with the aim of obtaining commercial products.

The FSU team developed the basis of the bundles theory as a new modification of combinatorial configurations on graphs involving Golomb ruler theory and proposed a new approach to the synthesis of technical devices and to engineering technology.

The US team developed the basis of Golomb ruler theory and proposed areas of their possible applications.

Equipment: 1) PC TSDX-4-120 540M, SVGA 0.28 LR NI 1M, 1, 2+1, 44; 2) Printer EPSON Stylus 800; 3) Telecommunications Services: Scanner HEWLETT PACKARD Jet-555, Fax-modem US Robotics Sportster; 4) Writing materials, floppy disk.

The FSU and U.S. co-investigators the project implementation and assess progress ar regular intervals (monthly) by using Fax and E-mail.

PLANNED STEPS

Title of stages	Stage duration	Anticipated results
Theoretical research on Ideal Numerical Rings (INR)	6 mos	Conditions of INR existence will be determined
Research of properties of extended Galois Field cyclic groups	6 mos	Patterns in the distribution of cyclic group elements will be established
Construction of INRs and Ideal numbere ring configurations	6 mos	Catalog of INRs
Applied research and engineering design of specific innovative devices and technologies	6 mos	Creation of concrete innovative devices and technologies

CONCLUSION

The Ideal Numerical Bundles (INB)s provide, essentially, a new conceptual model of technical systems. Moreover, the optimization has been embedded in the underlying combinatorial models. The remarkable properties and structural perfection of one- and multidimensional INBs provide an ability to reproduce the maximum number of combinatorial varieties in the systems with a limited number of elements and bonds. The favorable qualities of the combinatorial structures provide many opportunities to apply them to numerous branches of science and advanced technology. A perfection, beauty and harmony exist not only in the abstract models but in the real world also.

Here is the print of the cover page of the project, worded by S. Golomb.

COVER SHEET FOR COOPERATIVE GRANTS PROGRAM APPLICATION

1. INFORMATION TO BE PROVIDED BY EITHER THE U.S. OR FCU CO-INVESTIGATOR

A. Amound Requested from CRDF: Year One $24700   Year Two $21600 **Total $46300**
B. General Scientific Field of Proposed Activity: Mathematics, Systems Ingeneering
C. Brief descriptive title for your proposal:
Researches and Applications of the Combinatorial Configurations for Innovative Devices and Process Engineering

11. INFORMATION ON CO-INVESTIGATOR FROM THE FORMER SOVIET UNION
A. Name
  Last **Riznyk**   First **Volodymyr**   Patronymic **Vasyljovych**

B. Sex M	C. Date of Birth (Month/Day/Year)
	May/21/1940

D. D.Sc., Professor
  Field Combinatorics in Systems Engineering   Year Awarded 1995
E. Office Phone +38(0322)398793, +38(0322)744300   Fax +380(322)744300
          E-mail rvv@polynet.lviv.ua
F. Professional Title/Position Lvivska Polytechnika State University
                  Department of Control Systems Automation

G. Professional Affiliation and Address	H. Mailing Address(if different then G)
12,Bandera Str., 290646, Lviv-13, Ukraine	

I. Total number of FSU based investigators (including principal investigator):Three persons

Signature   *[signature]*   Date   *17.02.96*

111. INFORMATION ON U.S. CO-INVESTIGATOR
A. Name
  Last   **Golomb**   First   **Solomon**   Middle   **W.**

B. Sex M	C. Date of Birth (Month/Day/Year)
	5/31/32

D. Highest Degree Earned Ph.D. Field Mathematics   Year Awarrded   1957
E. Office Phone (213)740-7333   Fax (213) 740-8729
          E-mail milly@mizar.usc.edu
F. Professional Title/Position University of Southern California , "University Profes-
  sor" (EE & Math.)   University Park Campus

G. Professional Affiliation and Address	H. Mailing Address (if different that G)
Los Angeles, CA 90089-2565, US	

I. Total number of U.S. based investigators (including principal investigator): one (1)
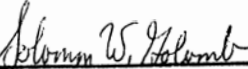
Signature   *[signature]* Date   March 5, 1996

Note, S. Golomb personally signed the date of his birthday 31.05.1932 (not 30.05.1932, as indicated in the Wikipedia [1]).

AFTERWORD

In mathematics, a Golomb ruler is a set of marks at integer positions along a ruler such that no two pairs of marks are the same distance apart. The Golomb ruler was named for Solomon W. Golomb. There is no requirement that a Golomb ruler be able to measure all distances up to its length, but if it does, it is called

a perfect Golomb ruler. It has been proved that no perfect Golomb ruler exists for five or more marks [2]. Unlike of them, an infinite quantity of one- and multidimensional IRBs exist, and the more long is an *n*-stage of IRB, the more invariants we can see by a majority. For example, the two variants of one-dimensional IRBs {1,3,10,2,5} and {1,1,2,3,4} exist for $n = 5$ [3], while exactly the 1717 ones with $R = 1$ for $n = 102$ [4, p.163]. Of very interest are two-dimensional IRBs, which properties hold for the same set of the rings in varieties permutations of terms in the set, e.g. set of two-dimensional five-stages ($n = 5$) ring sequences {(1,1),(1,0),(1,4),(1,3),(1,2)} and {(1,1),(1,3),(1,0),(1,2), (1,4)}, called "Gloria to Ukraine Stars" [5]. Examples of two paired pentagonal (*n*=5) such IRBs shown below.
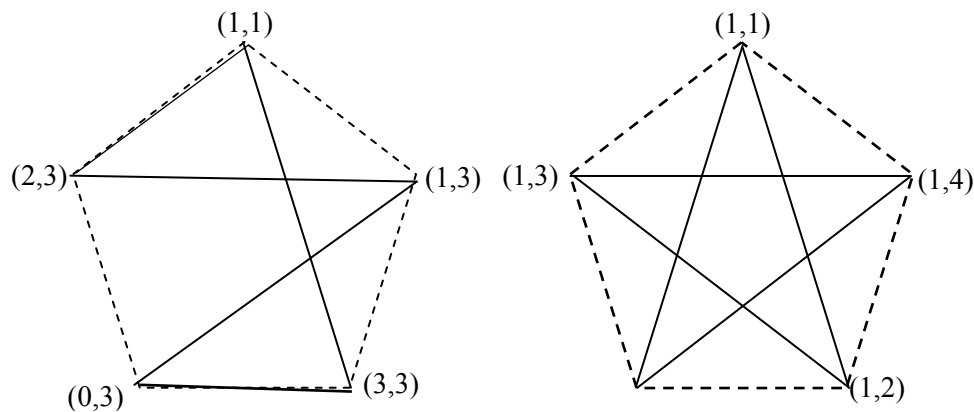
Two paired pentagonal (*n*=5) "Gloria to Ukraine Stars"

It is shown that the star{(1,1), (1,3), (3,3), (0,3),(2,3)} to be marked with dash edges, and the {(1,1), (2,3), (1,3), (0,3), (3,3)} – solid ones is the paired star (the outside star). The star {(1,1), (1,4), (1,2), (1,0), (1,3)} marked with dash edges, and the star {(1,1), (1,0), (1,4), (1,3), (1,2)} – solid ones is paired star also (the inner star). We have found numerous families of the two- and multidimensional stars, originated from the remarkable geometric properties and creative harmony of the real word [6].

S. Golomb's aptitude allowed him to see in the proposed project not only the "ideal ordered chain" combinatorial configurations but also the "ideal rings", which provide novel opportunities for the development of a new direction of fundamental and applied research in systems engineering with the direct use of one- and multidimensional combinatorial configurations of ring topology in radio electronics, communication, and numerous fields of advanced technologies. He not only approved our project, but also edited and substantiated the prospects for the implementation and further development of fundamental and applied research of combinatorial structures with ring topology, placing the right emphasis on the advantages of the latter over systems with a chain structure. Our collaboration was started in August 1996 from the report "Combinatorial Sequencing Theory for Optimisation of Signal Data Vectors Converting and Signal Processing" [7]. However, shortly we have got refusal letters from the CRDF in financial supporting the project.

Brief data on the scientific school of combinatorics at the Lviv Polytechnic National University

The scientific school of combinatorics at Lviv Polytechnic National University became known due to the fundamental and applied research of the "intelligent" two- and multidimensional combinatorial configurations prospected from the real world law of "elegant" deviding rotational symmetry into two complementary asymmetric parts. Each of them is an IRB with appropriate information parameters which being interrelated by this symmetry [6]. Design of systems with the "ideal" ring structures originated from solution of the engineering problem for expanding the range of time delays in transient analyzer on capacitor storage for researching dynamic processes in power electric stations on analog computers in 1968. One of the first publications for the perfect rings is connected with designing optimized memory devices [8]. The mathematical problem was to fix four switches on a moving rotor with different relative angular shifts of the ring switch, with the possibility of obtaining the widest possible range of time delays on a set of combination options for selecting the corresponding pair of swithes, one of them should bring the flowing voltage value to the memorizing element, and the second – to read the same value with a delay in time after turning the rotor of the switch to the appropriate angle [9]. Currently, we have a lot of patents, based on the idea of "perfect" one- and multidimensional IRBs.

The remarkable properties both optimal Golomb rulers and IRBs discover many opportunities to apply them to numerous branches of science and advanced technology, including vector information technologies and communications, vector data coding and multidimensional signal processing. These properties embedded in the laws of real world penetrating rotational symmetry.

ACKNOWLEDGMENTS

REFERENCES

1. *Solomon W. Golomb*. [Online]. Available: https://en.wikipedia.org/wiki/
2. *Golomb_ruler*. [Online]. Available: https://en.wikipedia.org/wiki/Golomb_ruler
3. *Ideal ring bundl*. [Online]. Available: https://uk.wikipedia.org/wiki/Ідеальна_ кільцева_в'язанка
4. V. Riznyk, *Synthesis of Optimal Combinatorial Systems*. Lviv: High School, 1989, 168 p.
5. V.V. Riznyk, "Information Technologies under the Manifold Coordinate Systems," *Perspective trajectory of scientific research in technical sciences: Collective*

monograph. Riga, Latvia: "Baltija Publishing", pp. 521–538, 2021. Available: https://doi.org/10.30525/978-9934-26-085-8-22

6. V. Riznyk, "Multi-modular Optimum Coding Systems Based on Remarkable Geometric Properties of Space," *Advances in Intelligent Systems and Computing*, no. 512, pp. 129–148, 2017. doi: 10.1007/978—319-45991-2_9.

7. S. Golomb, P. Osmera, and V. Riznyk, "Combinatorial Sequencing Theory for Optimisation of Signal Data Vectors Converting and Signal Processing," *Proc. All-European Workshop on Design Methodologies for Signal Processing, Zakopane, Poland, 1996*, pp. 43–44.

8. V.V. Riznyk, "Ideal Ring Relations and Possibilities of Their Practical Application," *Avtomatika*, no. 3, pp. 87–90, 1981.

9. *Certificate of authorship USSR № 527725 (1976), G 08 C9/06.*

INFORMATION ON THE ARTICLE

Volodymyr V. Riznyk, ORCID: 0000-0002-3880-4595, Institute of Computer Sciences and Information Technologies, Lviv Polytechnic National University, Ukraine, e-mail: ikv.riznyk@gmail.com

ДОСЛІДЖЕННЯ ТА ЗАСТОСУВАННЯ КОМБІНАТОРНИХ КОНФІГУРАЦІЙ ДЛЯ ІННОВАЦІЙНИХ ПРИСТРОЇВ І ТЕХНОЛОГІЙ / В.В. Різник

Анотація. Присвячено пам'яті Соломона Вольфа Ґоломба (1932–2016) — відомого американського математика, інженера, професора електротехніки, який зробив значний внесок у розвиток теорії лінійних регістрів зсуву і комбінаторної математики в теорії кодування та радіофізиці. Він цікавився розробленням методів підвищення якісних показників інженерних пристроїв і систем з погляду надійності, швидкості передавання, точності позиціонування і роздільної здатності на основі нових комбінаторних конфігурацій. У 1996 р. С. Ґоломб підтримав проєкт "Дослідження та застосування комбінаторних конфігурацій для інноваційних пристроїв та технологій" як наукову співпрацю дослідницької групи Державного університету «Львівська політехніка» (Україна) і Південно-каліфорнійського університету за спільною грантовою програмою Фонду цивільних досліджень та розвитку (США). Подано основний проєкт під редакцією С. Голомба, а також коротку інформацію про розвиток досліджень та застосування оптимізованих систем з кільцевою структурою.

Ключові слова: проєкт, комбінаторна конфігурація, ідеальна кільцева в'язанка, оптимізація, комбінаторна модель, наукова школа.

ІНТЕГРАЛЬНІ ЗОБРАЖЕННЯ ДОДАТНО ВИЗНАЧЕНИХ ЯДЕР

Ю.Є. БОХОНОВ

Анотація. Доведено можливість інтегрального зображення додатно визначеного ядра від двох пар змінних. Використано техніку побудови за цим ядром нового гільбертового простору, у якому формально комутують симетричні диференціальні оператори. При цьому ядро задовольняє систему диференціальних рівнянь із частинними похідними. Відомо, що ядро, задане в підобласті дійсної площини, не завжди припускає продовження на всю площину. Така можливість зумовлена проблемою існування комутувального самоспряженого розширення симетричних операторів. Застосовано результати, отримані автором, пов'язані з комутувальним самоспряженим розширенням у більш широкому гільбертовому просторі. Одержане інтегральне зображення за спектральною мірою, породженою розкладом одиниці операторів, дає змогу продовження додатно визначеного ядра на всю площину.

Ключові слова: гільбертовий простір, скалярний добуток, симетричний оператор, самоспряжений оператор, додатно визначене ядро, індекс дефекту, продовження оператора.

ВСТУП

Можливість інтегрального зображення додатно визначеного ядра (невиродженого) — одна з відомих класичних задач гармонічного аналізу. Існують різні підходи до її розв'язання. Один з них — побудова гільбертового простору зі скалярним добутком, що визначається за допомогою ядра, і знаходження симетричного (ермітового) оператора в цьому просторі, що припускає самоспряжене розширення. У разі необмеженості оператора ядро припускає інтегральне зображення за елементарними додатно визначеними ядрами. На цьому шляху доводиться, наприклад, відомий класичний факт Бохнера про інтегральне зображення додатно визначеної функції. У випадку ядра від кількох (парної кількості) змінних треба знайти симетричні оператори, що припускають комутувальне самоспряжене розширення в даному гільбертовому просторі або з виходом у більш широкий гільбертовий простір. Це вдається зробити не завжди, але існують умови на оператори, для яких таке продовження можливе. Якщо ядро визначено на підмножині простору змінних, таке інтегральне зображення дає можливість його продовжити на весь простір. Автор, спираючись на отримані ним результати [1, 2], про-

понує інтегральне зображення одного додатно визначеного ядра, функції $K(x_1, x_2, y_1, y_2)$, пари аргументів (x_1, x_2), (y_1, y_2) якої визначені на півсмузі двовимірної площини. На цьому шляху вдається продовжити цю функцію на площину зі збереженням додатної визначеності.

Нагадаємо основні конструкції, пов'язані з побудовою гільбертового простору, виходячи з розглядуваного додатно визначеного ядра, із симетричними операторами, що припускають комутувальне самоспряжене розширення. Міркування досить проводити для двох операторів.

Нехай є ланцюги сепарабельних комплексних гільбертових просторів з додатною і від'ємною нормами [3], у яких діє інволюція $h \to \overline{h}$:

$$H_-^{(1)} \supset H_0^{(1)} \supset H_+^{(1)}, H_-^{(2)} \supset H_0^{(2)} \supset H_+^{(2)} .$$

Використовуючи тензорні добутки, утворимо гільбертові простори

$$H_- = H_-^{(1)} \otimes H_-^{(2)}, H_0 = H_0^{(1)} \otimes H_0^{(2)}, H_+ = H_+^{(1)} \otimes H_+^{(2)}$$

і ланцюг

$$H_- \otimes H_- \supset H_0 \otimes H_0 \supset H_+ \otimes H_+ .$$

Позначатимемо через $(.,.)_0$ скалярний добуток у просторі $H_0 \otimes H_0$. Виходячи з конструкції побудови гільбертових просторів з додатною і від'ємною нормами, зазначимо, що цей скалярний добуток визначено для елементів $\alpha \in H_- \otimes H_-$, $w \in H_+ \otimes H_+ : (\alpha, w)_0$.

Узагальненим додатно визначеним ядром називається елемент $K \in H_- \otimes H_-$ такий, що $(K, u \otimes \overline{u}) \geq 0 \ \forall u \in H_+$. Будемо вважати це ядро невиродженим, тобто рівність $(K, u \otimes \overline{u}) = 0$ може справджуватись тоді і тільки тоді, коли $u = 0$. Це дає змогу ввести новий гільбертовий простір H_K, поповнивши H_+ за допомогою нового скалярного добутку $\langle .,. \rangle$:

$$\langle u, v \rangle = (K, v \otimes \overline{u}) \ \ \forall u, v \in H_+ .$$

Елементарним додатно визначеним ядром (ермітовим) називається елемент

$$\Omega_\lambda \in H_- \otimes H_-, \lambda \in \mathbb{R} : \|\Omega_\lambda\|_{H_- \otimes H_-} \leq C < \infty ;$$

$$(\Omega_\lambda, (A^* - \lambda I) v \otimes \overline{u})_0 = \left(\Omega_\lambda, v \otimes \overline{A^* - \lambda I u} \right)_0 = 0 .$$

Інакше кажучи, елементарне ядро — це узагальнений власний вектор оператора.

Далі замикання довільної множини $X \subset H_K$ позначатимемо через $[X]$.

Розглянемо оператори A_1, A_2 із всюди щільними, відповідно, у $H_+^{(1)}$, $H_+^{(2)}$ областями визначення $D(A_1) \subset H_+^{(1)}, D(A_2) \subset H_+^{(2)}$. Побудуємо оператори

$$B_1 = A_1 \otimes I, \ \ D(B_1) = D(A_1) \otimes H_+^{(2)}, \ B_2 = I \otimes A_2, D(B_2) = H_+^{(1)} \otimes D(A_2) .$$

Вони комутують у такому розумінні:

$$B_1 B_2 u = B_2 B_1 u \quad \forall u \in D(A_1) \otimes D(A_2).$$

Будемо вважати, що оператори B_1 і B_2 симетричні у H_K.

Нагадаємо, що для симетричного оператора A з областю визначення $D(A)$ у гільбертовому просторі H вводиться поняття дефектних чисел $d_z, d_{\bar{z}}$. Нехай $R(A,z) = \mathrm{Im}(A - zI) = (A - zI)D(A)$ і $N(A,z) = (R(A,z))^{\perp}$. Тоді $d_z = \dim N(A,z)$ — дефектне число для верхньої півплощини $z \in \mathbb{C}$, $\mathrm{Im}\, z > 0$, $d_{\bar{z}} = \dim N(A, \bar{z})$ для нижньої півплощини $\bar{z} \in \mathbb{C}$, $\mathrm{Im}\, \bar{z} < 0$. Пара $(d_z, d_{\bar{z}})$ називається індексом дефекту симетричного оператора. Індекс дефекту $(0, d_{\bar{z}})$ відповідає максимальному оператору, $(0,0)$ — самоспряженому. Зауважимо, що

$$N(A,z) = \{u \in D(A^*) : A^* u = \bar{z} u\}, \quad N(A, \bar{z}) = \{v \in D(A^*) : A^* v = z v\}.$$

Далі вважається, що, скажімо, симетричний оператор B_1 максимальний у H_K. Розглянемо його перетворення Келі за деякого $z_1 \in \mathbb{C}$, $\mathrm{Im}\, z_1 > 0$:

$$V_1(z_1) = (B_1 - \bar{z}_1 I)(B_1 - z_1 I)^{-1} : (B_1 - z_1 I)D(B_1) \to (B_1 - \bar{z}_1 I)D(B_1).$$

Із максимальності B_1 випливає, що одна з цих множин, наприклад, $(B_1 - z_1 I)D(B_1)$, всюди щільна у H_K.

Нагадаємо результат, отриманий у праці [1].

Теорема 1. Нехай оператори B_1 і B_2 симетричні в H_K, причому для довільного $w_2 \in H_+^{(2)}$ замикання у $[H_+^{(1)} \otimes w_2]$ звуження B_1 на $D(A_1) \otimes w_2$ є максимальним оператором за деякого $z_1 \in \mathbb{C}$, $\mathrm{Im}\, z_1 \neq 0$. Тоді існує комутувальне самоспряжене розширення цих операторів з виходом у більш широкий гільбертовий простір.

Застосуємо цей факт для одного конкретного прикладу.

ПОСТАНОВКА ЗАДАЧІ

Розглянемо додатно визначене невироджене ядро, яке є звичайною функцією: $K : D = [0, \infty) \times [0, \infty) \times [0, l] \times [0, l] \to \mathbb{C}$, $K, \dfrac{\partial K}{\partial x_1}, \dfrac{\partial K}{\partial y_1}, \dfrac{\partial^{l_1} K}{\partial x_1^{l_1}}, \dfrac{\partial^{l_2} K}{\partial y_2^{l_2}} \in$ $\in C(D)$, $l_1, l_2 = 1, 2$.

Нехай

$$p_1(x_1) = \exp(M x_1), M > 0 \text{ і } p(x_1, y_1) = p_1(x_1) p_1(y_1) = \exp(M(x_1 + y_1)).$$

Покладемо $\quad H_+ = L_{2, p_1}([0, \infty) \times [0, l]) = L_{2, p_1}[0, \infty) \otimes L_2[0, l] = H_+^{(1)} \otimes H_+^{(2)}$ [3, с. 709].

Будемо вважати, що виконуються такі умови:

1) справджується оцінка

$$\left|K(x_1, x_2, y_1, y_2)\right| \le \gamma \exp M(x_1 + y_1), \ \gamma, M > 0, \tag{1}$$

2) $\forall u \in H^+$

$$(K, u \otimes \overline{u}) = \int\limits_D K(x, y) u(y)\overline{u}(x) dx dy \overset{\Delta}{=}$$

$$\overset{\Delta}{=} \int\limits_0^\infty \int\limits_0^\infty \int\limits_0^l \int\limits_0^l K(x_1, x_2, y_1, y_2) u(y_1, y_2)\overline{u}(x_1, x_2) dx_1 dx_2 dy_1 dy_2 \ge 0, \tag{2}$$

причому рівність нулю можлива лише, якщо $u \equiv 0$,

3) функція K задовольняє рівняння

$$\frac{\partial K}{\partial x_1} + \frac{\partial K}{\partial y_1} = 0; \ \ \frac{\partial^2 K}{\partial x_2^2} + \frac{\partial^2 K}{\partial y_2^2} = 0. \tag{3}$$

Будемо також вважати, що за довільного $w_2 \in H_+^{(2)}$ і деякого $\beta > 0$ розбігається інтеграл

$$\int\limits_0^\infty \int\limits_0^\infty \int\limits_0^l \int\limits_0^l K(x_1, x_2, y_1, y_2) \exp(\beta(x_1 + y_1)) w_2(y_2)\overline{w_2(x_2)} dx_1 dx_2 dy_1 dy_2 = \infty, \tag{4}$$

ІНТЕГРАЛЬНЕ ЗОБРАЖЕННЯ ДОДАТНО ВИЗНАЧЕНОГО ЯДРА У ПІВСМУЗІ І ЙОГО ПРОДОВЖЕННЯ НА ПЛОЩИНУ

Визначимо на H_+ скалярний добуток за формулою

$$\langle u, v \rangle (K, v \otimes \overline{u}) = \int\limits_D K(x, y) v(y)\overline{u}(x) dx dy \overset{\Delta}{=}$$

$$\overset{\Delta}{=} \int\limits_0^\infty \int\limits_0^\infty \int\limits_0^l \int\limits_0^l K(x_1, x_2, y_1, y_2) v(y_1, y_2)\overline{u}(x_1, x_2) dx_1 dx_2 dy_1 dy_2.$$

Уведемо гільбертовий простір H_K як поповнення H_+ за нормою, породженою цим скалярним добутком.

Розглянемо оператори в H_K:

$$B_1 = A_1 \otimes I = -i\frac{\partial}{\partial x_1} \otimes I, \ \ B_2 = I \otimes A_2 = I \otimes \left(-\frac{\partial^2}{\partial x_2^2}\right),$$

де A_1, A_2 визначені на досить гладких фінітних функціях відповідно в областях $x_1, y_1 \in [0, \infty)$, $x_2, y_2 \in [0, l]$.

Використовуючи умови (3) і фінітність функцій з області визначення операторів A_1 і A_2, доведемо симетричність B_1 і B_2.

$$\langle B_1(u_1 \otimes u_2), v_1 \otimes v_2 \rangle =$$

$$= \int\limits_{0}^{\infty}\int\limits_{0}^{\infty}\int\limits_{0}^{l}\int\limits_{0}^{l} K(x_1,x_2,y_1,y_2)v_1(y_1)v_2(y_2)\overline{\left(-i\frac{\partial}{\partial x_1}\right)u_1(x_1)u_2(x_2)}\,dx_1dx_2dy_1dy_2 =$$

$$= i\int\limits_{0}^{\infty}\int\limits_{0}^{\infty}\int\limits_{0}^{l} K(x_1,x_2,y_1,y_2)v_1(y_1)v_2(y_2)\overline{u_1(x_1)u_2(x_2)}\Big|_{x_1=-\infty}^{\infty}\,dx_2dy_1dy_2 -$$

$$- i\int\limits_{0}^{\infty}\int\limits_{0}^{\infty}\int\limits_{0}^{l}\int\limits_{0}^{l} \frac{\partial}{\partial x_1}K(x_1,x_2,y_1,y_2)v_1(y_1)v_2(y_2)\overline{u_1(x_1)u_2(x_2)}\,dx_1dx_2dy_1dy_2 =$$

$$= i\int\limits_{0}^{\infty}\int\limits_{0}^{\infty}\int\limits_{0}^{l}\int\limits_{0}^{l} \frac{\partial}{\partial y_1}K(x_1,x_2,y_1,y_2)v_1(y_1)v_2(y_2)\overline{u_1(x_1)u_2(x_2)}\,dx_1dx_2dy_1dy_2 =$$

$$= i\int\limits_{0}^{\infty}\int\limits_{0}^{\infty}\int\limits_{0}^{l} K(x_1,x_2,y_1,y_2)v_1(y_1)v_2(y_2)\overline{u_1(x_1)u_2(x_2)}\Big|_{y_1=-\infty}^{\infty}\,dx_2dy_1dy_2 +$$

$$+ \int\limits_{0}^{\infty}\int\limits_{0}^{\infty}\int\limits_{0}^{l}\int\limits_{0}^{l} K(x_1,x_2,y_1,y_2)\left(i\frac{\partial}{\partial y_1}v_1(y_1)\right)v_2(y_2)\overline{u_1(x_1)u_2(x_2)}\,dx_1dx_2dy_1dy_2 =$$

$$= \langle u_1 \otimes u_2, B_1(v_1 \otimes v_2)\rangle.$$

Аналогічним чином доводиться симетричність оператора B_2.

Доведемо, що індекс дефекту оператора B_1 дорівнює $(0,1)$, тобто оператор максимальний.

Нехай $u \in N(A,z)$, $\operatorname{Im} z > 0$, тобто $A^*u = -i\dfrac{du}{dx_1} = \overline{z}u$. Звідси

$$u = C\exp(i\overline{z}\,x_1) = C\exp(\operatorname{Im} z\,x_1)\exp(i\operatorname{Re} z\,x_1).$$

Вибираючи $\operatorname{Im} z \geq \beta$ з інтегралу (4), упевнюємось в розбіжності інтеграла

$$\int\limits_{0}^{\infty}\int\limits_{0}^{\infty}\int\limits_{0}^{l}\int\limits_{0}^{l} K(x_1,x_2,y_1,y_2)\exp(\beta(x_1+y_1))w_2(y_2)\overline{w_2(x_2)}\,dx_1dx_2dy_1dy_2 = \infty.$$

Це означає, що $N(A,z) = \{0\}$ і дефектне число оператора B_1 для верхньої півплощини комплексної площини дорівнює нулю.

Нехай $v \in N(A,\overline{z})$, $\operatorname{Im} z > 0$. Звідси

$$v = C\exp(iz\,x_1) = C\exp(-\operatorname{Im} z\,x_1)\exp(i\operatorname{Re} z\,x_1).$$

Вибираючи $\operatorname{Im} z > M$, впевнимось, що $v \in N(A,\overline{z})$, $\operatorname{Im} z > 0$ породжується функцією $\exp(iz\,x_1)$, із чого випливатиме, що дефектне число оператора B_1 для нижньої півплощини комплексної площини дорівнює 1.

Згідно з оцінкою (1) маємо:

$$\int\limits_{0}^{\infty}\int\limits_{0}^{\infty}\int\limits_{0}^{l}\int\limits_{0}^{l} K(x_1,x_2,y_1,y_2)\exp(izy_1)\overline{\exp(izx_1)}w_2(y_2)\overline{w_2(x_2)}\,dx_1dx_2dy_1dy_2 \leq$$

$$\leq \gamma \int\limits_{0}^{\infty}\int\limits_{0}^{\infty}\int\limits_{0}^{l}\int\limits_{0}^{l} \exp(M - \operatorname{Im} z)(x_1 + y_1)\exp(M(x_2 + y_2)) \left| w_2(y_2)\overline{w_2(x_2)} \right| dx_1 dx_2 dy_1 dy_2 < \infty.$$

Очевидно, індекс дефекту оператора B_2 дорівнює $(1,1)$. Відповідно до результатів [1, 2] існує комутувальне самоспряжене розширення операторів B_1 і B_2 у більш широкому гільбертовому просторі. Тоді, згідно з працею [3], додатно визначене ядро K припускає інтегральне зображення від елементарних ядер за мірою $d\sigma(\lambda_1, \lambda_2)$, породженою розкладом одиниці (неортогональним) цих самоспряжених продовжень. Елементарні ядра породжуються фундаментальними системами розв'язків задач Коші:

$$-i\frac{du}{dx_1} = \lambda_1 u, \; u(0) = 1 \Rightarrow u(x_1, \lambda_1) = \exp(i\lambda_1 x_1);$$

$$-\frac{d^2 v_k}{dx_2^2} = \lambda_2 v_k, \;\; k = 0,1, \;\; v_0(0) = 1, \; v_0'(0) = 0, \; v_1(0) = 0, \; v_1'(0) = 1 \Rightarrow$$

$$\Rightarrow v_0(x_2, \lambda_2) = \cos\sqrt{\lambda_2}\, x_2, \, v_1(x_2, \lambda_2) = \frac{\sin\sqrt{\lambda_2}\, x_2}{\sqrt{\lambda_2}}.$$

У результаті доходимо до такого висновку.

Теорема 2. Нехай функція $K: D = [0,\infty) \times [0,\infty) \times [0,l] \times [0,l] \to C$, що задовольняє оцінку (1), є додатно визначеним ядром в розумінні (2) і задовольняє рівнянням (3). Тоді існує інтегральне зображення цього ядра за мірою, яка визначається неоднозначно:

$$K(x_1, x_2, y_1, y_2) =$$

$$= \int\limits_{-\infty}^{\infty}\int\limits_{-\infty}^{\infty} \exp(i\lambda_1(y_1 - x_1)) \sum_{j,k=0}^{1} v_k(y_2, \lambda_2)\overline{v_j(x_2, \lambda_2)} d\sigma(\lambda_1, \lambda_2). \tag{5}$$

Наслідок. Із виразу (5) випливає можливість продовження додатно визначеного ядра з півсмуги $(x_1, x_2),(y_1, y_2) \in [0,\infty) \times [0,l]$ на всю площину $(x_1, x_2),(y_1, y_2) \in \mathbb{R}^2$.

ВИСНОВКИ

Додатно визначені ядра, зокрема функції, відіграють важливу роль у різних розділах математики, зокрема, у гармонічному аналізі, теорії ймовірностей та теорії зображень груп. Для їх дослідження використовуються різні підходи. Один з них, використаний у роботі, належить М.Г. Крейну і базується на побудові за додатно визначеним ядром гільбертового простору і дослідженням формально комутувальних ермітових операторів. У разі існування їх комутувального самоспряженого продовження в даному просторі або з виходом з нього ядро припускає інтегральне зображення від елементарних додатно визначених ядер, які знаходяться як узагальнені власні функції цих операторів. У математичній літературі частіше розглядались ситуації, у яких самоспряжені комутувальні продовження будуються в гільбертовому прос-

торі. Автору належить кілька результатів, у яких доведено можливість побудови таких розширень у більш широкому гільбертовому просторі. Звичайно, в одержаному інтегральному зображенні ядра операторна міра знаходиться неоднозначно. Інші підходи до інтегральних зображень додатно визначених ядер містяться у працях [6, 7].

Слід також зауважити, що подібну техніку можна використати для інтегральних зображень додатно визначених ядер від нескінченної кількості змінних, які досліджуються, наприклад, у працях [4, 5].

ЛІТЕРАТУРА

1. Yu. Bokhonov, "Commuting self-adjoint extensions of systems of Hermitian operators," *Ukr. Math. Journ.*, vol. 40, no. 2, pp. 149–153, 1988.
2. Yu. Bokhonov, "On self-adjoint extensions of commuting Hermitian operators," *Ukr. Math. Journ.*, vol. 42, no. 5, pp. 695–697, 1990.
3. Yu. Berezansky, *Expansion in Eigenfunctions of Self-Adjoint Operators*. Kyiv: Naukova Dumka, 1965, 798 p.
4. Yu. Berezansky, *Self-adjoint operators in spaces of functions of an infinite number of variables*. Kyiv: Naukova Dumka, 1978, 360 p.
5. Yu. Berezansky and Yu. Kondratiev, *Spectral methods in infinite-dimensional analysis*. Kyiv: Naukova Dumka, 1988, 680 p.
6. *A.D. Manov,* "On the uniqueness of the extension of one function to a positive definite one," *Math. Notes*, **107**:4, pp. 639–652, 2020.
7. A.G. Sergeev, "Lectures on functional analysis," *Lekts. courses of the SEC of the MIAS*, vol. 23, pp. 3–101, 2014.

INFORMATION ON THE ARTICLE

Yurii E. Bokhonov, ORCID: 0000-0002-3355-008X, Educational and Scientific Institute for Applied System Analysis of the National Technical University of Ukraine "Igor Sikorsky Kyiv Polytechnic Institute", Ukraine, e-mail: yubochonoff@gmail.com

INTEGRAL REPRESENTATIONS OF POSITIVE DEFINITE KERNELS / Yu.E. Bokhonov

Abstract. The paper proposes proof of the possibility of an integral representation of a positive definite kernel of two pairs of variables. Using this kernel, we use the technique of constructing a new Hilbert space in which symmetric differential operators formally commute. In this case, the kernel satisfies a system of differential equations with partial derivatives. It is known that a kernel given in a subdomain of the real plane, generally speaking, does not always imply an extension to the entire plane. This possibility is related to the problem of the existence of a commuting self-adjoint extension of symmetric operators. The author applies his own results related to a commuting self-adjoint extension in a wider Hilbert space. The resulting representation in the form of an integral of elementary positive-definite kernels with respect to the spectral measure generated by the resolution of the identity of the operators allows us to extend the positive-definite kernel to the entire plane.

Keywords: Hilbert space, scalar product, symmetric operator, self-adjoint operator, positive definite kernel, defect index, operator extension.

APPROACH TO POSITIONAL LOGIC ALGEBRA

M. KOVALOV

Abstract. The method of Boolean function representation in terms of positional logic algebra in compact operator form is offered. Compared with the known method, it uses position operators with a complexity of no more than two and only one type of equivalent transformations. The method is less labor intensive. It allows parallelizing logic calculations. The corresponding way of Boolean function implementation is developed. It competes with some known ways in terms of hardware complexity, resource intensity, and speed when implemented on an FPGA basis. Possibilities open up for creating effective automating means of representing Boolean functions from a large number of variables, synthesizing the corresponding LCs, and improving modern element bases.

Keywords: boolean functions, positional logic algebra, positional operators, equivalent transformations, logic circuits, FPGA.

INTRODUCTION

The development of information systems involves a significant expansion and complication of logic calculations. Therefore, the development of new directions in the study and implementation of Boolean functions (BF), one of which is positional logic algebra of (PLA), seems promising. It includes principles and methods that allow BF representing and calculating using equivalent transformations and positional operators with polynomial complexity [1]. The application of positionality principles for arithmetic and parallelization of logic calculations is substantiated in PLA [1, 2]. Therefore, effective application of its apparatus is possible for artificial intelligence, pattern recognition, cryptography and etc., where it is necessary to operate BF from a large number of variables.

However, the following problems might be identified within PLA framework:

• cumbersome apparatus of sequentially performed equivalent transformations α-, β-, γ-, μ, i-inversions; τ-permutations; multi-parametric Δ-, λ-, Θ-, ω-transformations) and complex positional operators). The known method of BF representing from n variables [1] actually includes cumbersome analysis of many n order operators. The operator, which generates the most similar BF and has identical level, is chosen from them. After that with no less difficulty a sequence of multi-parameter equivalent transformations is selected. Therefore, for large n value, the application of the method is significantly labor-intensive;

• researches within PLA framework were mainly theoretical (solving a complex systems of logic equations, determining ratios of NP- and P-complete problem classes, etc.). Its practical application has not been considered enough [2, 3].

In view of these problems, it is reasonable not to idealize PLA and to oppose it to Boolean algebra, but interaction. Therefore, a less labor-intensive method of BF representing was proposed. It does not involve enumeration of solutions, but the formation process of less complex operators, only one type of equivalent

transformations and some Boolean algebra apparatus. Also, prerequisites are created for logic calculations parallelization. In accordance with the method hardware implementation of the BF was developed, which competes with some known methods in terms of hardware complexity, resource intensity and speed.

BF REPRESENTATION

The essence of the offered method is in the following. An arbitrary BF is covered by its fragments given by the corresponding conjunctions. For each of them, a simple positional operator can be formed, which generates closed BF of the fragment, which must be corrected to obtain exact BF values:

$$f_i = \left(\bigwedge_{t=1}^{n-k} \widetilde{x}_{\alpha t} \right) \wedge (f_{cor\,i}^1(X_k) \vee (S_{j_i}^k[X_k] \wedge f_{cor\,i}^0(X_k))), \tag{1}$$

here X_k — input argument vector with k digit capacity; $\left(\bigwedge_{t=1}^{n-k} \widetilde{x}_{\alpha t} \right)$ — ($n-k$)-rank conjunction ($\alpha_t \in \overline{1,n}$), which defines f_i fragment; $S_{j_i}^k$ — simple positional operator (j_i — binary vector of operator with dimension ($k+1$), $0 \le j \le 2^{k+1}-1$; k — operator order, $k \le n$), which generates the BF-prototype (the closest to the f_i). BF-correction $f_{cor\,i}^1$ has "1" values on those X_k vectors, where $S_{j_i}^k$ has "0" values but f_i has "1" values; BF-correction $f_{cor\,i}^0$ has "0" values on those X_k vectors, where $S_{j_i}^k$ has "1" values but f_i has "0" values.

The covering process begins with shaping and analysis of great fragments. With a large number of differences between BF-prototypes and fragments its sizes should be reduced. For this reason, the BF might be covered by the operator's records (1) fast enough. If we disjunctively combine records (1) and transform the resulting expression to the operator form, it will be received a representation of the original BF in PLA terms. Obviously, it is necessary to minimize complexity of such representation. There is no general decision of this minimization task. Larger fragments may have many corrections, but smaller fragments may result in a large number of fragments and records (1) respectively. Therefore, the following rule is developed. If $f_{cor\,i}^1$ and $f_{cor\,i}^0$ don't require large number of operators (usually two), it is not further defragmentation. And according record (1) includes in BF representation. On the other hand, the method does not need more complex transformations of input arguments as inverting. For this reason, from large number of equivalent transformations it is expedient to use one-parameter λ_w transformation. It inverts binary digits of argument corresponding to "1" in binary w code. For example, $\overline{a}b\overline{c}d = S_{16}^4\lambda_{10}[abcd]$. It is obvious that the implementation of such transformation is trivial. So, the process of BF representing is as follows:

1. The set F of fragment representations in the form (1) that cover BF is assumed to be empty. In set G of conjunctions that define analyzed fragments include initial BF Z.

2. If set G is empty, then go to step 9.

3. For each analyzed fragment in the set G generate:

– a binary vector $j = (j_0...j_k)$ of a simple positional operator $S_{j_l}^k$ that generates the BF-prototype, the closest to $f_{pr\,l}(X_k)$. Here $j_m = 1$ $(0 \le m \le k)$, if the case number when $f_l=1$ on vectors X_k with m 1's digits exceeds half of the total number of such vectors, else $j_m = 0$;

– estimate the operator number for describing of BF corrections $f_{corr\,l}^1(X_k)$ and $f_{corr\,l}^0(X_k)$ based on mismatches between f_l and $f_{pr\,l}(X_k)$.

4. Select a fragment f_s with the simplest records of BF corrections.

5. If $f_{corr\,l}^1(X_k)$ and $f_{corr\,l}^0(X_k)$ records in PLA terms don't require large number of operators (typically two) then go to step 7.

6. Include in set G all conjunctions of the next $(n-k+1)$-rank, which define non-empty f_s fragments. Go to step 8.

7. The selected fragment f_s written in form (1) include in the set *F*.

8. Exclude from G conjunction defining f_s and alternative conjunctions obtained with it in step 7, except the conjunction with which chosen conjunction can be glued. Go to step 2.

9. Disjunctively merge all records in form (1) of fragments included in the set *F*, obtaining a combined original BF representation. It includes positional operators and logic operations of Boolean algebra:

$$Z = \overset{r}{\underset{i=1}{\vee}} f_i, \tag{2}$$

where r — number of resulting fragments f_i $(1 \le i \le r)$.

10. Open all brackets in (2) and simplify it using Boolean algebra relations.

11. The original BF representation obtained in previous step is finally reduced to an operator form using relations between PLA and Boolean algebra, for example:

$$\widetilde{a}_n \wedge ... \wedge \widetilde{a}_1 = S_{2^n}^n \lambda_w[a_n...a_1]; \tag{3}$$

$$a_n \vee ... \vee a_1 = S_{2^{n+1}-2}^n[a_n...a_1]; \tag{4}$$

$$\widetilde{a}_n \wedge ... \wedge \widetilde{a}_{k+1} \wedge S_j^k[a_k...a_1] = S_{2^{n-k+1}}^{n-k} S_j^k \lambda_w[a_n...a_1]. \tag{5}$$

Example. Let some BF $F = f(X_5)$ has values "1" on vectors 1–3, 13–15, 19, 21–23 and 25–28. Following the known method [1], BF can be represented by a complex positional operator and a sequence of equivalent two-parameter transformations like this:

$$Z = S_4^1 S_{14}^4 \omega_{30}^{17} \omega_{29}^{19} \omega_{24}^{21} \omega_{20}^{23} \omega_{18}^{16} \omega_{17}^{16}[x5x4x3x2x1]. \tag{6}$$

The BF representation following the proposed method looks like:

s. 1: $F = \{\}; G = \{Z\}$.

Cycle 1:

s. 2: G is non-empty, go to s. 3.

s. 3–5: for Z form: $f_{pr\,Z}(x5x4x3x2x1) = S_{24}^{5}[x5x4x3x2x1]$.
$f_{corr\,Z}^{1}(x5x4x3x2x1)$ has values "1" on vectors 1–3, $f_{corr\,Z}^{0}(x5x4x3x2x1)$ has values "0" on vectors 1–3, 7, 11, 29, 30. To record them more than 2 operators are required, hence go to s. 6.

s. 6, 8: $G = \{x1, x2, x3, x4, x5, \overline{x1}, \overline{x2}, \overline{x3}, \overline{x4}, \overline{x5}\}$.

Cycle 2:

s. 2: G is non-empty, go to s. 3.

s. 3–5: the fragment defined by the conjunction $\overline{x1}$ requires the simplest corrections. For it $f_{pr\,\overline{x1}}(x5x4x3x2) = S_{8}^{4}[x5x4x3x2]$. There is no need in $f_{corr\,\overline{x1}}^{0}(x5x4x3x2)$, only one operator is enough for $f_{\kappa op\,\overline{x1}}^{1}(x5x4x3x2)$ defining on vector 1 ($x5x4x3x2$=0001), hence go to s. 7.

s.7: write the selected fragment in the form (1) as $f_{\overline{x1}} = \overline{x1}(S_{8}^{4}[x5x4x3x2] \vee \overline{x5x4x3x2})$. Hence $F = \{\overline{x1}(S_{8}^{4}[x5x4x3x2] \vee \overline{x5x4x3x2})\}$.

s. 8: $G = \{x1\}$.

Cycle 3:

s. 2: G is non-empty, go to s. 3.

s. 3–5: for the fragment defined by conjunction $x1$, form $f_{pr\,x1}(x5x4x3x2) = S_{13}^{4}[x5x4x3x2]$. $f_{corr\,x1}^{1}(x5x4x3x2)$ has value "1" on vector 1, a $f_{corr\,x1}^{0}(x5x4x3x2)$ — has value "0" on vectors 3, 5, 14. More than 2 operators are required to write them, hence go to s. 6.

s. 6, 8: $G = \{x1x2, x1x3, x1x4, x1x5, x1\overline{x2}, x1\overline{x3}, x1\overline{x4}, x1\overline{x5}\}$.

Cycle 4:

s. 2: G is non-empty, go to s. 3.

s. 3–5: the fragment defined by the conjunction $x1\overline{x2}$ does not require correction. For it $f_{pr\,x1\overline{x2}}(x5x4x3) = S_{5}^{3}[x5x4x3]$. Go to s. 7.

s. 7: write the selected fragment in the form (1) as $f_{x1\overline{x2}} = x1\overline{x2}S_{5}^{3}[x5x4x3]$. Hence $F = \{\overline{x1}(S_{8}^{4}[x5x4x3x2] \vee \overline{x5x4x3x2}), x1\overline{x2}S_{5}^{3}[x5x4x3]\}$.

s. 8: $G = \{x1x2\}$.

Cycle 5:

s. 2: G is non-empty, go to s. 3.

s. 3–5: for the fragment defined by conjunction $x1x2$, form $f_{prx1x2}(x5x4x3) = S_{5}^{3}[x5x4x3]$. $f_{corr\,x1x2}^{1}(x5x4x3)$ has value "1" on vector 4, only one operator is enough for it, there is no need in $f_{\kappa op\,x1x2}^{0}$. Go to s. 7.

s. 7: write the selected fragment in the form (1) as $f_{x1x2} =$ $= x1x2(S_5^3[x5\,x4\,x3] \vee x5\,\overline{x4}\,\overline{x3})$. Therefore $F = \{\overline{x1}(S_8^4[x5\,x4\,x3\,x2] \vee \overline{x5x4x3x2}),$ $x1\overline{x2}S_5^3[x5x4x3], x1x2(S_5^3[x5x4x3] \vee x5\overline{x4x3})\}$.

s. 8: $G = \{x1\}$.

The set G is empty. Entire original BF is covered with fragments from the set F, so go to s. 9.

s. 9: Get first Z representation:

$$Z = \overline{x1}(S_8^4[x5x4x3x2] \vee \overline{x5x4x3x2}) \vee x1\overline{x2}S_5^3[x5x4x3] \vee$$

$$\vee x1x2(S_5^3[x5x4x3] \vee x5\overline{x4x3}). \tag{7}$$

s. 10: Open brackets in (7):

$$Z = \overline{x1}S_8^4[x5x4x3x2] \vee \overline{x5x4x3x2\overline{x1}} \vee x1\overline{x2}S_5^3[x5x4x3] \vee$$

$$\vee x1x2S_5^3[x5x4x3] \vee x5\overline{x4x3}x2x1.$$

Glue 3rd and 4th conjunctions and select common variables in the 2nd and 5th conjunctions:

$$Z = \overline{x1}S_8^4[x5x4x3x2] \vee \overline{x4x3}x2(\overline{x5x1} \vee x5x1) \vee x1S_5^3[x5x4x3]. \tag{8}$$

s. 11: expression in brackets of the second term in (8) might be written as $S_5^2[x5x1]$, for each conjunction, use (5). It is necessary to use corresponding one-parameter transformations λ_w for variable inverting (3):

$$Z = S_4^1 S_8^4 \lambda_{16}[x1x5x4x3x2] \vee S_{16}^3 S_5^2 \lambda_{24}[x4x3x2x5x1] \vee S_4^1 S_5^3[x1x5x4x3].$$

Now apply (4) and finally get original BF representing as:

$$Z = S_{14}^3[S_4^1 S_8^4 \lambda_{16}[x1x5x4x3x2], S_{16}^3 S_5^2 \lambda_{24}[x4x3x2x5x1], S_4^1 S_5^3[x1x5x4x3]]. \tag{9}$$

This example shows that the internal operators in complex positional operators serve to set the BF-prototypes of fragments, and the external ones set conjunctions that uniquely determine these fragments. Therefore, the complexity of positional operators in such representing in most does not exceed two, while maintaining their compactness.

According to representation (9), it is possible to build a flow graph of logic calculations (Fig. 1). If it is assumed that transformation and operator are performed during the same time, then the calculation of the BF will take 4 steps. The sequential process of calculating the same BF according to expression (6) lasts 8 steps. It might also be seen that, compared with the known method, the proposed method also allows parallelize execution of positional operators and equivalent transformations, reducing the time for BF calculating.

It is difficult to compare the complexities of the proposed and known [1] methods directly. However, it might be done by evaluating the number of analyzed fragments in the maximum case and positional operators of order *n*. In accordance with the proposed method, first, the entire original BF is considered,

then — $(2n)$ fragments depend on $(n$–$1)$ variables, then — $(2^2(n-1))$ fragments on $(n$–$2)$ variables, etc. Therefor the maximum number of fragments is evaluated as $N_f \approx 2^{n+1}$. Estimating the number of operators analyzed in accordance with the known method reduces to the combinatorial task of partitioning the number n into terms. Using the Hardy-Ramanujan formula [4] and considering that for any complexity and order n it might be build (2^{n+1}) operators at least,

get $N_{op} \approx \dfrac{2^{n+1} e^{\pi\sqrt{\frac{2n}{3}}}}{4n\sqrt{3}}$ all types positional operators. Obviously, the developed

method is significantly less labor intensive.
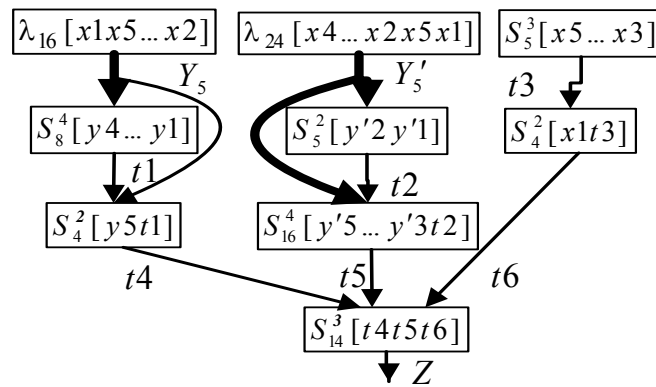
Fig. 1. Flow graph of logic calculations $Z = f(X_5)$

HARDWARE IMPLEMENTATION

The BF implementation in accordance with the proposed method is a combinational logic circuit (LC). It should be based on the form (2). For example, hardware implementation of the conjunctions and disjunctions in (1) and (2) is more efficient directly using logic elements. And BF corrections are implemented in accordance with their disjunctive normal form. The maximum number of fragments in form (2) is a power of two. Hence the same number of identical functional blocks (FBs) is applicable for its implementation, as well as the corresponding number of other logic blocks and elements. Thus, structure of such LC (Fig. 2) includes:

(2^{n-k-1}) blocks for determining the number of "1" in the input argument vector X_k;

(2^{n-k}) FBs for fragments f_i implementing;

OR logic element 4 for disjunction implementing in accordance with the form (2).

Each FB contains:

group of logic elements 1, which with the corresponding block for determining the number of "1" implements a simple positional operator $S_{j_i}^{k}[X_k]$ for current fragment;
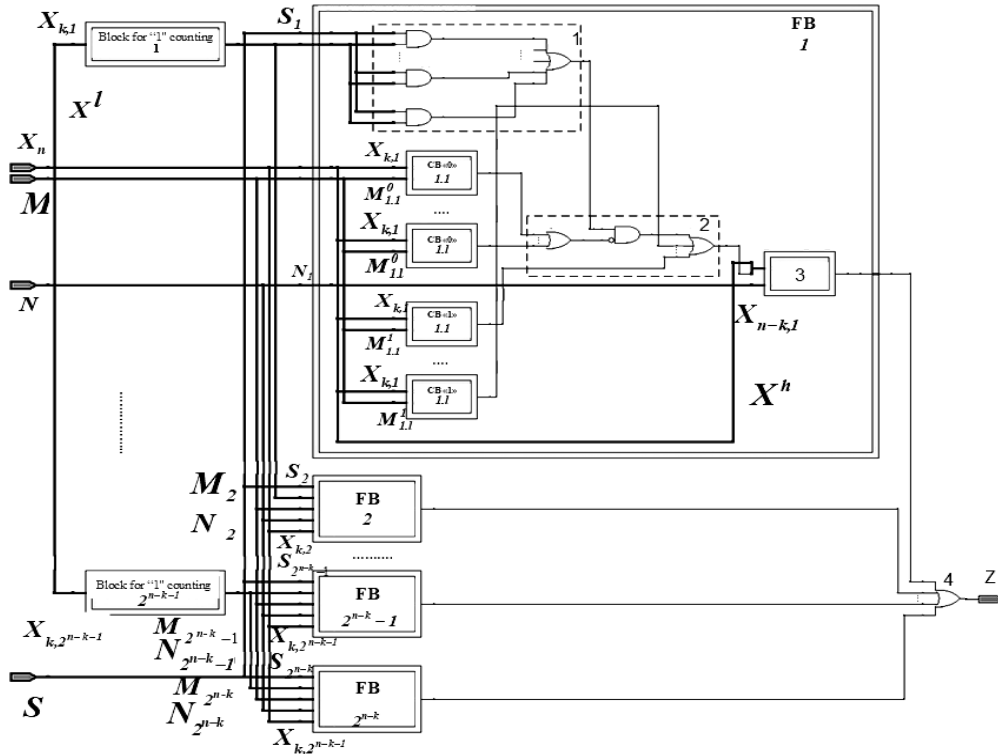
Fig. 2. LC for the BF implementation by the proposed method

l correction blocks (CBs "0" or "1"), that implement respectively BF-corrections $f_{corr\,i}^0(X_k)$ and $f_{corr\,i}^1(X_k)$ with a group of logic elements 2. Each of them is a k-input logic element AND with controlled input inverters;

block 3 of logic element AND, one input of which is the f_i value. Remaining $(n-k)$ inputs have controlled inverters for the implementation of the conjunction $\left(\overset{n-k}{\underset{t=1}{\wedge}} \tilde{x}_{\alpha\,t} \right)$ accordance with (1).

Input signals of the LC:

input vector of arguments X_n (input X);

2^{n-k} vectors of positional operators (input S);

2^{n-k} control signals for CB inverters (input M);

2^{n-k} control signals for inverters of block 3 (input N).

The number of BFs, calculable by the LC, is directly determined by thes number and bit capacity k of FBs, CBs:

$$N_{BF\,PAL} \approx (N_{BF\,fr}(k,l))^{2^{n-k}} \prod_{i=0}^{n-k-1} (n-i)^{2^i}, \qquad (10)$$

where $N_{BF\,fr}(k,l)$ – the number of BFs depending on k variables, which, taking into account l CBs "0" and "1", are calculated by one FB.

Being a complex combinatorial dependence $N_{BF\,PAL} >> 2^{n+1}$ (number of all simple positional operators). Therefore, this LC is capable to calculate a large number of practically used regular BFs depend on *n* variables. In addition, many partially defined BFs might be extended to a form convenient for calculating on similar LCs.

The following hardware characteristics of the proposed LC were defined:

– complexity as a number of two-input logic elements:

$$L(n,2)_{PAL} = 2^{n-k-2}(3k^2 + 4n + k(8l+5)) - 1;\qquad(11)$$

– LC depth defined as a number of cascades on signal way from input to output through the block for determining the number of "1", groups 1, 2 of logic elements and block 3:

$$T_{PAL} = n + k +]\log_2 k[+]\log_2(n-k)[+1;\qquad(12)$$

– input numbers:

$$N_{in\,PAL} = n + 2^{n-k}(2n + k(2l-1)+1).\qquad(13)$$

The developed LC allows to simply change the number and bit capacity of the main logic blocks. It allows flexible change the ratio between its functionality and hardware requirements, that follows from (10)–(13).

Let's implement BF considered in the example by this LC. According the LC structure, it is necessary transform (7) so that all operators have same order 3. Simple positional operator $S_j^k[X_k]$ might be represented with simple operators of smaller order in the next way:

$$S_j^k[x_k...x_i...x_1] = x_i S_{j1}^{k-1}[x_k...x_{i+1}x_{i-1}...x_1] \vee \overline{x_i} S_{j2}^{k-1}[x_k...x_{i+1}x_{i-1}...x_1].\qquad(14)$$

Using (14), represent the first operator in (7) as:

$$S_8^4[x5x4x3x2] = x2 S_8^3[x5x4x3] \vee \overline{x2} S_4^3[x5x4x3].$$

Transform (7) to the form:

$$Z = \overline{x1}x2(S_8^3[x5x4x3] \vee \overline{x5x4x3}) \vee \overline{x1}x2 S_4^3[x5x4x3] \vee$$

$$\vee x1\overline{x2} S_5^3[x5x4x3] \vee x1x2(S_5^3[x5x4x3] \vee x5\overline{x4x3}),\qquad(15)$$

getting 4 fragments described by operators $S_8^3, S_4^3, S_5^3, S_5^3$. The first and last of them are corrected by $f_{corr1}^1 = \overline{x5x4x3}$ and $f_{corr4}^1 = x5\overline{x4x3}$ respectively. Therefore, for BF calculating in the form (15) it is suitable LC that includes 3-bit 2 blocks determining the number of "1" and 4 FBs, including one CB per block. The input variables are inverted according to the input control signals M and N. Zero values might be entered to the information inputs of unused CBs of FBs 2 and 3. Thus, LC inputs (Fig. 2) are:

blocks determining the number of "1": $X_1^h = X_2^h \equiv x1x2$; $X_1^l = X_2^l \equiv$ $= x5x4x3$;

FB 1: $S_1 \equiv 1000$, $M_1 \equiv 111$, $N_1 \equiv 10$;

FB 2: $S_1 \equiv 0100$, $M_2 \equiv 000$, $N_2 \equiv 11$;

FB 3: $S_3 \equiv 0101$, $M_3 \equiv 000$, $N_3 \equiv 01$;

FB 4: $S_4 \equiv 0101$, $M_4 \equiv 011$, $N_4 \equiv 00$.

PRACTICAL RESEARCH

In practical research, in addition to the developed method some known ways of BF implementation [5] were considered. They implement any BF depend on n variables with optimal hardware complexity:

– multiplexer with $(n-1)$ selector inputs based on a rectangular decoder [6]. The values of its hardware complexity, depth and number of inputs are:

$$L(n,2)_{MUX} = 3\left(2^{n-1} + 2^{\frac{n}{2}} - 3 \right), \tag{16}$$

$$T_{MUX} = \frac{3n}{2}, \tag{17}$$

$$N_{in\ MUX} = 2^{n-1} + n - 1; \tag{18}$$

– LC based on the cascade method [7]:

$$L(n,2)_{casc} = 3(2^{n-1} - 1), \tag{19}$$

$$T_{casc} = 2(n-1), \tag{20}$$

$$N_{in\ casc} = 2^{n-1} + n - 1. \tag{21}$$

Dependences of hardware complexity, depth, number of LC inputs are based on (10)–(13), (16)–(21). Also, for the developed LC structure with a different number of FBs and CBs (*l* CB "0" and "1" in each FB) the number of countable BFs depend on the number of variables *n* is obtained. The parameters of resource intensity and speed of the FPGA-based (Field Programmable Gate Array) implementation of the proposed LC were gotten. Schemes were described on VHDL, synthesis and modeling were carried out using Intel Quartus Prime and Siemens Modelsim. Comparative studies are made.

Dependencies on Fig. 3 and 4 (given on a logarithmic scale) show that FB number increasing (a *k* decreasing at invariable *n*) leads to the significant increase of the calculable BF number and hardware complexity of the proposed LC (dependencies 2, 5 and 7). However, it makes sense to increase, the number of CBs within the FB. This can increase the functionality of the proposed LC to the level provided by a large number of FBs, but with lower hardware costs (dependencies 4–6). When $n > 7$ developed LC structure provides an overwhelming advantage sod.
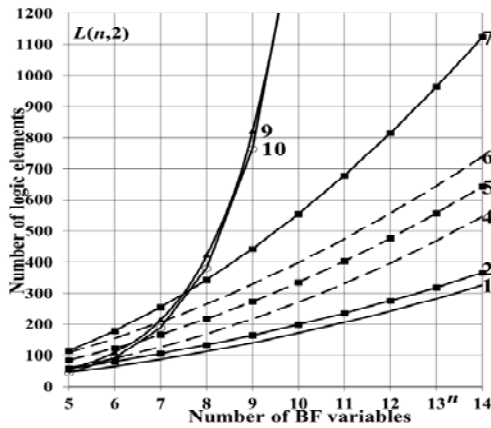
Fig. 3. Hardware complexity of *LCs*
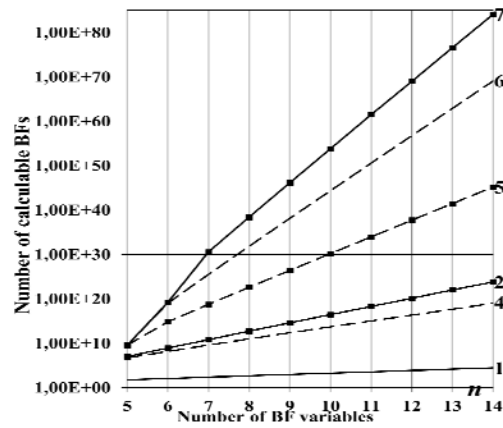
Fig. 4. Number of calculable *BFs*

The resource intensity of the FPGA-based LC implementations (Fig. 5) at most corresponds its hardware complexity (Fig. 3). When $n > 10$ the proposed LC provides a significant advantage over the known ways also in the LC input numbers (Fig. 6). From these dependences it is shown that for functionality expanding and equipment minimizing more effectively increase the CB number.
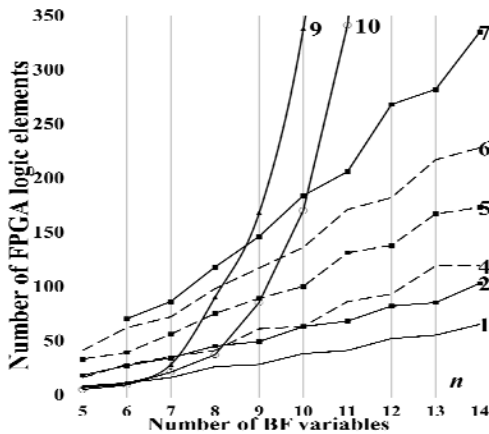

Fig. 5. Resource intensity of the LC integral implementations
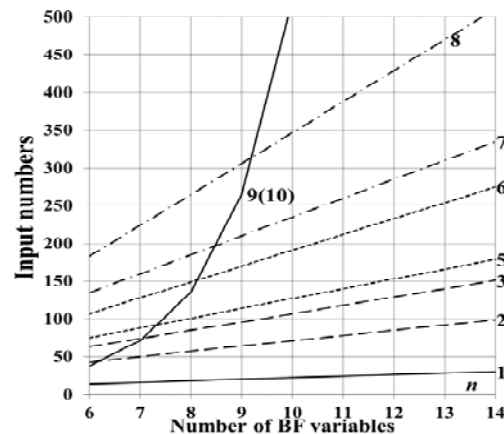
Fig. 6. LC input numbers

The depth of the developed LC (Fig. 7) depends mainly on *n*, so the dependences 1, 2, 5 and 7 are close to each other. A similar trend is observed for the performance of LC integral implementations (dependencies 1, 2, 4–7 on Fig. 8). Although the LCs based on multiplexer or cascade method, when implemented on FPGA basis, have less depth, but the difference in performance is practically leveled. The proposed LC structure may provide higher performance when a large number of variables (*n*>11).

CONCLUSIONS

In comparison with the known method the developed method of boolean function representation in terms of PLA is characterized by the following:

– uses positional operators with complexity no more than two and only one type of equivalent transformations;

– less labor intensive and compactness of BF representation;

– allows to parallelize execution of equivalent transformations and operators, reducing BF calculation time.
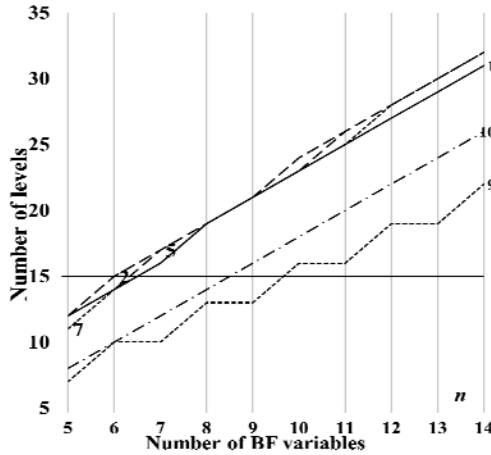

Fig. 7. Depth of the LCs
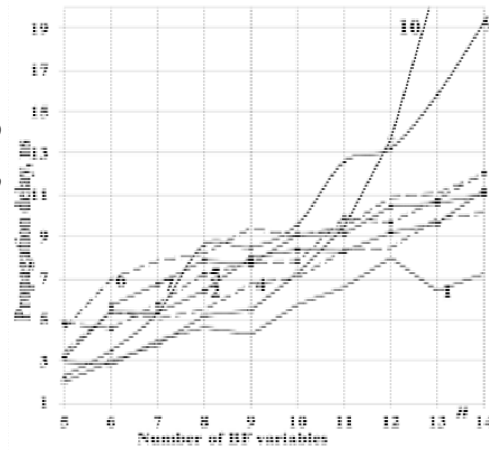
Fig. 8. Performance of the LC integral implementations

1 — proposed LC ($n-k=0, l=0$); 2 — proposed LC ($n-k=1, l=1$);
3 — proposed LC ($n-k=1, l=2$); 4 — proposed LC ($n-k=2, l=0$);
5 — proposed LC ($n-k=2, l=1$); 6 — proposed LC ($n-k=2, l=2$);
7 — proposed LC ($n-k=3, l=1$); 8 — proposed LC ($n-k=3, l=2$;
9 — multiplexer; 10 — LC based on the cascade method

The developed LC structure, in comparison with some known ways of BF implementation, has a significantly fewer hardware complexity when $n>7$. As a result, corresponding FPGA-based implementation also requires fewer logic resources and input number without losing in performance. To expand its functionality, it is more efficient to increase the number of CBs in FBs. The regularity and scalability of the LC structure provide effective control the involvement in operation process its parts by using, for example, "operand isolation" technology [8, 9]. This creates the prerequisites to change flexible the ratio between LC functionality, technical and economic parameters of the integral implementation, "bypassing" possible failures, increasing its reliability. In addition, possibilities for creating effective automating means of representing BF from a large number of variables, synthesizing the corresponding LCs and modern element bases improvement open up.

REFERENCE*S*

1. M. Telpiz, *Algebra of positional operators and equivalent transformations*. M.: Scientific advice on a complex problem, 1988.
2. C.M. Hamann and L. Chtcherbanski, "Positional Logic Algebra — PLA – A Fascinating Alternative Approach,"*ICSI Technical Report TR-97-039*, Sep. 1997.
3. M.I. Telpiz, "Sigma-notation and the equivalence of p and np classes,"*J. Inf. Organ. Sci.*, vol. 29, no. 2, Mar. 2012.
4. T. Jiang and K. Wang, "A generalized Hardy-Ramanujan formula for the number of restricted integer partitions,"*Journal of Number Theory*, vol. 201, pp. 322–353, Aug.

2019. Accessed on: Feb. 6, 2023. [Online]. Available: https://doi.org/ 10.1016/j.jnt.2019.02.006

5. D. Harris and S. Harris, *Digital Design and Computer Architecture: ARM Edition*. Morgan Kaufmann, 2015.

6. A.N. Borodzhieva, I.I. Stoev, and V.A. Mutkov, "FPGA Implementation of Boolean Functions Using Multiplexers," in *2019 IEEE XXVIII International Scientific Conference Electronics (ET), Sozopol, Bulgaria, Sep. 12–14, 2019*. Accessed on: Feb. 6, 2023. [Online]. Available: https://doi.org/10.1109/et.2019.8878504

7. A.N. Borodzhieva, I.I. Stoev, I.D. Tsvetkova, S.L. Zaharieva, and V.A. Mutkov, "FPGA Design of Boolean Functions Using a Cascade of Decoders and Logic Gates," in *2020 43rd International Convention on Information, Communication and Electronic Technology (MIPRO), Opatija, Croatia, Sep. 28–Oct. 2, 2020, IEEE, 2020*. Accessed on: Feb. 6, 2023. [Online]. Available: https://doi.org/10.23919/ mipro48935.2020.9245448

8. A.A. M. Bsoul, S.J.E. Wilton, K.H. Tsoi, and W. Luk, "An FPGA Architecture and CAD Flow Supporting Dynamically Controlled Power Gating,"*IEEE Transactions on Very Large-Scale Integration (VLSI) Systems*, vol. 24, no. 1, pp. 178–191, Jan. 2016. Accessed on: Feb. 6, 2023. [Online]. Available: https://doi.org/10.1109/ tvlsi.2015.2393914

9. C. Ashok Kumar, B.K. Madhavi, and K.L. Kishore, "Enhanced Clock Gating Technique for Power Optimization in SRAM and Sequential Circuit,"*Journal of Automation, Mobile Robotics and Intelligent Systems*, pp. 32–38, Jan. 2022. Accessed on: Feb. 6, 2023. [Online]. Available: https://doi.org/10.14313/jamris/2-2021/11

INFORMATION ON THE ARTICLE

Mykola O. Kovalov, ORCID: 0000-0002-2590-4052, National Technical University of Ukraine "Igor Sikorsky Kyiv Polytechnic Institute", Ukraine, e-mail: kovua@yahoo.com

ПІДХІД ДО ПОЗИЦІЙНОЇ АЛГЕБРИ ЛОГІКИ / М.О. Ковальов

Анотація. Запропоновано метод подання булевих функцій у термінах позиційної алгебри логіки в компактній операторній формі. Порівняно з відомим методом у ньому застосовуються позиційні оператори зі складністю не більше двох і лише одного виду еквівалентних перетворень. Метод відрізняється меншою трудомісткістю і розкриває паралелізм логічних обчислень. Запропоновано відповідний спосіб реалізації булевих функцій. Він становить конкуренцію деяким відомим способам за апаратною складністю, ресурсомісткістю та швидкістю із застосуванням базису FPGA. Відкриваються можливості для створення ефективних засобів автоматизації подання булевих функцій від великої кількості змінних, синтезу відповідних комбінаційних схем та вдосконалення сучасних елементних баз.

Ключові слова: булеві функції, позиційна алгебра логіки, позиційні оператори, еквівалентні перетворення, комбінаційні схеми, FPGA.

MATHEMATICAL MODELLING OF CRYSTALLIZATION OF POLYMER SOLUTIONS

K. ZELENSKY

Abstract. The processes of homogenization and crystallization of polymer solutions in cylindrical pipes are considered, which are described by the convective-diffusion equation with respect to the solution temperature and kinetic equations with respect to homogenization and crystallization of the polymer known as the thermokinetic nonlinear boundary value problem. A numerical-analytical iterative method for solving this problem is proposed, which consists of stepwise obtaining solutions of kinetic equations with respect to homogenization and crystallization of polymer solutions depending on the solution temperature and obtaining a solution of the convective-diffusion problem with respect to melt temperature. The accuracy of the obtained solution is determined by the norm of the difference between two adjacent iterations. The value of the crystallization coefficient, which is close to unity, determines the length of the dosing zone and the transition to the next zone – the flow of homogenized polymer into the distribution head of the extruder. The results of mathematical modelling are given.

Keywords: homogenization, integral transformations, iterative method, crystallization, mathematical model, nonlinear boundary value problem.

INTRODUCTION

The solution of the problem of polymer crystallization can be carried out on the basis of a mathematical model that describes the heat transfer processes of polymer melts and the cooling agent.

The main difference between the crystallization of polymers and the crystalliza\-tion of other types of materials (eg, metals) is that the crystallization of polymer melts is carried out in the space-time domain. With regard to the crystallization of polymer solutions in extrusion devices, the situation is complicated by the movement not only of the crystallization front, but also by the motion of the solid mixture heated to the melting temperature under the rotational motion of the screw worm. The crystallization process is phase, accompanied by the release of heat and leads to stresses. Determining the values of the coordinate $z = L$, in which the degree of crystallization becomes close to unity, determines the length of the dosing zone of the polymer, after which the polymer enters the extruder head. This factor plays a crucial role in ensuring the formation of a quality source product (for example, the quality of the insulating coating of the cable or the quality of the polyethylene film) at the outlet of the extruder.

PROBLEM STATEMENT

The goal of solving the problem of crystallization of polymer solutions is to develop an optimal strategy for cooling polymer solutions in order to reduce processing time and limit the use of excessively low cooling temperatures.

Overview of approaches to building models

A significant number of scientific and applied works [1, 6–8,10–15] are devoted to the construction of mathematical models of crystallization for various purposes.

Mathematical models of polymer crystallization in the form of a thin disk (one-dimensional model) are considered in [1, 12, 13]. The model consists of two nonlinear differential equations for the degree of crystallinity $y(r,t)$, defined as the average volume fraction of the space occupied by crystals, and the temperature field $T(r,t)$, combined using the norm of the nucleation and growth function $b_N(T)$ and $b_G(T)$, the nucleation initiation function and the aggregation $k(y) = 1 - y^2$ and saturation function of nuclei $\beta(y) = y(1-y)$:

$$\frac{\partial y}{\partial t} = \beta(y(r,t))b_G(T(r,t)) + v_0 k(y(r,t))b_N(T(r,t));$$

$$\frac{\partial T}{\partial t} = \sigma\left(\frac{\partial^2 T}{\partial r^2} + \frac{1}{r}\frac{\partial T}{\partial r}\right) + a_G \beta(y(r,t))b_G(T(r,t)).$$

In the given mathematical model of crystallization of the polymer solution, there are no connections of the determining components b_G, b_N from the temperature of the solution.

In [4], a mathematical model is considered, in which the dependence of the crystallization coefficient on the temperature of the polymer melt is specified explicitly.

In [8], the mathematical model takes into account the clear dependence of not only the crystallization coefficient, but also the polymerization coefficient, since these characteristics are interconnected.

Two macrokinetic parameters α and β, which determine the specific contribution of the polymer and crystalline phases, respectively, are introduced. The degree of polymerization $\alpha(t)$ determines the degree of completion of the polymerization process and can take values from 0 (the polymer content is 0) to 1 (all the monomer has turned into a polymer). The degree of crystallization $\beta(t)$ determines the degree of completion of the crystallization process and can take values from 0 (the content of the crystalline phase is 0) to 1 (the entire amorphous phase of the polymer has turned into a crystalline one). To quantitatively characterize the degree of completion of the phase transformation $\beta \in [0,1]$, a parameter called the relative degree of crystallinity is used.

Determination of temperature fields $T(r,z)$ and the degree of crystallinity $\beta(r,z)$ in insulation consists in the joint solution of the heat conduction equation and the kinetic equation:

$$V\frac{\partial T}{\partial z} = \frac{1}{c\rho}\left[\frac{1}{r}\frac{\partial}{\partial r}\left(r\lambda\frac{\partial T}{\partial r}\right) + \frac{\partial}{\partial z}\left(\lambda\frac{\partial T}{\partial z}\right)\right] + Q_v, \quad r \in (R_g, R_{iz}),\ z \in (0, L); \quad (1)$$

$$\frac{\partial \beta}{\partial z} = \frac{1}{V}\left[K_0 \exp\left(-\frac{U}{RT} - \frac{\psi T_{iz}}{T(T_{iz} - T)}\right)\right](1 + C_0\beta)[\beta_p(T) - \beta]; \quad (2)$$

$$r \in (R_g, R_{iz}), \ z \in (0, L), \quad Q_v = \frac{VQ_m}{c} \frac{\partial \beta}{\partial z}.$$

The problem is solved under appropriate boundary and initial conditions. Note that the equations (1), (2) are written relative to the processes in the insulation, and the boundary conditions contain the conditions for the current-conducting core. In addition, the equation for the degree of crystallization is written relative to the variable , that is, a stationary problem is considered.

The presented mathematical model of polymer crystallization refers, according to the authors, to the processes of applying polymer insulation to a conductive core. However, the process of crystallization of the polymer solution is carried out even before the insulation is applied to the core, that is, in the dosing zone of the extruder. Therefore, such an approach to the study of the crystallization process of polymer solutions cannot be considered to correspond to the essence of the matter. For this reason, the mathematical model does not take into account the convective transfer of the polymer melt during the cooling process in the dosing zone.

Formulation of the problem

Assuming that technological stresses do not affect the temperature and flow of the crystallization process, it is necessary to solve the problem of determining the temperature fields and the degree of homogenization and crystallization, or the thermokinetic problem.

The problem of determining temperature fields and the degree of polymerization and crystallization is described by the following boundary value problem:

$$c(T)\rho(T)\left[\frac{\partial T(x,t)}{\partial t} + v_r \frac{\partial T}{\partial r} + v_z \frac{\partial T}{\partial z}\right];$$

$$= \mathrm{div}(\lambda(T)\,\mathrm{grad}\,T(x,t)) + \left(Q_\alpha \frac{d\alpha}{dt} + Q_\beta \frac{d\beta}{dt}\right); \ x \in V;$$

kinetic equation of polymerization

$$\frac{d\alpha(t)}{dt} = K_\alpha (1 - \alpha)(c_0 + \alpha); \tag{3}$$

kinetic equation of crystallization

$$\frac{d\beta(t)}{dt} = K_\beta(T)(A_0 + \beta)(\alpha \beta_p(T) - \beta); \tag{4}$$

$$K_\alpha = k_\alpha \exp\left(-\frac{U}{RT}\right); \ K_\beta = k_\beta \exp\left(-\frac{E}{RT} - \frac{\Psi T_p}{T_p - T}\right); \tag{5}$$

$$b_0 = E/R, \ b_1 = \Psi - b_0.$$

Initial and boundary conditions:

$$\alpha(x,0) = 0; \ \beta(x,0) = 0, \ T(x,0) = T_0; \tag{6}$$

$$\lambda(T)n \cdot \mathrm{grad}\,T(x,t) = h(T(x,t) - T_{av}); \ n \cdot \mathrm{grad}\,T(x,t) = 0, \ x \in S_2; \tag{7}$$

$$T(x,t) = T^*(x,t); \ x \in S_1, \tag{8}$$

where c is the specific heat capacity; ρ — density; λ — thermal conductivity coefficient; Q_α, Q_β — intensities of heat sources due to polymerization and crystallization, respectively; R — universal gas table; $U, E, k_\alpha, k_\beta, c_0, c_1$ — kinetic steels determined experimentally from calorimetric measurements; melting point; β_p — equilibrium degree of crystallization;

$$\beta_b = 0,52\sqrt{1-(T/T_p)^4} \approx \frac{0,26}{T_p^2}(T_p^4 - T^4) = E_1(T_p^4 - T^4).$$

Thermophysical properties of low density polymer (PENG):

$$c = 2,4 \ \cdot kJ/(kg^\circ\mathrm{C})); \ \lambda = 0,182 \ W/(m^\circ\mathrm{C}) ;$$

$$T_p = 170^\circ\mathrm{C} ; \ \rho = 1080 \ \mathrm{kg/m}^3 ; \ T_c = 60^\circ\mathrm{C}.$$

Taking into account the fact that at the melting temperature of the polymer, the thermophysical coefficients can be considered constant, the differential equations describing the processes of heat release in the dosing zone, taking into account the smallness of the gradients relative to the axial component of the speed of movement of the polymer solution, take the form:

$$\frac{\partial v_z}{\partial t} + v_r \frac{\partial v_z}{\partial r} + v_z \frac{\partial v_z}{\partial z} = -\frac{1}{\rho}\frac{\partial p}{\partial z} + \mu_e \Delta v_z + g_z; \tag{9}$$

$$c\rho\left[\frac{\partial T}{\partial t} + v_r \frac{\partial T}{\partial r} + v_z \frac{\partial T}{\partial z}\right] = \lambda\Delta T + Q_\alpha \frac{d\alpha}{dt} + Q_\beta \frac{d\beta(t)}{dt}. \tag{10}$$

Initial and boundary conditions:

$$\alpha(r,z,t)|_{t=0} = 1, \ \beta(r,z,t)|_{t=0} = 0; \ T(r,z,t)|_{t=0} = T_p;$$

$$\left[\frac{\partial T}{\partial r} - h_0(T - T_0)\right]|_{R_1} = 0; \ \left[\frac{\partial T}{\partial r} + h_1(T - T_0)\right]|_{R_2} = 0.$$

Cooling channel:

$$v_z|_{z=0} = f_2(r); \ \frac{\partial v_r}{\partial r}|_{r=0} = 0, \ \frac{\partial v_z}{\partial z}|_{r=0} = 0.$$

On hard surfaces for the components of the agent that cools, meet the conditions of adhesion and impenetrability.

In the equations, the following are indicated: λ — thermal conductivity coefficient; Q_α — thermal effect of polymerization; Q_β — the thermal effect of crystallization (the rate of specific heat release during PENG crystallization); k_α, k_β — polymerization and crystallization rate constants; U — activation energy of the polymerization process; Ψ — characteristic temperature of the polymer; R — universal gas table; h_0, h_1 — coefficients of heat exchange with the environment; $T_p = 415\,\mathrm{K}$ is the equilibrium melting temperature.

PROBLEM SOLVING

So, we have a system of differential equations (9), (10), (3), (4) with respect to the temperature of the polymer melt and the degree of homogenization α and crystallization β with the corresponding initial and boundary conditions (6)–(8).

This system of equations is nonlinear, its solution will be sought by an iterative scheme by analogy with the previous sections.

Let's consider the equations regarding the degree of polymerization and the degree of crystallization β. At the same time, at the first stage, we consider, $K_\alpha \sim k_\alpha$, $K_\beta \sim k_\beta$.

Since these equations contain a nonlinear component relative to $T(r,z,t)$, the exponent must be approximated, for example, by a fractional-rational expression [16]. Let's denote $e_0 = U/R$. Then we will have

$$K_\alpha(T) \approx k_\alpha\left(1 - \frac{e_0 T}{e_1 + e_2 T + e_3 T^2}\right) = k_\alpha \frac{e_1 - e_2 T + e_3 T^2}{e_1 + e_2 T + e_3 T^2};$$

$$e_1 = e_0^2/12, \quad e_2 = e_0/2, \quad e_3 = 1.$$

By analogy, we approximate K_β in (6) $b_0 = E/R$, $b_1 = \Psi - b_0$).

$$K_\beta = k_\beta \exp\left[-\frac{b_0 + b_1 T}{T(T_p - T)}\right] \approx k_\beta \frac{d_0 + d_1 T + d_2 T^2 + d_3 T^3 + d_4 T^4}{c_0 + c_1 T + c_2 T^2 + c_3 T^3 + c_4 T^4}. \qquad (11)$$

Consider the equation (3) and denote

$$N_\alpha = -\frac{1}{e_1} T\left[(e_2 + T)\frac{d\alpha}{dt} - (e_2 - T)k_\alpha(1-\alpha)(c_0 + \alpha)\right].$$

Then we will have

$$\frac{d\alpha}{dt} = k_\alpha(1-\alpha)(c_0 + \alpha) + N_\alpha(\alpha, T). \qquad (12)$$

We get the solution of the equation (12) without taking into account $N_\alpha(\alpha, T)$:

$$\frac{d\alpha^{(1)}}{dt} + k\alpha = k - k_\alpha \alpha^2, \quad k = k_\alpha c_0; \quad \alpha(0) = 0.$$

The solution of this equation in the first approximation:

$$\alpha^{(1)}(t) = \frac{1}{c_0}[(2kt + 1)e^{-kt} - e^{-2kt} - 1].$$

Further iterations in determining the expressions for the solutions in this form leads to a significant increase in the exponential terms in the solution, which actually makes it impossible to use the iterative procedure.

Therefore, it is worth now to apply the simplification algorithm and obtain the following solution of the equation (12):

$$\alpha^{(1)}(t) \approx A_2 + e^{-\gamma_\alpha t}[\overline{a}_0 f_1(\omega_\alpha t) + \overline{a}_1 f_2(\omega_\alpha t)]. \qquad (13)$$

Now further iterations to determine the expression for the polymerization coefficient can be implemented according to the standard algorithmic procedure [16].

Let's go back to the expression (12). It contains an expression for the melting temperature of the polymer:

$$v_r(r,z,t) = \sum_{n=1}^{M} R_n(r) \sum_{k=1}^{N} Z_k(z) vr_{n,k}(t); \quad v_z(r,z,t) = \sum_{n=1}^{M} R_n(r) \sum_{k=1}^{N} Z_k(z) vz_{n,k}(t);$$

$$T(r,z,t) = \sum_{m=1}^{M} \sum_{k=1}^{N} R_m(r) Z_k(z) tt_{n,k}(t);$$

$$tt_{n,k}(t) = t1^0_{n,k} - e^{-t1^4_{n,k}t}(t1^1_{n,k} f_1(t1^5_{n,k}t) + t1^2_{n,k} f_2(t1^5_{n,k}t)). \tag{14}$$

This expression is obtained in [17]. Application of integral transformations by spatial variables gives:

$$\overline{\overline{N_\alpha^{(1)}}}(t) = \int_{r_2}^{r_2+\alpha} R_n(\beta r) R_{n_1}(\beta r) \int_{z_0}^{L} Z_k(\delta_k z) Z_{k_1}(\delta_{k_1} z) N_\alpha(r,z,t) dr dz.$$

Substituting the expression for the melt temperature in the image space by the spatial variables in gives:

$$\overline{\overline{N_\alpha^{(1)}}}(t) = \sum_{n_1,k_1} \overline{\overline{tt}}_{n_1,k_1}(t)\left[\left(\overline{\overline{tt}}_{n_1,k_1}(t) - e_2\right)\alpha^{(1)} - \left(\overline{\overline{tt}}_{n_1,k_1}(t) + e_2\right)\frac{d\alpha^{(1)}}{dt}\right].$$

Substituting (13) and (14) into this expression, performing the corresponding transformations gives

$$\overline{\overline{\overline{N_\alpha^{(1)}}}}(p) \approx \frac{N_2}{p} + \frac{N_0 + N_1 p}{N_3 + N_4 p + p^2} \rightarrow \overline{\overline{N}}_\alpha^{(1)}(t) =$$

$$= na_0 + e^{-na_4 t}(na_1 f_1(na_5 t) + na_2 f_2(na_5 t)).$$

Taking into account (13)

$$\alpha^{(2)}(t) = \alpha^{(1)}(t) + \overline{\overline{N}}_\alpha^{(1)}(t) = A_0^{(2)} + e^{-A_4^{(2)}t}(A_1^{(2)} f_1(A_5^{(2)}t) + A_2^{(2)} f_2(A_5^{(2)}t)).$$

In Fig. 1, 2 graphs of the distribution of the proportion of melt homogenization at fixed time values are given. It can be seen that the distribution of the homogenization (and crystallization) process is evened out due to the decrease in the temperature of the polymer melt.

In the space of originals by spatial variables:

$$\alpha(r,z,t) \approx \sum_{n,k} R_n(\beta_n r) Z_k(\delta_k z) \times$$

$$\times\left[A_{n,k}^0 + e^{-(x\gamma_\alpha)_{n,k}t}(A_{n,k}^1 f_1((\omega_\alpha)_{n,k}t) + A_{n,k}^2 f_2((\omega_\alpha)_{n,k}t))\right]. \tag{15}$$
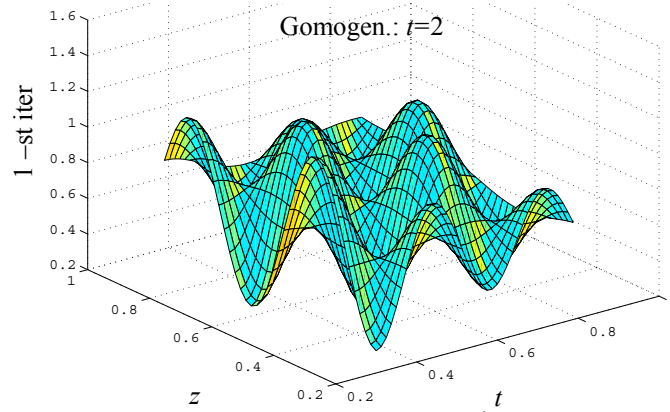
Fig. 1. Graph of distribution of polymer melt homogenization at the 1st iteration

Taking (11) into account, the equation (4) for determining the degree of crystallization takes the form

$$(c_0 + c_1 T + c_2 T^2 + c_3 T^3 + c_4 T^4)\frac{d\beta(t)}{dt} =$$

$$= (d_0 + d_1 T + d_2 T^2 + d_3 T^3 + d_4 T^4)(E_0 + \beta))[\alpha(t)E_1(T_p^4 - T^4) - \beta];$$

$$E_1 = 0{,}26/T_p^2.$$

$$c_0 \frac{d\beta(t)}{dt} = d_0(e_0 + e_1\beta + e_2(\beta)^2) + N_\beta(T,\beta); \tag{16}$$

$$N_\beta(T,\beta) = T(d_1 + d_2 T + d_3 T^2 + d_4 T^3)(e_0 + e_1\beta + e_2\beta^2).$$
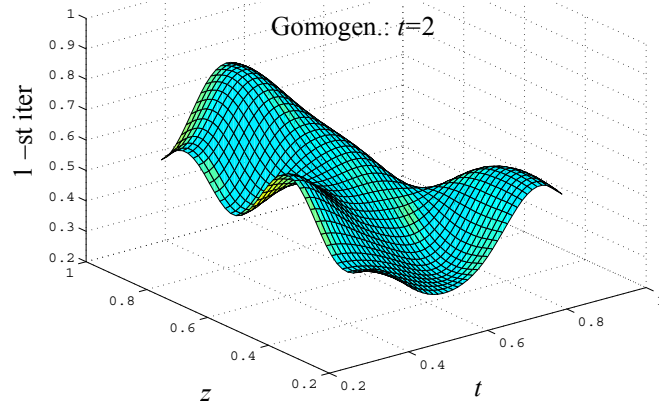

Fig. 2. Distribution graph of polymer melt homogenization at the 3rd iteration

$$- T(c_1 + c_2 T + c_3 T^2 + c_4 T^3)\frac{d\beta(t)}{dt}. \tag{17}$$

By analogy with (13) we obtain the solution of the equation (16)

$$\beta^{(1)}(t) \approx b_0 + e^{-\gamma_\beta t}[\bar{b}_1 f_1(\omega_\beta t) + \bar{b}_2 f_2(\omega_\beta t)].$$

In the next step, we will add to the obtained solution the dependence on the temperature of the melt $T(x,t)$, perform the transformation for $N_\beta(T,t)$ according to (17). Due to the algorithms of equivalent simplification, the solution of the equation (16) can be written in the form

$$\beta(r,z,t) = \sum_{n,k} R_n(\beta_n r) Z_k(\delta_k z) \times$$

$$\times \left[B_{n,k}^0 + e^{-(\gamma_\beta)_{n,k}t} (B_{n,k}^1 f_1((\omega_\beta)_{n,k}t) + B_{n,k}^2 f_2((\omega_\beta)_{n,k}t)) \right].$$

Now we need to define an expression for

$$L_T = Q_p \frac{d\alpha(t)}{dt} + Q_{cr} \frac{d\beta(t)}{dt}.$$

Taking into account the obtained solutions regarding the degree of polymerization and crystallization and the calculation of the time-dependent ones, we have:

$$L_T = Q_p e^{-\gamma_\alpha t} \left[-(\gamma_\alpha A_0 + \omega_\alpha A_1)(\omega_\alpha t) + (\omega_\alpha A_0 - \gamma_\alpha A_1)(\omega_\alpha t) \right] +$$

$$+ Q_{cr} e^{-\gamma_\beta t} \left[-(\gamma_\beta B_0 + \omega_\beta B_1)(\omega_\beta t) \right] + (\omega_\beta B_0 - \gamma_\beta B_1)(\omega_\beta t)].$$

We have

$$F_{n,k}^T(t) = f_0^{n,k} + e^{-\gamma_f^{n,k}t} [f_1^{n,k}(\omega_f^{n,k}t) + f_2^{n,k}(\omega_f^{n,k}t)].$$

Therefore, the temperature field of the polymer in the cooling zone is determined by the expression:

$$T(r,z,t) = T_{\text{pol}}(r,z,t) \approx \sum_{n=1}^{M} \sum_{k=1}^{M} R(\delta_n r) Z(\beta_k z) F_{n,k}^T(t).$$

The coefficients in these expressions are calculated using the appropriate C program.

Calculations were performed for the following values of the problem parameters:

$$c = 57,3 \, kJ/(kg\,°C); \ \rho = 1,1 \cdot 10^3 \, \text{kg/m}^3; \ \lambda_0 = 2,14848 \cdot 10^{-2} \, \text{kJ/(m\,c\,°C)};$$

$$Q_n = 4,297 \, \text{J/(sm}^3); Q_{kr} = 8,3552 \, \text{J/(sm}^3); k_\alpha = 0,83 \, 1/c; k_\beta = 0,041 \, 1/c;$$

$$U = 0,0443 \, kJ/kg; \ A = 10^2; \ R = 8,314; \Psi = 45°C; \ E = 0,034 \, kJ/kg.$$

In fig. 3 shows the graph of the distribution of the fraction of crystallization for a fixed value of time.
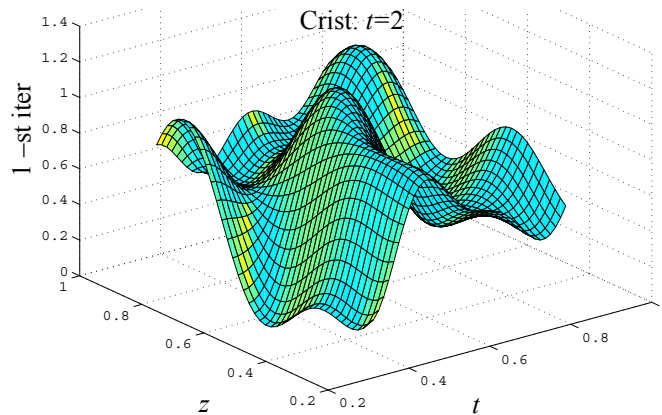

Fig. 3. Distribution graph of polymer melt crystallization on the 3rd iteration

CONCLUSIONS

1. The purpose of mathematical modeling of polymerization and crystallization processes was to determine the equilibrium state of these processes and to determine the length of the dosing zone.

2. The problem of determining the degree of polymerization and crystallization of the polymer melt in the dosing zone of the extruder is formulated in the form of a system of nonlinear differential equations with respect to the temperature of the melt (mass and heat transfer equations), taking into account the cooling boundary conditions and nonlinear kinetic equations of the degree of polymerization and crystallization of the polymer melt.

3. The solution of the system of equations of motion of the polymer melt (thermal conductivity) and kinetic equations of the degree of polymerization and crystallization is carried out by a numerical-analytical iterative method, which made it possible to obtain a solution in quadrature.

4. The distribution of the temperature of the melt crystallizing in the dosing zone, the degree of polymerization and crystallization of the polymer are obtained.

5. The proposed numerical analytical method for solving nonlinear differential equations made it possible to automate the software implementation of the iterative procedure and obtain an approximate solution for the distribution of the crystallization field of polymer solutions. Four iterations were performed to achieve a relative solution error of 5%.

6. The proposed iterative numerical analytical method proved the effectiveness of its application to a wide range of problems described by systems of nonlinear equations of the parabolic type.

REFERENCES

1. N.A. Belyaeva, *Mathematical modeling of deformation of viscoelastic structured polymer (composite) systems: Author. dr. diss*. Chelyabinsk, 2008, 35 p.
2. K.Kh. Zelensky, "A numerical-analytical method for solving space-time problems with moving boundaries," *Interv. science and technology coll. "Adaptive automatic control systems"*, no. 14 (34), pp. 107–117, 2009.
3. K.Kh. Zelensky, *Mathematical modeling of nonlinear polymer materials in extruders: Author.diss... of Doctor of Technical Sciences*. Kyiv, 2021, 43 p.
4. R.R. Zinatullin and N.M. Trufanova, "*Numerical modeling of technological stresses during the production of plastic wire insulation*," Computational Mechanics of Solid Media, vol. 2, no. 1, pp. 38–53, 2009.
5. T.G. Kulikova and N.A. Trufanov, "Numerical solution of the boundary value problem of thermomechanics for a crystallizing viscoelastic polymer," *Ex. Mechanics of continuous media*, vol. 1, no. 2, pp. 38–52, 2008.
6. V.N. Mitroshin, "Structural modeling of the cooling process of an insulated cable core when it is produced on an extrusion line," *Vestn. Samar Mr. technical Univ. Ser.: "Technical Sciences"*, no. 40, pp. 22–33, 2006.
7. O.S. Sakharov, V.I. Sivetskyi, and O.L. Sokolskyi, *Modeling of processes of melting and homogenization of polymer compositions in worm equipment: monograph*. Kyiv: VP "Edelweiss", 2012, 120 p.
8. I.N. Shardakov and N.A. Trufanov, "Modeling of thermomechanics of crystallizing polymers," *Izv. Tula State University. Natural sciences*, vol. 2, pp. 117–123, 2008.

9. D. Andreucci, A. Fasano, and M. Primicerio, "Numerical simulation of polymer crystallization,"*Mathematical Models and Methods in Applied Sciences*, November 2011, 11 p.
10. V. Capasso, H. Engl, J. Periaux (Eds.), "Computational Mathematics Driven by Industrial Problems," in *Mathematical models for polymer crystallization processes,* Springer, Berlin/Heidelberg, 2000, pp. 39–67.
11. V. Capasso, R. Escobedo, and C. Salani, "Moving Bands and Moving Boundaries in a Hybrid Model for the Crystallization of Polymers," in *Free Boundary Problems Theory and Applications*, vol. 147, ed. by P. Colli, C. Verdi, A. Visintin, Birkhauser, 2004, pp. 75–86.
12. R. Escobedo and L. Fernandez, "Free boundary problems (FBP) and optimal control of axisymmetric polymer crystallization processes," *Computers and Mathematics with applications*, 68, pp. 27–43, 2014.
13. R. Escobedo and L. Fernandez, "Optimal control of chemical birth and growth processes in a deterministic model," J. Math. Chem., 48, pp. 118–127, 2010.
14. A. Friedman and A. Velazquez, "A free boundary problem associated with crystallization of polymers in a temperature field," *Indiana Univ. Math. J.*, 50, pp. 1609–1649, 2001.
15. J. Ramos, "Propagation and interaction of moving fronts in polymer crystallization," *Appl. Math. Comput.*, 189, pp. 780–795, 2007.
16. O. Trofymchuk, K. Zelensky, V. Pavlov, and K. Bovsunovska, "Modeling of heat and mass transfer processes in the melting zone of polymer," *System Research & Information Technologies*, no. 4, pp. 68–80, 2021.
17. N. Zelenskaya and K. Zelensky, "Approximation of Bessel functions by rational functions," *Electronics and control systems*, no. 2 (44), pp. 123–129, 2015.

INFORMATION ON THE ARTICLE

Kyryl Kh. Zelensky, ORCID: 0000-0003-1501-8214, National Technical University of Ukraine "Igor Sikorsky Kyiv Polytechnic Institute", Ukraine, e-mail: zelensky126@ukr.net

МАТЕМАТИЧНЕ МОДЕЛЮВАННЯ КРИСТАЛІЗАЦІЇ РОЗЧИНІВ ПОЛІМЕРІВ / К.Х. Зеленський

Анотація. Розглянуто процеси гомогенізації та кристалізації розчинів полімерів у циліндричних трубах, які описуються рівнянням конвективно-дифузійної залежності від температури розчину та кінетичними рівняннями з гомогенізації та кристалізації полімера, відомими як термокінетична нелінійна крайова задача. Запропоновано числово-аналітичний ітераційний метод розв'язування цієї задачі, який полягає в поетапному отриманні розв'язків кінетичних рівнянь з гомогенізації та кристалізації розчинів полімерів залежно від температури розчину та отримання розв'язку конвективно-дифузійної задачі щодо температури розплаву. Точність отриманого розв'язку визначається нормою різниці двох сусідніх ітерацій. Значення коефіцієнта кристалізації, близьке до одиниці, визначає довжину зони дозування і перехід до наступної зони – потоку гомогенізованого полімера в розподільну головку екструдера. Наведено результати математичного моделювання.

Ключові слова: усереднення, інтегральні перетворення, ітераційний метод, кристалізація, математична модель, нелінійна крайова задача.

ВІДОМОСТІ ПРО АВТОРІВ

Андрушко Станіслав Дмитрович,

отоларинголог Чернівецької центральної лікарні, Україна, Чернівці

Баран Данило Романович,

старший інженер із розроблення програмного забезпечення компанії «Codeimpact B.V.», Україна, Київ

Бохонов Юрій Євгенович,

доцент, кандидат фізико-математичних наук, доцент кафедри математичних методів системного аналізу ІПСА КПІ ім. Ігоря Сікорського, Україна, Київ

Виклюк Ярослав Ігорович,

професор, доктор технічних наук, професор кафедри систем штучного інтелекту Національного університету «Львівська політехніка», Україна, Львів

Газдюк Катерина Петрівна,

доктор філософії за спеціальністю 121 (інженерія програмного забезпечення), асистент кафедри програмного забезпечення комп'ютерних систем Чернівецького національного університету імені Юрія Федьковича

Гапон Сергій Вікторович,

завідувач лабораторії географічних інформаційних систем Світового центру даних з геоінформатики та сталого розвитку КПІ ім. Ігоря Сікорського, Україна, Київ

Єфремов Костянтин Вікторович,

кандидат технічних наук, доцент кафедри штучного інтелекту КПІ ім. Ігоря Сікорського, директор Світового центру даних з геоінформатики та сталого розвитку КПІ ім. Ігоря Сікорського, Україна, Київ

Згуровський Михайло Захарович,

академік НАН України, професор, доктор технічних наук, ректор КПІ ім. Ігоря Сікорського, Україна, Київ

Зеленський Кирило Харитонович,

доцент, доктор технічних наук, професор кафедри біомедичної кібернетики факультету біомедичної інженерії КПІ ім. Ігоря Сікорського, Україна, Київ

Клименко Анастасія Іллівна,

співробітник Національної комісії, що здійснює державне регулювання у сферах енергетики та комунальних послуг, Україна, Київ

Коваленко Світлана Миколаївна,

доцент, кандидат технічних наук, доцент кафедри програмної інженерії та інтелектуальних технологій управління Національного технічного університету «ХПІ», Україна, Харків

Коваленко Сергій Володимирович,

доцент, кандидат технічних наук, доцент кафедри системного аналізу та інформаційно-аналітичних технологій Національного технічного університету «ХПІ», Україна, Харків

Ковальов Микола Олександрович,

кандидат технічних наук, доцент кафедри інформаційних систем та технологій КПІ ім. Ігоря Сікорського, Україна, Київ

Куценко Олександр Сергійович,

професор, доктор технічних наук, професор кафедри системного аналізу та інформаційно-аналітичних технологій Національного технічного університету «ХПІ», Україна, Харків

Левицька Світлана Анатоліївна,

професор, доктор медичних наук, професор кафедри дитячої хірургії та отоларингології Буковинського державного медичного університету, Україна, Чернівці

Міронов Юрій Глібович,

аспірант кафедри ІПЗ ФККПІ Національного авіаційного університету, Україна, Київ

Мусієнко Данило Ігорович,

аспірант ІПСА КПІ ім. Ігоря Сікорського, Україна, Київ

Невінський Денис Володимирович,

доцент, кандидат технічних наук, асистент кафедри електронних засобів інформаційно-комп'ютерних технологій Інституту телекомунікацій, радіоелектроніки та електронної техніки Національного університету «Львівська політехніка», Україна, Львів

Палій Марина Анатоліївна,

отоларинголог Чернівецької центральної лікарні, Україна, Чернівці

Панкратова Наталія Дмитрівна,

член-кореспондент НАН України, професор, доктор технічних наук, заступник директора з наукової роботи ІПСА КПІ ім. Ігоря Сікорського, Україна, Київ

Писарчук Ілля Олексійович,

студент кафедри обчислювальної техніки факультету інформатики та обчислювальної техніки КПІ ім. Ігоря Сікорського, Україна, Київ

Писарчук Олексій Олександрович,

професор, доктор технічних наук, професор кафедри обчислювальної техніки факультету інформатики та обчислювальної техніки КПІ ім. Ігоря Сікорського, Україна, Київ

Пишнограєв Іван Олександрович,

доцент, кандидат фізико-математичних наук, доцент кафедри штучного інтелекту КПІ ім. Ігоря Сікорського, Україна, Київ

Подколзін Гліб Борисович,

доцент, кандидат фізико-математичних наук, доцент кафедри математичних методів системного аналізу ІПСА КПІ ім. Ігоря Сікорського, Україна, Київ

Різник Володимир Васильович,

професор, доктор технічних наук, професор кафедри автоматизованих систем управління Інституту комп'ютерних наук та інформаційних технологій Національного університету "Львівська політехніка", Україна, Львів

Статкевич Віталій Михайлович,

кандидат фізико-математичних наук, науковий співробітник відділу прикладного нелінійного аналізу ІПСА КПІ ім. Ігоря Сікорського, Україна, Київ

Шкода Мирослав,

PhD, проректор з міжнародних зв'язків та акредитації DTI University, Дубніца-над-Вагом, Словаччина

Pradip M. Paithane,

Doctor of Philosophy, Department of Computer Engineering of Vidya Pratishthan's Kamalnayan Bajaj Institute of Engineering and Technology, India, Pune

Sarita Jibhau Wagh,

Assistant Professor, Environment Science Department, T.C. College Baramati, India, Maharashtra

Sangeeta N. Kakarwal,

Professor, Department of Computer Science and Engineering of ICEEM College, India, Aurangabad